AFRL-AFOSR-UK-TR-2012-0041

Waveform Design and Diversity for Advanced Space-Time Adaptive Processing and Multiple Input Multiple Output Systems

Professor Antonio De Maio

Universita Degli Studi Federico II
Departimento Di Ingegneria
Via Claudio 21
Napoli, Italy 80125

EOARD Grant 09-3006

Report Date: August 2012

Final Report from 1 April 2009 to 31 March 2012

Air Force Research Laboratory
Air Force Office of Scientific Research
European Office of Aerospace Research and Development
Unit 4515 Box 14, APO AE 09421

REPORT DOCUMENTATION PAGE

Form Approved OMB No. 0704-0188

1. REPORT DATE *(DD-MM-YYYY)*	2. REPORT TYPE	3. DATES COVERED *(From – To)*
28 August 2012	Final Report	1 April 2009 – 31 March 2012

4. TITLE AND SUBTITLE

Waveform Design and Diversity for Advanced Space-Time Adaptive Processing and Multiple Input Multiple Output Systems

5a. CONTRACT NUMBER

FA8655-09-1-3006

5b. GRANT NUMBER

Grant 09-3006

5c. PROGRAM ELEMENT NUMBER

61102F

6. AUTHOR(S)

Professor Antonio De Maio

5d. PROJECT NUMBER

5d. TASK NUMBER

5e. WORK UNIT NUMBER

7. PERFORMING ORGANIZATION NAME(S) AND ADDRESS(ES)

Universita Degli Studi Federico II
Departimento Di Ingegneria
Via Claudio 21
Napoli, Italy 80125

8. PERFORMING ORGANIZATION REPORT NUMBER

N/A

9. SPONSORING/MONITORING AGENCY NAME(S) AND ADDRESS(ES)

EOARD
Unit 4515 BOX 14
APO AE 09421

10. SPONSOR/MONITOR'S ACRONYM(S)

AFRL/AFOSR/RSW (EOARD)

11. SPONSOR/MONITOR'S REPORT NUMBER(S)

AFRL-AFOSR-UK-TR-2012-0041

12. DISTRIBUTION/AVAILABILITY STATEMENT

Approved for public release; distribution is unlimited.

13. SUPPLEMENTARY NOTES

14. ABSTRACT

Waveform diversity refers to the adaptivity of the radar waveform to dynamically optimize the radar performance for the particular scenario and tasks. It may also exploit adaptivity in other domains, including the antenna radiation pattern (both on transmit and receive), time domain, frequency domain, coding domain, and polarization domain. As this definition indicates, the term waveform diversity does not refer to a tangible object, but to a remote sensing paradigm. The basic elements of the paradigm are: measurement diversity, knowledge-aided processing and design, and transmitter adaptivity. The waveform diversity paradigm arose from the insatiable demands for remote sensing performance that are always present in military applications, and the application of waveform diversity has led to many interesting and promising remote sensing concepts. In this report we focus on some challenging problems concerning waveform design and diversity and propose innovative solutions. Specifically, in Chapter 1, we consider the problem of waveform design for radar sensors that operate in a noncooperative network. In Chapter 2, we deal with the problem of Pareto-optimal waveform design in the presence of colored Gaussian noise, under a similarity and an energy constraint. In Chapter 3, we consider the problem of knowledge-aided transmit signal and receive filter design for point like target in signal-dependent clutter. In Chapter 4, a network of radars sharing the same frequency band, and using properly coded waveforms to improve features attractive from the radar point of view is considered. In Chapter 5, we deal with the design of radar receive filters jointly optimized with respect to sidelobe energy and sidelobe peaks via Pareto-optimal theory. Finally, in Chapter 6, we consider the problem of cognitive transmit signal and receive filter design for a point-like target embedded in a high reverberating environment.

15. SUBJECT TERMS

EOARD, Phased Arrays, radar

16. SECURITY CLASSIFICATION OF:			17. LIMITATION OF ABSTRACT	18, NUMBER OF PAGES	19a. NAME OF RESPONSIBLE PERSON
a. REPORT	b. ABSTRACT	c. THIS PAGE			JAMES LAWTON Ph. D.
UNCLAS	UNCLAS	UNCLAS	SAR	289	**19b. TELEPHONE NUMBER** *(Include area code)* +44 (0)1895 616187

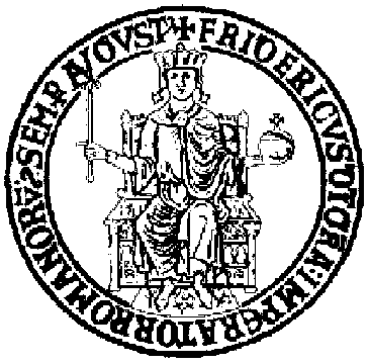

Waveform Design and Diversity for Advanced Space-Time Adaptive Processing and Multiple Input Multiple Output Systems

A. De Maio A. Farina* M. Wicks*

*collaborating engineer from SELEX Sistemi Integrati

*collaborating engineer from the Air Force Research Laboratory

March 2012

This work has been funded by EOARD grant FA8655-09-1-3006 on "European Office of Aerospace Research and Development".

Effort sponsored by the EOARD, European Office of Aerospace Research and Development, under grant number FA8655-09-1-3006. The U.S. Government is authorized to reproduce and distribute reprints for Government purpose notwithstanding any copyright notation thereon.

The authors certify that there were no subject inventions to declare during the performance of this grant.

Contents

List of Figures

List of Tables

List of Algorithms

Preface

IEEE Radar Standard P686/D2 (Jan. 2008) defines waveform diversity as: Adaptivity of the radar waveform to dynamically optimize the radar performance for the particular scenario and tasks. May also exploit adaptivity in other domains, including the antenna radiation pattern (both on transmit and receive), time domain, frequency domain, coding domain, and polarization domain. As this definition indicates, the term waveform diversity does not refer to a tangible object, but to a remote sensing paradigm. The basic elements of the paradigm are: measurement diversity, knowledge-aided processing and design, and transmitter adaptivity. The waveform diversity paradigm arose from the insatiable demands for remote sensing performance that are always present in military applications, and the application of waveform diversity has led to many interesting and promising remote sensing concepts.

In this report we focus on some challenging problems concerning waveform

design and diversity and propose innovative solutions.

Precisely, in Chapter 1, we consider the problem of waveform design for radar sensors that operate in a noncooperative network. This is a system in which multiple radars share some common features (for example, the same carrier frequency), but they do not cooperate in the detection stage of processing (namely, each sensor performs detection processing independently). Our goal is to increase the performance of an element of the sensor network, and, at the same time, to limit the interference induced by this element of interest on remaining sensors. The resulting problem is in general Nondeterministic Polynomial-hard, namely an optimal solution can not be calculated in polynomial time. However, it is possible to relax the original problem into a Semidefinite Programming problem, which is convex. This last problem can easily be solved in polynomial time. Starting from an optimal solution to the relaxed problem, we construct a *good* solution of the original nonconvex problem, and evaluate its quality via the approximation bound. The proposed technique, referred to as "Waveform Design in Noncooperative Environment" (WDNE), enjoys the benfits of polynomial time complexity. Finally, we analyze via simulation the performance of the WDNE procedure.

In Chapter 2, we deal with the problem of Pareto-optimal waveform design in the presence of colored Gaussian noise, under a similarity and an energy constraint. At the design stage, we determine the optimal radar code according the following criterion: constrained maximization of the detection performance and constrained minimization of the (Cramer Rao Lower Bound) CRLB on the Doppler estimation accuracy. This is tantamount to jointly maximizing two quadratic forms under two quadratic constraints, so that the problem can be formulated in terms of a non-convex multi-objective optimization problem. In order to solve it, we resort to the scalarization technique, which reduces the vectorial problem into a scalar one using a Pareto weight defining the relative importance of the two objective functions. At the analysis stage, we assess the performance of the proposed waveform design scheme in terms of detection performance, region of achievable Doppler estimation accuracy, and ambiguity function. In particular, we analyze the role of the Pareto weight in the optimization process.

In Chapter 3, we consider the problem of knowledge-aided transmit signal and receive filter design for point like target in signal-dependent clutter. We suppose that the radar system has access to a (possibly dynamic) database con-

taining a Geographical Information System (GIS), characterizing the terrain to be illuminated, and some a-priori electromagnetic reflectivity and spectral clutter models, allowing the raw prediction of the actual scattering environment. Hence, we devise an optimization procedure for the transmit signal and the receive filter which sequentially improves the Signal to Interference plus Noise Ratio (SINR). Each iteration of the algorithm, whose convergence is analytically proved, requires the solution of both a convex and an hidden convex optimization problem. The resulting computational complexity is linear with the number of iterations and polynomial with the receive filter length. At the analysis stage, we assess the performance of the proposed technique in the presence of either an homogeneous ground clutter scenario or an heterogeneous mixed land and sea clutter environment.

In Chapter 4, a network of radars sharing the same frequency band, and using properly coded waveforms to improve features attractive from the radar point of view is considered. Non-cooperative games aimed at code design for maximization of the Signal-to-Interference-plus-Noise Ratio (SINR) of each active radar are presented. Code update strategies are proposed, and, resorting to the theory of potential games, the existence of Nash equilibria is analytically

proven. In particular, we propose non-cooperative code update procedures for the cases in which a matched filter, a minimum integrated sidelobe level filter, and a minimum peak to sidelobe level filter is used at the receiver. The case that the received data contain a non-negligible Doppler shift is also analyzed. Experimental results confirm that the proposed procedures reach an equilibrium in few iterations, as well as that the SINR values at the equilibrium are largely superior to those in the case in which classical waveforms are used and no optimization of the radar code is performed.

In Chapter 5, we deal with the design of radar receive filters jointly optimized with respect to sidelobe energy and sidelobe peaks via Pareto-optimal theory. We prove that this criterion is tantamount to jointly minimizing two quadratic forms, so that the design can be analytically formulated in terms of a multi-objective optimization problem. In order to solve it, we resort to the scalarization technique, which reduces the vectorial problem into a scalar one using a Pareto weight defining the relative importance of the two objective functions. At the analysis stage, we assess the performance of the receive filters in correspondence of different values of the Pareto weight highlighting the performance compromises between the Integrated Sidelobe Level (ISL) and the Peak

Sidelobe Level (PSL).

Finally, in Chapter 6, we consider the problem of cognitive transmit signal and receive filter design for a point-like target embedded in a high reverberating environment. We focus on phase-only waveforms, sharing either a continuous or a finite alphabet phase, hence we devise constrained optimization procedures which sequentially improves the Signal to Interference plus Noise Ratio (SINR), accounting for a similarity constraint between the transmitted signal and a prescribed radar waveform. The computational complexity of the proposed algorithms is linear with the number of iterations and polynomial with the receive filter length. At the analysis stage, the performances of the techniques are assessed in the presence of a homogeneous clutter scenario.

Chapter 1

Waveform Design for Noncooperative Radar Networks

1.1 Introduction

In the last decade, the importance of radar has grown progressively with the increasing dimension of the system: from a single colocated antenna to a large sensor network [1]. The concept of heterogeneous radars working together has been thoroughly studied, opening the door to the the concept of Multiple-Input-Multiple-Output (MIMO) radar [2] [3], Over-The-Horizon (OTH) radar networks [4], and Distributed Aperture Radar (DAR) [5] [6]. These three

scenarios are examples of *cooperative radar networks*, in the sense that every single element contributes to the overall detection process. Unfortunately, in many practical situations, it is not possible to design the network *a-priori*. As such, the elements are just simply added to the already existing network (*plug and fight*), and each sensor exhibits its own detection scheme. This is the case in *noncooperative radar networks* [7] [77]. In this scenario, it becomes extremely important that each additional sensor interferes as little as possible with the pre-existing elements, and, to this end, some techniques are easily adopted. The usual approaches rely upon the employment of spatial and/or frequency diversity: the former resorts to forming multiple orthogonal beams, while the latter uses separated carrier frequencies to reduce interference [9] [10]. Another possibility is to exploit waveform diversity [32]: in which the basic concept is to suitably modulate the waveform of the new sensor so as to optimize the detection capabilities of the specific sensor, but, at the same time, controlling the interference introduced into the network. Notice that this is different from the approach employed in cooperative sensor network, where one must design waveforms so as to optimize the joint performance of the system [11] [12]. In the noncooperative case, the optimization of radar wave-

forms has been discussed in the literature [13] and [14]. In the former, the design is based upon the maximization of the global Signal-to-Interference-Plus-Noise Ratio (SINR), and classic constraints such as phase-only or finite energy are considered [13]. In the latter, the problem of parameter estimation (e.g. direction of arrival) for a noncooperative radar is analyzed [14].

In this report, we propose a different approach: we maximize the Signal-to-Noise Ratio (SNR), but at the same time, we control the interference induced by our sensor on the other elements of the network. Furthermore, we apply a constraint to the transmitted signal, limiting the energy to a specific maximum value. The resulting problem is Nondeterministic Polynomial (NP) -hard, namely an optimal solution can not be found in polynomial time. Since an optimal approach is not possible for real-time applications, we propose a new algorithm, referred to as WDNE (Waveform Design in Noncooperative Environment), to generate a suboptimal solution with a polynomial time computational complexity. The procedure is based on the *relaxation and randomization* theory [15]: first we relax the feasible set of the problem, obtaining a solution; then we use this solution to generate a waveform that is feasible for our original problem. The quality of the solution is guaranteed by the *ap-*

proximation bound that ensures that the WDNE technique achieves at least a fraction $R \in (0, 1]$ of the optimal value of the relaxed problem [16].

This chapter is organized as follows. In Section 1.2, we present a model for the generic signal received by an element of the network. In Section 1.3, we discuss some relevant guidelines for waveform design. In Section 1.4, we introduce the optimization procedure. In Section 1.5, we analyze via simulation the performance of the proposed waveform design method. Finally, in Section 1.6, we draw conclusions and outline possible future research tracks.

1.1.1 Notation

We adopt the following notation: boldface for vectors $\boldsymbol{a}$ (lower case), and matrices $\boldsymbol{A}$ (upper case). $a(i)$ for $i = 0, \ldots, N-1$ is the i-th element of the $N-$dimensional vector $\boldsymbol{a}$, while $\boldsymbol{A}(n, m)$ for $(n, m) \in \{0, \ldots, N-1\} \times \{0, \ldots, M-1\}$ is the (n, m)-th entry of the $N \times M$ matrix $\boldsymbol{A}$. The transpose, the conjugate transpose, and the conjugate operators are denoted by the symbols $(\cdot)^T$, $(\cdot)^\dagger$, and $(\cdot)^*$ respectively. tr$(\cdot)$, rank$(\cdot)$, $\lambda_{min}(\cdot)$, and $\lambda_{max}(\cdot)$ are the trace, the rank, the minimum eigenvalue, and the maximum eigenvalue of the square matrix argument, respectively. $\boldsymbol{I}$ and $\boldsymbol{0}$ denote the identity matrix and the matrix with

zero entries (their size is determined from the context). diag($\boldsymbol{x}$) represents a diagonal matrix with diagonal entries $x(0), \ldots, x(N-1)$. The letter j denotes the imaginary unit (i.e. $j = \sqrt{-1}$). For a complex number x, $|x|$ is the modulus and x^* is the conjugate of x. $||.||$ denotes the Euclidean norm of a complex vector. The symbol $\odot$ represents the Hadamard element-wise product [17]. $E[\cdot]$ denotes statistical expectation. Finally, the curled inequality symbol $\succeq$ (and its strict form $\succ$) is used to denote generalized inequality: $\boldsymbol{A} \succeq \boldsymbol{0}$ means that $\boldsymbol{A}$ is an Hermitian positive semidefinite matrix ($\boldsymbol{A} \succ \boldsymbol{0}$ for positive definiteness).

1.2 System Model

We consider a network of L noncooperative monostatic radar systems, where each sensor transmits a coherent burst of pulses

$$s_l(t) = a_l^{tx} u_l(t) \exp[j(2\pi f t + \phi_l)]\,, \qquad l = 0, \ldots, L-1\,,$$

with a_l^{tx} the transmit signal amplitude,

$$u_l(t) = \sum_{i=0}^{N-1} c_l(i) p(t - iT_r)$$

the signal's complex envelope, $p(t)$ the single pulse shape of the transmitted signal, assumed of duration T_p and with unit energy, i.e.

$$\int_0^{T_p} |p(t)|^2 dt = 1\,,$$

T_r ($T_r > T_p$) is the pulse repetition period (see also **Figure 1.1**), $\boldsymbol{c}_l = [c_l(0), c_l(1), \ldots, c_l(N-1)]^T \in \mathbb{C}^N$ the radar code associated with the l-th sensor, f is the carrier frequency, and ϕ_l a random phase associated with the l-th transmitted waveform. In other words, we are considering a network of noncooperative homogeneous sensors, which do not cooperate in the detection process, yet exploit the same kind of waveform, namely a linearly coded pulse train with possibly different codes. Assume that the 0-th sensor is the radar of interest: the received signal under the alternative hypothesis (target presence) is the sum of L transmitted signals scattered by the target. Each term of this sum has a characteristic amplitude, delay and Doppler shift (which depend both on the l-th transmitter and the 0-th receiver), so we can express the signal

received by the radar sensor of interest as

$$r_0(t) = \sum_{l=0}^{L-1} \alpha_{0,l}^{rx} e^{j2\pi(f+f_{0,l})(t-\tau_{0,l})} u_l(t-\tau_{0,l}) + n_0(t)\,, \tag{1.1}$$

where $n_0(t)$ is an additive disturbance due to clutter and thermal noise, $\alpha_{0,l}^{rx}$, $\tau_{0,l}$, and $f_{0,l}$, $l \in \{0,\ldots,L-1\}$ are respectively the complex echo amplitude (accounting for the transmit amplitude, phase, target reflectivity, and channel propagation effects), the delay, and the target Doppler frequency relative to the l-th transmitter and the 0-th receiver. No synchronization is assumed among the sensors, namely $\tau_{0,l}$, $l = 1,\ldots,L-1$, is considered unknown to the 0-th radar system. To simplify the notation, we use the symbol γ_0 instead of $\gamma_{0,0}$ when the index of the receiver (first index) is equal to the index of the transmitter (second index), where $\gamma_{0,l}$ can be one of the parameters $\alpha_{0,l}^{rx}$, $\tau_{0,l}$, or $f_{0,l}$. We can separate in the Right Hand Side (RHS) of equation (1.1) the term due to the 0-th transmitter:

$$r_0(t) = \alpha_0^{rx} e^{j2\pi(f+f_0)(t-\tau_0)} u_0(t-\tau_0) + \sum_{l=1}^{L-1} \alpha_{0,l}^{rx} e^{j2\pi(f+f_{0,l})(t-\tau_{0,l})} u_l(t-\tau_{0,l}) + n_0(t)\,.$$

This signal is down-converted to baseband and filtered through a linear system with impulse response $h(t) = p^*(-t)$. Let the filter output be

$$v_0(t) = \alpha_0^{rx} e^{-j2\pi f \tau_0} \sum_{i=0}^{N-1} c_0(i) e^{j2\pi i f_0 T_r} \chi_p \left(t - iT_r - \tau_0, f_0\right) +$$

$$\sum_{l=1}^{L-1} \alpha_{0,l}^{rx} e^{-j2\pi f \tau_{0,l}} \sum_{i=0}^{N-1} c_l(i) e^{j2\pi i f_{0,l} T_r} \chi_p \left(t - iT_r - \tau_{0,l}, f_{0,l}\right) + w_0(t)$$

where $\chi_p(\lambda, \nu)$ is the (pulse waveform) ambiguity function [18], i.e.

$$\chi_p(\lambda, \nu) = \int_{-\infty}^{+\infty} p(\beta) p^*(\beta - \lambda) e^{j2\pi\nu\beta} d\beta,$$

and $w_0(t)$ is the down-converted and filtered disturbance. The signal $v_0(t)$ is sampled at $t_k = \tau_0 + kT_r$, $k = 0, \ldots, N-1$, providing the observables

$$v_0(t_k) = \alpha_0 c_0(k) e^{j2\pi k f_0 T_r} \chi_p(0, f_0) + \sum_{l=1}^{L-1} \alpha_{0,l} \sum_{i=0}^{N-1} c_l(i) e^{j2\pi i f_{0,l} T_r} \chi_p \left(\Delta\tau_{0,l}(k-i), f_{0,l}\right) + w_0(t_k)\,,$$

where $\alpha_{0,l} = \alpha_{0,l}^{rx} e^{-j2\pi f \tau_{0,l}}$, with $l \in \{0, \ldots, L-1\}$ (again, we use the simplified notation $\alpha_0 = \alpha_{0,0}$), and $\Delta\tau_{0,l}(h) = hT_r - \tau_{0,l} + \tau_0$, $l = 1, \ldots, L-1$. Moreover,

denoting by

$$\boldsymbol{p}_{0,l} = [1, e^{j2\pi f_{0,l} T_r}, \ldots, e^{j2\pi(N-1) f_{0,l} T_r}]^T$$

the temporal steering vector (with $\boldsymbol{p}_0 = \boldsymbol{p}_{0,0}$),

$$\boldsymbol{v}_0 = [v_0(t_0), v_0(t_1), \ldots, v_0(t_{N-1})]^T,$$

$$\boldsymbol{w}_0 = [w_0(t_0), w_0(t_1), \ldots, w_0(t_{N-1})]^T,$$

and

$$\boldsymbol{i}_{0,l} = \left[\sum_{i=0}^{N-1} c_l(i) e^{j2\pi i f_{0,l} T_r} \chi_p\left(\Delta\tau_{0,l}(-i), f_{0,l}\right), \ldots, \sum_{i=0}^{N-1} c_l(i) e^{j2\pi i f_{0,l} T_r} \chi_p\left(\Delta\tau_{0,l}(N-1-i), f_{0,l}\right) \right]^T,$$

we get the following vectorial model for the scattered signal

$$\boldsymbol{v}_0 = \alpha_0 \chi_p(0, f_0) \boldsymbol{c}_0 \odot \boldsymbol{p}_0 + \sum_{l=1}^{L-1} \alpha_{0,l} \boldsymbol{i}_{0,l} + \boldsymbol{w}_0 \,. \tag{1.2}$$

In (4.1), we can distinguish the first term due to the 0-th radar ($\alpha_0 \chi_p(0, f_0) \boldsymbol{c}_0 \odot \boldsymbol{p}_0$), the second term due to the interference induced by the other radars

$(\sum_{l=1}^{L-1} \alpha_{0,l} \boldsymbol{i}_{0,l})$, and, finally, the disturbance $(\boldsymbol{w}_0)$ accounting for clutter and thermal noise.

Moreover, since $\chi_p(t,\nu) = 0\,,$ for $|t| \geq T_p\,,$ the vector $\boldsymbol{i}_{0,l}$ shares a structure which belongs to the finite set $\mathcal{A}_{0,l}$ (of cardinality $2N$) whose elements are

$$\begin{bmatrix} \\ c_l(N-1)e^{j2\pi(N-1)f_{0,l}T_r} \\ \\ 0 \\ \\ \vdots \\ \\ 0 \\ \\ \end{bmatrix} \chi_p\left(\Delta\tau_{0,l}(-N+1), f_{0,l}\right)\,,$$

$$\begin{bmatrix} \\ c_l(N-2)e^{j2\pi(N-2)f_{0,l}T_r} \\ \\ c_l(N-1)e^{j2\pi(N-1)f_{0,l}T_r} \\ \\ 0 \\ \\ \vdots \\ \\ 0 \\ \\ \end{bmatrix} \chi_p\left(\Delta\tau_{0,l}(-N+2), f_{0,l}\right) ,$$

$$\vdots$$

$$\begin{bmatrix} \\ c_l(0) \\ \\ c_l(1)e^{j2\pi f_{0,l}T_r} \\ \\ \vdots \\ \\ c_l(N-1)e^{j2\pi(N-1)f_{0,l}T_r} \\ \\ \end{bmatrix} \chi_p\left(\Delta\tau_{0,l}(0), f_{0,l}\right) ,$$

$$\vdots$$

$$\begin{bmatrix} \\ 0 \\ \\ \vdots \\ \\ 0 \\ \\ c_l(0) \\ \\ c_l(1)e^{j2\pi f_{0,l}T_r} \\ \\ \end{bmatrix} \chi_p\left(\Delta\tau_{0,l}(N-2), f_{0,l}\right) ,$$

$$\begin{bmatrix} \\ 0 \\ \\ \vdots \\ \\ 0 \\ \\ c_l(0) \\ \\ \end{bmatrix} \chi_p\left(\Delta\tau_{0,l}(N-1), f_{0,l}\right) ,$$

and the N-dimensional vector $\mathbf{0}$. Defining $\tilde{\boldsymbol{i}}_{0,l}$

$$\tilde{\boldsymbol{i}}_{0,l} = \left[c_l(0), c_l(1)e^{j2\pi f_{0,l}T_r} \ldots, c_l(N-1)e^{j2\pi(N-1)f_{0,l}T_r}\right]^T = (\boldsymbol{c}_l \odot \boldsymbol{p}_{0,l})^T,$$

and

$$\boldsymbol{i}_{0,l}(h) = \boldsymbol{J}_h \tilde{\boldsymbol{i}}_{0,l} \chi_p \left(\Delta\tau_{0,l}(h), f_{0,l} \right) , \tag{1.3}$$

with $\boldsymbol{J}_h$ the $N \times N$ matrix whose entries are

$$\boldsymbol{J}_h(i,j) = \begin{cases} 1 & i - j = h \\ \\ \\ 0 & \text{elsewhere} \end{cases}$$

with $-N+1 \leq h \leq N-1$, the set $\mathcal{A}_{0,l}$ can be compactly written as

$$\mathcal{A}_{0,l} = \bigcup_{-N+1 \leq h \leq N-1} \left\{ \boldsymbol{i}_{0,l}(h) \right\} \quad \mathbf{0} \, .$$

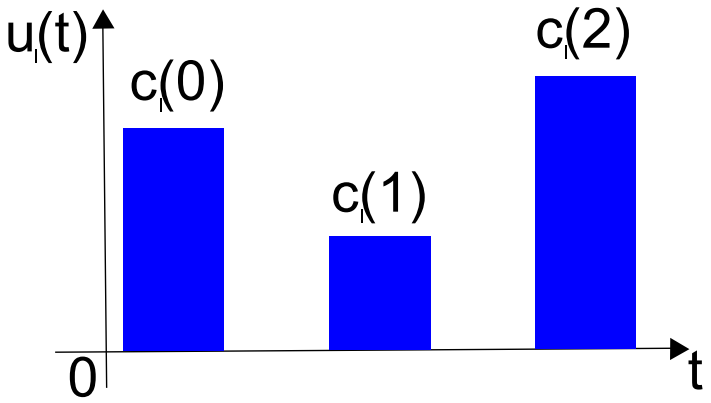

Figure 1.1: Coded pulse train $u_l(t)$ for $N = 3$, duty cycle$= T_p/T_r = 1/2$, and $p(t)$ with rectangular shape.

1.3 Problem Formulation

In this section, we formulate the problem of designing the code used by the sensor of interest. The design principle is the maximization of the SNR for the sensor of interest (the 0-th), mitigating the mutual interference induced by the sensor of interest on other sensors in the network, and forcing an energy constraint. To this end, it is necessary to introduce explicitly the definition of SNR and the constraints which are required to control the mutual interference and the transmitted energy.

1.3.1 Signal-to-Noise Ratio

Assuming that the disturbance $\boldsymbol{w}_m$, for $m = 0, \ldots, L-1$, is a zero-mean complex circular Gaussian vector with known positive definite covariance matrix

$$E[\boldsymbol{w}_m \boldsymbol{w}_m^\dagger] = \boldsymbol{M}\,,$$

it is known that the Generalized Likelihood Ratio Test (GLRT) for the detection of a target component $\boldsymbol{c}_0 \odot \boldsymbol{p}_0$ with unknown complex amplitude in the presence of $\boldsymbol{w}_0$ only (i.e. in the absence of mutual interference among the sensors), is given by

$$|\boldsymbol{v}_0^\dagger \boldsymbol{g}_0|^2 = |\boldsymbol{v}_0^\dagger \boldsymbol{M}^{-1}(\boldsymbol{c}_0 \odot \boldsymbol{p}_0)|^2 \underset{H_0}{\overset{H_1}{\gtrless}} G\,,$$

where $\boldsymbol{g}_0 = \boldsymbol{M}^{-1}(\boldsymbol{c}_0 \odot \boldsymbol{p}_0)$ is the 0-th pre-processed steering vector, and G is the detection threshold, set according to a desired value of the false alarm Probability (P_{fa}). This decision rule also coincides with the optimum test (according to the Neyman-Pearson criterion) if the phase of α_0 is uniformly distributed in $[0, 2\pi[$ [19]. From a geometric point of view, it is tantamount to projecting the received vector on the pre-processed steering direction and then comparing the energy of the projection with a threshold. An analytical expression of the

detection Probability (P_d), for a given value of P_{fa}, is available. Precisely, for nonfluctuating targets,

$$P_d = Q\left(\sqrt{2|\alpha_0\chi_p(0,f_0)|^2(\boldsymbol{c}_0\odot\boldsymbol{p}_0)^\dagger\boldsymbol{M}^{-1}(\boldsymbol{c}_0\odot\boldsymbol{p}_0)},\Psi\right),$$

where $Q(\cdot,\cdot)$ denotes the Marcum Q function of order 1, and $\Psi = \sqrt{-2\ln P_{fa}}$. This last expression shows that, given P_{fa}, P_d depends on the radar code, the disturbance covariance matrix, and the temporal steering vector only through the SNR, defined as

$$\text{SNR} = |\alpha_0\chi_p(0,f_0)|^2(\boldsymbol{c}_0\odot\boldsymbol{p}_0)^\dagger\boldsymbol{M}^{-1}(\boldsymbol{c}_0\odot\boldsymbol{p}_0)\,.$$

Moreover, P_d is an increasing function of SNR and, as a consequence, the maximization of P_d can be obtained maximizing

$$(\boldsymbol{c}_0\odot\boldsymbol{p}_0)^\dagger\boldsymbol{M}^{-1}(\boldsymbol{c}_0\odot\boldsymbol{p}_0) = \boldsymbol{c}_0^\dagger\boldsymbol{R}_{f_0}\boldsymbol{c}_0 \tag{1.4}$$

over the radar code $\boldsymbol{c}_0$, with

$$\boldsymbol{R}_{f_0} = \boldsymbol{M}^{-1} \odot (\boldsymbol{p}_0 \boldsymbol{p}_0^{\dagger})^* \,. \tag{1.5}$$

Evidently, (1.5) requires the specification of f_0; as a consequence, the solution depends on this pre-assigned value. It is thus necessary to provide some guidelines on the importance and the applicability of the proposed framework. To this end, we highlight that:

- the matched performance (namely when the actual Doppler is exactly f_0) which can be obtained through the optimal solution of (1.4), represents an upper bound to that achievable by any practical system;
- a single coded waveform designed for the challenging condition of slowly moving targets (i.e. $f_0 \simeq 0$) can be devised;
- a single coded waveform optimized over an average scenario may be designed. Otherwise stated, this code might be chosen so as to maximize (1.4) with $\boldsymbol{R}_{f_0}$ replaced by $\boldsymbol{R}_a = \boldsymbol{M}^{-1} \odot \left(E\left[\boldsymbol{p}_0 \boldsymbol{p}_0^{\dagger} \right] \right)^*$, where the expectation operator is over the normalized Doppler frequency. If this last quantity is modeled as a uniformly distributed random variable, i.e. $f_0 T_r \sim \mathcal{U}(-\epsilon, \epsilon)$,

with $0 < \epsilon < 1/2$, the expectation can be readily evaluated, leading to

$$\boldsymbol{R}_a = \boldsymbol{M}^{-1} \odot \boldsymbol{\Sigma}_\epsilon \,, \tag{1.6}$$

where $\boldsymbol{\Sigma}_\epsilon(m,n) = \text{sinc}\,[2\epsilon(m-n)]$, and $\text{sinc}(x) = \frac{\sin(\pi x)}{\pi x}$.

Summarizing, we can express the objective function as

$$\boldsymbol{c}_0^\dagger \boldsymbol{R} \boldsymbol{c}_0 \,, \tag{1.7}$$

with $\boldsymbol{R}$ equal to $\boldsymbol{R}_a$ or $\boldsymbol{R}_{f_0}$ according to the chosen design context. We highlight that in both cases $\boldsymbol{R} \succ \boldsymbol{0}$, since $\boldsymbol{R}$ is the Hadamard product of a positive definite matrix ($\boldsymbol{M}^{-1}$) and a positive semidefinite matrix with positive diagonal entries ($\boldsymbol{p}_0\boldsymbol{p}_0^\dagger$ or $\boldsymbol{\Sigma}_\epsilon$) [20].

1.3.2 Mutual Interference Constraints

To mitigate interference induced by the 0-th sensor, we force our code to produce a small energy level when projected on the l-th pre-processed steering vector, namely on the receiving direction of the l-th sensor. Otherwise stated,

we impose the design constraints

$$E\left[|\boldsymbol{i}_{l,0}^{\dagger}\boldsymbol{g}_l|^2\right] \leq \hat{\delta}_l, \quad l = 1, \ldots, L-1\,, \tag{1.8}$$

where $\hat{\delta}_l > 0$ are parameters ruling the acceptable levels of interference: the smaller $\hat{\delta}_l$, the smaller the interference of the radar of interest on the l-th sensor.

As indicated in (1.3), $\boldsymbol{i}_{l,0}$ depends on the particular shift h, i.e. $\boldsymbol{i}_{l,0} = \boldsymbol{i}_{l,0}(h)$; hence, in order to circumvent this drawback, we can resort to an average approach, imposing the constraint on the average of all the admissible nonzero $\boldsymbol{i}_{l,0}(h)$ (assumed equiprobable), i.e. (1.8) becomes

$$E\left[\sum_{h=-N+1}^{N-1} |\boldsymbol{i}_{l,0}^{\dagger}(h)\boldsymbol{g}_l|^2\right] \leq \hat{\delta}_l(2N-1), \quad l = 1, \ldots, L-1\,. \tag{1.9}$$

As to the expectation operator, it acts over the parameters $\tau_{l,0}$, τ_l, $f_{l,0}$ and f_l, for $l = 1, \ldots, L-1$, which are practically unknown, and can be reasonably modeled as random variables. Now,

$$E\left[\sum_{h=-N+1}^{N-1} |\boldsymbol{i}_{l,0}^{\dagger}(h)\boldsymbol{g}_l|^2\right] = E\left[\sum_{h=-N+1}^{N-1} |\boldsymbol{i}_{l,0}^{\dagger}(h)\boldsymbol{M}^{-1}(\boldsymbol{c}_l \odot \boldsymbol{p}_l)|^2\right] \leq \hat{\delta}_l(2N-1)\,, \tag{1.10}$$

or equivalently

$$E\left[\sum_{h=-N+1}^{N-1} \boldsymbol{i}_{l,0}^{\dagger}(h)\boldsymbol{M}^{-1}(\boldsymbol{c}_l \odot \boldsymbol{p}_l)(\boldsymbol{c}_l \odot \boldsymbol{p}_l)^{\dagger}\boldsymbol{M}^{-1}\boldsymbol{i}_{l,0}(h)\right] \leq \delta_l,$$

for $l = 1, \ldots, L-1$, with $\delta_l = \hat{\delta}_l(2N-1)$. Hence, denoting by

$$\boldsymbol{S}_l = \boldsymbol{M}^{-1}\mathrm{diag}(\boldsymbol{c}_l)\boldsymbol{p}_l\boldsymbol{p}_l^{\dagger}\mathrm{diag}(\boldsymbol{c}_l^{*})\boldsymbol{M}^{-1}\,,$$

the constraints can be recast as

$$E\left[\sum_{h=-N+1}^{N-1} \boldsymbol{i}_{l,0}^{\dagger}(h)\boldsymbol{S}_l\boldsymbol{i}_{l,0}(h)\right] \leq \delta_l, \qquad l = 1, \ldots, L-1\,. \tag{1.11}$$

According to (1.3),

$$\boldsymbol{i}_{l,0}(h) = \boldsymbol{J}_h(\boldsymbol{c}_0 \odot \boldsymbol{p}_{l,0})\chi_p(\Delta\tau_{l,0}(h), f_{l,0}) = \left(\boldsymbol{J}_h\boldsymbol{c}_0 \odot \boldsymbol{J}_h\boldsymbol{p}_{l,0}\right)\chi_p(\Delta\tau_{l,0}(h), f_{l,0})\,,$$

so (1.11) becomes

$$E\left[\sum_{h=-N+1}^{N-1} \boldsymbol{c}_0^{\dagger}\boldsymbol{J}_h^{\dagger}\boldsymbol{S}_{l,h}\boldsymbol{J}_h\boldsymbol{c}_0\right] \leq \delta_l, \qquad l = 1, \ldots, L-1\,,$$

with $\boldsymbol{S}_{l,h} = |\chi_p(\Delta\tau_{l,0}(h), f_{l,0})|^2 \boldsymbol{S}_l \odot \left(\boldsymbol{J}_h \boldsymbol{p}_{l,0} \boldsymbol{p}_{l,0}^\dagger \boldsymbol{J}_h^\dagger\right)^*$. Moreover, denoting by

$$\boldsymbol{R}_l = \sum_{h=-N+1}^{N-1} \boldsymbol{J}_h^\dagger E\left[\boldsymbol{S}_{l,h}\right] \boldsymbol{J}_h, \qquad l = 1, \ldots, L-1\,,$$

the mutual interference constraint (1.9) can be expressed as

$$c_0^\dagger \boldsymbol{R}_l \boldsymbol{c}_0 \leq \delta_l\,, \qquad l = 1, \ldots, L-1\,. \tag{1.12}$$

Notice that the constraints in (1.12) can be evaluated, assuming a suitable model for the random variables $f_{l,0}$, f_l, $\tau_{l,0}$ and τ_l, with $l = 1, \ldots, L-1$. Assuming f_l, $f_{l,0}$, τ_l and $\tau_{l,0}$ statistically independent, we can factorize $E\left[\boldsymbol{S}_{l,h}\right]$ as

$$E\left[\boldsymbol{S}_{l,h}\right] = \boldsymbol{C}_l \odot \boldsymbol{H}_h\,,$$

where the term $\boldsymbol{C}_l$ depends on the code $\boldsymbol{c}_l$, while the term $\boldsymbol{H}_h$ depends on the shift h. In particular,

$$\boldsymbol{C}_l = E\left[\boldsymbol{S}_l\right] = \boldsymbol{M}^{-1} \mathrm{diag}(\boldsymbol{c}_l) E\left[\boldsymbol{p}_l \boldsymbol{p}_l^\dagger\right] \mathrm{diag}(\boldsymbol{c}_l^*) \boldsymbol{M}^{-1}\,,$$

and

$$\boldsymbol{H}_h = E\left[|\chi_p(\Delta\tau_{l,0}(h), f_{l,0})|^2 \left(\boldsymbol{J}_h \boldsymbol{p}_{l,0} \boldsymbol{p}_{l,0}^\dagger \boldsymbol{J}_h^\dagger\right)^*\right] .$$

Moreover, assuming the normalized Doppler frequencies $f_l T_r$ uniformly distributed in the interval $[-\Delta, \Delta]$, i.e. $f_l T_r \sim \mathcal{U}(-\Delta, \Delta)$, with $0 < \Delta < 1/2$, we get

$$E\left[\boldsymbol{p}_l \boldsymbol{p}_l^\dagger\right] = \boldsymbol{\Sigma}_\Delta .$$

1.3.3 Energy Constraint

It remains to force a constraint on the transmitted energy by the radar of interest, namely we suppose that the normalized code energy is less than or equal to N, i.e.

$$\|\boldsymbol{c}_0\|^2 \leq N . \tag{1.13}$$

1.4 Code Design

1.4.1 Equivalent Problem Formulations

Now, according to (1.7), (1.12), and (1.13), we can formulate the code design in terms of the following Quadratic optimization Problem (QP)

$$\text{QP} \begin{cases} \underset{\boldsymbol{c}_0}{\text{maximize}} & \boldsymbol{c}_0{}^{\dagger}\boldsymbol{R}\boldsymbol{c}_0 \\ \text{subject to} & \boldsymbol{c}_0{}^{\dagger}\boldsymbol{R}_l\boldsymbol{c}_0 \leq \delta_l, \qquad l = 1, \ldots, L-1 \\ & \boldsymbol{c}_0{}^{\dagger}\boldsymbol{c}_0 \leq N\,. \end{cases} \tag{1.14}$$

Letting $\boldsymbol{R}_{\delta_l} = \delta_l^{-1}\boldsymbol{R}_l$, for $l = 1, \ldots, L-1$, problem (1.14) can be recast as

$$\text{QP} \begin{cases} \underset{\boldsymbol{c}_0}{\text{maximize}} & \boldsymbol{c}_0{}^{\dagger}\boldsymbol{R}\boldsymbol{c}_0 \\ \text{subject to} & \boldsymbol{c}_0{}^{\dagger}\boldsymbol{R}_{\delta_l}\boldsymbol{c}_0 \leq 1, \qquad l = 0, \ldots, L-1 \end{cases} \tag{1.15}$$

with $\boldsymbol{R}_{\delta_0} = N^{-1}\boldsymbol{I}$. Now, we have a homogeneous quadratic optimization problem defined in complex field $\mathbb{C}^N$. Moreover, $\boldsymbol{R}_{\delta_l}$ are positive semidefinite matri-

ces. The equivalent matrix formulation of QP is

$$\text{QP}\begin{cases} \underset{\boldsymbol{C}_0}{\text{maximize}} & \text{Tr}\left(\boldsymbol{C}_0\boldsymbol{R}\right) \\ \text{subject to} & \text{Tr}\left(\boldsymbol{C}_0\boldsymbol{R}_{\delta_l}\right) \leq 1, \qquad l = 0, \ldots, L-1 \\ & \boldsymbol{C}_0 = \boldsymbol{c}_0\boldsymbol{c}_0^{\dagger} \end{cases} \tag{1.16}$$

Unfortunately, in general this problem is NP-hard (there are some exception when $L \leq 3$) [16] [21]. One approach to approximating the solution to the NP-hard quadratic programs is the relaxation and randomization technique [15]: first relax the feasible solution set of the problem, obtaining a Convex Problem (CP) that can be solved in polynomial time through the *interior point methods*[1]; then use the optimal solution of the relaxed problem to produce a random feasible solution for the original problem.

In the following, we present the WDNE procedure to obtain a *good* solution of the original problem (1.14), and report the approximation bound [16],[21].

[1]The interior point methods are iterative algorithms which terminate once a pre-specified accuracy ζ is reached. The number of iterations necessary to achieve convergence usually ranges between 10 and 100 [22].

1.4.2 Relaxation and Randomization

Problem (1.16) can be relaxed into the following Semidefinite Programming (SDP) problem CP

$$\text{CP}\begin{cases} \underset{\boldsymbol{C}_0}{\text{maximize}} & \text{Tr}\left(\boldsymbol{C}_0\boldsymbol{R}\right) \\ \text{subject to} & \text{Tr}\left(\boldsymbol{C}_0\boldsymbol{R}_{\delta_l}\right) \leq 1, \qquad l = 0, \ldots, L-1 \\ & \boldsymbol{C}_0 \succeq \mathbf{0} \end{cases} \tag{1.17}$$

obtained removing the rank-one constraint from (1.16) An SDP is a convex problem which can be solved using interior point methods [22], so CP can be easily solved in polynomial time, obtaining the optimal solution $\overline{C}$ (the fact that the optimal value of CP is attainable is proved in Appendix).

Now if $\text{rank}(\overline{C}) = 1$ then $\overline{C} = \overline{c}\overline{c}^{\dagger}$ and, as a consequence, $\overline{c}$ is optimal for (1.15). Otherwise, we can obtain a *good* feasible solution of (1.15) through the following randomization procedure [16, 21]:

1. Simulate $\boldsymbol{\xi}$ as a complex normal random vector with zero-mean and covariance matrix $\overline{C}$, i.e. $\boldsymbol{\xi} \sim \mathcal{CN}\left(\mathbf{0}, \overline{C}\right)$.

2. Let

$$\boldsymbol{c}_\xi = \frac{\boldsymbol{\xi}}{\sqrt{\max\limits_{0\le l\le L-1} \boldsymbol{\xi}^\dagger \boldsymbol{R}_{\delta_l} \boldsymbol{\xi}}},$$

The last step can be possibly repeated P times and one can take the instance of $\boldsymbol{c}_\xi$ leading to the highest objective function. Usually, with a modest number of randomizations[2] , it is possible to achieve an accurate approximation of the optimal solution [23] [24].

1.4.3 Approximation Bound

A "measure of goodness" of the randomization algorithm is provided by the approximation bound which characterizes the quality of the produced solutions. In the literature, a randomized approximation method for a maximization problem has a bound (or performance guarantee, or worst case ratio) $R \in (0, 1]$, if for all instances of the problem, it always delivers a feasible solution whose expected value is at least R times the maximum value of the relaxed problem [15].

[2]In Chapter 1.5, we have set $P = 10$.

With reference to the WDNE algorithm, we have

$$R \times v(\text{CP}) \leq v_{_{WDNE}}(\text{QP}) \leq v(\text{CP}) \,,$$

where R is the approximation parameter, $v(\text{CP})$ is the optimal value of CP, and $v_{_{WDNE}}(\text{QP})$ is the objective value of QP achieved by the WDNE algorithm. It has been proven in [21][p. 173, Theorem 10.1.2] that the approximation parameter for this technique is

$$R = \frac{1}{\ln\left(34\mu\right)} \,,$$

where $\mu = \sum_{l=0}^{L-1} \min\left\{\text{rank}(\boldsymbol{R}_{\delta_l}), \sqrt{L}\right\}$.

However, we remark that the approximation bound is a worst-case result [15], and, in practice, the actual performance $v_{_{WDNE}}(\text{QP})$ might be substantially better than the lower bound $R \times v(\text{CP})$ (see Chapter 1.5.1): such behavior is quite common for randomized techniques [23] [24].

Summarizing, the WDNE procedure to generate a *good* solution $\boldsymbol{c}_{_{WDNE}}$ of problem (1.14), can be formulated as reported in **Algorithm 1**.

Algorithm 1 Waveform Design in Noncooperative Environment (WDNE)

Input: $\boldsymbol{R}$, $\boldsymbol{R}_{\delta_l}$ for $l = 0, \ldots, L-1$;

Output: $\boldsymbol{c}_{WDNE}$;

1: solve CP finding an optimal solution $\overline{\boldsymbol{C}}$;
2: evaluate $r = \text{rank}(\overline{\boldsymbol{C}})$;
3: **if** $r = 1$ **then**
4: decompose $\overline{\boldsymbol{C}} = \overline{\boldsymbol{c}}\overline{\boldsymbol{c}}^{\dagger}$;
5: set $\boldsymbol{c}_{WDNE} = \overline{\boldsymbol{c}}$;
6: **else**
7: generate $\boldsymbol{\xi} \sim \mathcal{CN}\left(\boldsymbol{0}, \overline{\boldsymbol{C}}\right)$;
8: set

$$\boldsymbol{c}_{WDNE} = \frac{\boldsymbol{\xi}}{\sqrt{\max\limits_{0 \leq l \leq L-1} \boldsymbol{\xi}^{\dagger} \boldsymbol{R}_{\delta_l} \boldsymbol{\xi}}} ;$$

9: **end**

1.5 Performance Analysis

The present section discusses the performance of the proposed waveform design scheme. The analysis is conducted in terms of normalized average[3] SNR, SNR_{norm} (sub-section 1.5.1) and average normalized interference level induced by the m-th sensor on the l-th one I_m^l (sub-section 1.5.2), respectively defined as

$$\text{SNR}_{norm} = \frac{E_{\boldsymbol{\xi}}\left[\boldsymbol{c}_0^{\dagger} \boldsymbol{R} \boldsymbol{c}_0\right]}{N \lambda_{max}\left(\boldsymbol{R}\right)} ,$$

[3]The average is performed over 100 trials, so as to make the result independent of the specific randomization $\boldsymbol{\xi}$.

and

$$I_m^l = \frac{E_{\boldsymbol{\xi}}\left[\boldsymbol{c}_m^\dagger \boldsymbol{R}_l \boldsymbol{c}_m\right]}{N\lambda_{max}\left(\boldsymbol{R}_l\right)}\,.$$

Notice that $N\lambda_{max}\left(\boldsymbol{R}\right)$ can be viewed as the optimal value of the Unconstrained Problem (UP),

$$\text{UP}\begin{cases} \underset{\boldsymbol{c}_0}{\text{maximize}} & \boldsymbol{c}_0^\dagger \boldsymbol{R} \boldsymbol{c}_0 \\ \text{subject to} & \boldsymbol{c}_0{}^\dagger \boldsymbol{c}_0 \leq N \end{cases}$$

where the constraints on the interference have been removed. Obviously, the optimal value $v(\text{UP})$ is greater than the optimal value of the problem QP, i.e. $v(\text{UP}) \geq v(\text{QP})$, and, as a consequence, $\text{SNR}_{norm} \leq 1$. Sub-section 1.5.3 illustrates the computational complexity of the proposed algorithm.

Finally, we assume that the disturbance covariance matrix is exponentially shaped with one-lag correlation coefficient $\rho = 0.95$, i.e.

$$\boldsymbol{M}(m,n) = \rho^{|m-n|}\,, \qquad (m,n) \in \{0,\ldots,N-1\}^2.$$

Moreover, we choose the pulse $p(t)$ with rectangular shape, and duty cycle $T_p/T_r = 1/3$. Finally, we model the normalized delay $\Delta\tau_{m,l}(h)/T_r$ and the nor-

malized Doppler shift $f_{m,l}T_r$ as independent random variables, uniformly distributed in the interval $[-1, 1]$ and $[-0.3, 0.3]$ respectively, i.e. $\Delta\tau_{m,l}(h)/T_r \sim \mathcal{U}(-1, 1)$ and $f_{m,l}T_r \sim \mathcal{U}(-0.3, 0.3)$. The convex optimization MATLAB© toolbox SeDuMi [25] is exploited to solve the SDP relaxation.

1.5.1 Maximization of the SNR

In this sub-section, we analyze the effect of three different parameters on the SNR_{norm} : normalized Doppler shift on the reference sensor, length of the code, number of interfering sensors. We consider the case of a WDNE code $\boldsymbol{c}_0$ of length N, and temporal steering vector $\boldsymbol{p}_0$ with a known normalized Doppler shift $f_d = f_0 T_r$, i.e.

$$\boldsymbol{p}_0 = \left[1, e^{j2\pi f_d}, \ldots, e^{j2\pi f_d(N-1)}\right]^T .$$

All the acceptable interfering levels δ_l with $l = 1, \ldots, L-1$, are set equal to δ, defined as

$$\delta = \delta_{norm}\left(\Lambda_{max} - \Lambda_{min}\right) + \Lambda_{min} ,$$

where

$$\Lambda_{max} = \min_{l=1,\ldots,L-1} \{N\lambda_{max}(\boldsymbol{R}_l)\} ,$$

$$\Lambda_{min} = \max_{l=1,\ldots,L-1} \{N\lambda_{min}(\boldsymbol{R}_l)\} ,$$

and $\delta_{norm} \in (0,1)$.

Finally, the operating environment has $L-1=4$ interfering sensors. All the interfering radars use a phase code with the same length and the same maximum energy[4] as our WDNE code. In particular, the first radar uses a Barker code, the second a generalized Barker code, the third a Zadoff code, and the fourth a P4 code [18].

In **Figure 1.2**, we plot SNR_{norm} versus δ_{norm} for $N=13$, $L=5$, and four different values of f_d. For comparison purposes, we also plot SNR_{norm} of a Barker code of length 13. As expected, the higher δ_{norm} the higher SNR_{norm}: this can be easily explained observing that increasing δ_{norm} is tantamount to enlarging the feasibility region, so higher and higher optimal values can be found. It is also noticeable that WDNE codes outperforms the classical Barker code for $\delta_{norm} \geq 0.3$. Finally, at any Doppler frequency the SNR_{norm} of the WDNE algorithm for $\delta_{norm} \to 1$ almost reaches the maximum (i.e. $\text{SNR}_{norm} = 0$

[4]We recall that the maximum code energy of our WDNE code is equal to N, as required by (1.13).

dB).

In **Figure 1.3**, we illustrate the effect of the length N on the code. In particular, we consider the normalized Doppler frequency $f_d = 0.15$, $L = 5$ sensors in the network, while the length N of the code $\boldsymbol{c}_0$ can be 4, 5, 7, or 13. For comparison purpose, we plot the SNR_{norm} of a Barker code of length 13. In particular, we plot SNR_{norm} versus δ_{norm} for the considered values of N. Evidently, increasing N leads to higher values of SNR_{norm}. This can be explained observing that the parameter N rules the energy constraint: the higher N, the higher the maximum energy. Moreover, increasing N enlarges the number of degrees of freedom. Finally, we can observe that the WDNE code of length 13 outperforms the Barker code of the same length for $\delta_{norm} \geq 0.1$.

In **Figure 1.4**, we analyze the effect of the size L of the network. We plot SNR_{norm} versus δ_{norm} with normalized Doppler frequency $f_d = 0.15$, length $N = 7$, and different values of L. In this figure, we also plot SNR_{norm} of a Barker code of length 7. The curves show that increasing the dimension of the network, leads to degraded performance. In fact, increasing L reduces feasibility region of the optimization problem, so lower and lower optimal values may be achieved. It can also be observed that for high values of δ_{norm}, the algorithm

reaches the maximum value of SNR_{norm} (i.e. $v(\text{UP}) = v_{_{WDNE}}(\text{QP})$), and even for small values of δ_{norm} (i.e. $\delta_{norm} = 0.1$) the WDNE code exhibits a gain of at least 1 dB over the classic Barker code. Summarizing, there is a trade-off between the SNR_{norm} of the sensor of interest and the interference induced on the remaining sensors: δ_{norm} is the parameter that rules this relationship.

Now, we study the robustness of the proposed algorithm, considering a mismatch between the *nominal* steering vector $\boldsymbol{p}_0$ with $f_d = 0.15$ (assumed to design the code) and the *actual* steering vector

$$\boldsymbol{p}_F = \left[1, e^{j2\pi F}, \ldots, e^{j2\pi F(N-1)}\right]^T ,$$

with F representing the actual normalized Doppler frequency. We also analyze the WDNE version of the code with $\boldsymbol{R} = \boldsymbol{R}_a$, as indicated in (2.17), assuming $\epsilon = 0.2$. To evaluate the performance of the algorithm, we consider the actual average normalized SNR, defined as

$$\text{SNR}_F = \frac{E_{\boldsymbol{\xi}}\left[\boldsymbol{c}_0^\dagger \boldsymbol{R}_F \boldsymbol{c}_0\right]}{N\lambda_{max}\left(\boldsymbol{R}_F\right)} ,$$

where $\boldsymbol{R}_F = \boldsymbol{M}^{-1} \odot \left(\boldsymbol{p}_F \boldsymbol{p}_F^\dagger\right)^*$.

In **Figure 1.5**, we plot SNR_F versus F for $\delta_{norm} = 0.9$, $N = 13$ and $L = 5$. For comparison purpose, we plot the performance of the Barker code of length 13. The classic version of the proposed code (i.e. with $\boldsymbol{R} = \boldsymbol{R}_{f_0}$) outperforms the Barker code when the effective normalized Doppler frequency F is close to the nominal value f_d. On the contrary, the average version of WDNE (i.e. with $\boldsymbol{R} = \boldsymbol{R}_a$) achieves an higher value of SNR_F than the Barker code in the interval $[-0.2, +0.2]$. As expected, this robustness has a price: a loss of 1 dB in the case of perfect knowledge of the steering vector (i.e. $F = 0.15$).

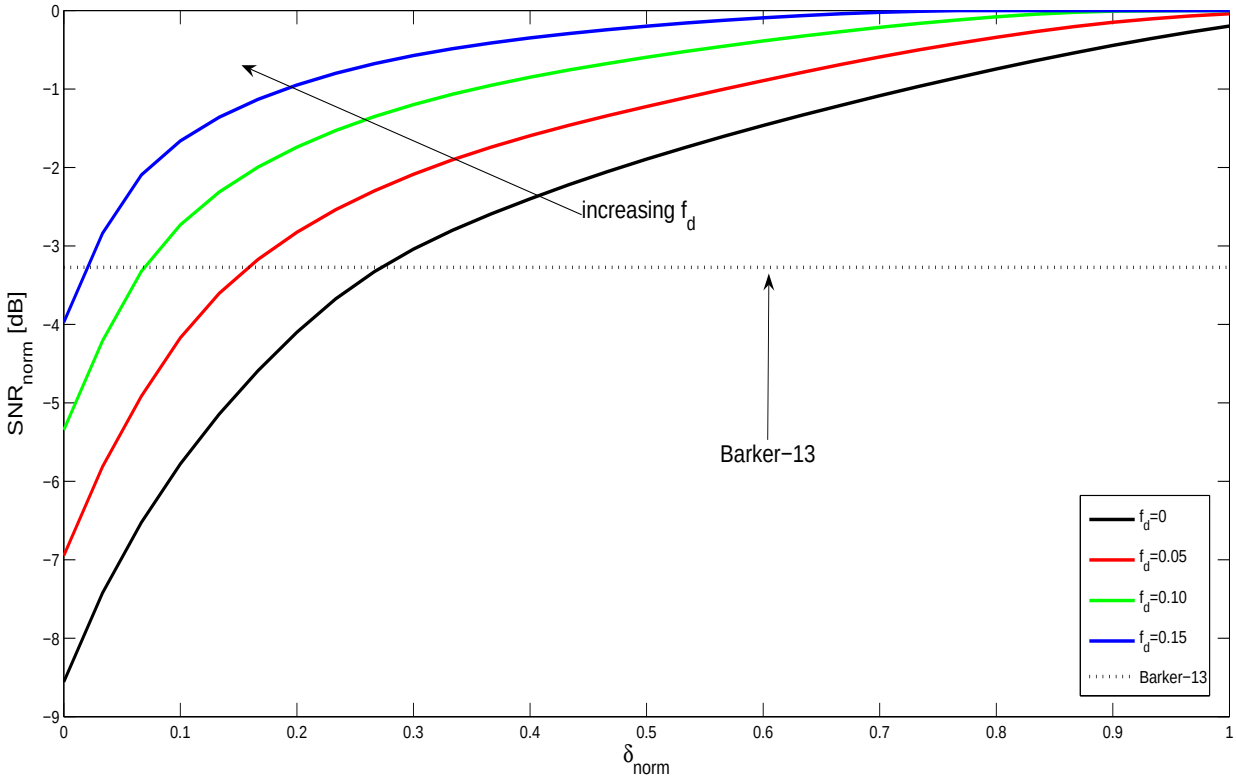

Figure 1.2: SNR_{norm} versus δ_{norm} for $N = 13$, $L = 5$, and some normalized Doppler shifts f_d, i.e. $f_d \in \{0; 0.05; 0.10; 0.15\}$ (solid curves). Barker code of length 13 (dotted line).

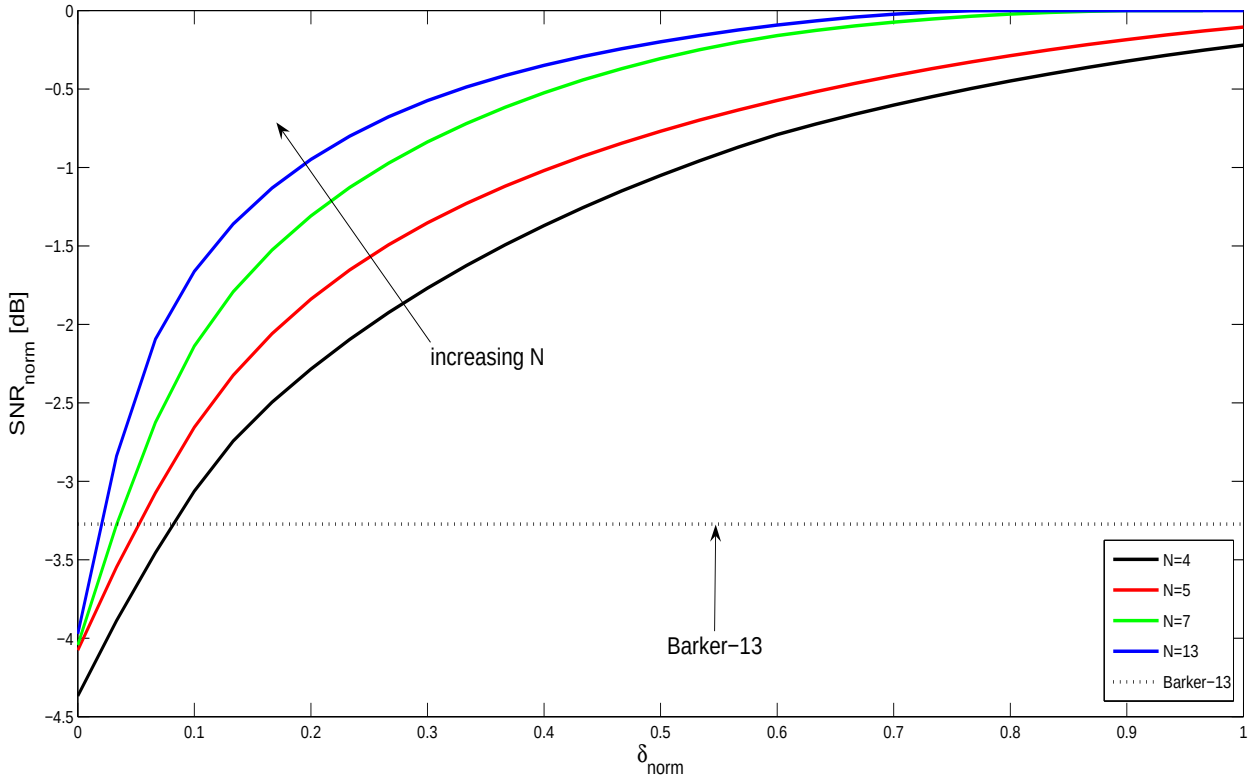

Figure 1.3: SNR_{norm} versus δ_{norm} for $L = 5$, normalized Doppler shift $f_d = 0.15$, and some values of N, i.e. $N \in \{4; 5; 7; 13\}$ (solid curves). Barker code of length 13 (dotted line).

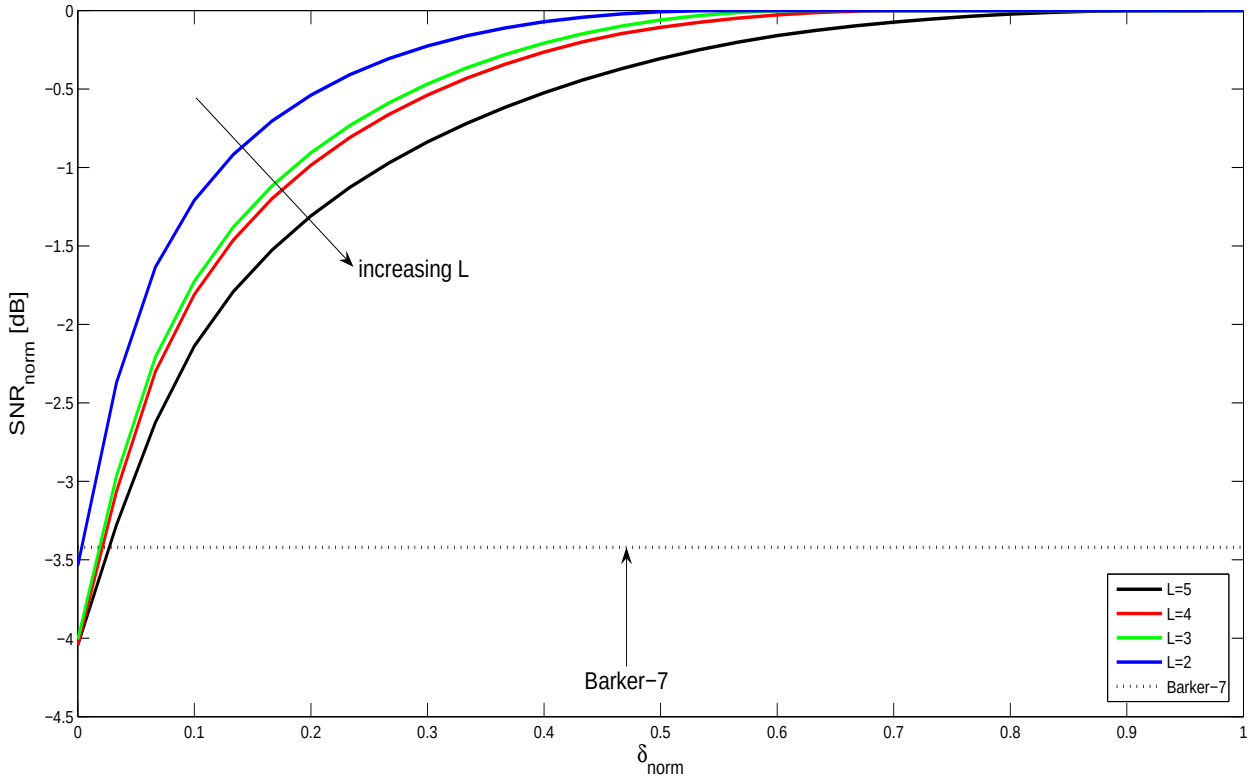

Figure 1.4: SNR_{norm} versus δ_{norm} for $N = 7$, normalized Doppler shift $f_d = 0.15$, and some values of L, i.e. $L \in \{2; 3; 4; 5\}$ (solid curves). Barker code of length 7 (dotted line).

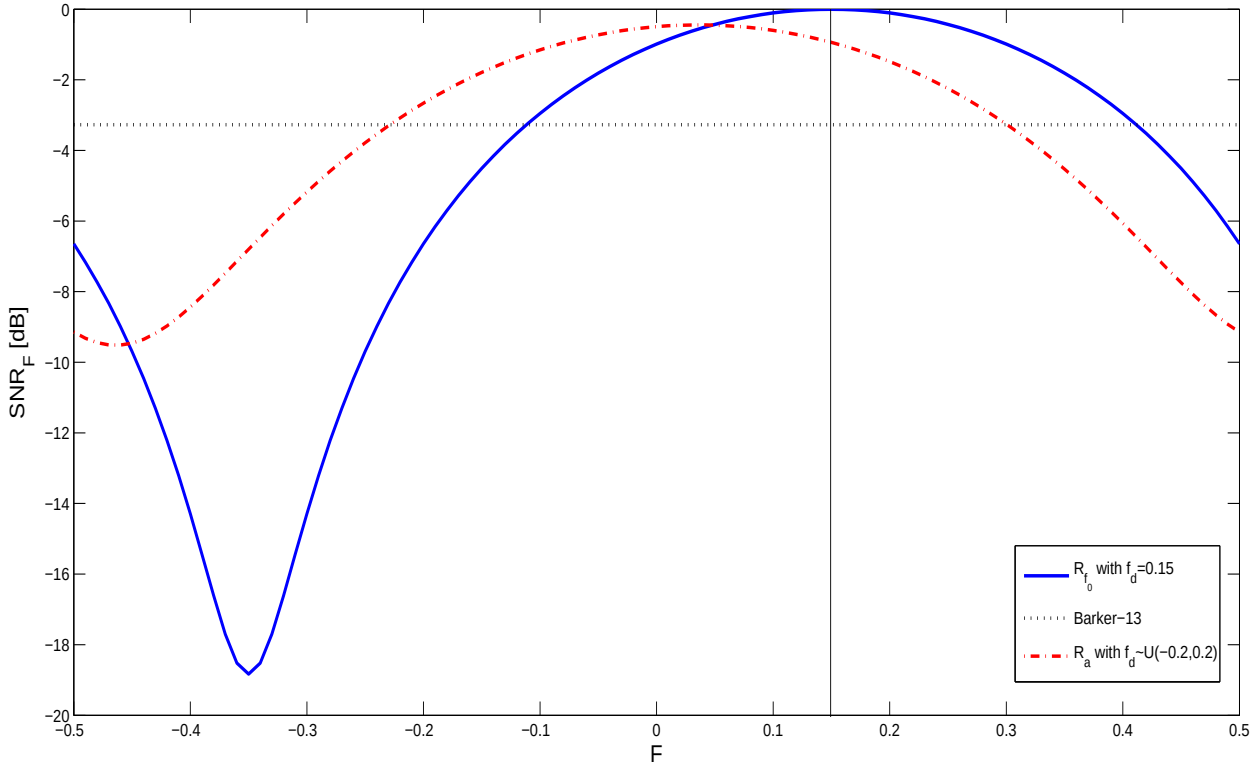

Figure 1.5: SNR_F versus F for $\delta_{norm} = 0.9$, $N = 13$, $L = 5$. Barker code of length 13 (dotted curve). Robust (i.e. $\boldsymbol{R} = \boldsymbol{R}_a$ with $f_d \sim \mathcal{U}(-0.2, 0.2)$) WDNE code (dot-dashed curve). Matched (i.e. $\boldsymbol{R} = \boldsymbol{R}_{f_0}$ with $f_d = 0.15$) WDNE code (solid curve).

1.5.2 Control of the induced interference

In this sub-section, we analyze the behavior of the induced interference I_m^l for different network scenarios. In the first case, we study an operating environment with three pre-existing radar sensors, which use a Barker code $(\boldsymbol{c}_1)$, a generalized Barker code $(\boldsymbol{c}_2)$, and a Zadoff code $(\boldsymbol{c}_3)$ respectively.

In **Figure 1.6a**, we plot the interference induced on the Barker code $\boldsymbol{c}_1$ (i.e. I_m^1, with $m \in \{0, 2, 3\}$) versus δ_{norm}, for normalized Doppler frequency $f_d = 0.15$, and length $N = 4$. In particular, we plot the interference induced by our code (I_0^1), and, for comparison purpose, we also plot the interference induced by the generalized Barker code and by the Zadoff code (I_2^1 and I_3^1 respectively). We notice that, as δ_{norm} increases, the interference level increases. It is noticeable that the interference induced by the WDNE code is lower than I_2^1 and I_3^1 for a large interval (i.e. for $\delta_{norm} \leq 0.8$). In Figure 1.6b-1.6c, we consider the interferences induced on the generalized Barker code $\boldsymbol{c}_2$ and on the Zadoff code $\boldsymbol{c}_3$ respectively. Analogous considerations can be done in these two cases.

In the second scenario, described in Figure 1.6d, we consider an operating environment with only one pre-existing sensor. This allows us to analyze the effect of a particular code on the algorithm. We selected four possible inter-

fering codes, all of them with energy $N = 4$: three phase codes (Barker, generalized Barker, and Zadoff codes), and an amplitude-phase modulated code (Huffman code). The Huffman code [26] has been obtained using the procedure described in [18]. In Figure 1.6d, we plot I_0^1 versus δ_{norm} for normalized Doppler frequency $f_d = 0.15$, network size $L = 2$, and different interfering codes $\boldsymbol{c}_1$. We observe that our code, for high value of δ_{norm}, induces almost the same level of interference over all the proposed codes: there is less than 1 dB among all the considered I_0^1, for $\delta_{norm} \geq 0.8$.

Finally, in the third scenario, we consider a network with $L - 1 = 3$ pre-existing radar sensors, all of them with a code of length and energy $N = 4$. Moreover, the first code ($\boldsymbol{c}_1$) is a Barker code, while the other two codes ($\boldsymbol{c}_2$ and $\boldsymbol{c}_3$) belong to a certain class: phase codes, Gold codes, orthogonal PN codes, or WDNE codes. When the sensors use phase codes, we set $\boldsymbol{c}_2$ and $\boldsymbol{c}_3$ as generalized Barker and Zadoff codes, respectively. In the case of Gold codes [27], they are simulated according to the procedure in [18], while the PN sequences [28] are simulated so that they are orthogonal. Finally, in the last case, we have an initial Barker code $\boldsymbol{c}_1$, a WDNE code $\boldsymbol{c}_2$ devised assuming $L = 2$ and $\delta_{norm} = \delta^0$, and a WDNE code $\boldsymbol{c}_3$, with $L = 3$ and $\delta_{norm} = \delta^0$ (see **Figure**

1.7 for a pictorial description of the different scenarios).

In **Figure 1.8**, we plot the normalized overall induced interference on the radar sensor which uses the Barker code $\boldsymbol{c}_1$, i.e. I^1_{TOT}, defined as

$$I^1_{TOT} = \frac{I^1_0 + I^1_2 + I^1_3}{L-1},$$

versus δ_{norm}, for normalized Doppler frequencies $f_d = 0.15$, and different classes of codes. The last class WDNE is also parameterized on three different values of δ^0. First of all, we notice that Gold codes, achieve lower values of induced interference than phase or PN codes. Moreover, WDNE codes can achieve the same performance as Gold sequences for $\delta^0 = 0.3$, while the overall induced interference can increase in correspondence of higher values of δ^0, or decrease for smaller δ^0 values.

Summarizing, the joint analysis in the last two sub-sections has shown that for a certain range of δ_{norm}, our proposed algorithm can achieve both higher values of SNR and lower values of induced interference than other considered codes.

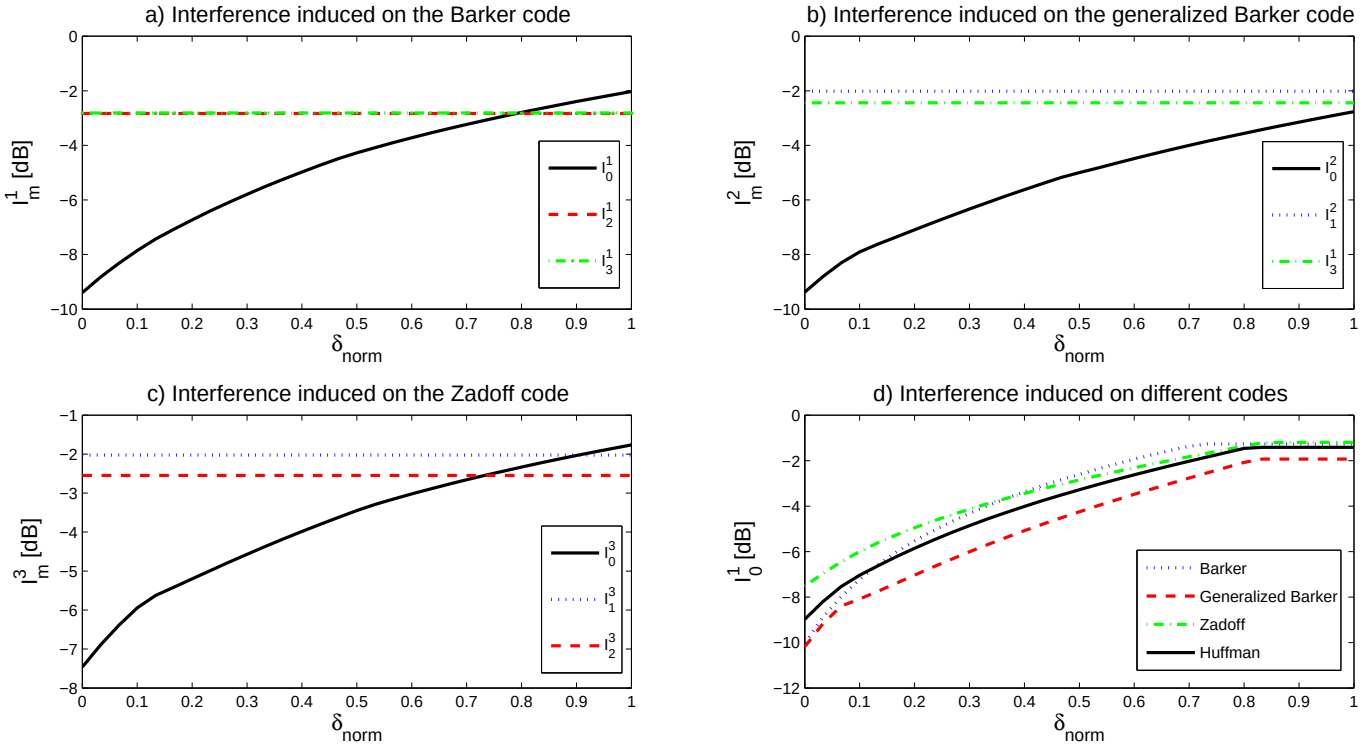

Figure 1.6: (a,b,c) I_m^l versus δ_{norm} for $N = 4$, $L = 4$, and normalized Doppler shift $f_d = 0.15$: a) I_m^1; b) I_m^2 c) I_m^3; I_0^l (solid curves); I_1^l (dotted lines); I_2^l (dashed lines); I_3^l (dot-dashed lines); **(d)** $I_0^1(\boldsymbol{c}_1)$ versus δ_{norm} for $N = 4$, $L = 2$, normalized Doppler shift $f_d = 0.15$, and different codes $\boldsymbol{c}_1$: Barker code (dotted curve), generalized Barker code (dashed curve), Zadoff code (dot-dashed curve), Huffman code (solid curve).

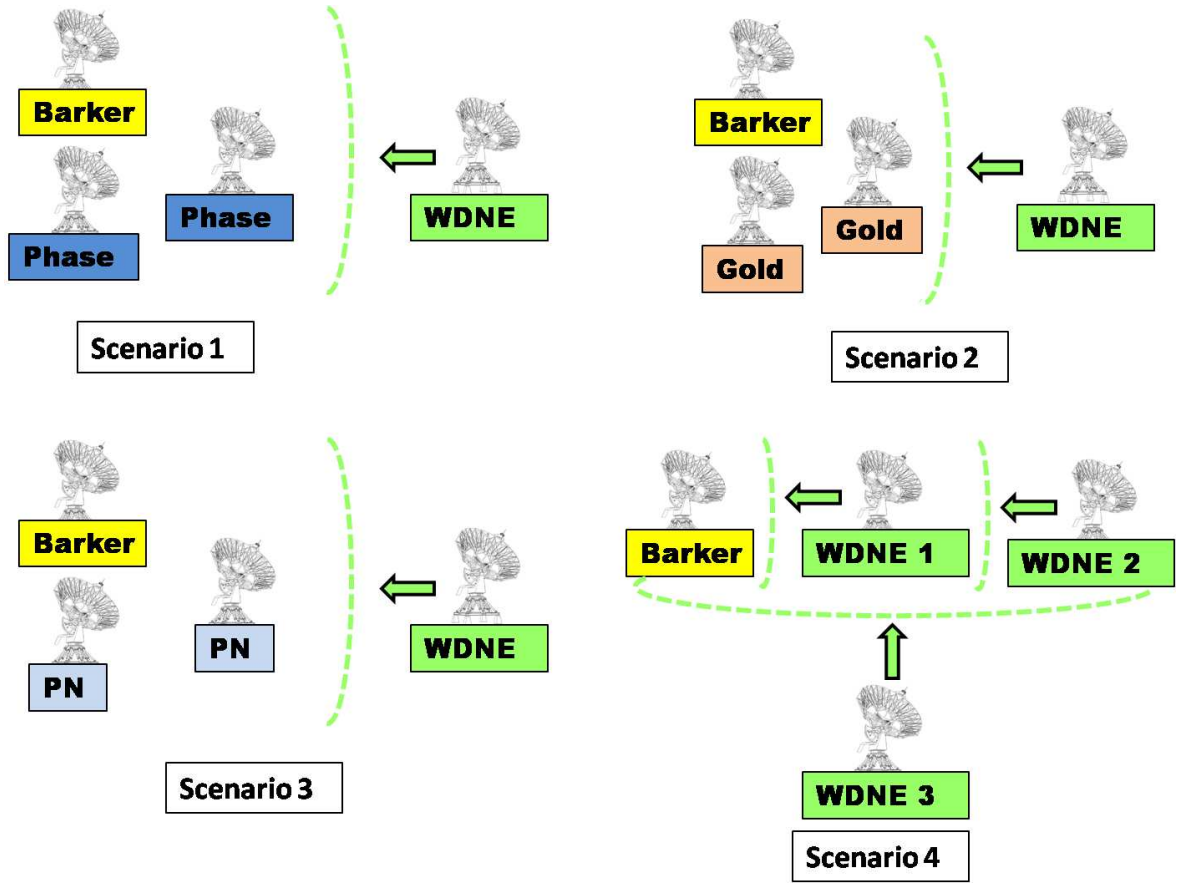

Figure 1.7: Some scenarios where WDNE can be applied.

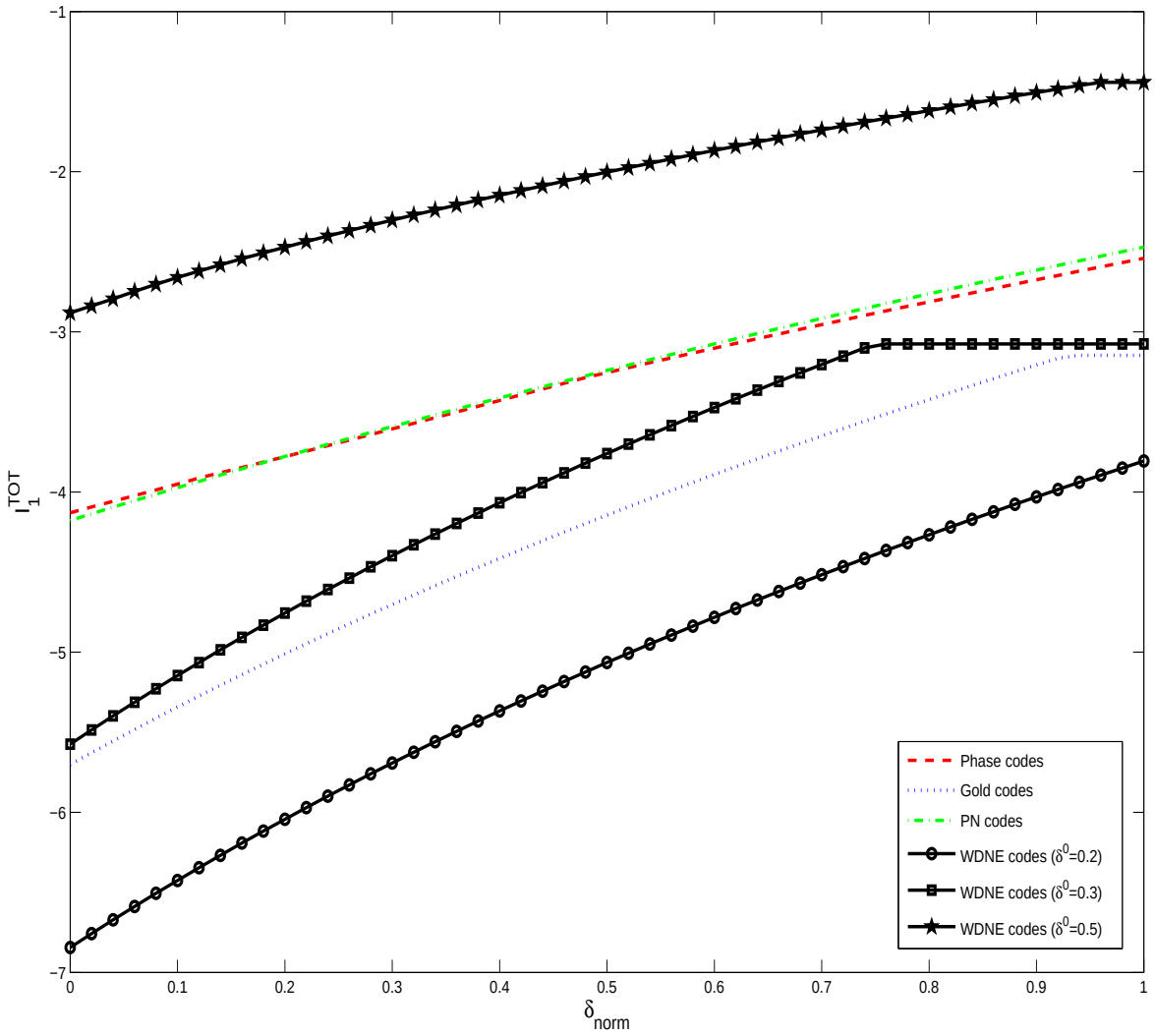

Figure 1.8: I^1_{TOT} versus δ_{norm} for $N = 4$, $L = 4$, normalized Doppler shift $f_d = 0.15$, and different classes of codes $\boldsymbol{c}_2$ and $\boldsymbol{c}_3$: phase codes (dashed curve), Gold code (dotted curve), orthogonal PN codes (dot-dashed curve), WDNE codes (solid curves): for $\delta^0 = 0.2$ (o-marked), for $\delta^0 = 0.3$ (square-marked), and for $\delta^0 = 0.5$ (star-marked).

Table 1.1: Average N_{it} and average T_{CPU} required to solve problem (1.17).

δ_{norm}	N	L	Average N_{it}	Average T_{CPU}
0.2	4	5	8	0.46
0.5	4	5	9	0.51
0.8	4	5	10	0.56
0.2	13	5	13	0.71
0.5	13	5	14	0.80
0.8	13	5	15	0.83

1.5.3 Computational complexity

Among the five steps of the WDNE algorithm, the most burdensome in terms of computational complexity, is the first step. In fact, the solution of CP has a computational complexity $O\left(N^{3.5}\right)$ [29]. We recall that the complexity is based on a worst-case analysis, and usually the interior point methods are much faster [22]. In Table 1.1, we report the number of iterations N_{it} and the CPU time T_{CPU} in seconds required to solve CP using the toolbox SeDuMi [25]. We have indicated also the corresponding value of δ_{norm} used in the simulation, the dimension N of the problem, and the number L of constraints. The reported averaged values have been evaluated over 100 trials. Finally, the computer used to obtain these results is equipped with a 3 GHz Intel XEON processor.

1.6 Conclusions

In this chapter, we have considered the problem of code design for a single radar that operates in a noncooperative network. We try to maximize the SNR of the radar, controlling, at the same time, the interference induced by our sensor on the other sensors of the network, and forcing a constraint on the transmitted energy by our radar. The resulting problem is in general NP-hard. Using the well established relaxation and randomization theory [16], we have presented a new waveform design procedure (referred to as WDNE), which in polynomial time generates a suboptimal solution of the original problem. Numerical simulations confirm that the WDNE technique can effectively increase the detection performance of each sensor of the network controlling the induced interference. Possible future research tracks might concern the extension of the WDNE: for instance, it might be interesting to add a constraint on the resulting ambiguity function of the code [30], or on the achievable region of Doppler estimation accuracy [31]. Moreover, it will be of interest to study this procedure applied to a real scenario.

1.7 Appendix: Solvability of CP

In this appendix, we prove that problem CP is solvable. To this end, we show that CP and its dual DP are strictly feasible. Hence by Corollary 1.7.1 of [29], we can conclude that CP and DP are solvable and the optimal values are equal to each other.

CP is evidently strictly feasible (for instance $\boldsymbol{I}/(1+\max_{l=0,\ldots,L-1}\mathrm{Tr}(\boldsymbol{R}_{\delta_l}))$ is a strictly feasible solution). As to the dual problem DP of CP, i.e.

$$\mathrm{DP}\begin{cases} \underset{y_0,\ldots,y_{L-1}}{\text{minimize}} & y_0+\ldots+y_{L-1} \\ \text{subject to} & y_0\boldsymbol{R}_{\delta_0}+\ldots+y_{L-1}\boldsymbol{R}_{\delta_{L-1}} \succeq \boldsymbol{R} \\ & y_l \geq 0\,, \quad l=0,\ldots,L-1 \end{cases}$$

it also admits a strict feasible solution $\boldsymbol{y}_\star = (y_0^\star,\ldots,y_{L-1}^\star)$. This is evident, observing that $\boldsymbol{R}_{\delta_0} \succ \boldsymbol{0}$. In fact, due to the positive definiteness of $\boldsymbol{R}_{\delta_0}$, for any $(y_1^\star,\ldots,y_{L-1}^\star)$ it is possible to choose $y_0^\star$ sufficiently large such as $\boldsymbol{y}_\star$ is a strictly

feasible solution of DP, i.e.

$$y_0^\star \boldsymbol{R}_{\delta_0} + \ldots + y_{L-1}^\star \boldsymbol{R}_{\delta_{L-1}} - \boldsymbol{R} \succ 0\,.$$

Chapter 2

Pareto-Optimal Radar Waveform Design

2.1 Introduction

More and more sophisticated algorithms for radar waveform design have been recently developed, due to the considerable advances in high speed signal processing hardware and digital array technology, as well as the growing interest for better and better radar performances [32, 33].

Some recent studies concerning waveform optimization in the presence of colored disturbance can be found in [34]. Therein, some algorithms, exploiting

the degrees of freedom provided by a possibly rank deficient clutter covariance matrix, are developed. In [30], a signal design approach relying on the maximization of the SNR under a similarity constraint with a given waveform is proposed and assessed. In [31], focusing on the class of linearly coded pulse trains (both in amplitude and in phase), the authors introduce a code selection algorithm which maximizes the detection performance but, at the same time, is capable of controlling both the region of achievable values for the Doppler estimation accuracy and the degree of similarity with a pre-fixed radar code. Further algorithms are also available attempting to determine the radar waveforms optimizing P_d under structural constraints (for instance a phase-only modulation) [24, 35] or possibly for airborne Space Time Adaptive Processing (STAP) scenarios [36].

In this chapter, we still focus on constrained code optimization, in the presence of colored Gaussian disturbance, assuming the same signal model as in [31]. At the design stage, we propose a waveform design algorithm based on the following criterion: joint optimization of the detection performance and of the region of achievable values for the Doppler estimation accuracy, under a constraint on the transmitted energy and on the degree of similarity

with a pre-fixed radar code. This is tantamount to jointly maximizing two quadratic forms, so that the resulting waveform design problem can be formulated in terms of a non-convex multi-objective optimization problem. In order to solve it, we resort to the technique of scalarization, where the original vectorial problem is reduced to a scalar one through the use of the Pareto-optimal theory. Thus, the proposed codes are chosen as *Pareto-optimal points*[1] of the previously mentioned multi-objective optimization problem. This design technique represents the main novelty of the present work and, to the authors best knowledge, this chapter represents the first application of the Pareto-optimal theory to radar signal design.

At the analysis stage, we assess the performance of the new encoding algorithm in terms of detection performance, region of achievable Doppler estimation accuracy, and ambiguity function, highlighting the role of the Pareto weight in the optimization. The results show that it is possible to trade-off the aforementioned performance metrics. Precisely, detection capabilities can be swaped for desirable properties of the waveform ambiguity function and/or for an enlarged region of achievable Doppler estimation accuracies. Further-

[1] A Pareto-optimal solution is an optimal solution of a multi-objective optimization problem; it is defined as any solution that can't be improved with respect to component without worsening the others [22]

more, the trade-off is ruled by both the similarity constraint and the Pareto weight. Indeed, this last parameter defines the relative importance of the two objectives in the optimization problem. Otherwise stated, it represents the cost required for improving a given objective (namely the CRLB) making worse the other (namely the detection probability).

The chapter is organized as follows. In Section 2.2, we present the model for both the transmitted and the received coded signals. In Section 2.3, we formulate the code design problem, give some relevant guidelines to handle multi-objective optimization problems through scalarization, and present the algorithm which provides Pareto-optimal waveforms. In Section 2.4, we assess the performance of the proposed encoding method also in comparison with a standard radar code. Finally, in Section 2.5, we draw conclusions and outline possible future research tracks.

2.2 System Model and Problem Formulation

We consider a radar which transmits a coherent burst of pulses, such as in [31]:

$$s(t) = a_t u(t) \exp[j(2\pi f_0 t + \phi)] \,,$$

where a_t is the transmit signal amplitude,

$$u(t) = \sum_{i=0}^{N-1} a(i)p(t - iT_r)\,,$$

is the signal's complex envelope (see **Figure 2.1**), $p(t)$ is the signature of the transmitted pulse, T_r is the Pulse Repetition Time (PRT), $[a(0), a(1), \ldots, a(N-1)] \in \mathbb{C}^N$ is the radar code, f_0 is the carrier frequency, and ϕ is a random phase. Moreover, the pulse waveform $p(t)$ is of duration $T_p \leq T_r$ and has unit energy, i.e.

$$\int_0^{T_p} |p(t)|^2 dt = 1\,.$$

The signal backscattered by a target with a two-way time delay τ and received by the radar is

$$r(t) = \alpha_r e^{j2\pi(f_0+f_d)(t-\tau)} u(t-\tau) + n(t)\,,$$

where α_r is the complex echo amplitude (accounting for the transmit amplitude, phase, target reflectivity, and channels propagation effects), f_d is the target Doppler frequency, and $n(t)$ is additive disturbance due to clutter and thermal noise. This signal is down-converted to baseband and filtered through a linear system with impulse response $h(t) = p^*(-t)$.

Let the filter output be

$$v(t) = \alpha_r e^{-j2\pi f_0 \tau} \sum_{i=0}^{N-1} a(i) e^{j2\pi i f_d T_r} \chi_p(t - iT_r - \tau, f_d) + w(t)\,,$$

where $\chi_p(\lambda, f)$ is the pulse waveform ambiguity function [18], i.e.

$$\chi_p(\lambda, f) = \int_{-\infty}^{+\infty} p(\beta) p^*(\beta - \lambda) e^{j2\pi f \beta} d\beta,$$

and $w(t)$ is the down-converted and filtered disturbance component. The signal $v(t)$ is sampled at $t_k = \tau + kT_r$, $k = 0, \ldots, N-1$, providing the observables[2]

$$v(t_k) = \frac{\alpha}{\sqrt{N}} a(k) e^{j2\pi k f_d T_r} \chi_p(0, f_d) + w(t_k), \qquad k = 0, \ldots, N-1\,,$$

where $\alpha = \sqrt{N}\alpha_r e^{-j2\pi f_0 \tau}$. Assuming that the pulse waveform time-bandwidth product and the expected range of target Doppler frequencies are such that the single pulse waveform is insensitive to target Doppler shift[3], namely $\chi_p(0, f_d) \sim$

[2]We neglect range straddling losses and also assume that there are no target range ambiguities.

[3]Notice that this assumption might be restrictive for the cases of very fast moving targets such as fighters and ballistic missiles.

$\chi_p(0,0) = 1$, we can rewrite the samples $v(t_k)$ as

$$v(t_k) = \frac{\alpha}{\sqrt{N}} a(k) e^{j2\pi k f_d T_r} + w(t_k), \qquad k = 0, \ldots, N-1\,.$$

Moreover, denoting by $\boldsymbol{c} = [a(0), a(1), \ldots, a(N-1)]^T$ the N-dimensional column vector containing the code elements, $\boldsymbol{p} = \frac{1}{\sqrt{N}}[1, e^{j2\pi\nu_d}, \ldots, e^{j2\pi(N-1)\nu_d}]^T$ the temporal steering vector, $\nu_d = f_d T_r$ the normalized Doppler frequency, $\boldsymbol{v} = [v(t_0), v(t_1), \ldots, v(t_{N-1})]^T$, and $\boldsymbol{w} = [w(t_0), w(t_1), \ldots, w(t_{N-1})]^T$, we get the following vectorial model for the backscattered signal

$$\boldsymbol{v} = \alpha \boldsymbol{c} \odot \boldsymbol{p} + \boldsymbol{w}\,. \tag{2.1}$$

2.2.1 Performance Measures

In this sub-section, we focus on the key performance measures which are to be optimized or controlled during the selection of the radar code.

Detection Probability: it's well known that the problem of detecting a target in the presence of observables described by the model (2.1) can be formulated in terms of the following binary hypotheses test

$$\begin{cases} H_0: & \boldsymbol{v} = \boldsymbol{w} \\ \\ H_1: & \boldsymbol{v} = \alpha \boldsymbol{c} \odot \boldsymbol{p} + \boldsymbol{w} \end{cases} \tag{2.2}$$

Assuming that the disturbance vector is a zero-mean complex circular Gaussian vector with known positive definite covariance matrix

$$E[\boldsymbol{w}\boldsymbol{w}^{\dagger}] = \boldsymbol{M}\,,$$

($E[\cdot]$ denotes statistical expectation and conjugate transpose), the generalized likelihood ratio test (GLRT) detector for (2.2), which coincides with the optimum test (according to the Neyman-Pearson criterion) if the phase of α is uniformly distributed in $[0, 2\pi)$ [37, 19], is given by

$$|\boldsymbol{v}^{\dagger}\boldsymbol{M}^{-1}(\boldsymbol{c} \odot \boldsymbol{p})|^2 \underset{H_0}{\overset{H_1}{\gtrless}} G\,, \tag{2.3}$$

where G is the detection threshold set according to a desired value of the false alarm Probability (P_{fa}). An analytical expression of the detection Probability (P_d), for a given value of P_{fa}, is available both for the cases of nonfluc-

tuating and fluctuating target. In the former case (NFT)

$$P_d = Q\left(\sqrt{2|\alpha|^2(\boldsymbol{c}\odot\boldsymbol{p})^\dagger \boldsymbol{M}(\boldsymbol{c}\odot\boldsymbol{p})}, \sqrt{-2\ln P_{fa}}\right), \tag{2.4}$$

while, for the case of Rayleigh fluctuating target (RFT) with $E\left[|\alpha|^2\right] = \sigma_a^2$,

$$P_d = \exp\left(\frac{P_{fa}}{1+\sigma_a^2(\boldsymbol{c}\odot\boldsymbol{p})^\dagger \boldsymbol{M}^{-1}(\boldsymbol{c}\odot\boldsymbol{p})}\right), \tag{2.5}$$

where $Q(\cdot,\cdot)$ denotes the Marcum Q function of order 1. This expression shows that, given P_{fa}, P_d depends on the radar code, the disturbance covariance matrix and the temporal steering vector only through the SNR, defined as:

$$\text{SNR} = \begin{cases} |\alpha|^2(\boldsymbol{c}\odot\boldsymbol{p})^\dagger \boldsymbol{M}(\boldsymbol{c}\odot\boldsymbol{p}) & NFT \\ \\ \sigma_a^2(\boldsymbol{c}\odot\boldsymbol{p})^\dagger \boldsymbol{M}^{-1}(\boldsymbol{c}\odot\boldsymbol{p}) & RFT \end{cases}. \tag{2.6}$$

Moreover, P_d is an increasing function of SNR and, as a consequence, the maximization of P_d can be obtained optimizing the SNR over the radar code.

Doppler Accuracy: the Doppler accuracy is bounded below by Cramer-Rao Bound (CRB) and CRB-like techniques which provide lower bounds for the variances of unbiased estimates. A reliable measurement of the Doppler frequency is very important in radar signal processing because it is directly related to the target radial velocity useful to speed the track initiation, to improve the track accuracy [38], and to classify the dangerousness of the target; hence it's clear that it has to be taken in account in the code design operation. It can be shown that the CRB for known α is given by [31]:

$$\Delta_{CR}(f_d) = \frac{\psi}{\frac{\partial \boldsymbol{h}^{\dagger}}{\partial f_d} \boldsymbol{M}^{-1} \frac{\partial \boldsymbol{h}}{\partial f_d}} \tag{2.7}$$

where $\boldsymbol{h} = \boldsymbol{c} \odot \boldsymbol{p}$ and $\psi = \frac{1}{2|\alpha|^2}$. Notice that

$$\frac{\partial \boldsymbol{h}}{\partial f_d} = T_r \boldsymbol{c} \odot \boldsymbol{p} \odot \boldsymbol{u},$$

with $\boldsymbol{u} = [0, j2\pi, ..., j2\pi\,(N-1)]^T$, so that (2.7) can be rewritten as

$$\Delta_{CR}(f_d) = \frac{\psi}{2T_r^2\,(\boldsymbol{c} \odot \boldsymbol{p} \odot \boldsymbol{u})^{\dagger}\, \boldsymbol{M}^{-1}\,(\boldsymbol{c} \odot \boldsymbol{p} \odot \boldsymbol{u})} \tag{2.8}$$

Similarity Constraint: Designing a code which just optimizes the detection performance does not provide any kind of control on the shape of the resulting coded waveform. Precisely, it can lead to signals with significant modulus variations, poor range resolution, high peak sidelobe levels, and more in general with an undesired ambiguity function behavior. These drawbacks can be partially circumvented imposing a further constraint to the sought radar code. Precisely it is required that the solution to be similar to a known code $\boldsymbol{c}_0$ ($||\boldsymbol{c}_0||^2 = 1$), which shares constant modulus, reasonable range resolution and peak sidelobe level. This is tantamount to imposing that [30]:

$$||\boldsymbol{c} - \boldsymbol{c}_0||^2 \leq \epsilon, \tag{2.9}$$

where the parameter $\epsilon \geq 0$ rules the size of the similarity region. In other words, (2.9) permits to indirectly control the ambiguity function of the considered coded pulse train: the smaller ϵ the higher the degree of similarity between the ambiguity functions of the designed radar code and of the reference sequence.

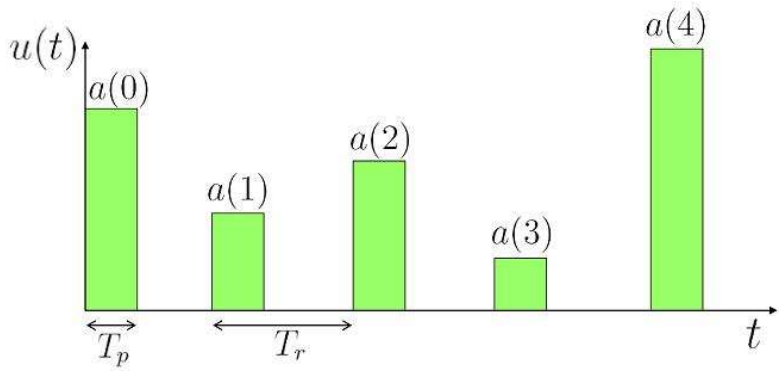

Figure 2.1: Coded pulse train $u(t)$ for $N = 5$ and $p(t)$ with rectangular shape.

2.3 Problem Formulation and Pareto-optimal Code Design

The idea pursued in this section is to design a radar code which optimizes jointly the detection performance and the CRLB on the Doppler estimation accuracy, under a similarity constraint with a known radar code $\boldsymbol{c}_0$ and an energy constraint. Specifically, exploiting the following relationships

$$(\boldsymbol{c} \odot \boldsymbol{p})^{\dagger} \boldsymbol{M} (\boldsymbol{c} \odot \boldsymbol{p}) = \boldsymbol{c}^{\dagger} \boldsymbol{R} \boldsymbol{c} \tag{2.10}$$

and

$$(\boldsymbol{c} \odot \boldsymbol{p} \odot \boldsymbol{u})^{\dagger} \boldsymbol{M}^{-1} (\boldsymbol{c} \odot \boldsymbol{p} \odot \boldsymbol{u}) = \boldsymbol{c}^{\dagger} \boldsymbol{R}_1 \boldsymbol{c}, \tag{2.11}$$

where $\boldsymbol{R} = \boldsymbol{M}^{-1} \odot \left(\boldsymbol{p}\boldsymbol{p}^{\dagger}\right)^{*}$ and $\boldsymbol{R}_1 = \boldsymbol{M}^{-1} \odot \left(\boldsymbol{p}\boldsymbol{p}^{\dagger}\right)^{*} \odot \left(\boldsymbol{u}\boldsymbol{u}^{\dagger}\right)^{*}$ are positive semidefinite [39, pag. 1352, A. 77], it appears that P_d is an increasing function of $\boldsymbol{c}^{\dagger}\boldsymbol{R}\boldsymbol{c}$, while the CRLB is a decreasing function of $\boldsymbol{c}^{\dagger}\boldsymbol{R}_1\boldsymbol{c}$. As a consequence, the joint optimization of the P_d and CRLB can be formulated in terms of a non-convex multi-objective optimization problem [22, pp. 174-187]:

$$\begin{cases} \max_{\boldsymbol{c}} \quad (\boldsymbol{c}^{\dagger}\boldsymbol{R}\boldsymbol{c}\,,\, \boldsymbol{c}^{\dagger}\boldsymbol{R}_1\boldsymbol{c}) \\ \text{s.t.} \quad ||\boldsymbol{c} - \boldsymbol{c}_0||^2 \leq \epsilon \\ \qquad\quad ||\boldsymbol{c}|| = 1. \end{cases} \tag{2.12}$$

Before proceeding with the presentation of the algorithm which solves (2.12) and provides radar codes, it is necessary to give a short introduction to the theory of multi-objective optimization problems as well as the terminology, and the concept of Pareto-optimal points.

2.3.1 Multi-Objective Optimization Problems

A multi-objective optimization problem presents a vector-valued objective function and can be written in the form

$$\begin{cases} \min_{\boldsymbol{x}} \quad \boldsymbol{f_0}(\boldsymbol{x}) \\ \text{s.t.} \quad f_i(\boldsymbol{x}) \leq 0, \qquad \forall i = 1, \ldots, m, \\ \qquad\quad h_i(\boldsymbol{x}) = 0, \qquad \forall i = 1, \ldots, p \end{cases} \tag{2.13}$$

where $\boldsymbol{x} \in \mathbb{R}^n$ is the optimization variable, $f_i(\boldsymbol{x})$, $i = 1, \ldots, m$ and $h_i(\boldsymbol{x})$, $i = 1, \ldots, p$ denote respectively the i-th inequality constraint and the i-th equality constraint function, $\mathbf{0}_0(\boldsymbol{x}) \ : \ \boldsymbol{x} \in \mathbb{R}^n \rightarrow \mathbb{R}^q$ is the vector-valued objective function whose q components $F_1(\boldsymbol{x}), \ldots, F_q(\boldsymbol{x})$ can be interpreted as q different scalar objectives, each of which we would like to minimize.

If $\boldsymbol{x}$ and $\boldsymbol{y}$ are both feasible, we say that $\boldsymbol{x}$ *is at least as good as* $\boldsymbol{y}$ according the i-th objective if $F_i(\boldsymbol{x}) \leq F_i(\boldsymbol{y})$, while $\boldsymbol{x}$ *is better than* $\boldsymbol{y}$ (or $\boldsymbol{x}$ beats $\boldsymbol{y}$) according the i-th objective if $F_i(\boldsymbol{x}) < F_i(\boldsymbol{y})$; so, if $F_i(\boldsymbol{x}) \leq F_i(\boldsymbol{y})$ for $i = 1, \ldots, q$ and, for al least one j, $F_j(\boldsymbol{x}) < F_j(\boldsymbol{y})$, we say that $\boldsymbol{x}$ *dominates* $\boldsymbol{y}$.

A point $\boldsymbol{x}^\star$ is defined optimal only if it complies with

$$F_i(\boldsymbol{x}^\star) \leq F_i(\boldsymbol{y}), \qquad i = 1, \ldots, q$$

for every feasible $\boldsymbol{y}$; otherwise stated, $\boldsymbol{x}^\star$ has to be simultaneously optimal for each of the scalar problems

$$\begin{cases} \min_{\boldsymbol{x}} & F_j(\boldsymbol{x}) \\ \text{s.t.} & f_i(\boldsymbol{x}) \leq 0 \qquad \forall i = 1, \ldots, m, \\ & h_i(\boldsymbol{x}) = 0, \qquad \forall i = 1, \ldots, p \end{cases}$$

for $j = 1, \ldots, q$. In the presence of an optimal point, the objectives are said *noncompeting*, since no compromises have to be made among them: each objective is as small as it could be made, even if the others were ignored.

However, the set of achievable values for problem (2.13) does not always present a minimum element, and thus the problem itself has not an optimal point and an optimal value. In these cases, one focuses on the *minimal* elements [22, pp. 45] of the set, namely on the so-called Pareto-optimal points.

A feasible point $\boldsymbol{x}^\star$ is referred to as Pareto-optimal only if $\mathbf{0}_0(\boldsymbol{x}^\star)$ is a minimal element of the set for achievable values of the problem; in this case, $\mathbf{0}_0(\boldsymbol{x}^\star)$ is a Pareto-optimal value for (2.13). Considering the q scalar components of the objective function $\mathbf{0}_0(\boldsymbol{x})$, $\boldsymbol{x}^\star$ can be considered Pareto-optimal only if it is feasible and no better feasible point exists. Precisely, if $\boldsymbol{y}$ is a feasible point and $F_i(\boldsymbol{y}) \leq F_i(\boldsymbol{x}^\star)$ for $i = 1, \ldots, q$, then necessarily $F_i(\boldsymbol{x}^\star) = F_i(\boldsymbol{y})$ for $i = 1, \ldots, q$. This also implies that: if a feasible point is not a Pareto-optimal, than there is at least another feasible point that is better. Hence, the search for "*good*" points can be limited to Pareto-optimal ones.

A standard technique to find Pareto-optimal points is the *scalarization*, where the vectorial problem (2.13) is reduced to the scalar one

$$\begin{cases} \min_{\boldsymbol{x}} & \boldsymbol{\lambda}^T \mathbf{0}_0(\boldsymbol{x}) \\ \text{s.t.} & f_i(\boldsymbol{x}) \leq 0 \\ & h_i(\boldsymbol{x}) = 0 \end{cases} \tag{2.14}$$

once it has been defined the vector of weights $\boldsymbol{\lambda} \succ 0$, namely a vector with

positive components. In fact, it can be shown [22, pp. 178] that if $\boldsymbol{x}^{\star}$ is an optimal point for problem (2.14), than it's also a Pareto-optimal point for the problem (2.13). Nevertheless it is worth pointing out that, for non-convex multi-objective optimization problems, it is possible through scalarization to obtain a sub-set, but not all, the Pareto-optimal points.

The choice of the parameter $\boldsymbol{\lambda}$ plays a primary role in the determination of the Pareto points, defining the *weight* given to each of the scalar components. Specifically, it quantifies our desire to make $F_i(\boldsymbol{x})$ small.

2.3.2 Pareto-optimal Code Design

In this sub-section, we design radar codes which are Pareto-optimal solutions to (2.12), through the scalarization technique explained in the previous

sub-section. Precisely, let us consider the scalarized problem

$$\begin{cases} \max_{\boldsymbol{c}} \quad \boldsymbol{c}^{\dagger}\left[\frac{\alpha_1}{\lambda_{max}(\boldsymbol{R})}\boldsymbol{R}+\frac{\alpha_2}{\lambda_{max}(\boldsymbol{R}_1)}\boldsymbol{R}_1\right]\boldsymbol{c} \\ \text{s.t.} \quad ||\boldsymbol{c}-\boldsymbol{c}_0||^2 \leq \epsilon \\ \qquad\quad ||\boldsymbol{c}|| = 1 \end{cases} \tag{2.15}$$

where $\frac{\alpha_1}{\lambda_{max}(\boldsymbol{R})} > 0$ and $\frac{\alpha_2}{\lambda_{max}(\boldsymbol{R}_1)} > 0$ are the weights. A code $\boldsymbol{c}$ is an optimal solution of (2.15) if and only if it is an optimal solution of

$$\begin{cases} \max_{\boldsymbol{c}} \quad \boldsymbol{c}^{\dagger}\boldsymbol{Q}(\gamma)\,\boldsymbol{c} \\ \text{s.t.} \quad ||\boldsymbol{c}-\boldsymbol{c}_0||^2 \leq \epsilon \\ \qquad\quad ||\boldsymbol{c}|| = 1 \end{cases} \tag{2.16}$$

where $\boldsymbol{Q}(\gamma) = \boldsymbol{R}+\gamma\boldsymbol{R}_1$, $\gamma = \frac{\alpha_2}{\alpha_1}\frac{\lambda_{max}(\boldsymbol{R})}{\lambda_{max}(\boldsymbol{R}_1)} > 0$. This claim is evident since the objective functions of problem (2.15) and (2.16) are proportional and the constraint sets are the same.

Given γ, an optimal solution to the previous scalarized problem can be found through the procedure proposed in [30]. Precisely, the Pareto-optimal point corresponding to γ can be constructed according to **Algorithm 2**.

Algorithm 2 Determination of a solution to problem (2.16)

Input: $\boldsymbol{c}_0$, ϵ, $\boldsymbol{R}$, $\boldsymbol{R}_1$, γ;

Output: an optimal solution $\hat{\boldsymbol{c}}$ of problem (2.16);

1: let $\boldsymbol{Q}(\gamma) \triangleq \boldsymbol{R} + \gamma \boldsymbol{R}_1$

2: let $\tilde{\boldsymbol{c}}$ be the unit norm eigenvector corresponding to the greatest eigenvalue of $\boldsymbol{Q}(\gamma)$;

3: define $\hat{\boldsymbol{c}} = \tilde{\boldsymbol{c}} e^{j \arg(\boldsymbol{c}_0^\dagger \tilde{\boldsymbol{c}})}$ (where $\arg(x)$ defines the argument of x);

4: **if** $\Re(\boldsymbol{c}_0^\dagger \hat{\boldsymbol{c}}) \geq 1 - \epsilon/2$ (where $\Re(x)$ defines the real part of x) **then**

5: $\quad \boldsymbol{c}_{opt}(\gamma) \equiv \hat{\boldsymbol{c}}$;

6: **else if** $\Re(\boldsymbol{c}_0^\dagger \hat{\boldsymbol{c}}) \leq 1 - \epsilon/2$ **then**

7: $\quad$ let $\lambda_{min}(\boldsymbol{Q}(\gamma))$ and $\lambda_{max}(\boldsymbol{Q}(\gamma))$ be, respectively, the smallest and the greatest eigenvalue of $\boldsymbol{Q}(\gamma)$;

8: $\quad$ define:

- $\rho \triangleq \frac{1}{(1-\epsilon/2)^2}$;
- $\eta_1 \triangleq \lambda_{max}(\boldsymbol{Q}(\gamma))$;
- $\eta_2 \triangleq \frac{\rho^{1/2}\left(\lambda_{max}(\boldsymbol{Q}(\gamma))\right) - \lambda_{min}(\boldsymbol{Q}(\gamma))}{\left(\rho^{1/2}-1\right)}$;

9: $\quad$ consider the equation $\frac{\boldsymbol{c}_0^\dagger \left(-\boldsymbol{Q}(\gamma)+\bar{\lambda}\boldsymbol{I}\right)^{-2} \boldsymbol{c}_0}{\left[\boldsymbol{c}_0^\dagger \left(-\boldsymbol{Q}(\gamma)+\bar{\lambda}\boldsymbol{I}\right)^{-1} \boldsymbol{c}_0\right]^2} = \rho$;

10: $\quad$ solve the equation above, via Newton's method, respect to $\bar{\lambda}$, with $\eta_1 < \bar{\lambda} \leq \eta_2$;

11: $\quad \boldsymbol{c}_{opt}(\gamma) = \left(1 - \frac{\epsilon}{2}\right) \frac{\left(-\boldsymbol{Q}(\gamma)+\bar{\lambda}\boldsymbol{I}\right)^{-1} \boldsymbol{c}_0}{\boldsymbol{c}_0^\dagger \left(-\boldsymbol{Q}(\gamma)+\bar{\lambda}\boldsymbol{I}\right)^{-1} \boldsymbol{c}_0}$;

12: **end**

The parameter γ can be interpreted as the *weight* given to the second ob-

jective (namely, the CRLB) with respect to the first one (namely, the P_d); otherwise stated, it represents the cost required for improving a component making worse the other.

A final remark concerns the applicability of the proposed framework in real scenarios. Evidently, the objective functions require the specification of ν_d; as a consequence, the solution depends on this pre-assigned value. It is thus necessary to provide some guidelines to set ν_d in practical scenarios. To this end, we highlight that:

- a single coded waveform designed for the challenging condition of slowly moving targets (i.e. $\nu_d \simeq 0$) can be devised;

- a single coded waveform optimized over an average scenario may be designed. Specifically, the code might be chosen so as to maximize the objectives with $\boldsymbol{R}$ replaced by $\boldsymbol{R}_a = \boldsymbol{M}^{-1} \odot \left(E\left[\boldsymbol{p}\boldsymbol{p}^{\dagger}\right]\right)^*$, where the expectation operator is over the normalized Doppler frequency. If this last quantity is modeled as a uniformly distributed random variable, i.e. $\nu_d \sim \mathcal{U}(-\epsilon, \epsilon)$, with $0 < \epsilon < 1/2$, the expectation can be readily evaluated, leading to

$$\boldsymbol{R}_a = \boldsymbol{M}^{-1} \odot \boldsymbol{\Sigma}_{\epsilon}\,, \tag{2.17}$$

where $\Sigma_\epsilon(m,n) = \text{sinc}\,[2\epsilon(m-n)]$, and $\text{sinc}(x) = \frac{\sin(\pi x)}{\pi x}$.

2.4 Performance Analysis

In this section, we assess the quality of the proposed waveform design technique. The analysis is conducted in terms of P_d, CRLB for Doppler estimation accuracy, and ambiguity function of the pulse train modulated with the designed code. Additionally, we provide the Pareto-optimal curve, i.e.

$$\begin{cases} F_1(\boldsymbol{c}_{opt}(\gamma)) \triangleq \boldsymbol{c}_{opt}^{\dagger}(\gamma)\boldsymbol{R}\boldsymbol{c}_{opt}(\gamma) \\ \\ F_2(\boldsymbol{c}_{opt}(\gamma)) \triangleq \boldsymbol{c}_{opt}^{\dagger}(\gamma)\boldsymbol{R}_1\boldsymbol{c}_{opt}(\gamma) \end{cases} \tag{2.18}$$

(where, according to (2.4) and (2.8), F_1 and F_2 rule, respectively, P_d and CRLB); namely the set of Pareto-optimal values, obtained through scalarization and varying the relative weight γ, for the considered optimization problem. Finally, we also explore the Pareto trade-off between P_d and CRLB arising through the variation of γ.

The analysis is developed assuming a disturbance covariance matrix $\boldsymbol{M}$

with the following structure:

$$\boldsymbol{M} = \boldsymbol{R}_{clutter} + 10^{-2}\boldsymbol{I}$$

where $\boldsymbol{R}_{clutter} = \rho^{|m-n|}$, with $\rho = 0.9$. Moreover, the P_{fa} of the receiver is fixed to 10^{-6}, $\nu_d = 0$; a NFT is considered, and the reference code is the generalized Barker sequence of length $N = 7$ [18, pp. 109-113] $\boldsymbol{c}_0 = [0.3780, 0.3780, -0.1072 - j0.3624, -0.0202 - j0.3774, 0.2752 + j0.2591, 0.1855 - j0.3293, 0.0057 + j0.3779]$, properly normalized in order to obtain a unitary norm vector.

In **Figure 2.2**, we plot the Pareto-optimal curve for several values of ϵ, namely different degrees of similarity between the devised and the pre-fixed code, assuming that γ ranges in the interval $]0, 10]$. This curve is also referred to as *optimal trade-off curve*, because it highlights the connection between the two objectives, F_1 and F_2, emphasizing the role of the weight γ in the determination of their Pareto-optimal values and the cost payed for increasing one component with respect to the other. The shaded region indicates the set of all the achievable values (F_1, F_2); for example, intercepting the curve with the vertical line $F_1 = \alpha$ (thus considering a certain value for P_d), we can observe how small F_2 (thus how large the corresponding CRLB) has to be in

order to achieve $F_1 \geq \alpha$. The same interpretation arises intercepting the curve with an horizontal line $F_2 = \beta$ (thus considering a certain value for the CRLB), which makes evident how small F_1 (thus the corresponding P_d) has to be in order to achieve $F_2 \geq \beta$. The slope of the optimal trade-off curve at a Pareto-optimal value shows the *local* optimal trade-off between the two objectives; steep slopes lead to large variations of F_2 in correspondence of small changes in F_1 (this is actually what happens in the lower right region of the curves in Figure 2.2).

Notice also how a reduction of ϵ (or, equivalently, an increase in the degree of similarity) leads to worse and worse otpimal values for both F_1 and F_2, namely to lower and lower Pareto-optimal curves. This result can be explained observing that decreasing ϵ is tantamount to reducing the size of the feasible set. However, the resulting loss (both in terms of detection capability and estimation accuracy) is compensated for an improvement of the coded pulse train ambiguity function, which appears more and more similar to that of the reference code. This is shown in **Figures 2.3a-2.3d**, where the ambiguity function modulus is plotted, for $\gamma = 1$ and some values of the similarity parameter ϵ. Comparing them with the ambiguity function of the code $\boldsymbol{c}_0$, plotted in **Figure**

2.4, it can be easily recognized a greater and greater degree of similarity as ϵ decreases.

The effects of the similarity parameter ϵ on the detection capability and the Doppler estimation accuracy are analyzed in **Figures 2.5a-2.5b**. Therein, we set $\gamma = 0.05$, and plot P_d (Figure 2.5a) or the normalized CRLB (CRLB$_n$ = T_r^2CRLB, Figure 2.5b) versus $|\alpha|^2$ for several values of ϵ ($\epsilon = \{0.1, 0.3, 0.7, 1.9998\}$). In order to compare the performance of our code with that of the similarity sequence, we also evaluate P_d and CRLB$_n$ obtained through the use of $\boldsymbol{c}_0$. As benchmark code, instead, we consider the sequence which maximizes the unconstrained (namely without forcing the similarity constraint) P_d or CRLB , i.e.

$$\boldsymbol{c}_{benchmark}^{P_d} = \arg\max_{\boldsymbol{c}} \{\boldsymbol{c}^\dagger \boldsymbol{R}\boldsymbol{c} \;/\; ||\boldsymbol{c}||^2 = 1\} \tag{2.19}$$

$$\boldsymbol{c}_{benchmark}^{CRLB} = \arg\max_{\boldsymbol{c}} \{\boldsymbol{c}^\dagger \boldsymbol{R}_1\boldsymbol{c} \;/\; ||\boldsymbol{c}||^2 = 1\} \tag{2.20}$$

The corresponding P_d and CRLB are referred to in the following as $P_d^{benchmark}$ and CRLB$_n^{benchmark}$. Usually, they are are not obtained in correspondence of the same code.

The curves in Figure 2.5a show that decreasing ϵ worse and worse P_d values

are obtained. This behavior can be explained observing that reducing ϵ is tantamount to reducing the size of the similarity region. Nevertheless, the quoted P_d loss is compensated for an improvement in the coded pulse train ambiguity function, which is forced to be more similar to the reference sequence. Different considerations apply to the curves of Figure 2.5b, representing the CRLB behavior for the same values of ϵ as in Figure 2.5a. In this case, due to the small value of the relative weight γ, the scalarization places almost all the emphasis on the P_d objective, which substantially rules the choice of the optimum code for the scalarized problem. As a consequence, enlarging the similarity region, we can find a new code improving P_d, but such a code can also lead to a degradation of the CRLB because the two objectives are competing.

Let us now analyze the effects of the Pareto weight γ, on the performance of the designed code, fixing the similarity constraint ϵ. To this end, in **Figure 2.6**, we plot the Pareto-optimal curve obtained for $\epsilon = 0.1561$, highlighting six different Pareto-optimal values (operating points in the following), related to six different weights. In **Figures 2.7a** and **2.7b** we study the impact of the Pareto weight on the optimization of the detection capability and Doppler es-

timation accuracy. Specifically, we plot P_d and CRLB$_n$ versus $|\alpha|^2$ for the six operating points of Figure 6. The performance follows the same qualitative behavior explained in Figure 2.2; namely, P_d and CRLB are both decreasing functions of γ.

Finally, it is important to point out that, although tied up to the same similarity value ϵ, the codes resulting from the optimization problem (2.16) are clearly affected by the chosen value for the weight γ. As a consequence, the corresponding pulse trains will exhibit different ambiguity functions as shown in **Figures 2.8a-2.8d**.

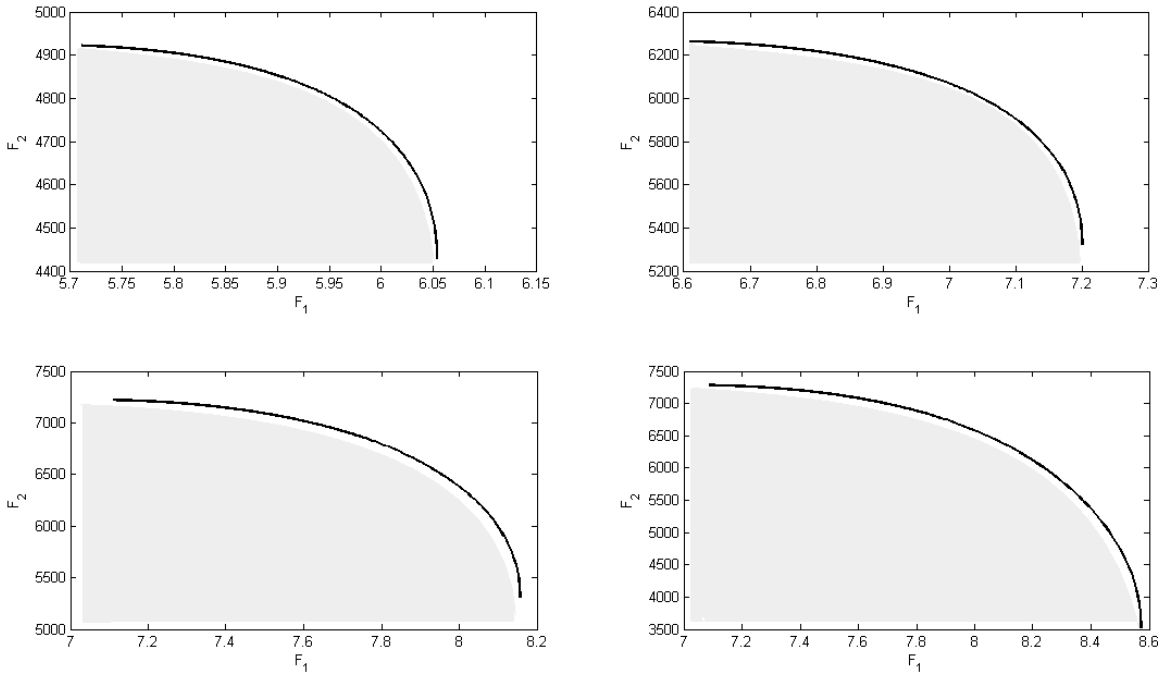

Figure 2.2: Pareto-optimal curves for $\gamma \in]0, 10]$, $\epsilon = 0.1$ (top-left), $\epsilon = 0.3$ (top-right), $\epsilon = 0.7$ (bottom-left) and $\epsilon = 1.9998$ (bottom-right), with the polyphase Barker code of length $N = 7$ as reference code. The set of achievable values under the curves is shaded in gray.

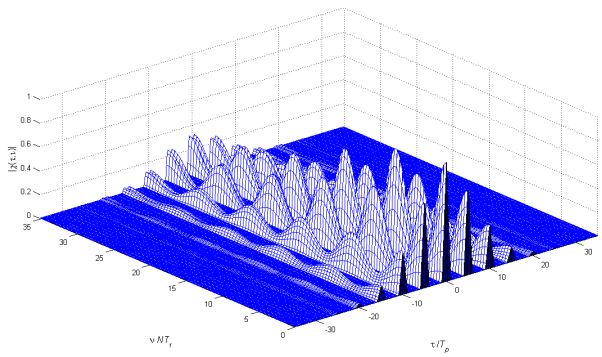

Figure 2.3: (a) Ambiguity function modulus of the designed code with $N = 7$, $T_r = 5T_p$, $\epsilon = 1.9998$ and $\gamma = 1$.

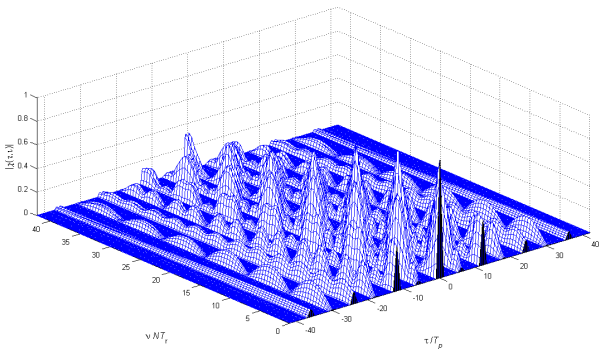

Figure 2.3: **(b)** Ambiguity function modulus of the designed code with $N = 7$, $T_r = 5T_p$, $\epsilon = 0.3$ and $\gamma = 1$.

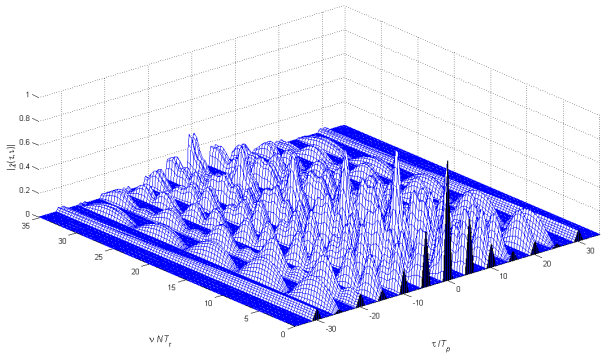

Figure 2.3: **(c)** Ambiguity function modulus of the designed code with $N = 7$, $T_r = 5T_p$, $\epsilon = 0.1561$ and $\gamma = 1$.

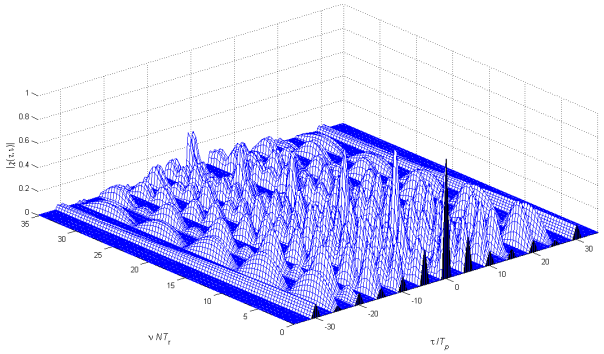

Figure 2.3: **(d)** Ambiguity function modulus of the designed code with $N = 7$, $T_r = 5T_p$, $\epsilon = 0.0506$ and $\gamma = 1$.

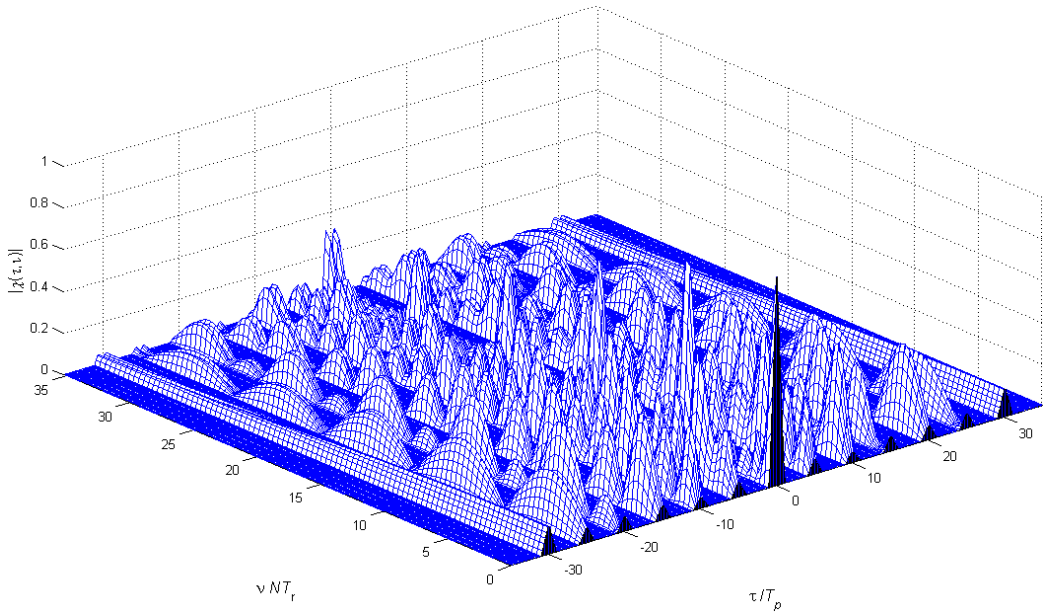

Figure 2.4: Ambiguity function modulus of the generalized Barker code c_0 of length $N = 7$ with $T_r = 5T_p$.

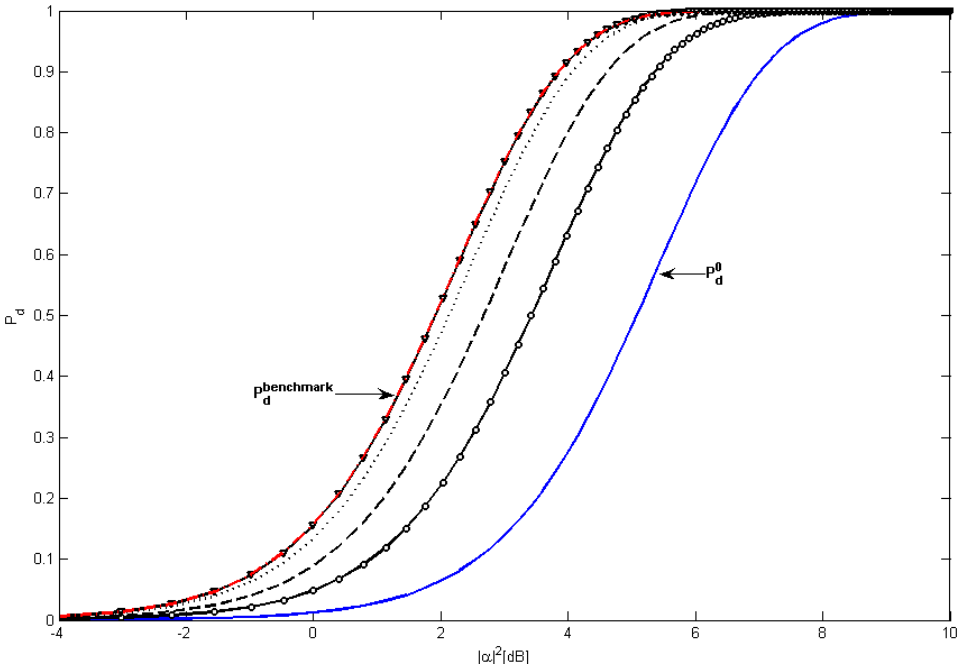

Figure 2.5: (a) P_d versus $|\alpha|^2$ for non-fluctuating target, $P_{fa} = 10^{-6}$, $N = 7$, $\gamma = 0.05$, and: $\epsilon = 0.1$ (solid-circle curve), $\epsilon = 0.3$ (dashed curve), $\epsilon = 0.7$ (dotted curve) and $\epsilon = 1.9998$ (solid-down triangle curve). The curves related to $\boldsymbol{c}_0$ (solid curve) and $\boldsymbol{c}_{benchmark}$ (dash-dotted curve) are highlighted directly on the figure; notice that the curve for $\epsilon = 1.9998$ overlaps with the benchmark one.

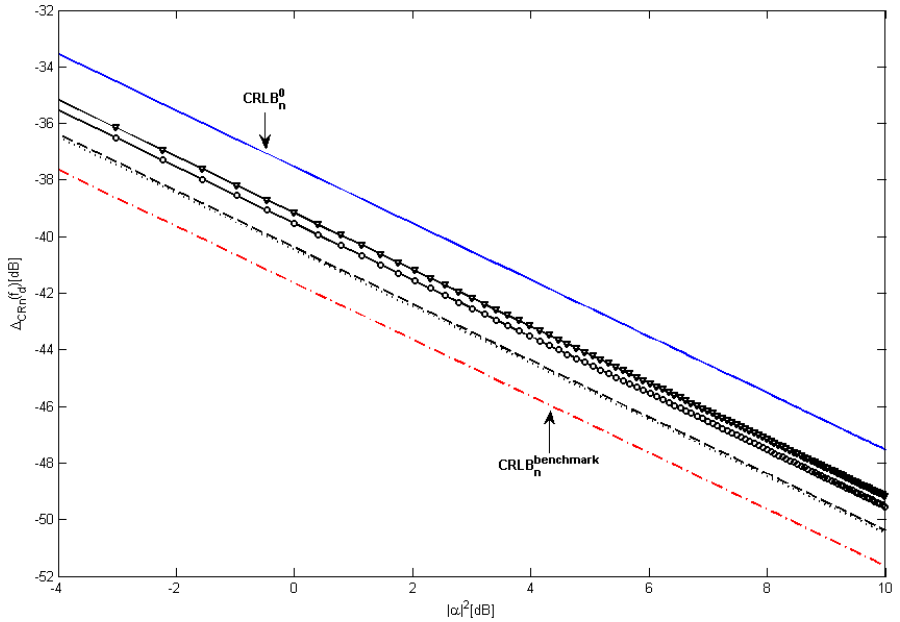

Figure 2.5: **(b)** CRLB_n versus $|\alpha|^2$ for non-fluctuating target, $P_{fa} = 10^{-6}$, $N = 7$, $\gamma = 0.05$, and: $\epsilon = 0.1$ (solid-circle curve), $\epsilon = 0.3$ (dashed curve), $\epsilon = 0.7$ (dotted curve) and $\epsilon = 1.9998$ (solid-down triangle curve). The curves related to $\boldsymbol{c}_0$ (solid curve) and $\boldsymbol{c}_{benchmark}$ (dash-dotted) are highlighted directly on the figure.

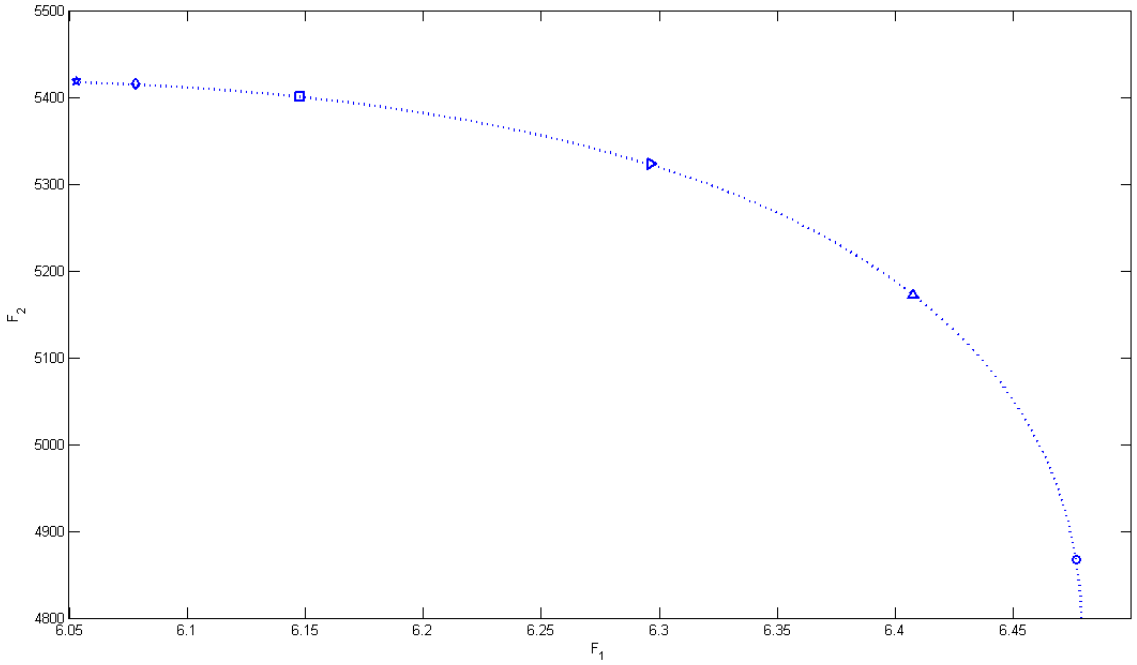

Figure 2.6: Pareto-optimal curve for $\epsilon = 0.1561$ and $\gamma \in]0, 10]$. Each marker represents an operative point for a given γ; $\gamma = 0.05$ (circle), $\gamma = 0.4$ (up-triangle), $\gamma = 1$ (right-triangle), $\gamma = 3$ (square), $\gamma = 6.5$ (diamond) and $\gamma = 10$ (star).

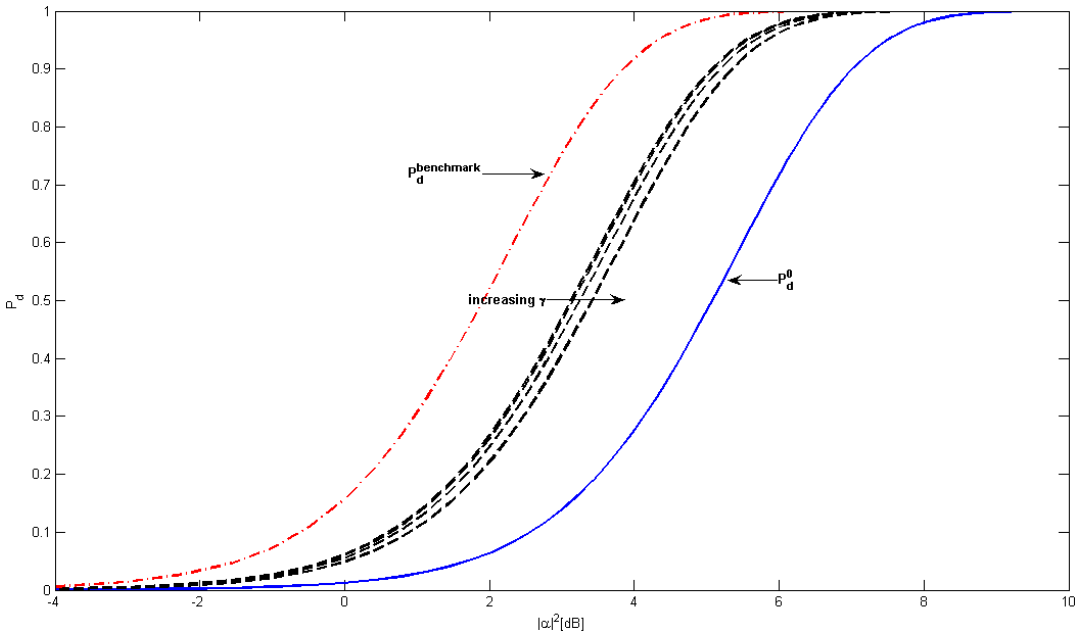

Figure 2.7: (a) P_d versus $|\alpha|^2$ for non-fluctuating target, $P_{fa} = 10^{-6}$, $N = 7$, $\epsilon = 0.1561$ and $\gamma = \{0.05; 0.4; 1; 3; 6.5; 10\}$. Generalized Barker code (solid curve). Designed codes (dashed curves). Benchmark code (dash-dotted curve

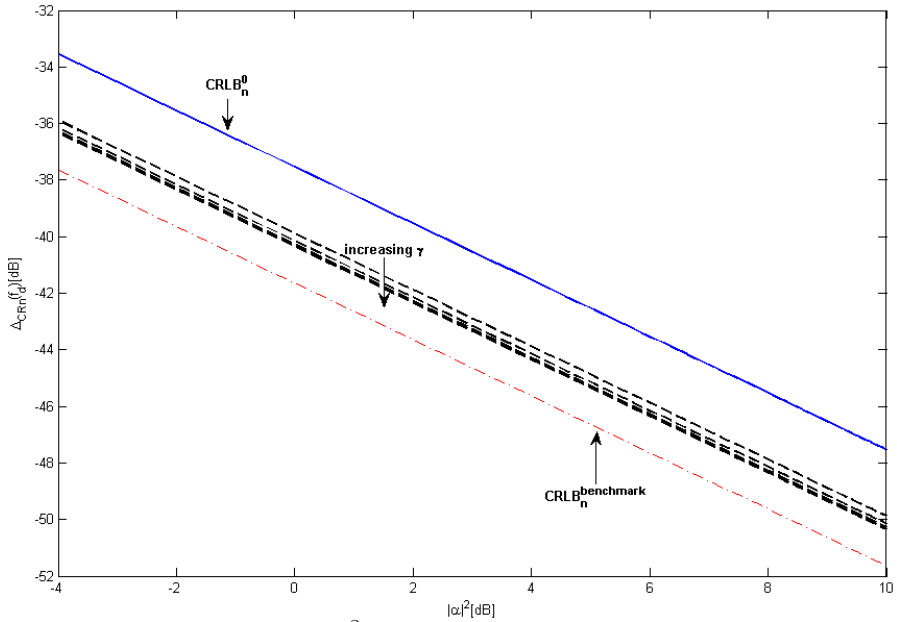

Figure 2.7: **(b)** CRLB$_n$ versus $|\alpha|^2$ for non-fluctuating target, $P_{fa} = 10^{-6}$, $N = 7$, $\epsilon = 0.1561$ and $\gamma = \{0.05; 0.4; 1; 3; 6.5; 10\}$. Generalized Barker code (solid curve). Designed codes (dashed curves). Benchmark code (dash-dotted curve).

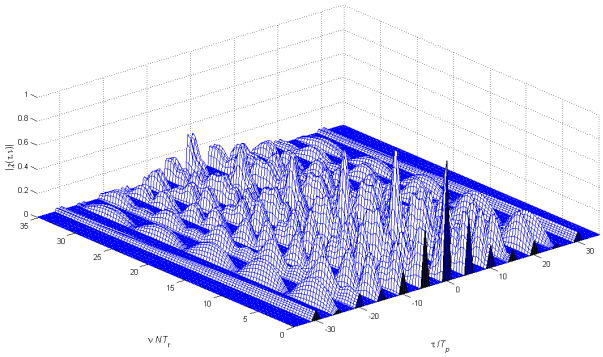

Figure 2.8: (a) Ambiguity function modulus of the designed code with $N = 7$, $T_r = 5T_p$, $\epsilon = 0.1561$ and $\gamma = 0.4$.

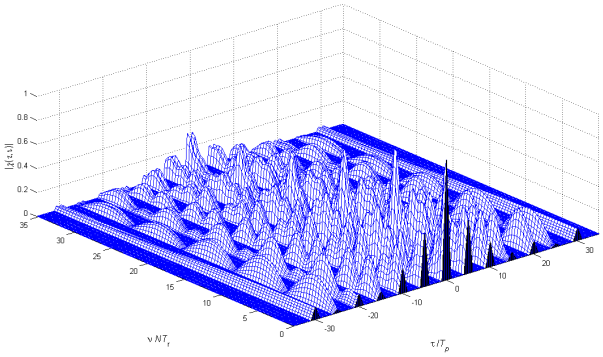

Figure 2.8: **(c)** Ambiguity function modulus of the designed code with $N = 7$, $T_r = 5T_p$, $\epsilon = 0.1561$ and $\gamma = 3$.

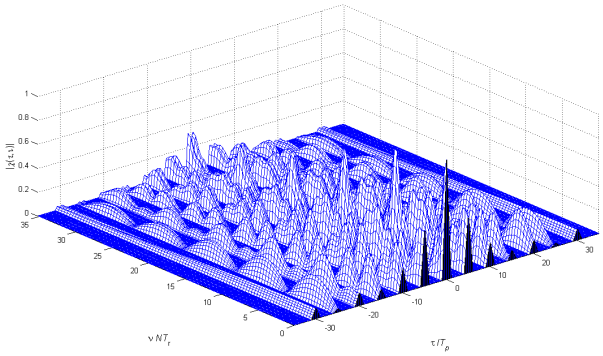

Figure 2.8: **(b)** Ambiguity function modulus of the designed code with $N = 7$, $T_r = 5T_p$, $\epsilon = 0.1561$ and $\gamma = 1$.

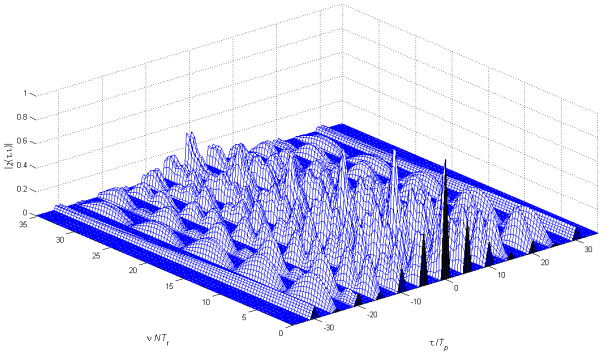

Figure 2.8: **(d)** Ambiguity function modulus of the designed code with $N = 7$, $T_r = 5T_p$, $\epsilon = 0.1561$ and $\gamma = 10$.

2.5 Conclusions

In this chapter, we have considered radar waveform design, in the presence of colored Gaussian disturbance, forcing an energy and a similarity constraints. The considered design criterion has been the joint constrained optimization of the detection performance and CRLB on Doppler estimation accuracy. The problem has been formulated in terms of a non-convex multi-objective optimization problem with two quadratic constraints. Hence, radar codes been have constructed as Pareto-optimal points of the aforementioned problem through the scalarization procedure.

At the analysis stage, we have evaluated the performance of the new algorithm in terms of detection performance, CRLB for Doppler estimation accuracy, and ambiguity function. Additionally, the Pareto-optimal curve has been studied showing the effects of the Pareto weight on the performance trade-off. Finally, we have also analyzed the impact of the similarity constraint on the performance, for a given value of the Pareto weight.

Possible future research tracks might concern the extension of the framework to situations where it is necessary to optimize more than two objectives (performance measures) and/or where it is necessary to force additional con-

straints on the structure of the radar waveform.

Chapter 3

Knowledge-Aided Transmit Signal and Receive Filter Design in Signal-Dependent Clutter

3.1 Introduction

Several papers, concerning radar waveform diversity and optimized receive filter design, have appeared in open radar literature during the last five decades. Such interest can be justified by the stressing performance requirements in terms of range-Doppler resolution, target tracking, and capability of clutter rejection with low sidelobes signals/filters, often imposed by defense applications in areas such as airborne early warning and homeland security [32, 33, 40]. Besides, new computing architectures, high speed and Off The Shelf (OTS) processors, digital arbitrary waveform generators, and solid state transmitters have paved the way for an increased capability, actually unthink-

able some years ago, to perform very complex and effective signal processing [41, Ch. 6, 11, 25]. As a consequence, new frontiers have been opened for radar signal processing such as the recent success story of the knowledge-aided paradigm (see [42], [43], and [44]). It suggests that a smart use of some a-priori information about the operating environment, when processing the received signal and designing the transmitted waveform, can lead to sensible performance improvements in the detection, classification, and tracking process. Following this processing philosophy, it is of primary importance the design of advanced algorithms, that, using a-priori knowledge sources (as for instance location of electromagnetic interferences, reflectivity characteristic of the environment, and weather conditions) adapt the synthesized transmit waveform and the receive filter to the operating environment.

Radar performance improvement through waveform optimization has been an ongoing topic of research since 1965, when H. Van Trees, in [45, 46], observed that a suitable transmitted waveform is more important than optimum receiver design, remarking that "the most effective way (within the limitations of our model) to combat reverberation is through proper signal design". Since then, many efforts have been directed, among radar community, towards

radar performance optimization through waveform diversity. Two research lines have been developed.

The former is focused on the signal-independent interference and well models, but is not limited to, radar environments where the main contribution to the disturbance is represented by system noise, and/or intentional interference (jammers), and/or unintentional emissions from telecommunication apparatuses, and/or terrain scattering due to signals from other radar platforms (hot clutter), [34]. The latter assumes signal-dependent disturbance, produced by the reflections of the signal, transmitted by the radar of interest, from the terrain and objects of no tactical importance within the illuminated area. Otherwise stated, this is a kind of self-induced radar interference, usually referred to as the reverberation phenomenon, due to the interaction of the transmitted wave with the scattering environment.

In the context of signal-independent noise, waveform design in the presence of colored disturbance with known covariance matrix has been addressed in [30]. The authors consider a waveform optimization problem, in an active sensing scenario, attempting to maximizing the Signal to Interference Plus Noise Ratio (SINR) at the output of the matched filter, restricting the sought

waveform to be similar to a desired signal. In [31], focusing on the class of linearly coded pulse trains (both in amplitude and in phase), the authors introduce a code selection algorithm which maximizes the detection performance but, at the same time, is capable of controlling both the region of achievable values for the Doppler estimation accuracy and the degree of similarity with a prescribed radar code. Further algorithms are also available attempting to determine the radar waveforms optimizing the detection probability under structural constraints [35] (for instance a phase-only modulation) [24] and (peak to average power ratio constraints) [47].

As to the signal-dependent clutter scenario, many papers have addressed along the years the problem of the joint transmitter-receiver design. In [48], the author devises an algorithm to find the transmit signal and the receive filter maximizing the SINR, for a point-like moving target embedded in a clutter environment produced by incoherent scatterers. Therein, an energy constraint is forced on the transmitted waveform. In [49], assuming the environment characterization of [48], dynamic range constraints on the transmitted waveform are added to the optimization problem. The resulting iterative algorithm, converges to a solution signal satisfying the Kuhn-Tucker conditions, which

are necessary for optimality, [50]. Implementation errors [49], amplitude and phase modulation limitations [51], and quantization error effects [52], have also been considered, modifying the procedure of [48]. In [53], considering a stochastic Gaussian extended target and modeling the signal-dependent noise as the output of a random Linear-Time-Invariant (LTI) filter (whose impulse response is assumed a realization of a stationary Gaussian random process), the transmitted waveform has been optimized forcing an energy constraint and considering as figure of merit both the SINR and the Mutual Information. In [54] and [55], the authors provide an analytical solution to the problem of optimizing the transmitted signal power spectrum so as to maximizing the detection performance of the optimal detector for a zero-Doppler Gaussian point-like target in the presence of signal-dependent clutter, still modeled as the output of a stochastic LTI filter with a stationary Gaussian impulse response. Finally, in [56], the author generalizes his results in [54] and [55] to a spatial-temporal processing resorting to the concept of the frequency-wavenumber spectrum.

In this report, we still deal with the joint design of the transmit signal and receive filter for a radar system, which operates in a high reverberant environ-

ment. Specifically, considering as figure of merit the SINR (no assumptions are made concerning the multivariate statistical characterization of the disturbance), we optimize both the radar code and the receive filter assuming a point-like moving target embedded in a clutter environment produced by incoherent scatterers. Other than an energy constraint, a similarity constraint is enforced on the transmitted radar signal, in order to control some relevant characteristics of the waveform, such as range-Doppler resolution, variations in the signal modulus, and peak sidelobe level.

We suppose that the radar system has access to an environmental (possibly dynamical) database including a geographical information system (and/or digital terrain maps) characterizing the scene to be illuminated, meteo data, and some theoretical (or possibly empirical) a-priori electromagnetic reflectivity (σ_0) and spectral clutter models allowing the prediction of the actual scattering environment. Hence, we devise an optimization procedure for the transmit signal and the receive filter which sequentially improves the SINR. Each iteration of the algorithm, whose convergence is analytically proved, requires the solution of both a convex and an hidden convex optimization problem. The resulting computational complexity is linear with the number of iterations and poly-

nomial with the receive filter length. The performance of the new algorithm is analyzed in two scenarios: homogeneous terrain as well as mixed land and sea clutter environment. The results show that significant SINR improvements can be obtained jointly optimizing the transmitter and the receiver.

The chapter is organized as follows. In Section 3.2, we describe the model for the transmitted signal, the received signal, and the signal-dependent clutter. In Section 3.3, we formulate the constrained optimization problem for the design of the radar code and the receive filter. Moreover, we propose a sequential optimization procedure, whose convergence properties are thoroughly studied, to find a good solution for the considered problem. In Section 3.4, we assess the performance of the proposed algorithm, and analyze the trade-off between the achievable SINR and the shape of the waveform ambiguity function. Finally, in Section 3.5, we draw conclusions and outline some possible future research tracks.

3.1.1 Notation

We adopt the notation of using boldface for vectors $\boldsymbol{a}$ (lower case), and matrices $\boldsymbol{A}$ (upper case). The transpose and the conjugate transpose operators are denoted by the symbols $(\cdot)^T$ and $(\cdot)^\dagger$ respectively. tr$(\cdot)$, rank$(\cdot)$, and $\lambda_{min}(\cdot)$ are respectively the trace, the rank, and the minimum eigenvalue of the square matrix argument. $\boldsymbol{I}$ and $\mathbf{0}$ denote respectively the identity matrix and the matrix with zero entries (their size is determined from the context). $\mathbb{R}^N$, $\mathbb{C}^N$, and $\mathbb{H}^N$ are respectively the sets of N-dimensional vectors of real numbers, the sets of N-dimensional vectors of complex numbers, and $N \times N$ Hermitian matrices. The curled inequality symbol $\succeq$ (and its strict form $\succ$) is used to denote generalized matrix inequality: for any $\boldsymbol{A} \in \mathbb{H}^N$, $\boldsymbol{A} \succeq \mathbf{0}$ means that $\boldsymbol{A}$ is a positive semidefinite matrix ($\boldsymbol{A} \succ \mathbf{0}$ for positive definiteness). The Euclidean norm of the vector $\boldsymbol{x}$ is denoted by $\|\boldsymbol{x}\|$. The letter j represents the imaginary unit (i.e. $j = \sqrt{-1}$), while the letter i often serves as index in this chapter. For any complex number x, we use $\Re(x)$ and $\Im(x)$ to denote respectively the real and the imaginary part of x, $|x|$ and arg(x) represent the modulus and the argument of x, and x^* is the conjugate of x. $\mathbb{E}[\cdot]$ denotes the statistical expectation. Finally, $\odot$ denotes the Hadamard product and for any optimization problem $\mathcal{P}$, $v(\mathcal{P})$

represents its optimal value.

3.2 System Model

We consider a monostatic radar system which transmits a coherent burst of N pulses. Let us denote by $\boldsymbol{s} = [s(1), s(2), \ldots, s(N)]^T \in \mathbb{C}^N$ the radar code, that we assume with unit norm. The waveform at the receiver end is down-converted to baseband, undergoes a pulse matched filtering operation, and then is sampled. The N-dimensional column vector $\boldsymbol{v} = [v(1), v(2), \ldots, v(N)]^T \in \mathbb{C}^N$ of the observations, from the range-azimuth cell under test, can be expressed as:

$$\boldsymbol{v} = \alpha_T \boldsymbol{s} \odot \boldsymbol{p}(\nu_{d_T}) + \boldsymbol{c} + \boldsymbol{n}, \tag{3.1}$$

with α_T a complex parameter accounting for channel propagation and backscattering effects from the target within the range-azimuth bin of interest, $\boldsymbol{p}(\nu_{d_T}) = [1, e^{j2\pi\nu_{d_T}}, \ldots, e^{j2\pi(N-1)\nu_{d_T}}]^T$ the temporal steering vector, ν_{d_T} the normalized target Doppler frequency, $\boldsymbol{c}$ the N-dimensional column vector containing the filtered clutter samples, and $\boldsymbol{n}$ the N-dimensional column vector of the filtered noise samples.

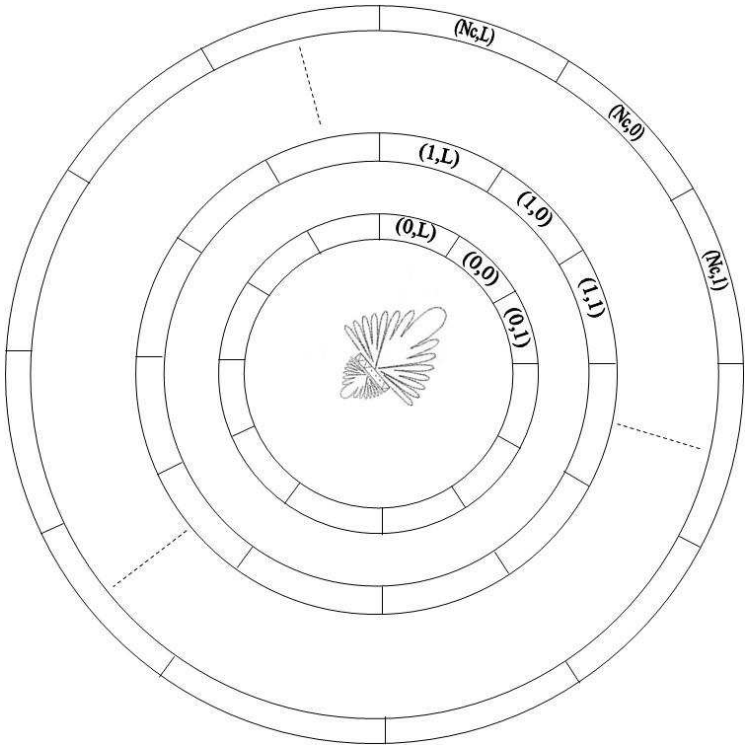

Figure 3.1: Range-azimuth bins of the illuminated area around the radar antenna pattern.

The vector $\boldsymbol{c}$ is the superposition of the returns from different uncorrelated scatterers, [57], each from the $(r, i)-$th range-azimuth bin[1] as depicted in **Figure 3.1**.

[1]The model can be easily generalized to account for the presence of clutter produced by multiple sources in the same range-azimuth bin. In this case, the clutter contribution from each range-azimuth bin can be expressed through a subspace model representation, namely $\boldsymbol{H\theta}$, where $\boldsymbol{H}$ denotes the steering matrix and $\boldsymbol{\theta}$ the vector of the backscattering complex amplitudes from each clutter source. In the following, we will focus on the single clutter source scenario even though the generalization to multiple sources is straightforward.

Specifically, the clutter vector $\boldsymbol{c}$ can be written as:

$$\boldsymbol{c} = \sum_{r=1}^{N_c-1} \sum_{i=0}^{L-1} \alpha_{(r,i)} \boldsymbol{J}_r \left(\boldsymbol{s} \odot \boldsymbol{p}(\nu_{d_{(r,i)}}) \right) + \sum_{i=0}^{L-1} \alpha_{(0,i)} \boldsymbol{c} \odot \boldsymbol{p}(\nu_{d_{(0,i)}}) \tag{3.2}$$

where $N_c \leq N$ is the number of range rings that interfere with the range-azimuth bin of interest $(0,0)$, L is the number of discrete azimuth sectors, $\alpha_{(r,i)}$ and $\nu_{d_{(r,i)}}$ are, respectively, the echo and the normalized Doppler frequency of the scatterer in the range-azimuth bin (r,i); furthermore, $\forall r \in \{1,\ldots,N-1\}$

$$\boldsymbol{J}_r(l,m) = \begin{cases} 1 \quad \text{if} \quad l-m=r \\ \\ 0 \quad \text{if} \quad l-m \neq r \end{cases} \qquad (l,m) \in \{1,\ldots,N\}^2$$

denotes the shift matrix, and $\boldsymbol{J}_{-r} = \boldsymbol{J}_r^T$. Notice that eq. (3.2), explicitly shows the functional dependence of the disturbance component over the transmitted signal $\boldsymbol{s}$ which modulates the temporal steering vector of each scatterer in the reverberant environment. Then, the return from an isolated point-like reflector is scaled by the backscattering amplitude $\alpha_{(r,i)}$ and time-shifted through the operator $\boldsymbol{J}_r$ so as to account for the specific range position. Finally, all the

contributions add together in the summation of eq. (3.2).

As to the characterization of the noise vector $\boldsymbol{n}$, we assume that it is a zero-mean white noise, i.e.:

$$\mathbb{E}[\boldsymbol{n}] = 0, \qquad \mathbb{E}\left[\boldsymbol{n}\boldsymbol{n}^{\dagger}\right] = \sigma_n^2 \boldsymbol{I}.$$

Let us analyze the characterization of the clutter vector $\boldsymbol{c}$. As previously stated, we suppose that the scatterers are uncorrelated; moreover, for each scatterer, we denote by $\sigma^2_{(r,i)} = \mathbb{E}\left[|\alpha_{(r,i)}|^2\right]$, assume that the expected value of its complex amplitude is zero[2], i.e. $\mathbb{E}\left[\alpha_{(r,i)}\right] = 0$, and that its normalized Doppler frequency is uniformly distributed around a mean Doppler frequency $\bar{\nu}_{d_{(r,i)}}$, i.e. $\nu_{d_{(r,i)}} \sim \mathcal{U}\left(\bar{\nu}_{d_{(r,i)}} - \frac{\epsilon_{(r,i)}}{2}, \bar{\nu}_{d_{(r,i)}} + \frac{\epsilon_{(r,i)}}{2}\right)$. As a consequence, we have:

$$\mathbb{E}[\boldsymbol{c}] = 0,$$

and

$$\boldsymbol{\Sigma}_{\boldsymbol{C}}(\boldsymbol{s}) = \mathbb{E}\left[\boldsymbol{c}\boldsymbol{c}^{\dagger}\right] = \sum_{r=1}^{N_c-1} \sum_{i=0}^{L-1} \sigma^2_{(r,i)} \boldsymbol{J}_r \boldsymbol{\Gamma}(\boldsymbol{s},(r,i)) \boldsymbol{J}_r^T + \sum_{i=0}^{L-1} \sigma^2_{(0,i)} \boldsymbol{\Gamma}(\boldsymbol{s},(0,i)), \tag{3.3}$$

[2]This is a reasonable assumption since $\arg(\alpha_{(r,i)})$ is accurately modeled as statistically independent of $|\alpha_{(r,i)}|$ and uniformly distributed in the interval $[-\frac{1}{2},\frac{1}{2}]$, i.e. $\arg(\alpha_{(r,i)}) \sim \mathcal{U}\left(-\frac{1}{2},\frac{1}{2}\right)$.

where $\mathbf{\Gamma}(\boldsymbol{s},(r,i)) = \mathrm{diag}\{\boldsymbol{s}\}\mathbf{\Phi}_{\epsilon_{(r,i)}}^{\bar{\nu}_{d_{(r,i)}}}\mathrm{diag}\{\boldsymbol{s}\}^{\dagger}$ with

$$\mathbf{\Phi}_{\epsilon}^{\bar{\nu}_d}(l,m) = \begin{cases} 1 & \text{if} \quad l = m \\ e^{(j2\pi\bar{\nu}_d(l-m))}\frac{\sin[\pi\epsilon(l-m)]}{[\pi\epsilon(l-m)]} & \text{if} \quad l \neq m \end{cases} \qquad (l,m) \in \{1,\ldots,N\}^2. \tag{3.4}$$

No assumption has been done about the multivariate statistical characterization of $\boldsymbol{c}$.

Some relevant cases, which can be described and modeled according to (6.2), will be now presented. One of them assumes that, for any (r,i) range-azimuth bin, the Radar Cross Section (RCS) $\sigma_0^{(r,i)}$ of the scatterer is predicted through the interaction between a digital terrain map, such as the National Land Cover Data (NLCD), and RCS clutter models, see [58], [59], and [41, Ch. 15, 16]. Precisely, through the NLCD interrogation, we can classify the environment illuminated by the radar, and consequently we can label each (r,i) range-azimuth bin as a specific reflectivity environment. In fact, the NLCD data, [58], hierarchically distinguish the terrain in nine major classifications such as urban areas, barren land, water and so on, and each major classification is sub-grouped into 21 minor classifications such as high-intensity residen-

tial urban areas, low-intensity residential urban areas and so on. Once each range-azimuth bin has been classified, we can determine its mean RCS using a clutter model specific for that type of environment.

Let us present some relevant RCS clutter models; if the (r, i)-th range-azimuth bin is classified as a hilly ground covered with trees, the RCS can be evaluated as, [60]:

$$\sigma_0^{(r,i)} = \frac{0.00032}{\lambda} A_{(r,i)} \sin \psi_{(r,i)}$$

where λ is the radar operating wavelength, while $A_{(r,i)}$ and $\psi_{(r,i)}$ are respectively the area and the grazing angle of the (r, i)-th bin. Moreover, if the (r, i)-th range-azimuth bin is classified as sea, the RCS can be obtained from, [60]:

$$\sigma_0^{(r,i)} = \frac{10^{0.6 K_b \sin \psi_{(r,i)}}}{2.51 \times 10^6 \lambda} A_{(r,i)}$$

where K_b is the constant on the Beaufort scale showing the sea-state, λ is the radar operating wavelength, while $A_{(r,i)}$ and $\psi_{(r,i)}$ are respectively the area and the grazing angle of the (r, i)-th bin.

More reliable sea clutter models could be alternatively used, as for instance the Georgia Institute of Technology (GIT) model, which also involves meteo pa-

rameters, [61, pp. 307-308]. Other information concerning reflectivity of some terrain types such as farmland-rural, desert, heavy woods, jungle, urban, at different frequency bands and grazing angles are available in [61, Ch. 7]. Whenever $\sigma_0^{(r,i)}$ has been estimated, as previously described, we can evaluate $\sigma^2_{(r,i)}$ as:

$$\sigma^2_{(r,i)} = \sigma_0^{(r,i)} K_r |G(\theta_i)|^2, \tag{3.5}$$

where K_r is a constant accounting for the channel propagation effects, such as the free space two-way path loss and additional system losses (radar equation), θ_i is the azimuth angle of the bin (r,i), and $G(\theta)$ is the one-way antenna gain for the angle θ[3].

Another interesting scenario, that can be modeled according to (6.2), encompasses the situation of a uniform scattering field corresponding to $\sigma_0 = \sigma_0^{(r,i)}$, which is meaningful when no knowledge of the clutter reflectivity is available. In this case, we have:

$$\sigma^2_{(r,i)} = \sigma_0 K_r |G(\theta_i)|^2, \tag{3.6}$$

[3]We are considering, for notational simplicity, a two-dimensional scenario (the generalization to the three-dimensional case is straightforward).

where, again, K_r is a constant accounting for the channel propagation effects, such as the free space two-way path loss and additional system losses (radar equation), θ_i is the azimuth angle of the bin (r, i), and $G(\theta)$ is the one-way antenna gain for the angle θ. In this setting, the basic parameters to characterize the second order statistical properties of the overall disturbance vector $\boldsymbol{c} + \boldsymbol{n}$ are the uncertainty ϵ on the clutter Doppler extension, the radiation pattern of the exploited antenna, and the Clutter to Noise Ratio (CNR), defined as:

$$\text{CNR} = \frac{\sigma_0}{\sigma_n^2},$$

whose value can be accurately estimated starting from some secondary data or clutter maps, [62].

To define the mean clutter Doppler frequency $\bar{\nu}_{d_{(r,i)}}$ and the uncertainty $\epsilon_{(r,i)}$ on the clutter Doppler extension of the (r, i)-th range-azimuth bin, a meaningful criterion is to set $\bar{\nu}_{d_{(r,i)}}$ equal to the frequency peak of the Power Spectral Density (PSD) of the clutter random process (characterizing the $(r, i)-$th bin) and to take $\epsilon_{(r,i)}$ equal to the $90/95-$percent power bandwidth, whose values can be obtained through a-priori models for the clutter spectrum. Again, we can make use of NLCD to classify each bin and, consequently, to determine an

adequate model of its PSD. For instance, it has been shown in [63], [14] that the exponential model for the PSD is one of the most accurate approximations of the windblown ground-clutter spectral measurements. It is given by:

$$S(f) = {\sigma_0}^g \left[\frac{d}{1+d}\delta(f) + \frac{1}{1+d}\frac{\beta\lambda}{4}\exp\left(-\frac{\beta\lambda}{2}|f|\right)\right]$$

where

1. $\delta(f)$ is the Dirac delta function;
2. d represents the Direct Current (DC) to Alternate Current (AC) ratio, which can be estimated [63] as $d = 489.8w^{-1.55}f_0^{1.21}$, where w is the wind speed in miles per hour (mi/h), and f_0 is the radar carrier frequency;
3. λ is the radar operating wavelength, expressed in meters;
4. β is the shape parameter, a function of the wind condition [63] through the relationship $\beta^{-1} = 0.1048\,(\log_{10} w + 0.4147)$.

Furthermore, in the case of sea clutter, it has been shown in [64] that the PSD can be roughly approximated as:

$$S(f) = {\sigma_0}^s \frac{1}{f_e\sqrt{\pi}}\exp\left[-\frac{(f-f_G)^2}{f_e}\right]$$

where

1. f_G is the peak of the Gaussian function, accounting for the mean Doppler frequency;

2. f_e is the Doppler spectrum width.

Typical values of f_G and f_e are reported in the tables given in [64].

Summarizing, the average clutter statistical parameters can be obtained jointly using geographical information, meteo measurements, and statistical (possibly empirical) models for the clutter RCS and PSD.

3.3 Problem formulation and Design Issues

We deal with the design of a radar code and a receive filter in order to maximize the SINR under some constraints on the shape of the code. Specifically, assuming that the vector of observations $\boldsymbol{v}$ is filtered through $\boldsymbol{w}$, the SINR at the output of the filter[4] can be written as:

$$\text{SINR} = \frac{|\alpha_T|^2 \left| \boldsymbol{w}^\dagger \left(\boldsymbol{s} \odot \boldsymbol{p}(\nu_{d_T}) \right) \right|^2}{\boldsymbol{w}^\dagger \boldsymbol{\Sigma_C}\left(\boldsymbol{s}\right) \boldsymbol{w} + \sigma_n^2 \|\boldsymbol{w}\|^2} \tag{3.7}$$

[4]Obviously, we assume that $\boldsymbol{w} \neq \boldsymbol{0}$

where $|\alpha_T|^2 \left|\boldsymbol{w}^\dagger(\boldsymbol{s} \odot \boldsymbol{p}(\nu_{d_T}))\right|^2$ is the useful energy at the output of the filter, $\sigma_n^2 \|\boldsymbol{w}\|^2$ and $\boldsymbol{w}^\dagger \boldsymbol{\Sigma_C}(\boldsymbol{s})\, \boldsymbol{w}$ represents respectively the noise and the clutter energy at the output of the filter. Notice that the clutter energy $\boldsymbol{w}^\dagger \boldsymbol{\Sigma_C}(\boldsymbol{s})\, \boldsymbol{w}$ functionally depends both on the receive processing $\boldsymbol{w}$ and the transmitted waveform through $\boldsymbol{\Sigma_C}(\boldsymbol{s})$ (namely it is a quartic polynomial in variables $\boldsymbol{w}$ and $\boldsymbol{s}$). This observation represents the main difference between a signal-dependent and a signal-independent environment where the output clutter energy is only a function of $\boldsymbol{w}$, being a homogeneous quadratic form in the variable $\boldsymbol{w}$.

An important remark is now necessary. For a standard radar processing, exploiting a fixed transmitted waveform $\bar{\boldsymbol{s}}$ and a matched filter receiver $\bar{\boldsymbol{s}} \odot \boldsymbol{p}(\nu_{d_T})$, the SINR becomes:

$$\mathrm{SINR}_{MF} = \frac{|\alpha_T|^2}{\bar{\boldsymbol{s}}^\dagger \left[\mathrm{diag}\left(\boldsymbol{p}(\nu_{d_T})^*\right) \boldsymbol{\Sigma_C}(\bar{\boldsymbol{s}})\, \mathrm{diag}\left(\boldsymbol{p}(\nu_{d_T})\right) + \sigma_n^2 \boldsymbol{I}\right] \bar{\boldsymbol{s}}}. \tag{3.8}$$

Moreover, since (6.3) can be upper-bounded by

$$\mathrm{SINR}_{UB} = \frac{|\alpha_T|^2}{\sigma_n^2 + \min\limits_{\boldsymbol{s}, \|\boldsymbol{s}\|=1} \lambda_{min}\left(\boldsymbol{\Sigma_C}(\boldsymbol{s})\right)}, \tag{3.9}$$

the following order relation holds true

$$\text{SINR}_{UB} \geq \max_{\boldsymbol{w},\boldsymbol{s}} \text{SINR} \geq \text{SINR}_{MF}. \tag{3.10}$$

It defines the region of potential performance improvements (in terms of SINR) which can be potentially achieved by an algorithm of joint transmitter/receiver design with respect to the classic processing. Evidently, the size of the interval $[\text{SINR}_{UB}, \text{SINR}_{MF}]$ depends on the specific environment (through the matrix $\boldsymbol{\Sigma_C}(\boldsymbol{s})$). If $\boldsymbol{\Sigma_C}(\boldsymbol{s})$ is proportional to the identity matrix then $\text{SINR}_{UB} = \text{SINR}_{MF}$, confirming the optimality of the matched filter in a white interference scenario.

To develop our SINR optimization algorithm, we introduce the following technical Lemma providing an alternative expression of the SINR.

Lemma 3.3.1. *An equivalent expression of the SINR is given by:*

$$SINR = \frac{|\alpha_T|^2 \left| \boldsymbol{s}^T \left(\boldsymbol{w}^* \odot \boldsymbol{p}(\nu_{d_T}) \right) \right|^2}{\boldsymbol{s}^T \boldsymbol{\Theta_C}(\boldsymbol{w}) \boldsymbol{s}^* + \sigma_n^2 \|\boldsymbol{w}\|^2} \tag{3.11}$$

where:

$$\boldsymbol{\Theta_C}(\boldsymbol{w}) = \sum_{r=1}^{N_c-1} \sum_{i=0}^{L-1} \sigma_{(r,i)}^2 \text{diag}\{\boldsymbol{J}_{-r}\boldsymbol{w}^*\} \boldsymbol{\Phi}_{\epsilon_{(r,i)}}^{\bar{\nu}_{d_{(r,i)}}} \text{diag}\{\boldsymbol{J}_{-r}\boldsymbol{w}\} + \sum_{i=0}^{L-1} \sigma_{(0,i)}^2 \text{diag}\{\boldsymbol{w}^*\} \boldsymbol{\Phi}_{\epsilon_{(0,i)}}^{\bar{\nu}_{d_{(0,i)}}} \text{diag}\{\boldsymbol{w}\}$$

Proof. See Appendix 3.6.1. □

As to the shape of the code, we assume that $\|\boldsymbol{s}\|^2 = 1$, to account for the finite energy transmitted by the radar. Moreover, a similarity constraint, [30], is enforced

$$\|\boldsymbol{s} - \boldsymbol{s}_0\|^2 \leq \delta\,, \tag{3.12}$$

where the parameter $\delta \geq 0$ rules the size of the similarity region and $\boldsymbol{s}_0$ ia a prefixed code. There are several reasons that justify the use of a similarity constraint in the design of a radar code. In fact, a code which optimizes the SINR at the output of the receiving filter does not provide any kind of control on the shape of the resulting coded waveform. Precisely, the unconstrained optimization of SINR can lead to signals with significant modulus variations, poor range resolution, high peak sidelobe levels, and more in general with an undesired ambiguity function behavior. These drawbacks can be partially circumvented imposing the similarity constraint (6.5) to the sought radar code. By doing so, it is required the solution to be similar to a known code $\boldsymbol{s}_0$ ($\|\boldsymbol{s}_0\|^2 = 1$), which shares some nice properties such as constant modulus, reasonable range resolution, and peak sidelobe level. In other words, imposing (6.5), it is possible to indirectly control the ambiguity function of the considered

coded pulse train: the smaller δ the higher the degree of similarity between the ambiguity functions of the designed radar code and $\boldsymbol{s}_0$.

Resorting to the previously mentioned guidelines and definitions, the joint design of the radar code and the receive filter can be formulated as the following constrained optimization problem:

$$\mathcal{P} \begin{cases} \max\limits_{\boldsymbol{s},\boldsymbol{w}} & \dfrac{|\alpha_T|^2 \left|\boldsymbol{w}^\dagger \left(\boldsymbol{s} \odot \boldsymbol{p}(\nu_{d_T})\right)\right|^2}{\boldsymbol{w}^\dagger \boldsymbol{\Sigma_C}\left(\boldsymbol{s}\right) \boldsymbol{w} + \sigma_n^2 \|\boldsymbol{w}\|^2} \\ \text{s.t.} & \|\boldsymbol{s}\|^2 = 1 \\ & \|\boldsymbol{s} - \boldsymbol{s}_0\|^2 \leq \delta, \end{cases} . \tag{3.13}$$

Problem $\mathcal{P}$ is a non-convex optimization problem (the objective function is a non-convex function and $\|\boldsymbol{s}\|^2 = 1$ defines a non-convex set), and the technique that we adopt to find a good solution is based on a sequential optimization procedure. The idea is to iteratively optimize the SINR. Specifically, starting from a receive filter $\boldsymbol{w}^{(n-1)}$, we search for an admissible radar code $\boldsymbol{s}^{(n)}$ at step n maximizing the SINR corresponding to the receive filter $\boldsymbol{w}^{(n-1)}$. Whenever $\boldsymbol{s}^{(n)}$ is found, we search for the adaptive filter $\boldsymbol{w}^{(n)}$ which maximizes the SINR corresponding to the radar code $\boldsymbol{s}^{(n)}$, and so on. Otherwise stated, $\boldsymbol{w}^{(n)}$ is used

as starting point at step $n+1$. To trigger the procedure, the optimal receive filter $\boldsymbol{w}^{(0)}$, to an admissible code $\boldsymbol{s}^{(0)}$, is considered. From an analytical point of view, $\boldsymbol{s}^{(n)}$ and $\boldsymbol{w}^{(n)}$ are the optimal solutions of the optimization problems $\mathcal{P}_{\boldsymbol{s}}{}^{(n)}$ and $\mathcal{P}_{\boldsymbol{w}}{}^{(n)}$, respectively defined as:

$$\mathcal{P}_{\boldsymbol{s}}{}^{(n)} \begin{cases} \max\limits_{\boldsymbol{s}} & \dfrac{|\alpha_T|^2 \left| \boldsymbol{w}^{(n-1)^\dagger} \left(\boldsymbol{s} \odot \boldsymbol{p}(\nu_{d_T}) \right) \right|^2}{\boldsymbol{w}^{(n-1)^\dagger} \boldsymbol{\Sigma}_{\boldsymbol{C}} \left(\boldsymbol{s} \right) \boldsymbol{w}^{(n-1)} + \sigma_n^2 \| \boldsymbol{w}^{(n-1)} \|^2} \\ \text{s.t.} & \| \boldsymbol{s} \|^2 = 1 \\ & \| \boldsymbol{s} - \boldsymbol{s}_0 \|^2 \leq \delta \end{cases}, \tag{3.14}$$

and

$$\mathcal{P}_{\boldsymbol{w}}{}^{(n)} \begin{cases} \max\limits_{\boldsymbol{w}} & \dfrac{|\alpha_T|^2 \left| \boldsymbol{w}^\dagger \left(\boldsymbol{s}^{(n)} \odot \boldsymbol{p}(\nu_{d_T}) \right) \right|^2}{\boldsymbol{w}^\dagger \boldsymbol{\Sigma}_{\boldsymbol{C}} \left(\boldsymbol{s}^{(n)} \right) \boldsymbol{w} + \sigma_n^2 |\boldsymbol{w}|^2} \end{cases}. \tag{3.15}$$

The proposed procedure shares some interesting properties summarized in the following

Proposition 3.3.2. *Assume that problems $\mathcal{P}_{\boldsymbol{w}}{}^{(n)}$ and $\mathcal{P}_{\boldsymbol{s}}{}^{(n)}$ are solvable*[5]*. Let $\left\{ \left(\boldsymbol{s}^{(n)}, \boldsymbol{w}^{(n)} \right) \right\}$ be a sequence of points obtained through the proposed sequential optimization procedure; let SINR$^{(n)}$ be the SINR value corresponding to the point*

[5]By "solvable", we mean that the problem is feasible and bounded, and the optimal value is attained, see [29, p. 13].

$\left(\boldsymbol{s}^{(n)}, \boldsymbol{w}^{(n)}\right)$ *at the* $n-$*th iteration. Then:*

- *the sequence* $\text{SINR}^{(n)}$ *is a monotonic increasing sequence;*
- *the sequence* $\text{SINR}^{(n)}$ *converges to a finite value* $\text{SINR}^{\star}$*;*
- *starting from the sequence* $\left\{\left(\boldsymbol{s}^{(n)}, \boldsymbol{w}^{(n)}\right)\right\}$*, it is possible to construct another sequence* $\left\{\left(\tilde{\boldsymbol{s}}^{(n')}, \tilde{\boldsymbol{w}}^{(n')}\right)\right\}$*, that converges to a feasible point* $(\tilde{\boldsymbol{s}}^{\star}, \tilde{\boldsymbol{w}}^{\star})$ *of the problem* $\mathcal{P}$*, such that the SINR evaluated in* $(\tilde{\boldsymbol{s}}^{\star}, \tilde{\boldsymbol{w}}^{\star})$ *is equal to* $\text{SINR}^{\star}$*.*

Proof. See Appendix 3.6.3. □

Let us observe that, from a practical point of view, the proposed optimization procedure requires a condition to stop the iterations. There are several ways to impose it; for instance considering the maximum number of tolerable iterations, or the difference between two consecutive values of the partial optimized SINR (i.e. forcing an iteration gain constraint), or mixing them. A pictorial representation of the joint optimization process of the radar code and the receive filter, based on the available information about the clutter environment, is given in **Figure 3.2**. Precisely, through the use of a site specific (possible dynamic) environment database, which contains a geographical information system, digital terrain maps, clutter models (in terms of electromag-

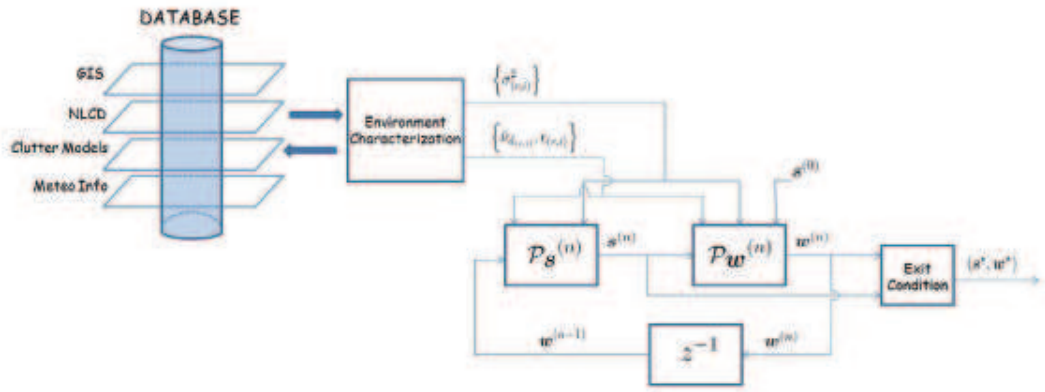

Figure 3.2: Block diagram of the proposed transmit-receive optimization procedure.

netic reflectivity and spectral density), and meteorological information, we get a description of clutter characterization in terms of $\sigma^2_{(r,i)}$, $\bar{\nu}_{d_{(r,i)}}$, and $\epsilon_{(r,i)}$ for each range-azimuth bin (r, i). Then, triggering the optimization procedure from an initial code $\boldsymbol{s}^{(0)}$, from which we obtain the adaptive filter $\boldsymbol{w}^{(0)}$, we sequentially optimize the SINR solving $\mathcal{P}_{\boldsymbol{s}}{}^{(n)}$ and $\mathcal{P}_{\boldsymbol{w}}{}^{(n)}$ and obtain, at the step n, $\left(\boldsymbol{s}^{(n)}, \boldsymbol{w}^{(n)}\right)$. The process continues until the exit condition is satisfied, returning the radar code $\boldsymbol{s}^{\star}$ and the receive filter $\boldsymbol{w}^{\star}$.

***Remark*:** The same optimization problem is obtained resorting to Information Theoretic arguments, namely optimizing, under the same constraints as in problem $\mathcal{P}$ (6.6), a lower bound to the Mutual Information (MI), see [65], between the received observations v and the complex backscattering target

amplitude α_T. See Appendix 3.6.4 for the detailed discussion and analysis.

The next subsections will be devoted to the study of the optimization problems $\mathcal{P}_{\boldsymbol{w}}{}^{(n)}$ and $\mathcal{P}_{\boldsymbol{s}}{}^{(n)}$ required for implementing the sequential optimization procedure.

3.3.1 Receive Filter Optimization: Solution of the Problem $\mathcal{P}_{\boldsymbol{w}}{}^{(n)}$

In this subsection, a relevant property of problem $\mathcal{P}_{\boldsymbol{w}}{}^{(n)}$ is analyzed. Precisely, we show that $\mathcal{P}_{\boldsymbol{w}}{}^{(n)}$ is solvable and find a closed form optimal solution $\boldsymbol{w}^{(n)}$, for any $\boldsymbol{s}^{(n)}$.

Lemma 3.3.3. *To find an optimal solution of $\mathcal{P}_{\boldsymbol{w}}{}^{(n)}$, it is sufficient to solve $\mathcal{P}_1$, given by:*

$$\mathcal{P}_1 \begin{cases} \min\limits_{\boldsymbol{w}} \quad \boldsymbol{w}^\dagger \boldsymbol{\Sigma}_{\boldsymbol{C}}\left(\boldsymbol{s}^{(n)}\right)\boldsymbol{w} + \sigma_n^2\|\boldsymbol{w}\|^2 \\ \\ \textit{s.t.} \quad \Re(\boldsymbol{w}^\dagger\left(\boldsymbol{s}^{(n)} \odot \boldsymbol{p}(\nu_{d_T})\right)) = 1 \end{cases} . \tag{3.16}$$

i.e. given an optimal solution $\boldsymbol{w}^\star$ of $\mathcal{P}_1$, $\boldsymbol{w}^\star$ is also an optimal solution of $\mathcal{P}_{\boldsymbol{w}}{}^{(n)}$.

Proof. See Appendix 3.6.7. □

From Lemma 3.3.3 and [66], an optimal solution of $\mathcal{P}_{\boldsymbol{w}^{(n)}}$ is given by:

$$\boldsymbol{w}^{(n)} = \frac{\left(\boldsymbol{\Sigma_C}\left(\boldsymbol{s}^{(n)}\right) + \sigma_n^2\boldsymbol{I}\right)^{-1}}{\left(\boldsymbol{s}^{(n)} \odot \boldsymbol{p}(\nu_{d_T})\right)^{\dagger}\left(\boldsymbol{\Sigma_C}\left(\boldsymbol{s}^{(n)}\right) + \sigma_n^2\boldsymbol{I}\right)^{-1}\left(\boldsymbol{s}^{(n)} \odot \boldsymbol{p}(\nu_{d_T})\right)}\left(\boldsymbol{s}^{(n)} \odot \boldsymbol{p}(\nu_{d_T})\right), \quad (3.17)$$

from which it is evident the dependence of $\boldsymbol{w}^{(n)}$ on $\boldsymbol{s}^{(n)}$ and the steering vector $\boldsymbol{p}(\nu_{d_T})$.

3.3.2 Radar Code optimization: Solution of the Problem $\mathcal{P}_{\boldsymbol{s}^{(n)}}$

In this subsection, the main properties of problem $\mathcal{P}_{\boldsymbol{s}^{(n)}}$ are analyzed. Specifically, we prove that the problem is solvable and describe an algorithm that finds an optimal solution of $\mathcal{P}_{\boldsymbol{s}^{(n)}}$. Firstly, using Lemma 6.3.1, $\mathcal{P}_{\boldsymbol{s}^{(n)}}$ is equivalent to $\mathcal{P}_2$:

$$\mathcal{P}_2 \begin{cases} \max\limits_{\boldsymbol{s}} & \dfrac{\left|\boldsymbol{s}^T\left(\boldsymbol{w}^{(n-1)^*} \odot \boldsymbol{p}(\nu_{d_T})\right)\right|^2}{\boldsymbol{s}^T\boldsymbol{\Theta_C}\left(\boldsymbol{w}^{(n-1)}\right)\boldsymbol{s}^* + \sigma_n^2\|\boldsymbol{w}^{(n-1)}\|^2} \\ \text{s.t.} & \|\boldsymbol{s}\|^2 = 1 \\ & \|\boldsymbol{s} - \boldsymbol{s}_0\|^2 \leq \delta. \end{cases} \quad (3.18)$$

This is a fractional quadratic problem and to solve it we follow the guidelines in [67]. Now, let us indicate with

$$\boldsymbol{S} = \left(\boldsymbol{w}^{(n-1)} \odot \boldsymbol{p}(\nu_{d_T})^*\right) \left(\boldsymbol{w}^{(n-1)} \odot \boldsymbol{p}(\nu_{d_T})^*\right)^\dagger$$

and

$$\boldsymbol{M} = \boldsymbol{\Theta}_{\boldsymbol{C}} \left(\boldsymbol{w}^{(n-1)}\right)^* + \sigma_n^2 \|\boldsymbol{w}^{(n-1)}\|^2 \boldsymbol{I}.$$

The homogenized version of $\mathcal{P}_2$ is

$$
\mathcal{P}_2' \left\{ \begin{array}{ll}
\underset{\boldsymbol{p},\, t}{\max} & \dfrac{\operatorname{tr}\left(\begin{bmatrix} \boldsymbol{S} & \boldsymbol{0} \\ \boldsymbol{0} & 0 \end{bmatrix}\begin{bmatrix} \boldsymbol{s}\boldsymbol{s}^\dagger & \boldsymbol{s}t^* \\ \boldsymbol{s}^\dagger t & |t|^2 \end{bmatrix}\right)}{\operatorname{tr}\left(\begin{bmatrix} \boldsymbol{M} & \boldsymbol{0} \\ \boldsymbol{0} & 0 \end{bmatrix}\begin{bmatrix} \boldsymbol{s}\boldsymbol{s}^\dagger & \boldsymbol{s}t^* \\ \boldsymbol{s}^\dagger t & |t|^2 \end{bmatrix}\right)} \\
\text{s.t.} & \operatorname{tr}\left(\begin{bmatrix} \boldsymbol{I} & -\boldsymbol{s}_0 \\ -\boldsymbol{s}_0^\dagger & \|\boldsymbol{s}_0\|^2 - \delta \end{bmatrix}\begin{bmatrix} \boldsymbol{s}\boldsymbol{s}^\dagger & \boldsymbol{s}t^* \\ \boldsymbol{s}^\dagger t & |t|^2 \end{bmatrix}\right) \leq 0 \\
& \operatorname{tr}\left(\begin{bmatrix} \boldsymbol{I} & \boldsymbol{0} \\ \boldsymbol{0} & 0 \end{bmatrix}\begin{bmatrix} \boldsymbol{s}\boldsymbol{s}^\dagger & \boldsymbol{s}t^* \\ \boldsymbol{s}^\dagger t & |t|^2 \end{bmatrix}\right) = 1 \\
& \operatorname{tr}\left(\begin{bmatrix} \boldsymbol{0} & \boldsymbol{0} \\ \boldsymbol{0} & 1 \end{bmatrix}\begin{bmatrix} \boldsymbol{s}\boldsymbol{s}^\dagger & \boldsymbol{s}t^* \\ \boldsymbol{s}^\dagger t & |t|^2 \end{bmatrix}\right) = 1 \\
& \boldsymbol{s} \in \mathbb{C}^N,\, t \in \mathbb{C}.
\end{array} \right. \tag{3.19}
$$

Problems $\mathcal{P}_2$ and $\mathcal{P}_2'$ are clearly equivalent. In fact, it is evident that $v(\mathcal{P}_2) \leq v(\mathcal{P}_2')$; on the other hand, the objective function of $\mathcal{P}_2$ evaluated at $\boldsymbol{s}^\star/t^\star$ is equal to the optimal value of $\mathcal{P}_2'$, provided that $(\boldsymbol{s}^\star, t^\star)$ is an optimal solution for $\mathcal{P}_2'$. The SemiDefinite Programming (SDP), see [29], relaxation of the problem $\mathcal{P}_2'$, obtained dropping the rank-one constraint, is problem $\mathcal{P}_3$:

$$\mathcal{P}_3 \begin{cases} \max\limits_{\boldsymbol{W}} & \frac{\mathrm{tr}(\boldsymbol{Q}_{-1}\boldsymbol{W})}{\mathrm{tr}(\boldsymbol{Q}_0\boldsymbol{W})} \\ \text{s.t.} & \mathrm{tr}\,(\boldsymbol{Q}_1\boldsymbol{W}) \leq 0 \\ & \mathrm{tr}\,(\boldsymbol{Q}_2\boldsymbol{W}) = 1 \\ & \mathrm{tr}\,(\boldsymbol{Q}_3\boldsymbol{W}) = 1 \\ & \boldsymbol{W} \succeq \boldsymbol{0}, \end{cases} \tag{3.20}$$

where $\boldsymbol{W} \in \mathbb{H}^{N+1}$, and the matrix $\boldsymbol{Q}_i$'s, are defined as follows:

$$\boldsymbol{Q}_{-1} = \begin{bmatrix} \boldsymbol{S} & \boldsymbol{0} \\ \boldsymbol{0} & 0 \end{bmatrix}, \boldsymbol{Q}_0 = \begin{bmatrix} \boldsymbol{M} & \boldsymbol{0} \\ \boldsymbol{0} & 0 \end{bmatrix}, \tag{3.21}$$

and

$$\boldsymbol{Q}_1 = \begin{bmatrix} \boldsymbol{I} & -\boldsymbol{s}_0 \\ -\boldsymbol{s}_0^\dagger & \|\boldsymbol{s}_0\|^2 - \delta \end{bmatrix}, \boldsymbol{Q}_2 = \begin{bmatrix} \boldsymbol{I} & \boldsymbol{0} \\ \boldsymbol{0} & 0 \end{bmatrix}, \boldsymbol{Q}_3 = \begin{bmatrix} \boldsymbol{0} & \boldsymbol{0} \\ \boldsymbol{0} & 1 \end{bmatrix}. \tag{3.22}$$

As shown in [67], the optimal solution $\boldsymbol{s}^{(n)}$ of $\mathcal{P}_2$, or equivalently of $\mathcal{P}_{2'}$, can be found in two steps. The first step consists in the solution of problem $\mathcal{P}_3$, or equivalently of the following SDP problem:

$$\mathcal{P}_4 \begin{cases} \underset{\boldsymbol{X},\ u}{\max} & \operatorname{tr}\left(\boldsymbol{Q}_{-1}\boldsymbol{X}\right) \\ \text{s.t.} & \operatorname{tr}\left(\boldsymbol{Q}_0\boldsymbol{X}\right) = 1 \\ & \operatorname{tr}\left(\boldsymbol{Q}_1\boldsymbol{X}\right) \leq 0 \\ & \operatorname{tr}\left(\boldsymbol{Q}_2\boldsymbol{X}\right) = u \\ & \operatorname{tr}\left(\boldsymbol{Q}_3\boldsymbol{X}\right) = u \\ & \boldsymbol{X} \succeq \boldsymbol{0},\ u \geq 0, \end{cases} \tag{3.23}$$

where $\boldsymbol{X} \in \mathbb{H}^{N+1}$ and $u \in \mathbb{R}$. In fact, problems $\mathcal{P}_3$ and $\mathcal{P}_4$ are solvable and have the equal optimal value; furthermore, if $(\boldsymbol{X}^\star, u^\star)$ solves $\mathcal{P}_4$, then $\boldsymbol{X}^\star/u^\star$ solves $\mathcal{P}_3$, and if $\boldsymbol{X}^\star$ solves $\mathcal{P}_3$, then $(\boldsymbol{X}^\star/\mathrm{tr}(\boldsymbol{Q}_0\boldsymbol{X}^\star), 1/\mathrm{tr}(\boldsymbol{Q}_0\boldsymbol{X}^\star))$ solves $\mathcal{P}_4$, see [67].

The second step consists in the construction of a rank-one optimal solution $\boldsymbol{x}^\star(\boldsymbol{x}^\star)^\dagger$ of $\mathcal{P}_3$, starting from $\boldsymbol{X}^\star$ (the obtained optimal solution of $\mathcal{P}_3$), resorting to a rank-one matrix decomposition theorem [68, Theorem 2.3], which is cited as the following lemma.

Lemma 3.3.4. *Let $\boldsymbol{X}$ be a non-zero $N \times N$ ($N \geq 3$) complex Hermitian positive semidefinite matrix and $\boldsymbol{A}_i$ be Hermitian matrix, $i = 1, 2, 3, 4$, and suppose that $(tr(\boldsymbol{Y}\boldsymbol{A}_1), tr(\boldsymbol{Y}\boldsymbol{A}_2), tr(\boldsymbol{Y}\boldsymbol{A}_3), tr(\boldsymbol{Y}\boldsymbol{A}_4)) \neq (0, 0, 0, 0)$ for any non-zero complex Hermitian positive semidefinite matrix $\boldsymbol{Y}$ of size $N \times N$. Then,*

- *if rank$(\boldsymbol{X}) \geq 3$, one can find, in polynomial time, a rank-one matrix $\boldsymbol{x}\boldsymbol{x}^\dagger$ such that $\boldsymbol{x}$ (synthetically denoted as $\boldsymbol{x} = \mathcal{D}_1(\boldsymbol{X}, \boldsymbol{A}_1, \boldsymbol{A}_2, \boldsymbol{A}_3, \boldsymbol{A}_4)$) is in range$(\boldsymbol{X})$, and*

$$\boldsymbol{x}^\dagger \boldsymbol{A}_i \boldsymbol{x} = tr(\boldsymbol{X}\boldsymbol{A}_i), \quad i = 1, 2, 3, 4;$$

- *if rank$(\boldsymbol{X}) = 2$, for any $\boldsymbol{z}$ not in the range space of $\boldsymbol{X}$, one can find a rank-one matrix $\boldsymbol{x}\boldsymbol{x}^\dagger$ such that $\boldsymbol{x}$ (synthetically denoted as $\boldsymbol{x} = \mathcal{D}_2(\boldsymbol{X}, \boldsymbol{A}_1, \boldsymbol{A}_2, \boldsymbol{A}_3, \boldsymbol{A}_4)$*

) is in the linear subspace spanned by $\{\boldsymbol{z}\} \cup$ *range*$(\boldsymbol{X})$*, and*

$$\boldsymbol{x}^{\dagger}\boldsymbol{A}_i\boldsymbol{x} = tr(\boldsymbol{X}\boldsymbol{A}_i)\,, \quad i = 1, 2, 3, 4.$$

Let us check the applicability of the lemma to both $\boldsymbol{X}^{\star}$ and the matrix parameters of $\mathcal{P}_3$. Indeed, the condition $N \geq 3$ is mild and practical (the number of transmitted pulses is usually greater than or equal to 3). Now, in order to verify

$$(\mathrm{tr}\,(\boldsymbol{Y}\boldsymbol{Q}_1)\,, \mathrm{tr}\,(\boldsymbol{Y}\boldsymbol{Q}_2)\,, \mathrm{tr}\,(\boldsymbol{Y}\boldsymbol{Q}_3)\,, \mathrm{tr}\,(\boldsymbol{Y}\boldsymbol{Q}_4)) \neq (0, 0, 0, 0), \text{ for any non-zero } \boldsymbol{Y} \succeq 0,$$

it suffices to prove that there is $(a_1, a_2, a_3, a_4) \in \mathbb{R}^4$ such that

$$a_1\boldsymbol{Q}_1 + a_2\boldsymbol{Q}_2 + a_3\boldsymbol{Q}_3 + a_4\boldsymbol{Q}_4 \succ \boldsymbol{0},$$

where

$$\boldsymbol{Q}_4 = \begin{bmatrix} \boldsymbol{S} - v(\mathcal{P}_3)\boldsymbol{M} & \boldsymbol{0} \\ \boldsymbol{0} & 0 \end{bmatrix}.$$

But this is evident for the matrix parameters[6] of $\mathcal{P}_4$. Since $\mathcal{P}_3$ is a relaxation of the homogenized fractional QPQC $\mathcal{P}_2'$, writing $\boldsymbol{x}^\star = \begin{bmatrix} \boldsymbol{y}^\star \\ \\ t^\star \end{bmatrix}$ the optimal solution of $\mathcal{P}_{\boldsymbol{s}^{(n)}}$ is $\boldsymbol{s}^{(n)} = \frac{\boldsymbol{y}^\star}{t^\star}$.

Algorithm 3 summarizes the procedure leading to an optimal solution $\boldsymbol{s}^{(n)}$ of $\mathcal{P}_{\boldsymbol{s}^{(n)}}$.

3.3.3 Transmit-Receive System Design: Optimization Procedure

In this subsection, the proposed sequential optimization procedure for the radar code and receive filter is summarized and schematized as **Algorithm 4**. To trigger the recursion, an initial radar code $\boldsymbol{s}^{(0)}$, from which we obtain the optimal receive filter $\boldsymbol{w}^{(0)}$, is required; a natural choice is obviously $\boldsymbol{s}^{(0)} = \boldsymbol{s}_0$.

As to the computational complexity, connected with the implementation of **Algorithm 4**, it depends on the number of iterations $\overline{N}$ as well as on and the complexity involved in each iteration. Precisely, the overall complexity is linear with respect to $\overline{N}$, while, in each iteration, it includes the computation of the

[6] In fact, taking $a_1 = a_4 = 0$ and $a_3 = a_2 = 1$, then $a_1\boldsymbol{Q}_1 + a_2\boldsymbol{Q}_2 + a_3\boldsymbol{Q}_3 + a_4\boldsymbol{Q}_4 = \boldsymbol{I} \succ \boldsymbol{0}$.

Algorithm 3 : Algorithm for Radar Code Optimization

Input: M, $\boldsymbol{S}$, $\boldsymbol{Q}_1$.

Output: An optimal solution $\boldsymbol{s}^{(n)}$ of $\mathcal{P}_{\boldsymbol{s}}{}^{(n)}$.

1: solve SDP $\mathcal{P}_4$ finding an optimal solution $(\boldsymbol{X}^\star, u^\star)$ and the optimal value $v^\star$;

2: let $\boldsymbol{X}^\star := \boldsymbol{X}^\star / u^\star$;

3: **if** Rank $(\boldsymbol{X}^\star) = 1$ **then**

4: perform an eigen-decomposition $\boldsymbol{X}^\star = \boldsymbol{x}^\star (\boldsymbol{x}^\star)^\dagger$, where $\boldsymbol{x}^\star = \begin{bmatrix} \boldsymbol{y}^\star \\ \\ t^\star \end{bmatrix}$; output $\boldsymbol{s}^{(n)^\star} := \boldsymbol{y}^\star / t^\star$ and terminate.

5: **else if** Rank $(\boldsymbol{X}^\star) = 2$ **then**

6: find $\boldsymbol{x}^\star = \mathcal{D}_2 \left(\boldsymbol{X}^\star, \begin{bmatrix} \boldsymbol{S} - v^\star \boldsymbol{M} & \boldsymbol{0} \\ \\ \boldsymbol{0} & 0 \end{bmatrix}, \begin{bmatrix} \boldsymbol{I} & -\boldsymbol{s}_0 \\ \\ -\boldsymbol{s}_0^\dagger & \|\boldsymbol{s}_0\|^2 - \delta \end{bmatrix}, \begin{bmatrix} \boldsymbol{I} & \boldsymbol{0} \\ \\ \boldsymbol{0} & 0 \end{bmatrix}, \begin{bmatrix} \boldsymbol{0} & \boldsymbol{0} \\ \\ \boldsymbol{0} & 1 \end{bmatrix} \right)$;

7: **else**

8: find $\boldsymbol{x}^\star = \mathcal{D}_1 \left(\boldsymbol{X}^\star, \begin{bmatrix} \boldsymbol{S} - v^\star \boldsymbol{M} & \boldsymbol{0} \\ \\ \boldsymbol{0} & 0 \end{bmatrix}, \begin{bmatrix} \boldsymbol{I} & -\boldsymbol{s}_0 \\ \\ -\boldsymbol{s}_0^\dagger & \|\boldsymbol{s}_0\|^2 - \delta \end{bmatrix}, \begin{bmatrix} \boldsymbol{I} & \boldsymbol{0} \\ \\ \boldsymbol{0} & 0 \end{bmatrix}, \begin{bmatrix} \boldsymbol{0} & \boldsymbol{0} \\ \\ \boldsymbol{0} & 1 \end{bmatrix} \right)$;

9: **end**

10: let $\boldsymbol{x}^\star = \begin{bmatrix} \boldsymbol{y}^\star \\ \\ t^\star \end{bmatrix}$; output $\boldsymbol{s}^{(n)} := \boldsymbol{y}^\star / t^\star$.

Algorithm 4 : Algorithm for Transmit-Receive System Design

Input: $\left\{\sigma_{(r,i)}\right\}$, $\left\{\bar{\nu}_{d_{(r,i)}}, \epsilon_{(r,i)}\right\}$, σ_n^2, $\boldsymbol{s}_0$, ν_{d_T}, $\boldsymbol{Q}_1$.

Output: A solution $(\boldsymbol{s}^\star, \boldsymbol{w}^\star)$ of $\mathcal{P}$.

1: set $n = 0$, $\boldsymbol{s}^{(n)} = \boldsymbol{s}_0$,

$$\boldsymbol{w}^{(n)} := \frac{\left(\boldsymbol{\Sigma_C}\left(\boldsymbol{s}_0\right) + \sigma_n^2 \boldsymbol{I}\right)^{-1}}{\left(\boldsymbol{s}_0 \odot \boldsymbol{p}(\nu_{d_T})\right)^\dagger \left(\boldsymbol{\Sigma_C}\left(\boldsymbol{s}_0\right) + \sigma_n^2 \boldsymbol{I}\right)^{-1} \left(\boldsymbol{s}_0 \odot \boldsymbol{p}(\nu_{d_T})\right)} \left(\boldsymbol{s}_0 \odot \boldsymbol{p}(\nu_{d_T})\right),$$

and $\text{SINR}^{(n)} = \text{SINR}$;

2: **do**

3: $n := n + 1$;

4: construct the matrices

$\boldsymbol{S} = \left(\boldsymbol{w}^{(n-1)} \odot \boldsymbol{p}(\nu_{d_T})^*\right)\left(\boldsymbol{w}^{(n-1)} \odot \boldsymbol{p}(\nu_{d_T})^*\right)^\dagger$ and $\boldsymbol{M} = \boldsymbol{\Theta_C}\left(\boldsymbol{w}^{(n-1)}\right)^* + \sigma_n^2 \|\boldsymbol{w}^{(n-1)}\|^2 \boldsymbol{I}$;

5: solve problem $\mathcal{P}_{\boldsymbol{s}^{(n)}}$ finding an optimal radar code $\boldsymbol{s}^{(n)}$, through the use of **Algorithm 3**;

6: construct the matrix $\boldsymbol{\Sigma_C}\left(\boldsymbol{s}^{(n)}\right)$;

7: solve problem $\mathcal{P}_{\boldsymbol{w}^{(n)}}$ finding an optimal receive filter

$$\boldsymbol{w}^{(n)} := \frac{\left(\boldsymbol{\Sigma_C}\left(\boldsymbol{s}^{(n)}\right) + \sigma_n^2 \boldsymbol{I}\right)^{-1}}{\left(\boldsymbol{s}^{(n)} \odot \boldsymbol{p}(\nu_{d_T})\right)^\dagger \left(\boldsymbol{\Sigma_C}\left(\boldsymbol{s}^{(n)}\right) + \sigma_n^2 \boldsymbol{I}\right)^{-1} \left(\boldsymbol{s}^{(n)} \odot \boldsymbol{p}(\nu_{d_T})\right)} \left(\boldsymbol{s}^{(n)} \odot \boldsymbol{p}(\nu_{d_T})\right),$$

and the optimal value of the SINR, for the pair $\left(\boldsymbol{s}^{(n)}, \boldsymbol{w}^{(n)}\right)$;

8: let $\text{SINR}^{(n)} = \text{SINR}$;

9: **while** $|\text{SINR}^{(n)} - \text{SINR}^{(n-1)}| \leq \zeta$

10: output $\boldsymbol{s}^\star = \boldsymbol{s}^{(n)}$ and $\boldsymbol{w}^\star = \boldsymbol{w}^{(n)}$.

inverse of $\Sigma_{\boldsymbol{C}}\left(\boldsymbol{s}^{(n)}\right)$ and the complexity effort of **Algorithm 3**. The former is in the order of $O(N^3)$ [69]. The latter corresponds to the complexity of solving the SDP $\mathcal{P}_4$, which is of order $O(N^{3.5}\log(1/\eta))$ (see [29, p. 250]), where η is a prescribed accuracy, and the complexity of the specific rank-one decomposition procedure which is $O\left(N^3\right)$ [68].

Some interesting comments are now in order:

- Evidently, **Algorithm 4** requires the specification of the target doppler ν_{d_T}; as a consequence, the radar code $\boldsymbol{s}^\star$ and the receive filter $\boldsymbol{w}^\star$ depend on these pre-assigned value. It is thus necessary to provide some guidelines on the importance and the applicability of the proposed framework. To this end, we highlight the following issues.

  1 A radar code and a receive filter designed for a challenging condition dictated by the clutter PSD shape (i.e. design target Doppler in correspondence of the PSD peak) can be synthesized (worst case optimization).

  2 A joint radar code and a receive filter optimized to an average scenario can be selected. Otherwise stated, the code might be chosen as the

solution to the problem,

$$\mathcal{P}^1 \begin{cases} \max\limits_{\boldsymbol{s},\boldsymbol{w}} & \dfrac{|\alpha_T|^2 \boldsymbol{w}^\dagger \mathrm{diag}\{\boldsymbol{s}\} \boldsymbol{\Phi}_{\epsilon_T}^{\bar{\nu}_{d_T}} \mathrm{diag}\{\boldsymbol{s}\}^\dagger \boldsymbol{w}}{\boldsymbol{w}^\dagger \boldsymbol{\Sigma}_{\boldsymbol{C}}(\boldsymbol{s})\, \boldsymbol{w} + \sigma_n^2 \|\boldsymbol{w}\|^2} \\ \text{s.t.} & \|\boldsymbol{s}\|^2 = 1 \\ & \|\boldsymbol{s} - \boldsymbol{s}_0\|^2 \leq \delta, \end{cases} . \tag{3.24}$$

where we are assuming that[7] $\nu_{d_T} \sim \mathcal{U}\left(\bar{\nu}_{d_T} - \frac{\epsilon_{(0,0)}}{2}, \bar{\nu}_{d_T} + \frac{\epsilon_{(0,0)}}{2}\right)$, and $\boldsymbol{\Phi}_{\epsilon_T}^{\bar{\nu}_{d_T}}$ is defined as in (3.4). In this case, the problem ${\mathcal{P}^1_{\boldsymbol{w}}}^{(n)}$, becomes

$${\mathcal{P}^1_{\boldsymbol{w}}}^{(n)} \begin{cases} \max\limits_{\boldsymbol{w}} & \dfrac{|\alpha_T|^2 \boldsymbol{w}^\dagger \mathrm{diag}\{\boldsymbol{s}^{(n)}\} \boldsymbol{\Phi}_{\epsilon_T}^{\bar{\nu}_{d_T}} \mathrm{diag}\{\boldsymbol{s}^{(n)}\}^\dagger \boldsymbol{w}}{\boldsymbol{w}^\dagger \boldsymbol{\Sigma}_{\boldsymbol{C}}\left(\boldsymbol{s}^{(n)}\right) \boldsymbol{w} + \sigma_n^2 |\boldsymbol{w}|^2} \end{cases} \tag{3.25}$$

and its optimal solution $\boldsymbol{w}^{(n)}$ is easily proved to be equal to the maximum eigenvector of the matrix

$$\left(\boldsymbol{\Sigma}_{\boldsymbol{C}}\left(\boldsymbol{s}^{(n)}\right) \boldsymbol{w} + \sigma_n^2 \boldsymbol{I}\right)^{-\frac{1}{2}} \mathrm{diag}\{\boldsymbol{s}^{(n)}\} \boldsymbol{\Phi}_{\epsilon_T}^{\bar{\nu}_{d_T}} \mathrm{diag}\{\boldsymbol{s}^{(n)}\}^\dagger \left(\boldsymbol{\Sigma}_{\boldsymbol{C}}\left(\boldsymbol{s}^{(n)}\right) \boldsymbol{w} + \sigma_n^2 \boldsymbol{I}\right)^{-\frac{1}{2}},$$

i.e. to a generalized eigenvector of the matrices $\left(\boldsymbol{\Sigma}_{\boldsymbol{C}}\left(\boldsymbol{s}^{(n)}\right) \boldsymbol{w} + \sigma_n^2 \boldsymbol{I}\right)$

[7] It can be straightforward generalized to other probability density functions for the normalized target Doppler frequency.

and

$\mathrm{diag}\{\boldsymbol{s}\}\boldsymbol{\Phi}_{\epsilon_T}\mathrm{diag}\{\boldsymbol{s}\}^{\dagger}$, corresponding to the maximum generalized eigenvalue. As to the solution of $\mathcal{P}_{\boldsymbol{s}}^{1\,(n)}$, we can again use **Algorithm 3**, replacing $\boldsymbol{S}$ with:

$$\boldsymbol{S}^1 = \mathrm{diag}(\boldsymbol{w}^{(n-1)})\boldsymbol{\Phi}_{\epsilon_T}^{\bar{\nu}_{d_T}{}^*}\mathrm{diag}(\boldsymbol{w}^{(n-1)^*}).$$

3 Assume that, after an uncoded (or a possibly standard coded) transmission a detection is declared in a given Doppler bin, using a high value of the false alarm Probability (P_{fa}). Then, our joint optimization procedure can be employed to shape the waveform and the receive filter for the next transmission in order to confirm the detection in the previously identified bin, possibly with a smaller value of the P_{fa} (confirmation process).

- As described in the block diagram of **Figure 3.2**, the proposed technique requires the knowledge of the clutter characterization. The knowledge-aided approach, see [70], [71], well fits with this need. Additionally, for an on-line implementation, a look ahead computing architecture has to

be considered. In fact, to adapt the radar code and the receive filter to the illuminated scene at the time instant t (in which we are interested to analyze the range-azimuth bin $(0,0)$), we need the environment characterization at that instant, as shown by the input parameters of **Algorithm 4**. Given the memory access latency and the computation time of **Algorithm 4**, it is necessary to know at the time instant $t-\Delta t$, where the radar will be positioned and what it will be doing, Δt time instants later, i.e. at the time instant t. Assuming that Δt is greater than the memory access latency and the processing time, then the sounder system is physically implementable [70, page 27].

3.4 Performance Analysis

In this section, the performance analysis of the proposed algorithm for the joint optimization of the radar code and the receive filter is presented. We consider an L-band radar whose operating frequency is $f_0 = 1.4$ GHz, and that exploits a broadside array with $N_a = 21$ elements, that points in the range-azimuth bin of interest $(0,0)$. Specifically, we consider a uniformly weighted linear array with uniform spacing equal to $d = \frac{\lambda}{2}$. Consequently, the radiation

pattern is given by:

$$G(\theta) = \begin{cases} \dfrac{1}{N_a} \dfrac{\sin\left(N_a \dfrac{\pi}{2}\cos(\theta)\right)}{\sin\left(\dfrac{\pi}{2}\cos(\theta)\right)} & \text{if} \quad 0 \leq \theta \leq \pi \\ G_{back} & \text{if} \quad \pi \leq \theta \leq 2\pi \end{cases},$$

with $G_{back} = 10^{-3}$ corresponding to the backlobes attenuation.

In the following subsections, we will focus on two main scenarios: the former refers to a uniform range-azimuth clutter characterization, the latter considers heterogenous clutter. In both cases, we assume that the number of range rings that interfere with the range-azimuth bin of interest $(0, 0)$ is $N_c = 2$ and that the number of azimuth cells in each ring (see **Figure 3.1**) is $L = 100$. Moreover, we consider a pulse train of length $N = 20$ and select, as similarity code $\boldsymbol{s}_0$, a generalized Barker code. It is a polyphase sequence whose autocorrelation function has minimal peak-to-sidelobe ratio excluding the outermost sidelobe. The description of generalized Barker codes can be found in [72] and [73], also for other values of N. The exit condition, see **Figure 3.2**, that we implement

to stop the procedure, is given by:

$$|\text{SINR}^{(n)} - \text{SINR}^{(n-1)}| \leq 10^{-3}, \tag{3.26}$$

namely when the increase in the objective function is lower than $\zeta = 10^{-3}$, the algorithm stops. Finally, in the numerical simulations, we exploit the MATLAB© toolbox SeDuMi [25] for solving the SDP relaxation, and the MATLAB© toolbox of [74] for plotting the ambiguity functions of the coded pulse trains.

3.4.1 Uniform Clutter Environment

In this subsection, we assess the performance of **Algorithm 4** for a uniform clutter environment. Such a choice proves effective to model a situation in which the reflectivity environment is physically uniform with respect to the range-azimuth bin, as depicted in right bottom corner of **Figure 3.3**, as well as a situation in which no a-priori information is available on the illuminated scene. As to the parameters of the uniform clutter, we consider a $\frac{\sigma_0}{\sigma_n^2} K_r = \text{CNR}\, K_r = 30$ dB, a mean Doppler frequency $\bar{\nu}_d = -0.1$, and Doppler uncertainty $\frac{\epsilon}{2} = 0.35$ for each range-azimuth bin. Additionally, we suppose the presence of a target with Signal to Noise Ratio (SNR) $\frac{|\alpha_T|^2}{\sigma_n^2} = \text{SNR} = 10$ dB and normalized

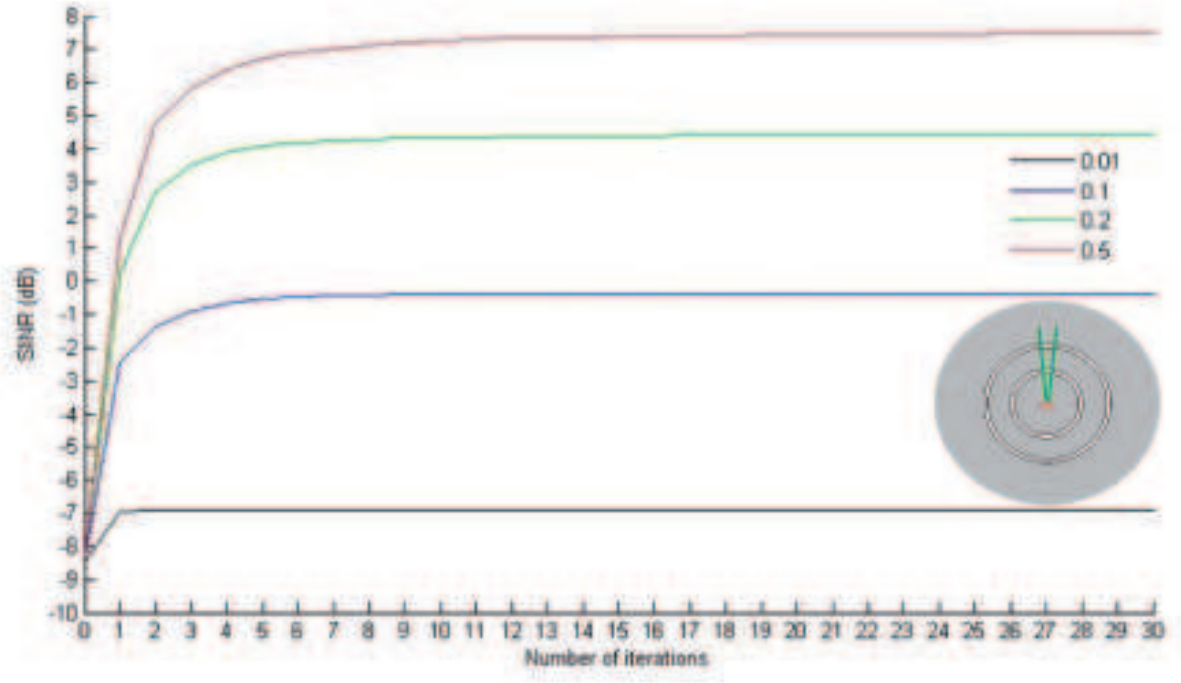

Figure 3.3: SINR behavior for $\delta = [0.01, 0.1, 0.2, 0.5]$. On the right bottom corner, the uniform terrain environment, illuminated by the radar positioned in correspondence of the red point, is illustrated. The range rings that contribute to the backscattering (white rings) are $N_c = 2$.

Doppler frequency $\nu_{d_T} = -0.4$.

In **Figure 3.3**, the SINR behavior is plotted versus the number of iterations, for different values of the similarity parameter δ. As expected, increasing δ, the optimal value of the SINR improves (actually, performance gains up to 15 dB can be observed for $\delta = 0.5$, even if this is just a potential value and in real conditions smaller gains could be experienced due to some inaccuracies in the a-priori information) since the feasible set of the optimization problem becomes larger and larger. achieve convergence, increases as well.

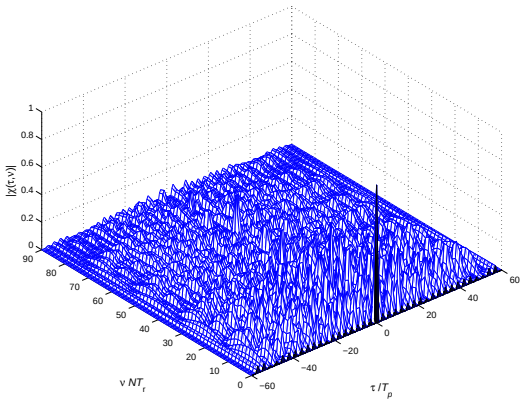

(a) Ambiguity Function modulus of the radar code s_0.

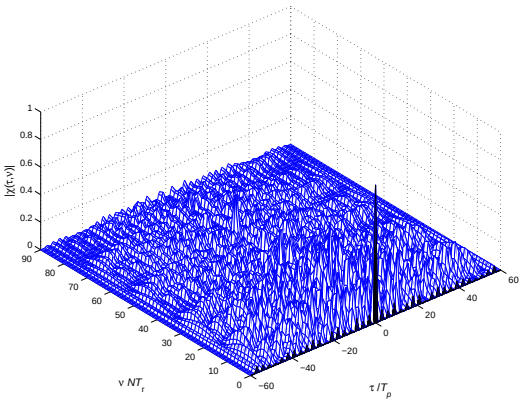

(b) Ambiguity Function modulus of the radar code $s^\star$ for $\delta = 0.01$.

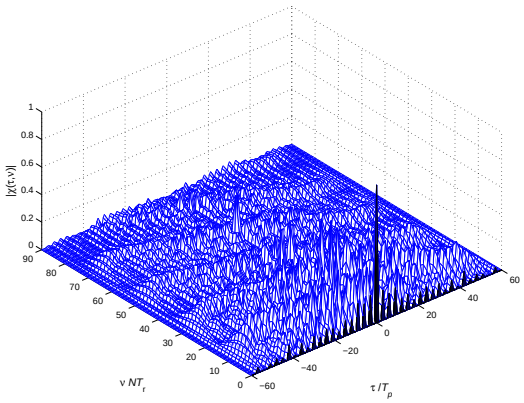

(c) Ambiguity Function modulus of the radar code $s^\star$ for $\delta = 0.2$.

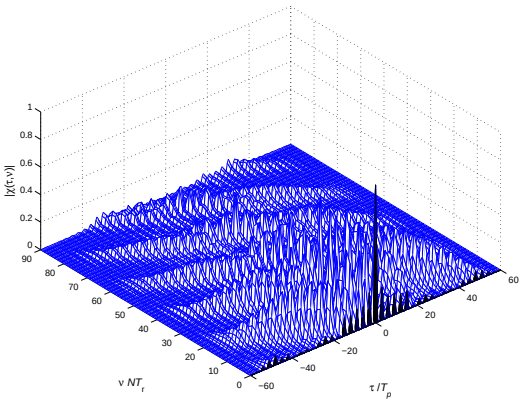

(d) Ambiguity Function modulus of the radar code $s^\star$ for $\delta = 0.5$.

Figure 3.4: Ambiguity Function modulus of the radar code, assuming $T_r = 3T_p$.

.

In **Figures 3.4**, the ambiguity function[8] of the optimal synthesized code $s^\star$ is plotted for different sizes of the similarity region. Indeed, we have an opposite behavior with respect to **Figure 3.3**. Precisely, increasing δ, the set of feasible points becomes larger and larger and worse and worse ambiguity functions can be obtained.

[8]We consider a coherent pulse train with ideal rectangular pulses of width T_p and pulse repetition time T_r.

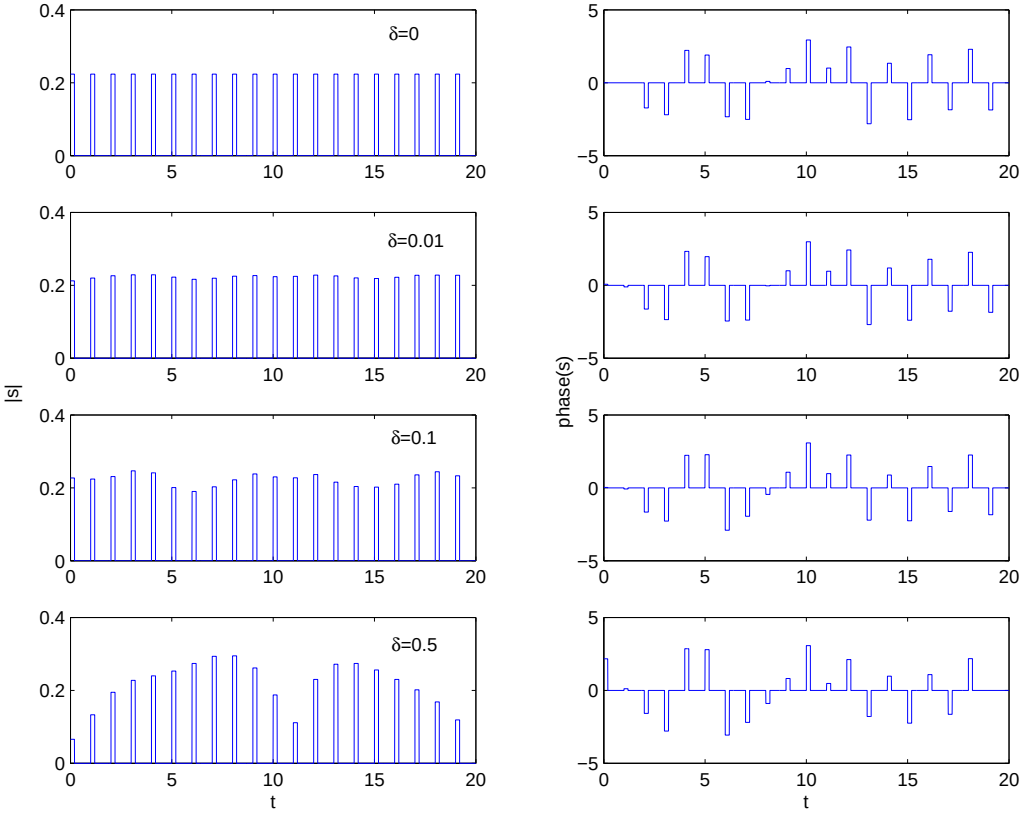

Figure 3.5: Temporal behavior of $s^\star$ in terms of amplitude (right plots), and phase (left plots).

Finally, let us consider the behavior of the radar codes in both the time and frequency domains. In **Figure 3.5**, we study the temporal behavior of the optimal code $s^\star$, in terms of the amplitude and phase of the coded train, for different values of δ. The plots highlight that increasing δ, the code becomes different and different from the initial Barker code s_0 and this agrees perfectly with the plots of **Figures 3.4**.

Furthermore, in **Figures 3.6**, we analyze the frequency behavior of the

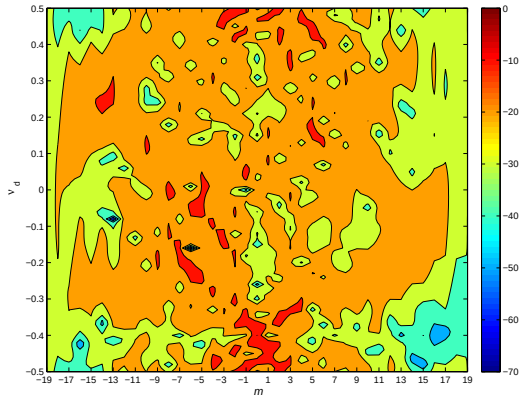

(a) Cross-Ambiguity Function of the radar code and receive filter $\left(\boldsymbol{s}^{(0)}, \boldsymbol{w}^{(0)}\right)$.

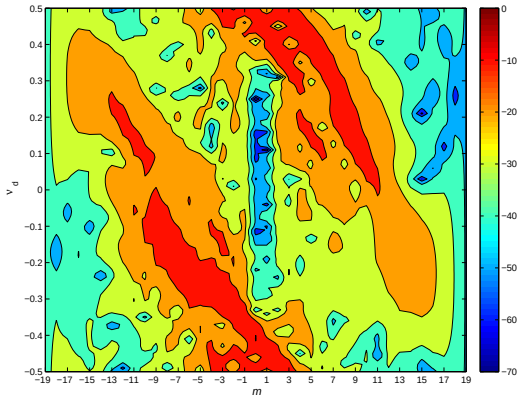

(b) Cross-Ambiguity Function of the radar code and receive filter $\left(\boldsymbol{s}^{(3)}, \boldsymbol{w}^{(3)}\right)$.

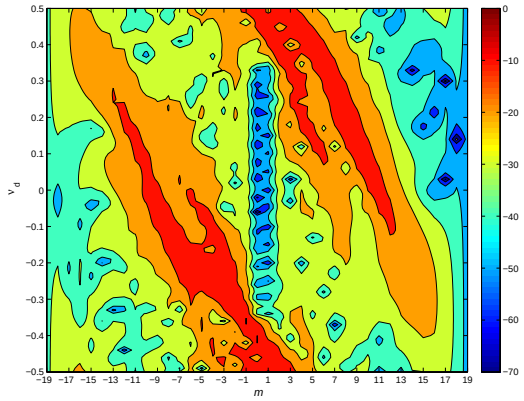

(c) Cross-Ambiguity Function of the radar code and receive filter $\left(\boldsymbol{s}^{(10)}, \boldsymbol{w}^{10}\right)$.

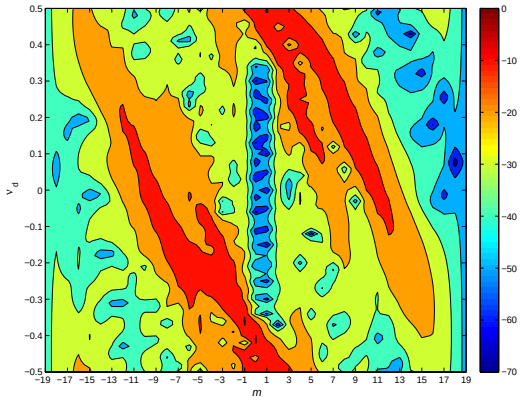

(d) Cross-Ambiguity Function of the radar code and receive filter $\left(\boldsymbol{s}^{(30)}, \boldsymbol{w}^{(30)}\right)$.

Figure 3.6: Cross-Ambiguity Function of the radar code and receive filter.

radar code and the receive filter, corresponding to $\delta = 0.5$, for different values of the iteration number ($n = [1, 3, 10, 30]$). Precisely, we plot the contour map of the cross-ambiguity function,

$$\mathrm{g}^{(n)}\left(m, \nu_d\right) = \left| \boldsymbol{w}^{(n)\dagger} \left(\boldsymbol{J}_m \left(\boldsymbol{s}^{(n)} \odot \boldsymbol{p}\left(\nu_d\right) \right) \right) \right|^2 \tag{3.27}$$

where m is the delay-lag and ν_d is the Doppler frequency of the incoming signal. As forced by the design procedure, the cross-ambiguity function is equal to one at $(m, \nu_d) = (0, -0.4)$, which corresponds to the range-Doppler position of the nominal target. Moreover, lower and lower values of $\mathrm{g}^{(n)}(m, \nu_d)$ can be observed in the strip $0 \leq m \leq 2$ $-0,35 \leq m \leq 0.35$ as the iteration step n grows up. Interestingly, this performance trend reflects the capability of the proposed joint transmit-receive optimization procedure to sequentially refine the shape of the cross-ambiguity function in order to get better and better clutter suppression levels. In **Figures 3.7**, we analyze the frequency behavior of SINR, for the synthesized radar code and receive filter in correspondence of $\delta = 0.5$ and different values of the iteration number ($n = [0, 3, 10, 30]$). Precisely, we plot

$$\mathrm{SINR}^{(n)} = \frac{|\alpha_T|^2 \left| \boldsymbol{w}^{(n)^\dagger} \left(\boldsymbol{s}^{(n)} \odot \boldsymbol{p}(\nu_d) \right) \right|^2}{\boldsymbol{w}^{(n)^\dagger} \boldsymbol{\Sigma_C} \left(\boldsymbol{s}^{(n)} \right) \boldsymbol{w}^{(n)} + \sigma_n^2 \|\boldsymbol{w}\|^2} \tag{3.28}$$

versus ν_d, which is tantamount to studying a normalized Doppler-cut of the cross-ambiguity function (i.e. for $m = 0$). These curves highlight that the SINR shares a quite flat shape within an interval of size $\Delta\nu_d = 0.008$, around the nominal Doppler frequency $\nu_{d_T} = -0.4$, namely, the proposed procedure

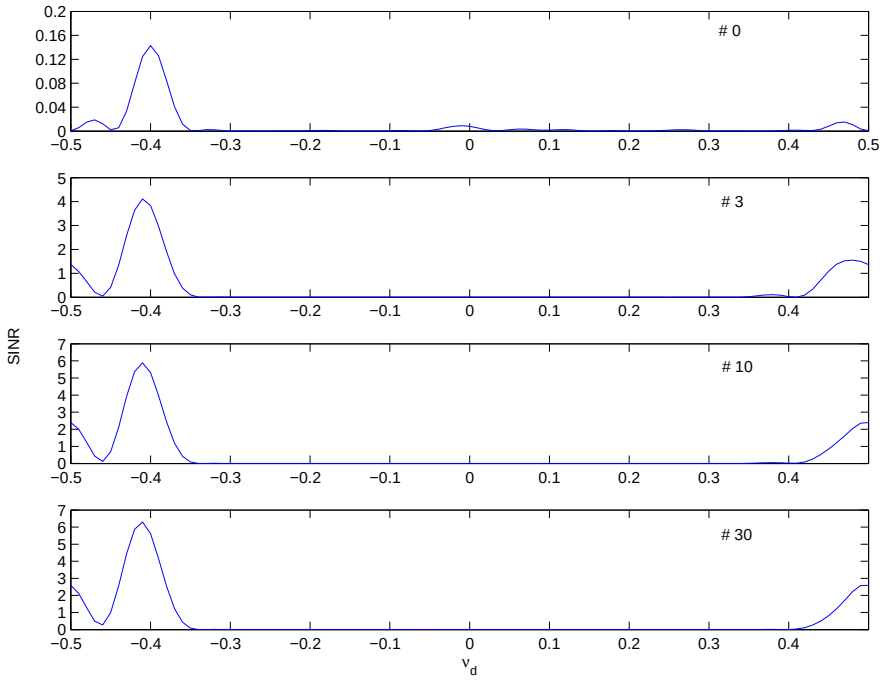

Figure 3.7: SINR$^{(n)}$ versus the normalized Doppler ν_d, for $n = [0, 3, 10, 30]$.

exhibits an intrinsic Doppler tolerance.

3.4.2 Heterogenous Clutter Environment

In this subsection, we assess the performance of **Algorithm 4** for an heterogenous clutter environment. We refer to the situation depicted in the bottom corner of **Figure 3.8**, namely a mixed clutter environment composed by ground and sea. As previously explained, the radar can acquire the geographic a-priori information through a query to the NLCD database. Let us now describe the statistical characterization of the ground and sea environments. As

to the ground range-azimuth bins, we consider a $\frac{\sigma_0^g}{\sigma_n^2}K_r = \text{CNR}_g K_r = 30$ dB, a mean Doppler frequency $\bar{\nu}_{d_g} = 0$, and Doppler uncertainty $\frac{\epsilon_g}{2} = 0.30$. Moreover, for the sea range-azimuth bins, we assume a $\frac{\sigma_0^s}{\sigma_n^2}K_r = \text{CNR}_s K_r = 25$ dB, a mean Doppler frequency $\bar{\nu}_{d_s} = -0.1$, and a relative Doppler uncertainty $\frac{\epsilon_s}{2} = 0.25$. Finally, we suppose that in each range ring the sea extends within the azimuth angular sector $\frac{\pi}{4} \leq \theta \leq \frac{\pi}{2} + \frac{\pi}{4}$, and that the reference target, with $\frac{|\alpha_T|^2}{\sigma_n^2} = \text{SNR} = 10$ dB and normalized Doppler frequency $\nu_{d_T} = -0.4$, is located in $\theta = 0$.

In **Figure 3.8**, the SINR behavior is plotted versus the number of iterations, for different values of the similarity parameter δ. In agreement with the uniform case, increasing δ, the optimal value of the SINR improves, since the feasible set of the optimization problem becomes larger and larger. Additionally, the number of iterations, required to achieve convergence, increases as well.

In **Figures 3.9**, the ambiguity function of the optimal synthesized code $\boldsymbol{s}^\star$ is plotted, for different sizes of the similarity region. Again, we have an opposite behavior with respect to **Figure 3.8**. Precisely, increasing δ, the set of feasible points becomes larger and larger and worse and worse ambiguity functions can be obtained, still in accordance with the unform clutter environment.

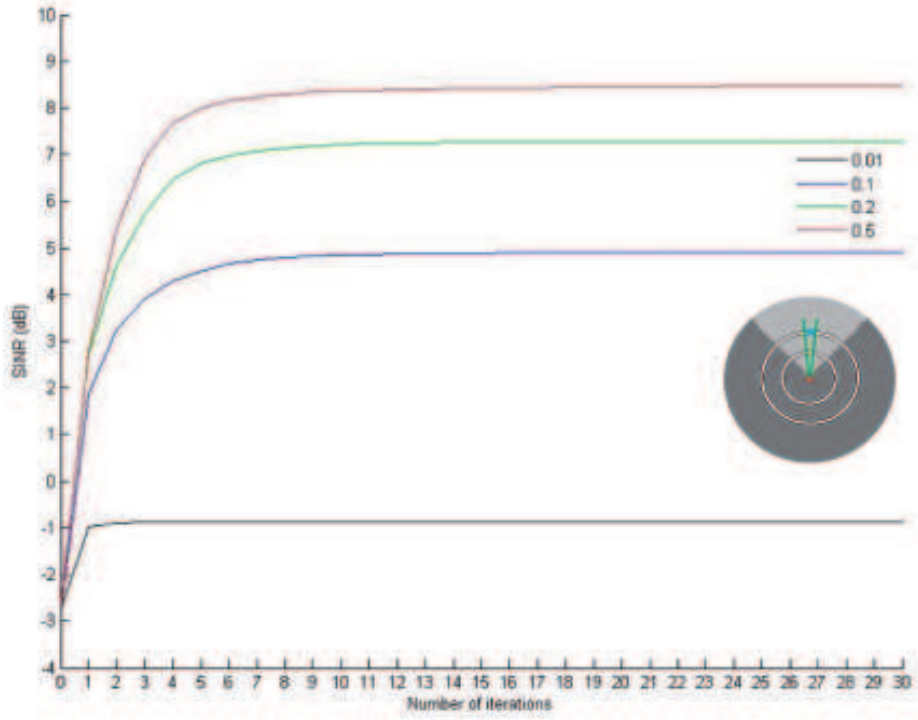

Figure 3.8: SINR behavior for $\delta = [0.01, 0.1, 0.2, 0.5]$. On the right bottom corner, the heterogenous terrain environment (ground, dark gray, and sea, light gray), illuminated by the radar positioned in correspondence of the red point, is illustrated. The range rings that contribute to the backscattering (white rings) are $N_c = 2$, and that the target is positioned on the blue point.

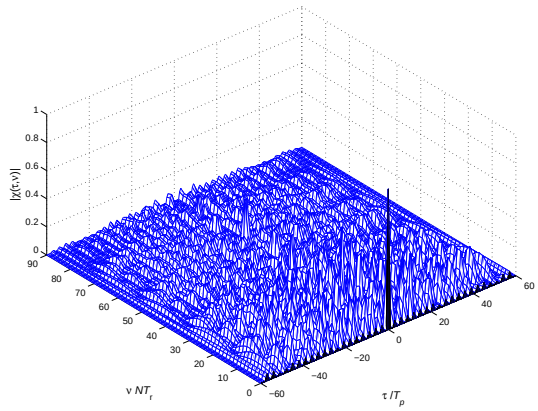

(a) Ambiguity Function modulus of the radar code $\boldsymbol{s}_0$, assuming $T_r = 3T_p$.

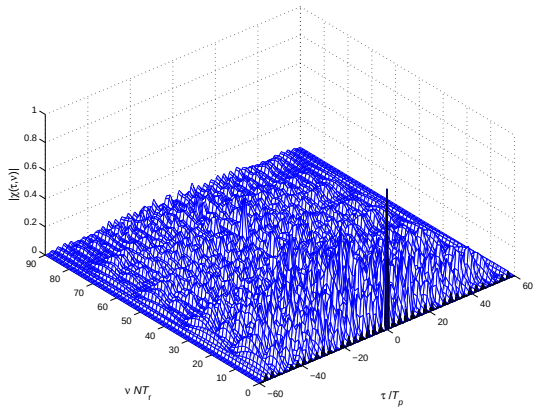

(b) Ambiguity Function modulus of the radar code $\boldsymbol{s}^\star$ for δ=0.01.

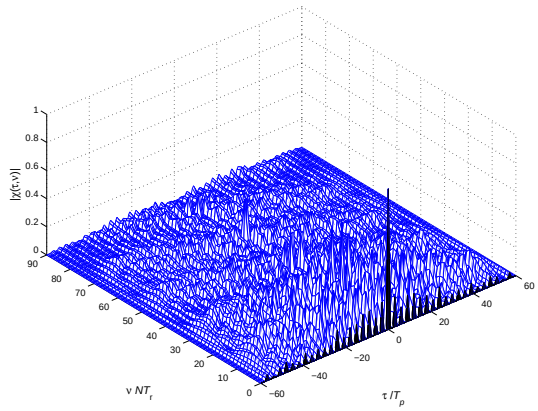

(c) Ambiguity Function modulus of the radar code $\boldsymbol{s}^\star$ for δ=0.2.

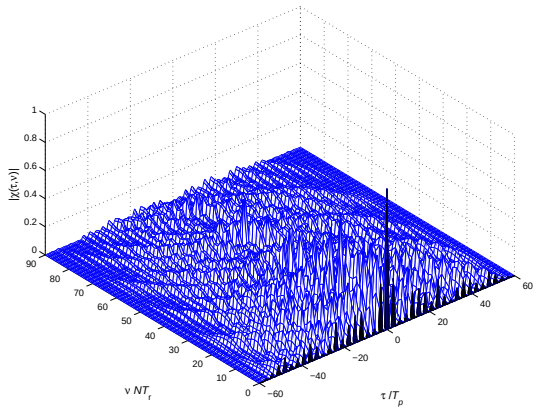

(d) Ambiguity Function modulus of the radar code $\boldsymbol{s}^\star$ for δ=0.5.

Figure 3.9: Ambiguity Function modulus of the radar code, assuming $T_r = 3T_p$.

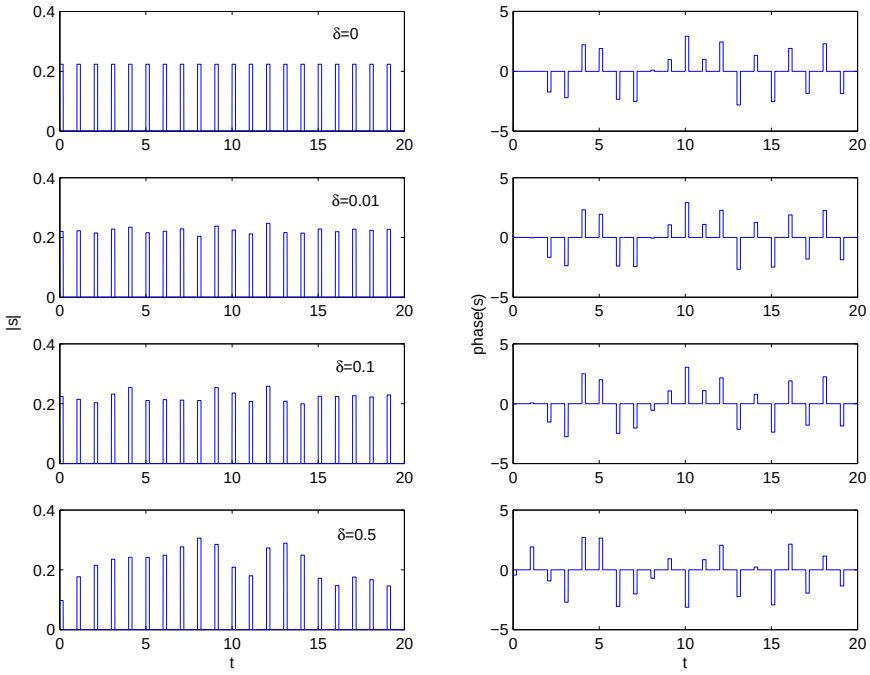

Figure 3.10: Temporal behavior of $s^\star$ in terms of amplitude (right plots), and phase (left plots).

Now, let us analyze the behavior of the radar codes in both the time and frequency domains. In **Figure 3.10**, we study the temporal behavior of the optimal code $s^\star$, in terms of the amplitude and phase of the coded train, for different values of δ. Increasing δ, the code becomes increasingly different from the initial Barker code s_0. Additionally, we can observe that the heterogenous setting leads to and optimal code exhibiting much more pronounced structural differences, with respect to the similarity code, than the optimal code obtained for the homogeneous scenario.

In **Figures 3.11**, we study the frequency behavior of the radar code and

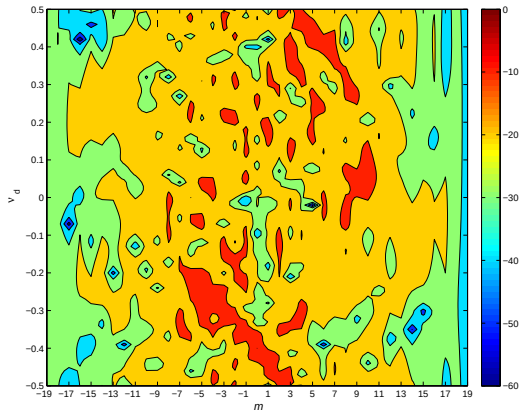

(a) Cross-Ambiguity Function for the radar code and receive filter $\left(\boldsymbol{s}^{(0)}, \boldsymbol{w}^{(0)}\right)$.

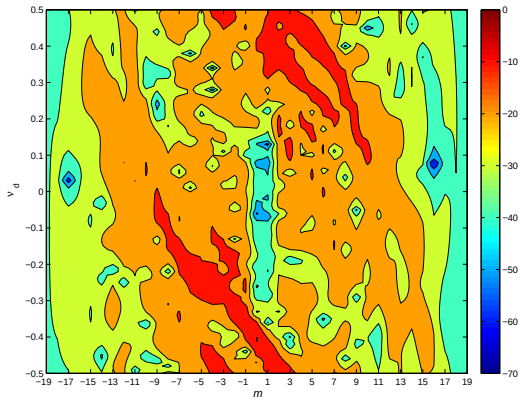

(b) Cross-Ambiguity Function for the radar code and receive filter $\left(\boldsymbol{s}^{(3)}, \boldsymbol{w}^{(3)}\right)$.

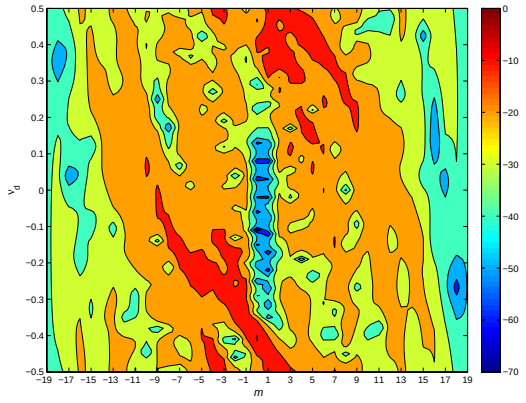

(c) Cross-Ambiguity Function for the radar code and receive filter $\left(\boldsymbol{s}^{(10)}, \boldsymbol{w}^{(10)}\right)$.

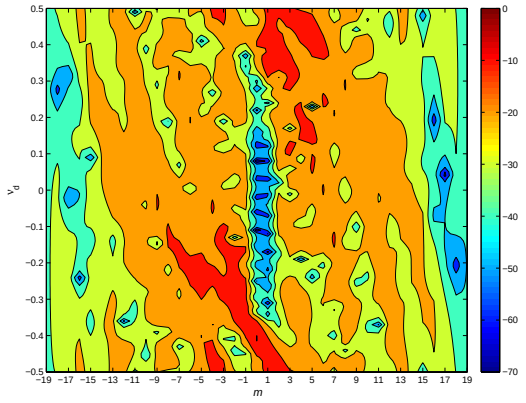

(d) Cross-Ambiguity Function for the radar code and receive filter $\left(\boldsymbol{s}^{(30)}, \boldsymbol{w}^{(30)}\right)$.

Figure 3.11: Cross-Ambiguity Function for the radar code and receive filter.

the receive filter, corresponding to $\delta = 0.5$, for different values of the iteration number. Precisely, we plot the contour map of the cross-ambiguity function, defined in (6.22). The quoted maps indicate that lower and lower values of $\mathrm{g}^{(n)}\left(m, \nu_d\right)$ can be observed in the strip $0 \leq m \leq 2$ $-0,35 \leq m \leq 0.3$ as the iteration step n grows up. Moreover, in correspondence of the sea clutter Doppler centroid $\nu_d = -0.1$, the cross-ambiguity function has a notch, account-

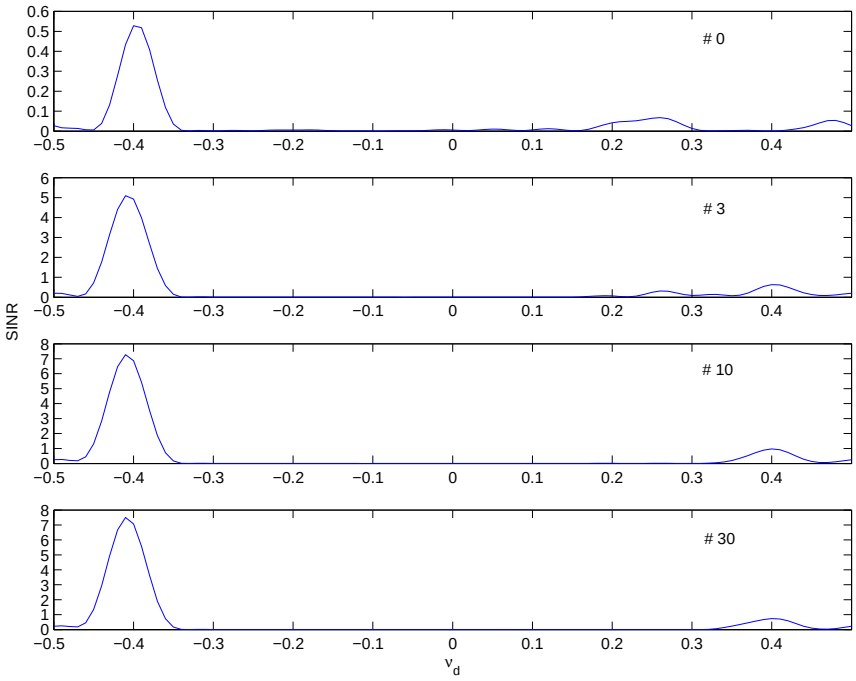

Figure 3.12: SINR$^{(n)}$ versus the normalized Doppler ν_d, for $n = [0, 3, 10, 30]$.

ing for the high probability event that the clutter Doppler frequency assumes a value very close to $\nu_d = -0.1$. As explained with reference to the uniform scenario, this performance behavior reflects the capability of the proposed joint transmit-receive optimization procedure to sequentially improve the clutter suppression.

Finally, in **Figures 3.12**, we analyze the frequency behavior of SINR versus ν_d. Specifically, we plot SINR$^{(n)}$, defined in (3.28), for the synthesized radar code and receive filter for $\delta = 0.5$ and different values of the iteration number ($n = [0, 3, 10, 30]$). The curves highlight that the SINR shares a quite flat shape

within an interval of size $\Delta\nu_d = 0.01$, around the nominal Doppler frequency $\nu_{d_T} = -0.4$. Otherwise stated, as for the homogeneous case, the proposed procedure shares a quite good Doppler tolerance.

3.5 Conclusions

In this chapter, we have considered the problem of knowledge-aided transmit signal and receive filter joint optimization in a signal-dependent clutter environment. First of all, we have defined the signal-dependent clutter model and have specified the a-priori information that the radar system needs to deal with this problem. At the design stage, we have assumed the interaction between the radar and a geographic database to acquire the topology of the scene to be illuminated. Then, based on the aforementioned geographic information, meteorological data, and some electromagnetic reflectivity and spectral clutter models, the radar can predict the scattering environment it is faced with.

Thus, we have devised and assessed an iterative algorithm for the joint design of the transmitted waveform and the receive filter. It involves in each iteration the solution of a convex and an hidden convex optimization problem. The resulting computational complexity is linear with the number of iterations

and polynomial with the receive filter length.

At the analysis stage, we have assessed the performance of the proposed algorithm in terms of SINR versus the number of iterations, ambiguity function of the resulting coded pulse train waveform, and cross-ambiguity function of the transmit signal and receive filter pair. The results have highlighted that, in the presence of a perfect a-priori knowledge, significant SINR gains (up to 15 dB) can be obtained jointly optimizing the transmitter and receiver.

Possible future research tracks might concern the analysis of the proposed algorithm on real radar data as well as the extension of the procedure according to a cognitive radar philosophy, see [70], [71], where each pulse of the transmitted train enjoys the information provided by its predecessor through a feedback network with the receiver. Finally, it might be of interest the generalization of the developed framework to an extended target scenario.

3.6 Appendix

3.6.1 Proof of Lemma 6.3.1

Proof. Let us start by analyzing the numerator of:

$$\text{SINR} = \frac{|\alpha_T|^2 \left| \boldsymbol{s}^T \left(\boldsymbol{w}^* \odot \boldsymbol{p}(\nu_{d_T}) \right) \right|^2}{\boldsymbol{s}^T \boldsymbol{\Theta}_{\boldsymbol{C}} \left(\boldsymbol{w} \right) \boldsymbol{s}^* + \sigma_n^2 \|\boldsymbol{w}\|^2}. \tag{3.29}$$

Using the property:

$$\boldsymbol{x} \odot \boldsymbol{y} = \text{diag}\{\boldsymbol{x}\}\boldsymbol{y}$$

we have:

$$\begin{aligned} \boldsymbol{w}^\dagger \left(\boldsymbol{s} \odot \boldsymbol{p}(\nu_{d_T}) \right) &= \boldsymbol{w}^\dagger \left(\text{diag}\{\boldsymbol{s}\}\boldsymbol{p}(\nu_{d_T}) \right) \\ &= \boldsymbol{s}^T \text{diag}\{\boldsymbol{w}^*\}\boldsymbol{p}(\nu_{d_T}) \\ &= \boldsymbol{s}^T \left(\boldsymbol{w}^* \odot \boldsymbol{p}(\nu_{d_T}) \right). \end{aligned} \tag{3.30}$$

Let us now consider the denominator of (3.29). Precisely, let us analyze $\boldsymbol{w}^\dagger \boldsymbol{\Sigma}_{\boldsymbol{C}} \left(\boldsymbol{s} \right) \boldsymbol{w}$. Using the property

$$\boldsymbol{x}^\dagger \boldsymbol{J}_r \text{diag}\{\boldsymbol{y}\} = \boldsymbol{y}^T \text{diag}\{\boldsymbol{J}_{-r}\boldsymbol{x}^*\}, \tag{3.31}$$

whose proof is given in Appendix 3.6.2, we have

$$
\begin{aligned}
\boldsymbol{w}^{\dagger}\boldsymbol{\Sigma}_{\boldsymbol{C}}(\boldsymbol{s})\,\boldsymbol{w} &= \boldsymbol{w}^{\dagger}\left(\sum_{r=1}^{N_c-1}\sum_{i=0}^{L-1}\sigma^2_{(r,i)}\boldsymbol{J}_r\boldsymbol{\Gamma}(\boldsymbol{s},(r,i))\boldsymbol{J}_r^T+\sum_{i=0}^{L-1}\sigma^2_{(0,i)}\boldsymbol{\Gamma}(\boldsymbol{s},(0,i))\right)\boldsymbol{w}\\
&= \sum_{r=1}^{N_c-1}\sum_{i=0}^{L-1}\sigma^2_{(r,i)}\boldsymbol{w}^{\dagger}\boldsymbol{J}_r\boldsymbol{\Gamma}(\boldsymbol{s},(r,i))\boldsymbol{J}_r^T\boldsymbol{w}+\sum_{i=0}^{L-1}\sigma^2_{(0,i)}\boldsymbol{w}^{\dagger}\boldsymbol{\Gamma}(\boldsymbol{s},(0,i))\boldsymbol{w}\\
&= \sum_{r=1}^{N-1}\sum_{i=0}^{L-1}\sigma^2_{(r,i)}\boldsymbol{w}^{\dagger}\boldsymbol{J}_r\mathrm{diag}\{\boldsymbol{s}\}\boldsymbol{\Phi}^{\bar{\nu}_{d_{(r,i)}}}_{\epsilon_{(r,i)}}\mathrm{diag}\{\boldsymbol{s}\}^{\dagger}\boldsymbol{J}_r^T\boldsymbol{w}\\
&\quad+\sum_{i=0}^{L-1}\sigma^2_{(0,i)}\boldsymbol{w}^{\dagger}\mathrm{diag}\{\boldsymbol{s}\}\boldsymbol{\Phi}^{\bar{\nu}_{d_{(0,i)}}}_{\epsilon_{(0,i)}}\mathrm{diag}\{\boldsymbol{s}\}^{\dagger}\boldsymbol{w}\\
&= \sum_{r=1}^{N_c-1}\sum_{i=0}^{L-1}\sigma^2_{(r,i)}\boldsymbol{s}^{T}\mathrm{diag}\{\boldsymbol{J}_{-r}\boldsymbol{w}^{*}\}\boldsymbol{\Phi}^{\bar{\nu}_{d_{(r,i)}}}_{\epsilon_{(r,i)}}\mathrm{diag}\{\boldsymbol{J}_{-r}\boldsymbol{w}\}\boldsymbol{s}^{*}\\
&\quad+\sum_{i=1}^{L-1}\sigma^2_{(0,i)}\boldsymbol{s}^{T}\mathrm{diag}\{\boldsymbol{w}^{*}\}\boldsymbol{\Phi}^{\bar{\nu}_{d_{(0,i)}}}_{\epsilon_{(0,i)}}\mathrm{diag}\{\boldsymbol{w}\}\boldsymbol{s}^{*}\\
&= \boldsymbol{s}^{T}\boldsymbol{\Theta}_{\boldsymbol{C}}(\boldsymbol{w})\,\boldsymbol{s}^{*} \qquad (3.32)
\end{aligned}
$$

from which, resorting to (3.30) and (3.32), the statement follows.

□

3.6.2 Proof of Equation (3.31)

Proof. Firstly, note that:

$$\begin{aligned} \boldsymbol{x}^\dagger \boldsymbol{J}_r &= \left(\boldsymbol{J}_r^\dagger \boldsymbol{x}\right)^\dagger \\ &= \left(\boldsymbol{J}_{-r}\boldsymbol{x}\right)^\dagger \qquad (3.33) \\ &= \begin{bmatrix} \boldsymbol{x}(r+1)^*, & \ldots, & \boldsymbol{x}(N)^*, & \mathbf{0}_r^T \end{bmatrix}. \qquad (3.34) \end{aligned}$$

Consequently,

$$\begin{aligned} \boldsymbol{x}^\dagger \boldsymbol{J}_r \mathrm{diag}\{\boldsymbol{y}\} &= \begin{bmatrix} \boldsymbol{x}(r+1)^*\boldsymbol{y}(1), & \ldots, & \boldsymbol{x}(N)^*\boldsymbol{y}(N-r), & \mathbf{0}_r^T \end{bmatrix} \\ &= \boldsymbol{y}^T \mathrm{diag}\{\boldsymbol{J}_{-r}\boldsymbol{x}^*\}, \qquad (3.35) \end{aligned}$$

where in (3.35) we used the fact that

$$\boldsymbol{J}_{-r}\boldsymbol{x}^* = \begin{bmatrix} \\ \boldsymbol{x}(r+1)^* \\ \\ \vdots \\ \\ \boldsymbol{x}(N)^* \\ \\ \mathbf{0}_r \\ \\ \end{bmatrix}.$$

Hence equation (3.31) is proved. □

3.6.3 Proof of Proposition 6.3.2

Proof. We first prove that $\text{SINR}^{(n)}$ is a monotone increasing sequence, i.e. $\text{SINR}^{(n)} \leq \text{SINR}^{(n+1)}$. In fact,

$$\text{SINR}^{(n)} = \frac{|\alpha_T|^2 \left| \boldsymbol{w}^{(n)^\dagger} \left(\boldsymbol{s}^{(n)} \odot \boldsymbol{p}(\nu_{d_T}) \right) \right|^2}{\boldsymbol{w}^{(n)^\dagger} \boldsymbol{\Sigma}_{\boldsymbol{C}} \left(\boldsymbol{s}^{(n)} \right) \boldsymbol{w}^{(n)} + \sigma_n^2 \|\boldsymbol{w}^{(n)}\|^2} \leq v(\mathcal{P}_{\boldsymbol{s}}{}^{(n+1)}), \tag{3.36}$$

$$
\begin{aligned}
v(\mathcal{P}_{\boldsymbol{s}^{(n+1)}}) &= \frac{|\alpha_T|^2 \left| \boldsymbol{w}^{(n)\dagger} \left(\boldsymbol{s}^{(n+1)} \odot \boldsymbol{p}(\nu_{d_T}) \right) \right|^2}{\boldsymbol{w}^{(n)\dagger} \boldsymbol{\Sigma}_{\boldsymbol{C}} \left(\boldsymbol{s}^{(n+1)} \right) \boldsymbol{w}^{(n)} + \sigma_n^2 \|\boldsymbol{w}^{(n)}\|^2} \leq v(\mathcal{P}_{\boldsymbol{w}^{(n+1)}}) \\
&= \frac{|\alpha_T|^2 \left| \boldsymbol{w}^{(n+1)\dagger} \left(\boldsymbol{s}^{(n+1)} \odot \boldsymbol{p}(\nu_{d_T}) \right) \right|^2}{\boldsymbol{w}^{(n+1)\dagger} \boldsymbol{\Sigma}_{\boldsymbol{C}} \left(\boldsymbol{s}^{(n+1)} \right) \boldsymbol{w}^{(n+1)} + \sigma_n^2 \|\boldsymbol{w}^{(n+1)}\|^2} = \text{SINR}^{(n+1)}, \quad (3.37)
\end{aligned}
$$

from (3.36) and (3.37) we obtain

$$
\text{SINR}^{(n)} \leq v(\mathcal{P}_{\boldsymbol{s}^{(n+1)}}) \leq v(\mathcal{P}_{\boldsymbol{w}^{(n+1)}}) = \text{SINR}^{(n+1)},
$$

and the monotonicity follows.

As to the convergence of the sequence $\text{SINR}^{(n)}$, let us observe that for all feasible points $(\boldsymbol{s}, \boldsymbol{w})$:

$$
\begin{aligned}
\frac{|\alpha_T|^2 \left| \boldsymbol{w}^\dagger \left(\boldsymbol{s} \odot \boldsymbol{p}(\nu_{d_T}) \right) \right|^2}{\boldsymbol{w}^\dagger \boldsymbol{\Sigma}_{\boldsymbol{C}} (\boldsymbol{s}) \boldsymbol{w} + \sigma_n^2 \|\boldsymbol{w}\|^2} &= \frac{|\alpha_T|^2 \left| \frac{\boldsymbol{w}}{\|\boldsymbol{w}\|}^\dagger \left(\boldsymbol{s} \odot \boldsymbol{p}(\nu_{d_T}) \right) \right|^2}{\frac{\boldsymbol{w}}{\|\boldsymbol{w}\|}^\dagger \boldsymbol{\Sigma}_{\boldsymbol{C}} (\boldsymbol{s}) \frac{\boldsymbol{w}}{\|\boldsymbol{w}\|} + \sigma_n^2} \\
&\leq \frac{|\alpha_T|^2}{\frac{\boldsymbol{w}}{\|\boldsymbol{w}\|}^\dagger \boldsymbol{\Sigma}_{\boldsymbol{C}} (\boldsymbol{s}) \frac{\boldsymbol{w}}{\|\boldsymbol{w}\|} + \sigma_n^2} \quad (3.38) \\
&\leq \frac{|\alpha_T|^2}{\sigma_n^2} \quad (3.39) \\
& \quad (3.40)
\end{aligned}
$$

where in (3.38) we used the Schwarz inequality and the fact that both $\frac{\boldsymbol{w}}{\|\boldsymbol{w}\|}$ and $\boldsymbol{s}$ have unit norm. Additionally, (3.39) stems from the fact that $\boldsymbol{\Sigma}_{\boldsymbol{C}}(\boldsymbol{s}) \succeq 0$. Consequently,

$$0 \leq \text{SINR}^{(n)} \leq \frac{|\alpha_T|^2}{\sigma_n^2}.$$

Since $\text{SINR}^{(n)}$ is a bounded above and monotone increasing sequence, it follows that $\text{SINR}^{(n)}$ converges to a finite value $\text{SINR}^{\star}$.

Finally, let us observe that given the sequence of points $\left\{\left(\boldsymbol{s}^{(n)}, \boldsymbol{w}^{(n)}\right)\right\}$, we can construct the sequence of feasible points $\left\{\left(\tilde{\boldsymbol{s}}^{(n)}, \tilde{\boldsymbol{w}}^{(n)}\right)\right\}$ of the problem $\mathcal{P}$, where $\tilde{\boldsymbol{s}}^{(n)} = \boldsymbol{s}^{(n)}$ and $\tilde{\boldsymbol{w}}^{(n)} = \frac{\boldsymbol{w}^{(n)}}{\|\boldsymbol{w}^{(n)}\|}$, satisfying the following conditions:

- $\widetilde{\text{SINR}}^{(n)} = \text{SINR}^{(n)} \quad \forall n$, where $\widetilde{\text{SINR}}^{(n)}$ is the value of the SINR evaluated in the point $\left(\tilde{\boldsymbol{s}}^{(n)}, \tilde{\boldsymbol{w}}^{(n)}\right)$;
- $\left(\tilde{\boldsymbol{s}}^{(n)}, \tilde{\boldsymbol{w}}^{(n)}\right) \in \mathcal{A} \quad \forall n$, where $\mathcal{A} = \left\{ (\boldsymbol{s}, \boldsymbol{w}) : \|\boldsymbol{s}\| = 1, \|\boldsymbol{s} - \boldsymbol{s}_0\| \leq \delta, \|\boldsymbol{w}\| = 1 \right\}$, is a compact set (closed and bounded set of $\mathbb{C}$).

Hence, we can extract from $\left(\tilde{\boldsymbol{s}}^{(n)}, \tilde{\boldsymbol{w}}^{(n)}\right)$ a converging subsequence, [29, Theorem A.4.2], $\left(\tilde{\boldsymbol{s}}^{(n')}, \tilde{\boldsymbol{w}}^{(n')}\right)$, whose limiting point $(\tilde{\boldsymbol{s}}^{\star}, \tilde{\boldsymbol{w}}^{\star}) \in \mathcal{A}$, i.e. $(\tilde{\boldsymbol{s}}^{\star}, \tilde{\boldsymbol{w}}^{\star})$ is a feasible point of the problem $\mathcal{P}$. Moreover, being SINR a continuous function

of $(\boldsymbol{s}, \boldsymbol{w})$, we have:

$$\text{SINR}^{*} = \lim_{n\to\infty} \widetilde{\text{SINR}}^{(n)} = \lim_{n'\to\infty} \widetilde{\text{SINR}}^{(n')} = \frac{|\alpha_T|^2 \left|\tilde{\boldsymbol{w}}^{\star\dagger} \left(\tilde{\boldsymbol{s}}^{\star} \odot \boldsymbol{p}(\nu_{d_T})\right)\right|^2}{\tilde{\boldsymbol{w}}^{\star\dagger} \boldsymbol{\Sigma}_{\boldsymbol{C}} \left(\tilde{\boldsymbol{s}}^{\star}\right) \tilde{\boldsymbol{w}}^{\star} + \sigma_n^2 \|\tilde{\boldsymbol{w}}^{\star}\|^2}. \tag{3.41}$$

Thus, the SINR evaluated in $(\tilde{\boldsymbol{s}}^{\star}, \tilde{\boldsymbol{w}}^{\star})$ is equal to SINR^{*} and the proof is concluded. □

3.6.4 Mutual Information Analysis

An interesting figure of merit, that can also be considered for designing the radar waveform, is the MI, see [65], between the received observations $\boldsymbol{v}$ and the complex backscattering target amplitude α_T, see [75]:

$$f_{MI}(\boldsymbol{s}) = \mathrm{I}\left(\alpha_T; \boldsymbol{v} | H_1, \boldsymbol{s}\right). \tag{3.42}$$

We follow a robust design, optimizing a lower bound to the MI given in (3.42), which depends only on the second order statistics of the independent random quantities α_T, $\boldsymbol{c}$, and $\boldsymbol{n}$. In fact, the MI (3.42) strongly depends on the probability density functions of α_T, $\alpha_{(r,i)}$, $\nu_{d_{(r,i)}}$, and $\boldsymbol{n}$, requiring too many a-priori information that can not be reasonably available at the design stage. Precisely,

it can be proved that, [76]:

Proposition 3.6.1. *Assuming that α_T, $\boldsymbol{c}$, and $\boldsymbol{n}$ are circularly invariant complex random vectors*[9]*, a lower bound to the MI (3.42) is:*

$$f_{MI}(\boldsymbol{s}) \geq \log\left(1 + (\boldsymbol{s} \odot \boldsymbol{p}(\nu_{d_T}))^{\dagger} \left[\boldsymbol{\Sigma}_{\boldsymbol{C}}(\boldsymbol{s}) + \boldsymbol{I}\right]^{-1} (\boldsymbol{s} \odot \boldsymbol{p}(\nu_{d_T}))\right) - D\left(\alpha_T, \alpha_T^G\right) \quad (3.43)$$

where α_T^G is a zero mean Gaussian random variable with the same variance of the backscattering target amplitude α_T, and $D\left(\alpha_T, \alpha_T^G\right)$ is the Kullback–Leibler divergence, see [65, Ch.9], between the distributions of the random variables α_T and α_T^G.

Proof. See Appendix 3.6.5. □

Consequently, considering the lower bound to the MI given in Proposition 3.6.1 as figure of merit, the design of the radar code can be formulated as the

[9] A complex random vector $\boldsymbol{x}$ is circularly invariant if the random vector $\exp(j\phi)\boldsymbol{x}$, where $\phi \sim \mathcal{U}\left(-\frac{1}{2}, \frac{1}{2}\right)$ is statistically independent of $\boldsymbol{x}$, is statistically equivalent to $\boldsymbol{x}$.

following constrained optimization problem:

$$\mathcal{P}_{MI} \begin{cases} \max\limits_{\boldsymbol{s}} & \log\left(1+\left(\boldsymbol{s}\odot\boldsymbol{p}(\nu_{d_T})\right)^{\dagger}\left[\boldsymbol{\Sigma_C}\left(\boldsymbol{s}\right)+\boldsymbol{I}\right]^{-1}\left(\boldsymbol{s}\odot\boldsymbol{p}(\nu_{d_T})\right)\right)-\mathrm{D}\left(\alpha_T,\alpha_T^G\right) \\ \text{s.t.} & \|\boldsymbol{s}\|^2=1 \\ & \|\boldsymbol{s}-\boldsymbol{s}_0\|^2\leq\delta, \end{cases} . \tag{3.44}$$

Since the function $\log(x)+\alpha$ is monotonically increasing in x, problem $\mathcal{P}_{MI}$ is equivalent to problem $\mathcal{P}'_{MI}$:

$$\mathcal{P}'_{MI} \begin{cases} \max\limits_{\boldsymbol{s}} & \left(\boldsymbol{s}\odot\boldsymbol{p}(\nu_{d_T})\right)^{\dagger}\left[\boldsymbol{\Sigma_C}\left(\boldsymbol{s}\right)+\boldsymbol{I}\right]^{-1}\left(\boldsymbol{s}\odot\boldsymbol{p}(\nu_{d_T})\right) \\ \text{s.t.} & \|\boldsymbol{s}\|^2=1 \\ & \|\boldsymbol{s}-\boldsymbol{s}_0\|^2\leq\delta, \end{cases} . \tag{3.45}$$

Finally, in order to solve problem $\mathcal{P}'_{MI}$, we prove the following Lemma:

Lemma 3.6.2. *Problem $\mathcal{P}'_{MI}$, given in (3.45), is equivalent to problem $\mathcal{P}$, pre-*

sented in (6.6), i.e. given an optimal solution $\boldsymbol{s}^{\star}_{MI}$ of $\mathcal{P}'_{MI}$ then

$$\left(\boldsymbol{s}^{\star}_{MI}, \frac{\left(\boldsymbol{\Sigma_c}\left(\boldsymbol{s}^{\star}_{MI}\right)+\sigma_n^2\boldsymbol{I}\right)^{-1}}{\left(\boldsymbol{s}^{\star}_{MI}\odot\boldsymbol{p}(\nu_{d_T})\right)^{\dagger}\left(\boldsymbol{\Sigma_c}\left(\boldsymbol{s}^{\star}_{MI}\right)+\sigma_n^2\boldsymbol{I}\right)^{-1}\left(\boldsymbol{s}^{\star}_{MI}\odot\boldsymbol{p}(\nu_{d_T})\right)}\left(\boldsymbol{s}^{\star}_{MI}\odot\boldsymbol{p}(\nu_{d_T})\right)\right)$$

is an optimal solution of $\mathcal{P}$, and conversely, given an optimal solution $(\boldsymbol{s}^{\star},\boldsymbol{w}^{\star})$ of $\mathcal{P}$, then $\boldsymbol{s}^{\star}$ is an optimal solution of $\mathcal{P}'_{MI}$.

Proof. See Appendix 3.6.6. □

Thus, we can use the optimization procedure of **Algorithm 4** to optimize the Mutual Information between the target backscattering and the received signal v. Furthermore, the optimal transmitted signal $\boldsymbol{s}^{*}$ in terms of SINR is also the optimal transmitted signal according to the lower bound to the MI, defined in Proposition 3.6.1.

3.6.5 Proof of Proposition 3.6.1

Proof. In order to prove Proposition 3.6.1, let us define the equivalent received vector:

$$\begin{aligned} \boldsymbol{y} &= \left[\boldsymbol{\Sigma_C}\left(\boldsymbol{s}\right)+\boldsymbol{I}\right]^{-\frac{1}{2}}\boldsymbol{v} \\ &= \left[\boldsymbol{\Sigma_C}\left(\boldsymbol{s}\right)+\boldsymbol{I}\right]^{-\frac{1}{2}}\left[\left(\boldsymbol{s}\odot\boldsymbol{p}(\nu_{d_T})\right)\alpha_T+\boldsymbol{c}+\boldsymbol{n}\right] \\ &= \bar{\boldsymbol{s}}\alpha_T+\boldsymbol{n}' \end{aligned} \tag{3.46}$$

where $\bar{\boldsymbol{s}}=\left[\boldsymbol{\Sigma_C}\left(\boldsymbol{s}\right)+\boldsymbol{I}\right]^{-\frac{1}{2}}\left(\boldsymbol{s}\odot\boldsymbol{p}(\nu_{d_T})\right)$ and $\boldsymbol{n}'=\left[\boldsymbol{\Sigma_C}\left(\boldsymbol{s}\right)+\boldsymbol{I}\right]^{-\frac{1}{2}}\left(\boldsymbol{c}+\boldsymbol{n}\right)$. Additionally, $\boldsymbol{n}'$ is a circularly symmetric white noise vector with unit variance statistically independent of α_T, because $\boldsymbol{c}$ and $\boldsymbol{n}$ are circularly symmetric random vectors statistically independent of α_T. Thus, the vectors $\boldsymbol{v}$ and $\boldsymbol{y}$ are related by an invertible mapping and, from the data processing inequality, see [65, pp. 32-33], we have that:

$$\mathrm{I}\left(\alpha_T;\boldsymbol{v}|H_1,\boldsymbol{s}\right)=\mathrm{I}\left(\alpha_T;\boldsymbol{y}|H_1,\bar{\boldsymbol{s}}\right) \tag{3.47}$$

Let us, now, expand the MI in the right hand side of (3.47) in the following way:

$$\mathrm{I}\left(\alpha_T; \boldsymbol{y}|H_1, \bar{\boldsymbol{s}}\right) = \mathrm{h}\left(\alpha_T|H_1, \bar{\boldsymbol{s}}\right) - \mathrm{h}\left(\alpha_T|H_1, \boldsymbol{y}, \bar{\boldsymbol{s}}\right), \tag{3.48}$$

where $\mathrm{h}\left(\boldsymbol{x}\right)$ and $\mathrm{h}\left(\boldsymbol{x}|\boldsymbol{z}\right)$ are, respectively, the differential entropy of the random vector $\boldsymbol{x}$, and the conditional differential entropy of the random vector $\boldsymbol{x}$ given $\boldsymbol{z}$, see [65, Ch. 9].

The conditional differential entropy $\mathrm{h}\left(\alpha_T|H_1, \boldsymbol{y}, \bar{\boldsymbol{s}}\right)$ can be upper bounded using the following chain of inequalities:

$$\begin{aligned}
\mathrm{h}\left(\alpha_T|H_1, \boldsymbol{y}, \bar{\boldsymbol{s}}\right) &= \mathrm{h}\left(\alpha_T|H_1, \boldsymbol{y}, \bar{\boldsymbol{s}}, \hat{\alpha}_T(\mathrm{y}, \bar{\boldsymbol{s}})\right) && (3.49)\\
&\leq \mathrm{h}\left(\alpha_T|H_1, \bar{\boldsymbol{s}}, \hat{\alpha}_T(\mathrm{y}, \bar{\boldsymbol{s}})\right) && (3.50)\\
&\leq \mathrm{h}\left(\epsilon_{\alpha_T}|H_1, \bar{\boldsymbol{s}}\right) && (3.51)
\end{aligned}$$

where $\hat{\alpha}_T(\mathrm{y}, \bar{\boldsymbol{s}})$ denotes an estimate of α_T, based on y and $\bar{\boldsymbol{s}}$, while $\epsilon_{\alpha_T} = \alpha_T - \hat{\alpha}_T(\mathrm{y}, \bar{\boldsymbol{s}})$ denotes the corresponding estimation error. Moreover, equality (3.49) follows from:

$$\mathrm{I}\left(\alpha_T; \hat{\alpha}_T(\mathrm{y}, \bar{\boldsymbol{s}})|H_1, \boldsymbol{y}, \bar{\boldsymbol{s}}\right) = 0$$

since, conditioned on $\boldsymbol{y}$, $\hat{\alpha}_T(\mathbf{y}, \bar{\boldsymbol{s}})$ is a deterministic quantity and then statistically independent of α_T. Inequalities (3.50) and (3.51) are due to the fact that conditioning reduces the entropy, [65, Ch. 9].

Letting $\hat{\alpha}_T(\mathbf{y}, \bar{\boldsymbol{s}})$ be the conditional Linear Minimum Mean Square Error (LMMSE) estimator, we have:

$$\hat{\alpha}_T = \sigma_T^2 \bar{\boldsymbol{s}}^\dagger \left(\bar{\boldsymbol{s}} \sigma_T^2 \bar{\boldsymbol{s}}^\dagger + \boldsymbol{I} \right)^{-1} \mathbf{y} \tag{3.52}$$

where we are assuming that both α_T and $\boldsymbol{y}$ have zero mean, and we have indicated with $\mathbb{E}\left[|\alpha_T|^2\right] = \sigma_T^2$. After some simple algebraic manipulations, the error variance of the estimator, in (3.52), can be expressed as:

$$\sigma_T^2 - \sigma_T^2 \bar{\boldsymbol{s}}^\dagger \left(\bar{\boldsymbol{s}} \sigma_T^2 \bar{\boldsymbol{s}}^\dagger + \boldsymbol{I} \right)^{-1} \bar{\boldsymbol{s}} \sigma_T^2. \tag{3.53}$$

In order to get a lower bound to (3.48), we will provide an upper bound to the conditional differential entropy of the error in (3.49). To this end, the entropy maximizing property of the Gaussian distribution with the same variance is

exploited, [65, Ch. 9]. Moreover, applying the inversion Lemma[10] to the variance in (3.53), we obtain:

$$\mathrm{h}\left(\alpha_T|H_1,\boldsymbol{y},\bar{\boldsymbol{s}}\right)\leq-\log\left(1+\left(\boldsymbol{s}\odot\boldsymbol{p}(\nu_{d_T})\right)^{\dagger}\left[\boldsymbol{\Sigma}_{\boldsymbol{C}}\left(\boldsymbol{s}\right)+\boldsymbol{I}\right]^{-1}\left(\boldsymbol{s}\odot\boldsymbol{p}(\nu_{d_T})\right)\right)+\mathrm{h}\left(\alpha_T^G\right) \tag{3.54}$$

Consequently, using (3.47), (3.48), and (3.54), we obtain

$$\mathrm{I}\left(\alpha_T;\boldsymbol{v}|H_1,\boldsymbol{s}\right)\geq\log\left(1+\left(\boldsymbol{s}\odot\boldsymbol{p}(\nu_{d_T})\right)^{\dagger}\left[\boldsymbol{\Sigma}_{\boldsymbol{C}}\left(\boldsymbol{s}\right)+\boldsymbol{I}\right]^{-1}\left(\boldsymbol{s}\odot\boldsymbol{p}(\nu_{d_T})\right)\right)-\mathrm{D}(\alpha_T,\alpha_T^G) \tag{3.55}$$

where we used $\mathrm{D}(\alpha_T,\alpha_T^G)=\mathrm{h}\left(\alpha_T^G\right)-\mathrm{h}\left(\alpha_T\right)$. □

3.6.6 Proof of Proposition 3.6.2

Proof. Let $\boldsymbol{s}_{MI}^{\star}$ be an optimal solution to $\mathcal{P}'_{MI}$; obviously, $v(\mathcal{P}'_{MI})\leq v(\mathcal{P})$, since

$$\left(\boldsymbol{s}_{MI}^{\star},\frac{\left(\boldsymbol{\Sigma}_{\boldsymbol{C}}\left(\boldsymbol{s}_{MI}^{\star}\right)+\sigma_n^2\boldsymbol{I}\right)^{-1}}{\left(\boldsymbol{s}_{MI}^{\star}\odot\boldsymbol{p}(\nu_{d_T})\right)^{\dagger}\left(\boldsymbol{\Sigma}_{\boldsymbol{C}}\left(\boldsymbol{s}_{MI}^{\star}\right)+\sigma_n^2\boldsymbol{I}\right)^{-1}\left(\boldsymbol{s}_{MI}^{\star}\odot\boldsymbol{p}(\nu_{d_T})\right)}\left(\boldsymbol{s}_{MI}^{\star}\odot\boldsymbol{p}(\nu_{d_T})\right)\right)$$

[10] We exploit in our derivation the fact that for any square matrix $\mathbf{A}=\mathbf{B}-\mathbf{B}\mathbf{C}^{\dagger}(\mathbf{C}\mathbf{B}\mathbf{C}^{\dagger}+\mathbf{D})^{-1}\mathbf{C}\mathbf{B}$, we may express its inverse as $\mathbf{A}^{-1}=\mathbf{B}^{-1}+\mathbf{C}^{\dagger}\mathbf{D}^{-1}\mathbf{C}$ and the well known relation $|\mathbf{A}|^{-1}=|\mathbf{A}^{-1}|$.

is a feasible point for $\mathcal{P}$. Conversely, let $(\boldsymbol{s}^\star, \boldsymbol{w}^\star)$ be an optimal solution of $\mathcal{P}$.

This implies that

$$\boldsymbol{w}^\star = \frac{\left(\boldsymbol{\Sigma_C}\left(\boldsymbol{s}^\star\right) + \sigma_n^2 \boldsymbol{I}\right)^{-1}}{\left(\boldsymbol{s}^\star \odot \boldsymbol{p}(\nu_{d_T})\right)^\dagger \left(\boldsymbol{\Sigma_C}\left(\boldsymbol{s}^\star\right) + \sigma_n^2 \boldsymbol{I}\right)^{-1} \left(\boldsymbol{s}^\star \odot \boldsymbol{p}(\nu_{d_T})\right)} \left(\boldsymbol{s}^\star \odot \boldsymbol{p}(\nu_{d_T})\right).$$

Consequently, the optimal value of the objective function of $\mathcal{P}$ is,

$$\left(\boldsymbol{s}^\star \odot \boldsymbol{p}(\nu_{d_T})\right)^\dagger \left[\boldsymbol{\Sigma_C}\left(\boldsymbol{s}^\star\right) + \boldsymbol{I}\right]^{-1} \left(\boldsymbol{s}^\star \odot \boldsymbol{p}(\nu_{d_T})\right)$$

which can also be achieved by $\mathcal{P}'_{MI}$, choosing $\boldsymbol{s}^\star_{MI} = \boldsymbol{s}^\star$. Then $v(\mathcal{P}'_{MI}) \geq v(\mathcal{P})$ and the proof is completed. □

3.6.7 Proof of Proposition 3.3.3

Proof. First of all, we prove that $\mathcal{P}_{\boldsymbol{w}^{(n)}}$ is equivalent to the problem $\mathcal{P}_{1'}$:

$$\mathcal{P}_{1'} \begin{cases} \max\limits_{\boldsymbol{w}} & \dfrac{|\alpha_T|^2 \left|\boldsymbol{w}^\dagger \left(\boldsymbol{s}^{(n)} \odot \boldsymbol{p}(\nu_{d_T})\right)\right|^2}{\boldsymbol{w}^\dagger \boldsymbol{\Sigma_C}\left(\boldsymbol{s}^{(n)}\right) \boldsymbol{w} + \sigma_n^2 \|\boldsymbol{w}\|^2} \\ \text{s.t.} & \boldsymbol{w}^\dagger \left(\boldsymbol{s}^{(n)} \odot \boldsymbol{p}(\nu_{d_T})\right) = 1 \end{cases}. \tag{3.56}$$

In fact, $v(\mathcal{P}_{\boldsymbol{w}^{(n)}}) \geq v(\mathcal{P}_{1'})$, because we are adding a constraint. Moreover, let $\boldsymbol{w}^{(n)}$ be an optimal solution of problem $\mathcal{P}_{\boldsymbol{w}^{(n)}}$. Then, $\boldsymbol{w}'_{1'} = \frac{\boldsymbol{w}^{(n)}}{\left|\boldsymbol{w}^{(n)\dagger}\left(\boldsymbol{s}^{(n)}\odot\boldsymbol{p}(\nu_{d_T})\right)\right|}$ $\exp(j\text{arg}(\boldsymbol{w}^{(n)^\dagger}\left(\boldsymbol{s}^{(n)}\odot\boldsymbol{p}(\nu_{d_T})\right)))$ is an optimal solution of $\mathcal{P}_{1'}$ with $v(\mathcal{P}_{\boldsymbol{w}^{(n)}}) = v(\mathcal{P}_{1'})$.

Obviously, $\mathcal{P}_{1'}$ is equivalent to $\mathcal{P}_{1''}$:

$$\mathcal{P}_{1''}\begin{cases}\min\limits_{\boldsymbol{w}} \quad \boldsymbol{w}^\dagger\boldsymbol{\Sigma}_{\boldsymbol{C}}\left(\boldsymbol{s}^{(n)}\right)\boldsymbol{w}+\sigma_n^2\|\boldsymbol{w}\|^2 \\ \\ \text{s.t.} \quad \boldsymbol{w}^\dagger\left(\boldsymbol{s}^{(n)}\odot\boldsymbol{p}(\nu_{d_T})\right)=1\end{cases}. \tag{3.57}$$

i.e. $v(\mathcal{P}_{1'}) = \frac{1}{v(\mathcal{P}_{1''})}$ and if $\boldsymbol{w}^\star_{1'}$ is an optimal solution of $\mathcal{P}_{1'}$ then it is also an optimal solution of $\mathcal{P}_{1''}$ and vice versa.

Finally, $\mathcal{P}_{1''}$ is equivalent to $\mathcal{P}_1$; in fact $v(\mathcal{P}_1) \leq v(\mathcal{P}_{1''})$, because we are adding a constraint. Moreover, let $\boldsymbol{w}_1^\star$ be an optimal solution of problem $\mathcal{P}_1$, then,

$$\boldsymbol{w}'_{1''} = \frac{\boldsymbol{w}_1^\star}{\left|\boldsymbol{w}_1^{\star\dagger}\left(\boldsymbol{s}^{(n)}\odot\boldsymbol{p}(\nu_{d_T})\right)\right|}\exp(j\text{arg}(\boldsymbol{w}_1^{\star\dagger}\left(\boldsymbol{s}^{(n)}\odot\boldsymbol{p}(\nu_{d_T})\right)))$$

is an optimal solution of $\mathcal{P}_{1''}$ and $v(\mathcal{P}_{1''}) = \frac{v(\mathcal{P}_1)}{\left|\boldsymbol{w}_1^{\star\dagger}\left(\boldsymbol{s}^{(n)}\odot\boldsymbol{p}(\nu_{d_T})\right)\right|^2}$. Since $\left|\boldsymbol{w}_1^{\star\dagger}\left(\boldsymbol{s}^{(n)}\odot\boldsymbol{p}(\nu_{d_T})\right)\right| \geq 1$, it follows that $\boldsymbol{w}'_{1''} = \boldsymbol{w}_1^\star$. From the above chain of equivalences, it follows that an optimal solution $\boldsymbol{w}_1^\star$ of $\mathcal{P}_1$ is an optimal solution of $\mathcal{P}_{\boldsymbol{w}^{(n)}}$. □

Chapter 4

Non-Cooperative Code Design in Radar Networks: A Game-Theoretic Approach

4.1 Introduction

In the last decade, the importance of radar has grown progressively with the increasing dimension of the system: from a single colocated antenna to a large sensor network [1]. The concept of heterogeneous radars working together has been thoroughly studied, opening the door to the ideas of Multiple-Input-Multiple-Output (MIMO) radar [2, 3], Over-The-Horizon (OTH) radar networks [4], and Distributed Aperture Radar (DAR) [5, 6]. These three scenarios are examples of *cooperative radar networks*, in the sense that every single element contributes to the overall detection process. Unfortunately, in many practical situations, it is not possible to design the network *a-priori*. As such,

the elements are just simply added to the already existing network (*plug and fight*), and each sensor exhibits its own detection scheme. This is the case in *non-cooperative radar networks* [7, 8]; in this scenario, it is extremely important that each additional sensor interferes as little as possible with the pre-existing elements, and, to this end, suitable techniques are to be adopted. The usual approaches rely upon the employment of spatial and/or frequency diversity: the former resorts to forming multiple orthogonal beams, while the latter uses separated carrier frequencies to reduce interference [9, 10]. Another possibility is to exploit waveform diversity [32]; here, the basic concept is to suitably modulate the waveform of the new sensor so as to optimize the detection capabilities of the specific sensor, but, at the same time, controlling the interference introduced into the network. Notice that this is different from the approach employed in cooperative sensor network, where one must design waveforms so as to optimize the joint performance of the system [11, 12].

With regard to the optimization of radar waveforms in a non-cooperative scenario, we cite here the studies [13] and [78]. In paper [13], the design is based upon the maximization of the global Signal-to-Interference-plus-Noise Ratio (SINR), and classic constraints such as phase-only or finite energy are

considered; in [78], instead, the problem of parameter estimation (e.g. direction of arrival) for a non-cooperative radar is analyzed. In the present report, we propose a different strategy, based upon a game-theoretic approach [79]; we thus deal with the active radars as if they were players of a properly modeled game, whose set of possible strategies is made up of a certain amount of pre-fixed transmit radar codes. We design *utility* functions, based on the framework of potential games [80], in order to improve the SINR of the active radars through a non-cooperative game. Thus, we present several non-cooperative games for radar-code optimization in a non-cooperative environment, considering different types of receive filters and accounting for the case of non-negligible Doppler shifts too.

The chapter is organized as follows. In Section 4.2, we give some background material on game theory and on potential games, which will be needed in the remaining part of the chapter. In Section 4.3, we present the considered radar network signal model and dwell on the proposed non-cooperative games for radar code updating. Section 4.4 is devoted to the analysis of the performance of the proposed games, while, finally, Section 4.5 contains the conclusions.

4.2 Brief preliminaries on game theory

Formally speaking, a game $\mathcal{G}$ in its normal form can be described as the triplet $\mathcal{G} = [\mathcal{K}, \{\mathcal{S}_k\}, \{u_k\}]$, wherein $\mathcal{K} = \{1, 2, \ldots, K\}$ is the set of players participating in the game, u_k is the k-th player's utility function (depending on the players' chosen strategies), and $\mathcal{S}_k$ is the set of possible actions (strategies) that player k can take. We will be considering one-shot games wherein players, in a round-robin fashion, update their strategies based on the strategies chosen by the other players, and aiming at their own utility function maximization. If, following such a strategy, an equilibrium is reached (or, in other words, if such an iterative procedure converges to a stable set of chosen strategies), then such an equilibrium is called Nash Equilibrium (NE), whose formal definition is here given. Let

$$(s_1, s_2, \ldots, s_K) \in \mathcal{S}_1 \times \mathcal{S}_2 \times \ldots \mathcal{S}_K$$

denote a certain strategy K-tuple for the active players. Letting, as customary in the game theory literature, $\boldsymbol{s}_{-k}$ denote the $(K-1)$-dimensional vector whose entries are the strategies of all the players except the k-th, the point

$(s_1, s_2, \ldots, s_K) = (s_k, \boldsymbol{s}_{-k})$ is an NE if, for any player k, we have

$$u_k(s_k, \boldsymbol{s}_{-k}) \geq u_k(s_k^*, \boldsymbol{s}_{-k}) \ ,$$

$\forall s_k^* \neq s_k$. Otherwise stated, at an NE, no user can *unilaterally* improve its own utility by taking a different strategy. A quick reading of this definition might lead to think that at NE users' utilities achieve their maximum values. Actually, this is not the case, since the existence of a NE point does not imply that no other strategy K-tuple exists that can lead to an improvement of the utilities of some players while not decreasing the utilities of the remaining ones. These latter strategies are usually said to be Pareto-optimal [79]. Otherwise stated, at an NE, each player, provided that the other players' strategies do not change, is not interested in changing its own strategy. However, if some sort of cooperation would be available, players might agree to simultaneously switch to a different strategy K-tuple, so as to improve the utility of some, if not all, players, while not decreasing the utility of the remaining ones. The gap existing between the achieved utilities at the NE and those achieved in correspondence of Pareto-optimal points is sometime colorfully named "the price of anarchy."

The concept of *best response dynamic* is also worth being introduced. Given a certain strategy profile $(s_k, \boldsymbol{s}_{-k})$ for the active players, we say that a player implements a best response dynamic if he chooses as its new strategy $\widetilde{s}_k = \arg\max_x u_k(x, \boldsymbol{s}_{-k})$. Given this definition, it descends that the set of chosen strategies at a NE is the best response for every active player.

4.2.1 Potential games [80]

A potential game is a normal form game wherein any change in the utility enjoyed by a given player in reaction to a unilateral (i.e., assuming that the other players do not change their strategies) change of strategy by that player is reflected by a similar change in a global function, that is usually referred to as potential function. Formally speaking, letting $\mathcal{S} = \mathcal{S}_1 \times \mathcal{S}_2 \times \cdots \times \mathcal{S}_K$, a normal form game is an *exact potential game* if there exists a function $T : \mathcal{S} \to \mathcal{R}$, known as the *exact potential function*, such that

$$u_k(s_k, s_{-k}) - u_k(\widetilde{s}_k, s_{-k}) = T(s_k, s_{-k}) - T(\widetilde{s}_k, s_{-k}) \ ,$$

for any $k \in \mathcal{K}$, $s_k, \widetilde{s}_k \in \mathcal{S}_k$, and for any $\boldsymbol{s}_{-k} \in \mathcal{S}_1 \times \cdots \mathcal{S}_{k-1} \times \mathcal{S}_{k+1} \times \cdots \mathcal{S}_K$. Given a normal form game, a potential function subsumes the effects that any uni-

lateral change of strategy may have on the utility enjoyed by that individual player. A moment of thought also reveals that every NE of an exact potential game must necessarily be a (possibly local) maximizer of the potential function, as well as that a best response dynamic in a potential game will converge to a NE in every game with continuous utility functions and compact strategy spaces. Finally, it is also worth underlining that, if the potential function does represent a global performance measure for the considered system, potential games are an instance wherein users can serve the greater good while playing a non-cooperative game and acting selfishly.

In the following, we will be using game theory concepts to model competition among a set of radars (the players) that tune their own transmitted code in order to maximize their SINR. Potential games will be used to come up with procedures convergent to an NE.

4.3 Problem Formulation and Code Updating Procedure

We consider a network of L non-cooperative monostatic radar systems, where each sensor transmits a coded pulse composed of N sub-pulses. The signal backscattered toward the l-th radar is filtered through a subpulse matched filter and then converted to digital. The vector $\boldsymbol{r}_l$ containing the received sequence $r_{k,l}$, $k = 1, \ldots, N$, assumed temporally aligned with the returns from the range bin of interest, can be written as [81, 82]

$$\boldsymbol{r}_l = \alpha_{0,l}\boldsymbol{c}_l + \sum_{k=-N+1,k\neq 0}^{N-1} \alpha_{k,l}\boldsymbol{J}_k\boldsymbol{c}_l + \sum_{h=1,h\neq l}^{L}\sum_{k=-N+1}^{N-1} \alpha_{k,h}\boldsymbol{J}_k\boldsymbol{c}_h + \boldsymbol{n}_l\,, \tag{4.1}$$

where $\boldsymbol{c}_l = [c_l(1)\ldots c_l(N)]^T$ denotes the unit-norm N-dimensional modulating sequence of the l-th radar, $\alpha_{k,h}$ are complex parameters accounting for the radar cross section of the k-th range bin illuminated by the h-th radar (0 is conventionally chosen as the range bin of interest), $\boldsymbol{n}_l$ is the vector containing the filtered thermal noise samples at the l-th radar (modeled as a zero-mean

complex circular white vector), and the matrix

$$\boldsymbol{J}_k = \boldsymbol{J}_{-k}^T = \begin{cases} \boldsymbol{J}_k(j,i) = 1 \quad i-j=k \\ \\ \boldsymbol{J}_k(j,i) = 0 \quad \text{otherwise} \end{cases} \tag{4.2}$$

($k = 0, \dots N-1$, $(i,j) \in \{1, \dots, N\}^2$) is the $N \times N$ shift matrix. As to the modulating sequence $\boldsymbol{c}_l$, we suppose that it belongs to a finite set Ω_l which contains all the possible sequences of length N that the l-th radar can transmit.

It is interesting to provide an interpretation of the contributions appearing in the right hand side of (4.1). Indeed, the first term represents the signal component from the range bin of interest for the l-th radar; the second contribution accounts for the self-induced interference, while the third addend represents the interference caused by the other radars of the network on the l-th one.

Now, the vector $\boldsymbol{r}_l$ is to be suitably processed in order to detect the possible presence of a target in the range cell of interest. We thus consider the following receiving structure: the vector $\boldsymbol{r}_l$ undergoes a linear transformation (projection over a suitable direction vector), and, then, its square modulus is compared

with a threshold, i.e. we consider the detection rule

$$|\boldsymbol{d}_l^\dagger(\boldsymbol{c}_l)\boldsymbol{r}_l|^2 \underset{H_0}{\overset{H_1}{\gtrless}} \eta_l \tag{4.3}$$

with $\boldsymbol{d}_l(\boldsymbol{c}_l)$ denoting an N-dimensional vector, function of the transmit code $\boldsymbol{c}_l$, to be suitably designed (it could be a standard matched filter or a mismatched filter [83, 84, 85] designed to optimize some performance metrics such as the Integrated Sidelobe Level (ISL) or the Peak to Sidelobe Level (PSL) - see more details in the sequel of the chapter), and η_l the detection threshold in the l-th radar. Given the detection rule (4.3), we can define a SINR for the l-th radar in the range cell of interest, γ_l say, as follows[1]

$$\gamma_l = \frac{\boldsymbol{G}(l,l)|\boldsymbol{d}_l^\dagger(\boldsymbol{c}_l)\boldsymbol{c}_l|^2}{\boldsymbol{d}_l^\dagger(\boldsymbol{c}_l)\boldsymbol{d}_l(\boldsymbol{c}_l) + \sum\limits_{h=1,h\neq l}^{L}\sum\limits_{k=-N+1}^{N-1}\boldsymbol{G}(h,l)|\boldsymbol{d}_l^\dagger(\boldsymbol{c}_l)\boldsymbol{J}_k\boldsymbol{c}_h|^2 + \boldsymbol{G}(l,l)\sum\limits_{k=-N+1,k\neq 0}^{N-1}|\boldsymbol{d}_l^\dagger(\boldsymbol{c}_l)\boldsymbol{J}_k\boldsymbol{c}_l|^2}, \tag{4.4}$$

where the matrix $\boldsymbol{G}$ models the beam-pattern of the receive antenna.

The SINR γ_l is indeed a measure of the detection capabilities of the l-th radar in the range cell of interest. Note that at the denominator we have the

[1]Actually, the SINR definition should include also the coefficients $\alpha_{\cdot,\cdot}$; however, no prior knowledge of these coefficients may be reasonably assumed, and we are thus omitting them in the SINR definition reported in (4.4).

contributions from the backscattered signals transmitted from the other (interfering) radars, weighted by the antenna pattern according to their direction of arrival; it thus follows that a proper design of the receive pattern helps to increase the detection capabilities.

4.3.1 Antenna beam pattern

The design of the receive antenna beam is of primary importance, especially in the case in which multiple radars operate in the same area. This problem is a classical one, and has been deeply analyzed in past years, especially with reference to wireless communications [86], where adaptive antennas are used in conjunction with power control and smart Multiple Access (MA) techniques. Obviously, it also plays a primary role in radar applications, where all the transmitting systems act as reciprocal sources of interference. Since we are considering here a non-cooperative scenario, no MA or a-priori coordination schemes can be applied. Likewise, since the ultimate goal of a radar is to maximize its detection capability, resorting to power control is unrealistic. In the radar scenario, the beam pattern of the antennas is used as a means to improve the received SINR and to weaken interfering echoes. A good model for

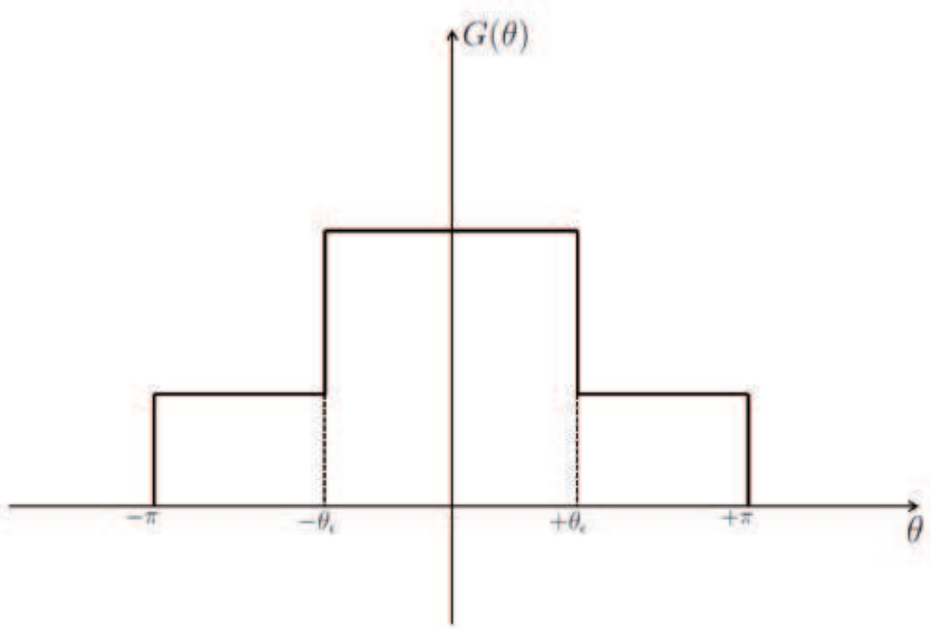

Figure 4.1: Antenna Beam Pattern. Main beam: $\theta \in [-\theta_\epsilon, +\theta_\epsilon]$. Side beam: $\theta \in [-\pi, -\theta_\epsilon] \cup [+\theta_\epsilon, +\pi]$

the beam pattern $G(\theta)$ is the one illustrated in **Figure 4.1**, where $\theta = 0$ is the radar search direction[2]; for instance, such a shape can be obtained through an N-element array [87]. Herein, we thus assume that the antenna gain may take two possible constant values, one for $\theta \in [-\theta_\epsilon, +\theta_\epsilon]$, and one (much lower than the former) outside the above interval: the side contributions are thus all equally weighted by the side beams. The effect of the antenna pattern can be therefore simply modeled as a proper $L \times L$ gain matrix $\boldsymbol{G}$, whose (h, l)-th element accounts for the effects of the h-th radar on the l-th system; the

[2]We are considering a bi-dimensional scenario where $G(\theta)$ is the azimuth beam pattern. However, the extension to a three-dimensional situation accounting for both azimuth and elevation is quite easy.

coefficients for $l \neq h$ are assumed to be a proper constant. The $\boldsymbol{G}(l,l)$ elements on the principal diagonal represent the main beam gain, weighting the useful signal for the l-th radar.

Given the outlined system model, our actual goal now is to design a non-cooperative procedure for adapting the radar codes in order to maximize the individual detection performances.

4.3.2 Matched filter

Given equation (4.4), we begin with assuming that $\boldsymbol{d}_l = \boldsymbol{c}_l$, i.e. a conventional matched filter receiver is used, and consider minimization of the denominator in (4.4), which is equivalent to optimizing γ_l since $||\boldsymbol{c}_l|| = 1$. We thus obtain the optimization problem

$$\min_{\boldsymbol{c}_l \in \Omega_l} \left\{ \boldsymbol{c}_l^{\dagger} \left(\boldsymbol{I} + \sum_{h=1, h\neq l}^{L} \sum_{k=-N+1}^{N-1} \boldsymbol{G}(h,l) \boldsymbol{J}_k \boldsymbol{c}_h \boldsymbol{c}_h^{\dagger} \boldsymbol{J}_k^T + \boldsymbol{G}(l,l) \sum_{k=-N+1, k\neq 0}^{N-1} \boldsymbol{J}_k \boldsymbol{c}_l \boldsymbol{c}_l^{\dagger} \boldsymbol{J}_k^T \right) \boldsymbol{c}_l \right\} , \tag{4.5}$$

for $l = 1, \ldots, L$. The solution for $\boldsymbol{c}_l$ to problem (4.5) exists and can be found through an exhaustive optimization over the finite set Ω_l, with an acceptable computational complexity because in practice the quoted set contains a quite

small number of elements.

Unfortunately, when active radars update their own transmitted waveforms according to such a strategy, no sufficient condition has been analytically worked out for the existence of Nash equilibria, and, moreover, numerical simulations have confirmed that when radars, in a round-robin fashion, update their codes according to the strategy (4.5), an equilibrium is not always reached. The considered game has thus no pure strategy equilibrium. One possible way to circumvent such a problem is to properly modify the utility function to be considered so that the resulting game may have an NE point. In particular, if we choose to use the tool of potential games, the trick is to define a new utility function, strictly related to (4.4), but whose maximization by the competing radars leads to an NE. To this end, let us consider the opposite of the sum of the denominators of γ_l's for the L active radars, i.e.:

$$T(\boldsymbol{c}_1,\ldots,\boldsymbol{c}_L) = -\sum_{l=1}^{L} \boldsymbol{c}_l^{\dagger}\left(\boldsymbol{I} + \sum_{h=1,h\neq l}^{L}\sum_{k=-N+1}^{N-1} \boldsymbol{G}(h,l)\boldsymbol{J}_k\boldsymbol{c}_h\boldsymbol{c}_h^{\dagger}\boldsymbol{J}_k^{T} + \boldsymbol{G}(l,l)\sum_{k=-N+1,k\neq 0}^{N-1}\boldsymbol{J}_k\boldsymbol{c}_l\boldsymbol{c}_l^{\dagger}\boldsymbol{J}_k^{T}\right)\boldsymbol{c}_l \ . \tag{4.6}$$

Upon some straightforward algebraic manipulations, we have

$$T(\boldsymbol{c}_1,\ldots,\boldsymbol{c}_L) = -\boldsymbol{c}_j^\dagger\left(\boldsymbol{I}+\sum_{h=1,h\neq j}^{L}\sum_{k=-N+1}^{N-1}\boldsymbol{G}(h,j)\boldsymbol{J}_k\boldsymbol{c}_h\boldsymbol{c}_h^\dagger\boldsymbol{J}_k^T+\boldsymbol{G}(j,j)\sum_{k=-N+1,k\neq 0}^{N-1}\boldsymbol{J}_k\boldsymbol{c}_j\boldsymbol{c}_j^\dagger\boldsymbol{J}_k^T\right)\boldsymbol{c}_j - \sum_{h=1,h\neq j}^{L}\sum_{k=-N+1}^{N-1}\boldsymbol{G}(j,h)\boldsymbol{c}_j^\dagger\boldsymbol{J}_k^T\boldsymbol{c}_h\boldsymbol{c}_h^\dagger\boldsymbol{J}_k\boldsymbol{c}_j - T_1(\boldsymbol{c}_1,\ldots,\boldsymbol{c}_{j-1},\boldsymbol{c}_{j+1},\ldots,\boldsymbol{c}_L)\,, \tag{4.7}$$

where the function $T_1(\boldsymbol{c}_1,\ldots,\boldsymbol{c}_{j-1},\boldsymbol{c}_{j+1},\ldots,\boldsymbol{c}_L)$ does not depend on $\boldsymbol{c}_j$. In Eq. (4.7), we have isolated the terms depending on the j-th radar code $\boldsymbol{c}_j$; it thus readily follows that if we consider a game wherein the utility for the j-th sensor is expressed as

$$u_j = -\boldsymbol{c}_j^\dagger\left(\boldsymbol{I}+\sum_{h=1,h\neq j}^{L}\sum_{k=-N+1}^{N-1}\boldsymbol{G}(h,j)\boldsymbol{J}_k\boldsymbol{c}_h\boldsymbol{c}_h^\dagger\boldsymbol{J}_k^T+\boldsymbol{G}(j,j)\sum_{k=-N+1,k\neq 0}^{N-1}\boldsymbol{J}_k\boldsymbol{c}_j\boldsymbol{c}_j^\dagger\boldsymbol{J}_k^T\right)\boldsymbol{c}_j - \sum_{h=1,h\neq j}^{L}\sum_{k=-N+1}^{N-1}\boldsymbol{G}(j,h)\boldsymbol{c}_j^\dagger\boldsymbol{J}_k^T\boldsymbol{c}_h\boldsymbol{c}_h^\dagger\boldsymbol{J}_k\boldsymbol{c}_j\,, \tag{4.8}$$

we obtain an exact potential game with potential function $T(\cdot)$. Summing up, we propose the radar code update procedure reported in **Algorithm 5**.

As already discussed, since at each iteration the potential function in (4.7) gets increased, and since it is upper bounded, it necessarily follows that the above iterative algorithm must reach a fixed point (NE). Notice however that

Algorithm 5 : Radar update procedure - Matched filter

Input: Ω_j, L;

Output: a NE solution for the potential game with utility (4.8);

1: assume that radar codes are arbitrarily chosen;
2: **while** the convergence is not reached **do**
3: **for** $j = 1$ to L **do**
4: update the j-th radar code according to

$$\boldsymbol{c}_j = \arg\max_{\boldsymbol{x}\in\Omega_j} -\boldsymbol{x}^\dagger \left(\boldsymbol{I} + \sum_{h=1,h\neq j}^{L} \sum_{k=-N+1}^{N-1} \boldsymbol{G}(h,j)\boldsymbol{J}_k \boldsymbol{c}_h \boldsymbol{c}_h^\dagger \boldsymbol{J}_k^T + \boldsymbol{G}(j,j) \sum_{k=-N+1,k\neq 0}^{N-1} \boldsymbol{J}_k \boldsymbol{x}\boldsymbol{x}^\dagger \boldsymbol{J}_k^T \right) \boldsymbol{x} - \sum_{h=1,h\neq j}^{L} \sum_{k=-N+1}^{N-1} \boldsymbol{G}(j,h)\boldsymbol{x}^\dagger \boldsymbol{J}_k^T \boldsymbol{c}_h \boldsymbol{c}_h^\dagger \boldsymbol{J}_k \boldsymbol{x} \tag{4.9}$$

5: **end for**
6: **end while**

there is in general no guarantee that such a fixed point is the global maximizer of the potential function, or just a local extremum.

4.3.3 Minimum ISL filter

The matched filter, considered in the previous section, is obviously the classical receiving structure used in detection problems. However, it does not allow to completely control the sidelobe energies, a feature that may be critical in radar applications. Indeed, this limitation may strongly affect the range resolution and the target detection capabilities of the radar system, especially

in scenarios where multiple radars have to co-exist in the same area, thus becoming themselves the main source of reciprocal interference.

Therefore, viable alternatives to the matched filter may be sought. From this point of view, relevant metrics to be considered are the ones related to the energies in the sidelobes, which, with reference to the l-th radar of (4.1), can be modeled as $\frac{|\boldsymbol{d}_{\boldsymbol{l}}^{\dagger}(\boldsymbol{c}_l)\boldsymbol{J}_k\boldsymbol{c}_l|^2}{|\boldsymbol{d}_l(\boldsymbol{c}_l)\boldsymbol{c}_l|^2}$, $k=\pm 1,\ldots,\pm N-1$. Specifically, if one wants to constraint the total energy underlying the sidelobes, it is possible to consider the ISL

$$\text{ISL}=\frac{\sum_{k=N+1,k\neq 0}^{N-1}|\boldsymbol{d}_l(\boldsymbol{c}_l)^{\dagger}\boldsymbol{J}_k\boldsymbol{c}_l|^2}{|\boldsymbol{d}_l(\boldsymbol{c}_l)^{\dagger}\boldsymbol{c}_l|^2}. \tag{4.10}$$

Indeed, designing a filter with minimum ISL is tantamount to minimizing the total energy in the range sidelobes - see, for instance, [88, 81]. In particular, with reference to the l-th radar of model (4.1), the optimal ISL filter may be found as the solution to the following minimization problem:

$$\min_{\boldsymbol{x}\in\mathbb{C}^N}\frac{\boldsymbol{x}^{\dagger}\boldsymbol{R}_l\boldsymbol{x}}{|\boldsymbol{x}^{\dagger}\boldsymbol{c}_l|^2} \tag{4.11}$$

where

$$\boldsymbol{R}_l\triangleq\sum_{k=_N+1,k\neq 0}^{N-1}\boldsymbol{J}_k\boldsymbol{c}_l\boldsymbol{c}_l^{\dagger}\boldsymbol{J}_k^{\dagger}.$$

It is easy to verify that a solution to (4.11) also solves the following constrained minimization problem

$$\begin{aligned} \min_{\boldsymbol{x}\in\mathbb{C}^N} \quad & \boldsymbol{x}^\dagger \boldsymbol{R}_l \boldsymbol{x} \\ \text{s.t.} \quad & \Re(\boldsymbol{x}^\dagger \boldsymbol{c}_l) = b, \end{aligned} \tag{4.12}$$

in the sense that $v(4.11) = \dfrac{v(4.12)}{b^2}$.

It is well known that problem (4.12) has a closed form solution $\boldsymbol{x}^\star(\boldsymbol{c}_l) = b^2 e^{\sqrt{-1}\psi}\boldsymbol{Q}_l\boldsymbol{c}_l$, for any given phase ψ and constant $b > 0$, with $\boldsymbol{Q}_l \triangleq \dfrac{\boldsymbol{R}_l^{-1}}{\boldsymbol{c}_l^\dagger \boldsymbol{R}_l^{-1}\boldsymbol{c}_l}$ (indeed, it is possible to prove that $\boldsymbol{R}$ is strictly positive definite and thus invertible, provided $c_l(1) \neq 0$ and $c_l(N) \neq 0$ [89]); as a consequence, in order to solve (4.11), it suffices to focus on (4.12) with $b = 1$ and $\psi = 0$.

In particular, due to the direct connection between the radar code $\boldsymbol{c}_l$ and the optimal ISL filter, as well as the energy constraint in (4.12), maximizing the SINR reported in equation (4.1) is equivalent to the minimization of its denominator, i.e. the quadratic form

$$\min_{\boldsymbol{c}_l\in\Omega_l} \left\{ \boldsymbol{c}_l^\dagger \left[\boldsymbol{Q}_l^\dagger \left(\boldsymbol{I} + \sum_{h=1,h\neq l}^{L} \sum_{k=-N+1}^{N-1} \boldsymbol{G}(h,l)\boldsymbol{J}_k\boldsymbol{c}_h\boldsymbol{c}_h^\dagger\boldsymbol{J}_k^T + \boldsymbol{G}(l,l) \sum_{k=-N+1,k\neq 0}^{N-1} \boldsymbol{J}_k\boldsymbol{c}_l\boldsymbol{c}_l^\dagger\boldsymbol{J}_k^T \right) \boldsymbol{Q}_l \right] \boldsymbol{c}_l \right\} . \tag{4.13}$$

A solution to problem (4.13) can be again computed through an exhaustive search over the finite set Ω_l; however, there is no guarantee that an equilibrium is reached as all the radars iteratively update their codes in a sequential fashion. As for the previous section, we can resort to the potential games framework to obtain an utility function for the players, such that the resulting game admits an NE. We thus consider the following potential

$$\begin{aligned} T(\boldsymbol{c}_1,\ldots,\boldsymbol{c}_L) = -\sum_{l=1}^{L} \boldsymbol{c}_l^{\dagger}\Bigg[\boldsymbol{Q}_l^{\dagger}\Bigg(\boldsymbol{I} + \sum_{h=1,h\neq l}^{L}\sum_{k=-N+1}^{N-1} \boldsymbol{G}(h,l)\boldsymbol{J}_k\boldsymbol{c}_h\boldsymbol{c}_h^{\dagger}\boldsymbol{J}_k^T + \boldsymbol{G}(l,l) \\ \sum_{k=-N+1,k\neq 0}^{N-1} \boldsymbol{J}_k\boldsymbol{c}_l\boldsymbol{c}_l^{\dagger}\boldsymbol{J}_k^T\Bigg)\boldsymbol{Q}_l\Bigg]\boldsymbol{c}_l \ , \end{aligned} \tag{4.14}$$

which can be rewritten as

$$\begin{aligned} T(\boldsymbol{c}_1,\ldots,\boldsymbol{c}_L) = -\boldsymbol{c}_j^{\dagger}\Bigg[\boldsymbol{Q}_j^{\dagger}\Bigg(\boldsymbol{I} + \sum_{h=1,h\neq j}^{L}\sum_{k=-N+1}^{N-1} \boldsymbol{G}(h,j)\boldsymbol{J}_k\boldsymbol{c}_h\boldsymbol{c}_h^{\dagger}\boldsymbol{J}_k^T + \boldsymbol{G}(j,j) \\ \sum_{k=-N+1,k\neq 0}^{N-1} \boldsymbol{J}_k\boldsymbol{c}_j\boldsymbol{c}_j^{\dagger}\boldsymbol{J}_k^T\Bigg)\boldsymbol{Q}_j\Bigg]\boldsymbol{c}_j - \sum_{h=1,h\neq j}^{L}\sum_{k=-N+1}^{N-1} \boldsymbol{G}(j,h)\boldsymbol{c}_j^{\dagger}\boldsymbol{Q}_j^{\dagger}\boldsymbol{J}_k^T\boldsymbol{c}_h\boldsymbol{c}_h^{\dagger}\boldsymbol{J}_k\boldsymbol{Q}_j\boldsymbol{c}_j \\ - T_1(\boldsymbol{c}_1,\ldots,\boldsymbol{c}_{j-1},\boldsymbol{c}_{j+1},\ldots,\boldsymbol{c}_L) \ . \end{aligned} \tag{4.15}$$

Therefore, in order to obtain an exact potential game with potential function

$T(\cdot)$, we can consider the following expression for the utility of the j-th user:

$$u_j = -\boldsymbol{c}_j^\dagger \left[\boldsymbol{Q}_j^\dagger \left(\boldsymbol{I} + \sum_{h=1,h\neq j}^{L} \sum_{k=-N+1}^{N-1} \boldsymbol{G}(h,j)\boldsymbol{J}_k \boldsymbol{c}_h \boldsymbol{c}_h^\dagger \boldsymbol{J}_k^T + \boldsymbol{G}(j,j) \sum_{k=-N+1,k\neq 0}^{N-1} \boldsymbol{J}_k \boldsymbol{c}_j \boldsymbol{c}_j^\dagger \boldsymbol{J}_k^T \right) \boldsymbol{Q}_j \right] \boldsymbol{c}_j - \sum_{h=1,h\neq j}^{L} \sum_{k=-N+1}^{N-1} \boldsymbol{G}(j,h) \boldsymbol{c}_j^\dagger \boldsymbol{Q}_j^\dagger \boldsymbol{J}_k^T \boldsymbol{c}_h \boldsymbol{c}_h^\dagger \boldsymbol{J}_k \boldsymbol{Q}_j \boldsymbol{c}_j \,. \tag{4.16}$$

We summarize the steps for the radar code update procedure in the **Algorithm 6**.

Algorithm 6 : Radar update procedure - Minimum ISL filter

Input: $\boldsymbol{R}_j$, Ω_j, L;

Output: a NE solution for the potential game with utility (4.16);

1: assume that radar codes are arbitrarily chosen;

2: **while** the convergence is not reached **do**

3: **for** $j = 1$ to L **do**

4: update the j-th radar code according to

$$\boldsymbol{c}_j = \arg\max_{\boldsymbol{x}\in\Omega_j} -\boldsymbol{x}^\dagger \left[\boldsymbol{Q}_j^\dagger \left(\boldsymbol{I} + \sum_{h=1,h\neq j}^{L} \sum_{k=-N+1}^{N-1} \boldsymbol{G}(h,j)\boldsymbol{J}_k \boldsymbol{c}_h \boldsymbol{c}_h^\dagger \boldsymbol{J}_k^T + \boldsymbol{G}(j,j) \sum_{k=-N+1,k\neq 0}^{N-1} \boldsymbol{J}_k \boldsymbol{x}\boldsymbol{x}^\dagger \boldsymbol{J}_k^T \right) \boldsymbol{Q}_j \right] \boldsymbol{x} - \sum_{h=1,h\neq j}^{L} \sum_{k=-N+1}^{N-1} \boldsymbol{G}(j,h) \boldsymbol{x}^\dagger \boldsymbol{Q}_j^\dagger \boldsymbol{J}_k^T \boldsymbol{c}_h \boldsymbol{c}_h^\dagger \boldsymbol{J}_k \boldsymbol{Q}_j \boldsymbol{x} \tag{4.17}$$

5: **end for**

6: **end while**

4.3.4 Minimum PSL filter

Besides the minimum ISL receive filter, another customary approach in radar applications is to constrain the level of the sidelobe peaks; the metric to be taken into account in this case is the PSL that, with reference to the l-th radar, can be expressed as

$$\text{PSL} = \max_{k=\pm 1,\ldots,\pm N-1} \frac{|\boldsymbol{d}_l(\boldsymbol{c}_l)^\dagger \boldsymbol{J}_k \boldsymbol{c}_l|^2}{|\boldsymbol{d}_l(\boldsymbol{c}_l)\boldsymbol{c}_l|^2}. \tag{4.18}$$

Note that designing a filter minimizing the PSL is equivalent to cutting all the sidelobes in the filter response, and constraining the mainlobe peak to a desired level.

The computation of the minimum PSL filter is slightly more involved than the computation of the minimum ISL filter (which indeed was given in closed form), since it requires the detection of the range lobes with the highest peak level, and then their minimization; the problem can be thus formulated as the following fractional quadratic optimization problem:

$$\min_{\boldsymbol{x}\in\mathbb{C}^N} \max_{k=\pm 1,\ldots,\pm N-1} \frac{\boldsymbol{x}^\dagger \boldsymbol{R}_{l,k} \boldsymbol{x}}{|\boldsymbol{x}^\dagger \boldsymbol{c}_l|^2}\ , \tag{4.19}$$

where

$$\boldsymbol{R}_{l,k} \triangleq \boldsymbol{J}_k \boldsymbol{c}_l \boldsymbol{c}_l^\dagger \boldsymbol{J}_k^\dagger, \; k = \pm 1, \ldots, \pm N - 1.$$

Problem (4.19) can be restated into an equivalent form as

$$\begin{aligned} \min_{\boldsymbol{x} \in \mathbb{C}^N} \max_{k = \pm 1, \ldots, \pm N-1} \quad & \boldsymbol{x}^\dagger \boldsymbol{R}_{l,k} \boldsymbol{x} \\ \text{s.t.} \quad & \Re(\boldsymbol{x}^\dagger \boldsymbol{c}_l) = b, \end{aligned} \tag{4.20}$$

where the equivalence follows from the observation that $v((4.19)) = \frac{v((4.20))}{b^2}$, for any $b > 0$: we can thus directly focus on (4.20), for $b = 1$. Solving problem (4.20) requires the solution of a Linear Programming (LP) problem [85, 84] or a Second Order Cone Programming (SOCP) [82]. Indeed, we can recast (4.20) as

$$\begin{aligned} \min_{t, \boldsymbol{x}} \quad & t \\ \text{s.t.} \quad & t \geq \boldsymbol{x}^\dagger \boldsymbol{R}_{l,k} \boldsymbol{x}, k = \pm 1, \ldots, \pm N - 1, \\ & \Re(\boldsymbol{x}^\dagger \boldsymbol{c}_l) = 1, \end{aligned} \tag{4.21}$$

which belongs to the class of the LP [85, 84] or SOCP [82] problems for the

case of real or complex transmitted code sequence and optimization variable, respectively.

Obviously, an optimal solution $\boldsymbol{x}^{\star}$ for problem (4.21) is a function of the radar code $\boldsymbol{c}_l$ used by the player; therefore, the finite set Ω_l of the possible radar sequences and the set, say Σ_l, of the possible optimal PSL filters are related by a one-to-one correspondence. Otherwise stated, specifying Ω_l also leads to specify Σ_l, in the sense that the set of the filters can be computed directly off-line, and populated by the possible solutions for the problem (4.21).

Based on the above assumptions, the maximization of the SINR for the pair $(\boldsymbol{c}_l, \boldsymbol{d}(\boldsymbol{c}_l))$ relative to (4.21), leads to the following minimization

$$\min_{\boldsymbol{c}_l \in \Omega_l} \left\{ \boldsymbol{d}(\boldsymbol{c}_l)^{\dagger} \left(\boldsymbol{I} + \sum_{h=1, h\neq l}^{L} \sum_{k=-N+1}^{N-1} \boldsymbol{G}(h,l) \boldsymbol{J}_k \boldsymbol{c}_h \boldsymbol{c}_h^{\dagger} \boldsymbol{J}_k^T + \boldsymbol{G}(l,l) \sum_{k=-N+1, k\neq 0}^{N-1} \boldsymbol{J}_k \boldsymbol{c}_l \boldsymbol{c}_l^{\dagger} \boldsymbol{J}_k^T \right) \boldsymbol{d}(\boldsymbol{c}_l) \right\} . \tag{4.22}$$

where, for each transmitted sequence $\boldsymbol{c}_l \in \Omega_l$, it is necessary to consider the corresponding filter $\boldsymbol{d}(\boldsymbol{c}_l) \in \Sigma_l$.

Again, for the purpose of correctly modeling the game among the L users,

let us define the following potential:

$$T(\boldsymbol{c}_1,\ldots,\boldsymbol{c}_L) = -\sum_{l=1}^{L} \boldsymbol{d}(\boldsymbol{c}_l)^\dagger \left(\boldsymbol{I} + \sum_{h=1,h\neq l}^{L} \sum_{k=-N+1}^{N-1} \boldsymbol{G}(h,l)\boldsymbol{J}_k \boldsymbol{c}_h \boldsymbol{c}_h^\dagger \boldsymbol{J}_k^T + \boldsymbol{G}(l,l) \sum_{k=-N+1,k\neq 0}^{N-1} \boldsymbol{J}_k \boldsymbol{c}_l \boldsymbol{c}_l^\dagger \boldsymbol{J}_k^T \right) \boldsymbol{d}(\boldsymbol{c}_l) \ , \tag{4.23}$$

where we assume that the correspondence between filters and transmitted sequences has already been defined. Specifically, we may resort to a table I, that can be looked upon during the update procedure. After some algebraic transformations, we obtain

$$\begin{aligned} T(\boldsymbol{c}_1,\ldots,\boldsymbol{c}_L) = &- \boldsymbol{d}(\boldsymbol{c}_j)^\dagger \left(\boldsymbol{I} + \sum_{h=1,h\neq j}^{L} \sum_{k=-N+1}^{N-1} \boldsymbol{G}(h,j)\boldsymbol{J}_k \boldsymbol{c}_h \boldsymbol{c}_h^\dagger \boldsymbol{J}_k^T + \boldsymbol{G}(j,j) \sum_{k=-N+1,k\neq 0}^{N-1} \boldsymbol{J}_k \boldsymbol{c}_j \boldsymbol{c}_j^\dagger \boldsymbol{J}_k^T \right) \boldsymbol{d}(\boldsymbol{c}_j) - \sum_{h=1,h\neq j}^{L} \sum_{k=-N+1}^{N-1} \boldsymbol{G}(j,h)\boldsymbol{d}(\boldsymbol{c}_j)^\dagger \boldsymbol{J}_k^T \boldsymbol{c}_h \boldsymbol{c}_h^\dagger \boldsymbol{J}_k \boldsymbol{d}(\boldsymbol{c}_j) \\ &- T_1(\boldsymbol{c}_1,\ldots,\boldsymbol{c}_{j-1},\boldsymbol{c}_{j+1},\ldots,\boldsymbol{c}_L) \ . \end{aligned} \tag{4.24}$$

Given the above potential function, it is possible to define the utility for the

j-th user as

$$u_j = -\boldsymbol{d}(\boldsymbol{c}_j)^\dagger \left(\boldsymbol{I} + \sum_{h=1,h\neq j}^{L} \sum_{k=-N+1}^{N-1} \boldsymbol{G}(h,j)\boldsymbol{J}_k \boldsymbol{c}_h \boldsymbol{c}_h^\dagger \boldsymbol{J}_k^T + \boldsymbol{G}(j,j) \sum_{k=-N+1,k\neq 0}^{N-1} \boldsymbol{J}_k \boldsymbol{c}_j \boldsymbol{c}_j^\dagger \boldsymbol{J}_k^T \right) \boldsymbol{d}(\boldsymbol{c}_j) - \sum_{h=1,h\neq j}^{L} \sum_{k=-N+1}^{N-1} \boldsymbol{G}(j,h)\boldsymbol{d}(\boldsymbol{c}_j)^\dagger \boldsymbol{J}_k^T \boldsymbol{c}_h \boldsymbol{c}_h^\dagger \boldsymbol{J}_k \boldsymbol{d}(\boldsymbol{c}_j), \tag{4.25}$$

whose iterative maximization by the active radars leads to a new potential game admitting NE points. **Algorithm 7** summarizes the radar code update iterations for the case at hand.

Algorithm 7 : Radar update procedure - Minimum PSL filter

Input: $\boldsymbol{R}_{j,k}$, Ω_j, L;

Output: a NE solution for the potential game with utility functions (4.25);

1: solve the problem (4.21) for all $\boldsymbol{c}_j \in \Omega_j$, and compute the set Σ_j;

2: compute the table I so that $I(i,j) \triangleq (\boldsymbol{c}_i, \boldsymbol{d}_j(\boldsymbol{c}_i))$, where $\boldsymbol{c}_i \in \Omega_l$ and $\boldsymbol{d}_j \in \Sigma_j$;

3: assume that radar codes are arbitrarily chosen;

4: **while** the convergence is not reached **do**

5: **for** $j = 1$ to L **do**

6: update the j-th radar code according to

$$\boldsymbol{c}_j = \arg \max_{(\boldsymbol{x},\boldsymbol{y})\in I} -\boldsymbol{y}^\dagger \left(\boldsymbol{I} + \sum_{h=1,h\neq j}^{L} \sum_{k=-N+1}^{N-1} \boldsymbol{G}(h,j)\boldsymbol{J}_k \boldsymbol{c}_h \boldsymbol{c}_h^\dagger \boldsymbol{J}_k^T + \boldsymbol{G}(j,j) \sum_{k=-N+1,k\neq 0}^{N-1} \boldsymbol{J}_k \boldsymbol{x}\boldsymbol{x}^\dagger \boldsymbol{J}_k^T \right) \boldsymbol{y} - \sum_{h=1,h\neq j}^{L} \sum_{k=-N+1}^{N-1} \boldsymbol{G}(j,h)\boldsymbol{y}^\dagger \boldsymbol{J}_k^T \boldsymbol{c}_h \boldsymbol{c}_h^\dagger \boldsymbol{J}_k \boldsymbol{y}. \tag{4.26}$$

7: **end for**

8: **end while**

4.3.5 Non-negligible Doppler shift

So far, we have implicitly assumed that the received signal is affected by either null or negligible Doppler shift. However, it is well-known that if the targets illuminated by the network of radars rapidly change their position with unknown velocity and directions, then it is necessary to account for the effect (no more negligible) of the Doppler frequency shifts. To this end, we follow the same approach as in [82], extending it to the considered non-cooperative scenario. Specifically, let us assume that $\boldsymbol{\omega}_l = [\omega_{-N+1,l}, \ldots, \omega_{N-1,l}]$ is the Doppler shifts vector (in radiant per second) for the l-th radar, with $l = 1, \ldots, L$. Moreover, let

$$\boldsymbol{c}_l(\omega_{k,l}) = \left[c_l(1)e^{j\omega_{k,l}} \ldots c_l(N)e^{jN\omega_{k,l}}\right]^T \tag{4.27}$$

be the related Doppler shifted code sequence. The data model (4.1) can be thus modified as follows:

$$\boldsymbol{r}_l = \alpha_{0,l}\boldsymbol{c}_l(\omega_{0,l}) + \sum_{k=-N+1,k\neq 0}^{N-1} \alpha_{k,l}\boldsymbol{J}_k\boldsymbol{c}_l(\omega_{k,l}) + \sum_{h=1,h\neq l}^{L}\sum_{k=-N+1}^{N-1} \alpha_{k,h}\boldsymbol{J}_k\boldsymbol{c}_h(\omega_{k,h}) + \boldsymbol{n}_l\,, \tag{4.28}$$

wherein $\omega_{0,l}$ is the Doppler shift associated to the range bin of interest. Now, should such a Doppler shift be known at the receiver, the following detection

rule should be considered:

$$|\boldsymbol{d}_l^\dagger(\boldsymbol{c}_l(\omega_{0,l}))\boldsymbol{r}_l|^2 \underset{H_0}{\overset{H_1}{\gtrless}} \eta_l\,, \tag{4.29}$$

with $\boldsymbol{d}_l(\boldsymbol{c}_l(\omega_{0,l}))$ the N-dimensional detection vector, function of the (known) Doppler shifted code $\boldsymbol{c}_l(\omega_{0,l})$. Given Eq. (4.29), the SINR equation (4.4) may be easily reformulated as follows:

$$\gamma_l = \frac{\boldsymbol{G}(l,l)|\boldsymbol{d}_l^\dagger(\boldsymbol{c}_l(\omega_{0,l}))\boldsymbol{c}_l(\omega_{0,l})|^2}{\boldsymbol{d}_l^\dagger(\boldsymbol{c}_l(\omega_{0,l}))\left(\begin{array}{l}\boldsymbol{I}+\displaystyle\sum_{h=1,h\neq l}^{L}\sum_{k=-N+1}^{N-1}\boldsymbol{G}(h,l)\boldsymbol{J}_k\boldsymbol{c}_h(\omega_{k,h})\boldsymbol{c}_h^\dagger(\omega_{k,h})\boldsymbol{J}_k^T+ \\ +\ \boldsymbol{G}(l,l)\displaystyle\sum_{k=-N+1,k\neq 0}^{N-1}\boldsymbol{J}_k\boldsymbol{c}_l(\omega_{k,l})\boldsymbol{c}_l^\dagger(\omega_{k,l})\boldsymbol{J}_k^T\end{array}\right)\boldsymbol{d}_l(\boldsymbol{c}_l(\omega_{0,l}))}. \tag{4.30}$$

In practical radar applications, however, the target Doppler shift is usually unknown, and the available knowledge is limited to the range $[\omega_0, \omega_1]$ of variability of the Doppler frequencies. The customary approach thus relies on a quantization of the said range with a preassigned resolution $(\Delta\omega)$ (a typical value of $(\Delta\omega)$ is $\pi/(10N)$ [82]) and, at the reception side, a bank of detection vectors, each one keyed to one of the quantized Doppler frequencies, is considered, followed by a maximum selector. Otherwise stated, denoting by

$\omega(1), \omega(2), \ldots, \omega(P)$ the P sample frequencies obtained by sampling with step $(\Delta\omega)$ the interval $[\omega_0, \omega_1]$, the detection rule is actually expressed as

$$\max_{i\in\{1,2,\ldots,P\}} |\boldsymbol{d}_l^\dagger(\boldsymbol{c}_l(\omega(i)))\boldsymbol{r}_l|^2 \underset{H_0}{\overset{H_1}{\gtrless}} \eta_l \,. \tag{4.31}$$

Now, in order to come up with a code update procedure, we should still focus on the minimization of the denominator of Eq. (4.30); note however that such a denominator depends on the Doppler shifts $\{\omega_{k,l}\}$, with $l = 1, \ldots, L$ and $k = -N+1, \ldots, N-1$. In order to circumvent this drawback, a suitable technique is to consider the statistical expectation of the denominator of (4.30), averaged with respect to the set of Doppler shifts. Since in practice the detection vectors are considered only for a finite number of Doppler frequencies, in performing the average we model the detection vector as taking value in the discrete set $\{\boldsymbol{d}_l^\dagger(\boldsymbol{c}_l(\omega(1))), \boldsymbol{d}_l^\dagger(\boldsymbol{c}_l(\omega(2))), \ldots, \boldsymbol{d}_l^\dagger(\boldsymbol{c}_l(\omega(P)))\}$, while the frequencies inside the curly brackets in the denominator of Eq. (4.30) are assumed to be continous and uniform random variates taking value in the set $[\omega_0, \omega_1]$. For the case in which a matched filter is used at the receiver, the presence of non-negligible Doppler shifts thus leads to consider, in place of Eq. (4.7), the

following potential function:

$$T(\boldsymbol{c}_1,\ldots,\boldsymbol{c}_L) = -\sum_{l=1}^{L}\sum_{i=1}^{P}\left\{\boldsymbol{c}_l^{\dagger}(\omega(i))\left(\boldsymbol{I}+\sum_{h=1,h\neq l}^{L}\sum_{k=-N+1}^{N-1}\boldsymbol{G}(h,l)\boldsymbol{J}_k\overline{\boldsymbol{c}_h(\omega_{k,h})\boldsymbol{c}_h^{\dagger}(\omega_{k,h})}\boldsymbol{J}_k^T+\right.\right.$$
$$\left.\left.+\ \boldsymbol{G}(l,l)\sum_{k=-N+1,k\neq 0}^{N-1}\boldsymbol{J}_k\overline{\boldsymbol{c}_l(\omega_{k,l})\boldsymbol{c}_l^{\dagger}(\omega_{k,l})}\boldsymbol{J}_k^T\right)\boldsymbol{c}_l(\omega(i))\right\}\ , \tag{4.32}$$

wherein the overline $\overline{(\cdot)}$ denotes statistical expectation with respect to the Doppler shifts; note that, upon letting $\boldsymbol{F}_l = \overline{\boldsymbol{c}_l(\omega_{k,l})\boldsymbol{c}_l^{\dagger}(\omega_{k,l})}$, it is easily shown that the (n,m)-th entry of $\boldsymbol{F}_l$, say $\boldsymbol{F}_l(n,m)$, is expressed as

$$\boldsymbol{F}_l(n,m) = \frac{c_l(n)c_l^{\dagger}(m)}{\omega_1-\omega_0}\int_{\omega_0}^{\omega_1}e^{j(n-m)\omega}d\,\omega = \begin{cases}|c_l(n)|^2, & n=m,\\ \dfrac{c_l(n)c_l^{\dagger}(m)\left[e^{j(n-m)\omega_1}-e^{j(n-m)\omega_0}\right]}{j(n-m)[\omega_1-\omega_0]}, & n\neq m.\end{cases} \tag{4.33}$$

Now, given the potential function (4.32) a non-cooperative game can be obtained, similarly to the case of negligible Doppler shift, by isolating the terms depending on a given code, say the j-th. The utility function for the j-th radar

is thus written as

$$
\begin{aligned}
u_j = \; & -\sum_{i=1}^{P} \Bigg\{ \boldsymbol{c}_j^{\dagger}(\omega(i)) \Bigg(\boldsymbol{I} + \sum_{h=1,h\neq j}^{L} \sum_{k=-N+1}^{N-1} \boldsymbol{G}(h,j) \boldsymbol{J}_k \boldsymbol{F}_h \boldsymbol{J}_k^T + \\
& + \boldsymbol{G}(j,j) \sum_{k=-N+1,k\neq 0}^{N-1} \boldsymbol{J}_k \boldsymbol{F}_j(\boldsymbol{c}_j) \boldsymbol{J}_k^T \Bigg) \boldsymbol{c}_j(\omega(i)) \Bigg\} - \\
& \sum_{l=1,l\neq j}^{L} \sum_{i=1}^{P} \Bigg\{ \boldsymbol{c}_l^{\dagger}(\omega(i)) \Bigg(\sum_{k=-N+1}^{N-1} \boldsymbol{G}(j,l) \boldsymbol{J}_k \boldsymbol{F}_j(\boldsymbol{c}_j) \boldsymbol{J}_k^T \Bigg) \boldsymbol{c}_l(\omega(i)) \Bigg\} \; .
\end{aligned}
\tag{4.34}
$$

In writing the above equation, we have made explicit the functional dependence of the matrix $\boldsymbol{F}_j$ on the code $\boldsymbol{c}_j$, which is to be properly accounted for in the utility maximization. Summing up, for non-negligible Doppler shifts and matched filter reception, each radar should update its code in order to maximize the utility in (4.34), and the detection rule to be considered should be the one reported in Eq. (4.31).

Similar considerations can be done for the cases in which a minimum ISL or PSL filters are used. For the sake of brevity, however, we avoid providing more details on this, since it would not add conceptual value to our work.

4.4 Performance Analysis

In this section, we assess the performance of the proposed non-cooperative waveform design techniques; to this end, we test the outlined algorithms in two distinct scenarios, where the difference is mainly in the amount of involved radars, as well as their receive antenna pattern characterization. Precisely, we consider the following two games $\mathcal{G}_i = \{\mathcal{L}_i, \Omega_l, \{u_l\}\}$, for $i = \{1, 2\}$ where:

- $\mathcal{L}_1 = \{1, 2, 3, 4\}$ is the set of 4 players (*i.e.* the set of 4 radars actually transmitting), while $\mathcal{L}_2 = \{1, 2, 3, 4, 5, 6\}$ is the set of 6 players (*i.e.* the set of 6 radars actually transmitting);

- Ω_l is a set of cardinality $M = 653$ which contains the sequences of length $N = 16$ available to the l-th player. The same set is considered for each radar, i.e. Ω_l is actually independent of the index l (and indeed we will be denoting it by Ω in the following). The full details on the sequences of the set Ω are reported in the Appendix.

- $\{u_l\}$ represents the utility function for the l-th player, as defined in the discussed **Algorithms 5**, **6** and **7**, for $l = 1, \ldots, 4$ or $l = 1, \ldots, 6$ respectively for the first and the second game;

- $\boldsymbol{G}$ is the $L_i \times L_i$ matrix describing the antenna gain pattern of the L_i players, for $i = \{1, 2\}$. We consider a general scenario wherein each radar may have its own antenna beam pattern, but we normalize, without loss of generality, to 0 dB the maximum gain of each antenna. Indeed, we consider the following pattern models for the games $\mathcal{G}_1$ and $\mathcal{G}_2$:

$$\boldsymbol{G}_{\mathcal{G}_1} = \begin{bmatrix} 0 & -30 & -19 & -20 \\ -20 & 0 & -19 & -20 \\ -20 & -30 & 0 & -20 \\ -20 & -30 & -19 & 0 \end{bmatrix}, \qquad \boldsymbol{G}_{\mathcal{G}_2} = \begin{bmatrix} 0 & -30 & -19 & -20 & -15 & -23 \\ -20 & 0 & -19 & -20 & -15 & -23 \\ -20 & -30 & 0 & -20 & -15 & -23 \\ -20 & -30 & -19 & 0 & -15 & -23 \\ -20 & -30 & -19 & -20 & 0 & -23 \\ -20 & -30 & -19 & -20 & -15 & 0 \end{bmatrix},$$

respectively[3].

With reference to the simulation setup of **Figures 4.2a**, **4.3a**, and **4.4a**, we choose four transmit sequences from Ω and consider them as the initial strate-

[3]Recall that in the above gain matrices the (m, n)-th element is a coefficient weighting the interference from the m-th radar on the n-th receiver.

gies for $\mathcal{G}_1$. Moreover, for the corresponding figures of $\mathcal{G}_2$ (**Figures 4.2b**, **4.3b**, and **4.4b**), we add two more codes, still selected from Ω, to the four aforementioned initial strategies. The analysis is conducted in terms of SINR γ_l which each player is able to obtain through the non-cooperative code design, focusing on the performance provided by the three algorithms. The average SINR among the transmitting radars at the equilibrium, for all the players, as their number increases, is also plotted. The results emphasize how, as the number of interferers increases, the games actually are able to reduce the consequential loss of performances with respect to the case in which no code optimization procedure is performed.

In **Figures 4.2a** and **4.2b** we plot the SINR of each player versus the number of iterations required by **Algorithm 5** to converge to a NE, for the games $\mathcal{G}_1$ and $\mathcal{G}_2$, respectively; these plots show the impact of the chosen code (strategy) on the SINR of the set of players, as they pick up different codes from the set Ω. Note that the starting codes (strategies) do not provide satisfactory values of γ_l for all the set of players; indeed, in both the games the majority of the sensors experiment quite a low level of SINR, with the exception of the first two players. The curves highlight that, as the players change their transmit-

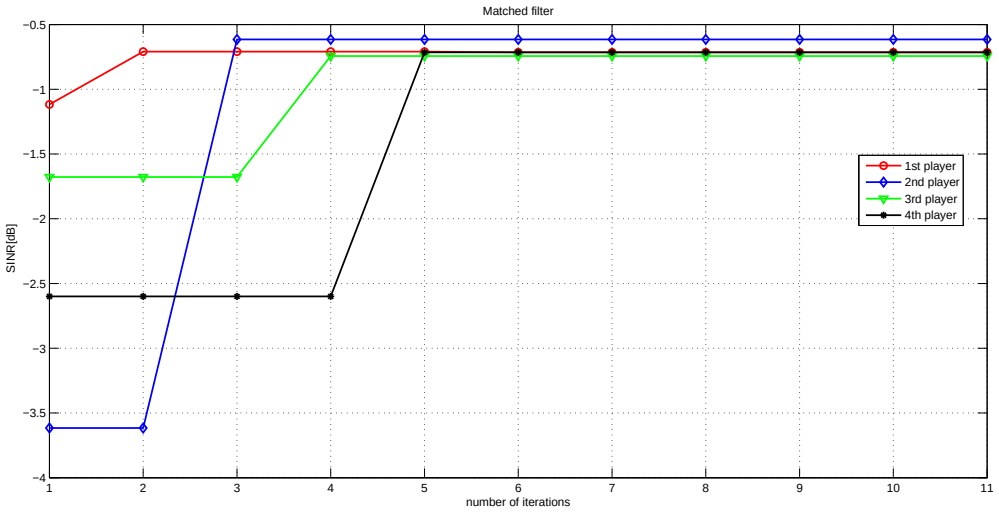

(a) SINR versus the number of iterations, for a set of $L = 4$ players, Algorithm 5.

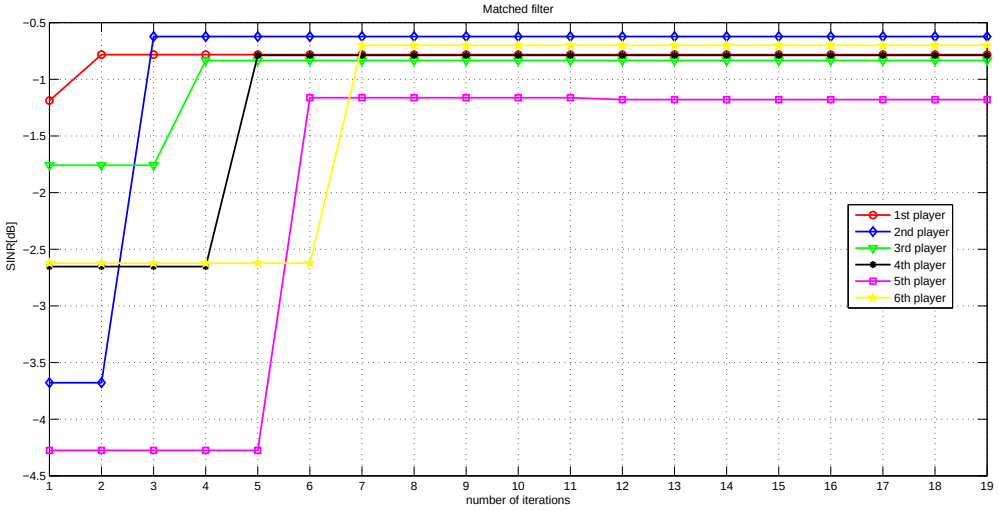

(b) SINR versus the number of iterations, for a set of $L = 6$ players, Algorithm 5.

Figure 4.2: SINR versus the number of iterations, Algorithm 5.

ting codes according to **Algorithm 5**, the SINR of each player converges to a fixed value: after a certain amount of iterations, the iterative algorithm thus reaches a fixed code (strategy). In particular, both the sets of players share an average increase in their respective performances, quantifiable in about 1.54 dB for the first game and 1.88 dB for the second game, and no particular loss is observed due to the growth of the number of transmitting radar. Moreover, convergence is reached after a few iterations.

In **Figures 4.3a** and **4.3b**, the same analysis is conducted for **Algorithm 6**. Again, the starting strategy seems to be quite disadvantageous for both the sets of active radars, and in particular for the second game (specifically, we experience unpleasant performances in the cases of radars 3 and 4, with reference to the 1-st game, and radars 3-6 for the second game). Resorting to the coding procedure of **Algorithm 6**, however, all the radars increase the respective performances; in particular, we observe an average increase, in the provided SINR values, of 1.84 dB for game $\mathcal{G}_1$ and 2.06 dB for game $\mathcal{G}_2$.

The analysis also shows a gain in terms of ISL values, due to the game approach. Specifically, in **Figure 4.4**, we provide a comparison between the average ISL, with respect to the increasing number of active radars (for the case

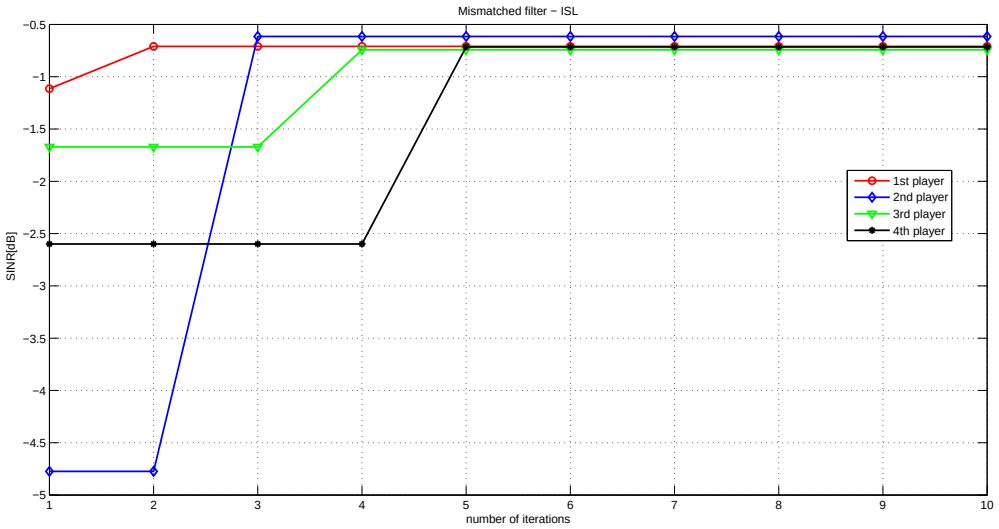

(a) SINR versus the number of iterations, for a set of $L = 4$ players, Algorithm 6.

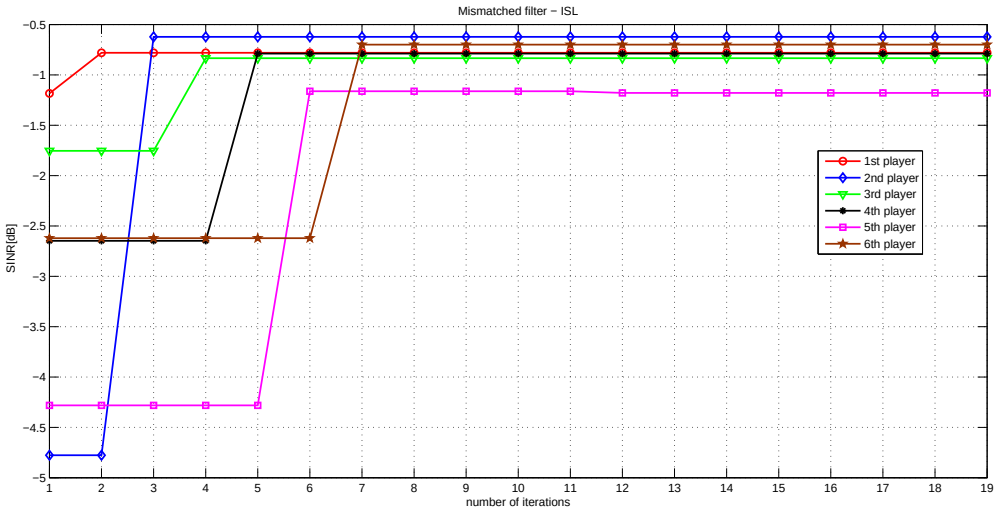

(b) SINR versus the number of iterations, for a set of $L = 4$ players, Algorithm 6.

Figure 4.3: SINR versus the number of iterations, Algorithm 6.

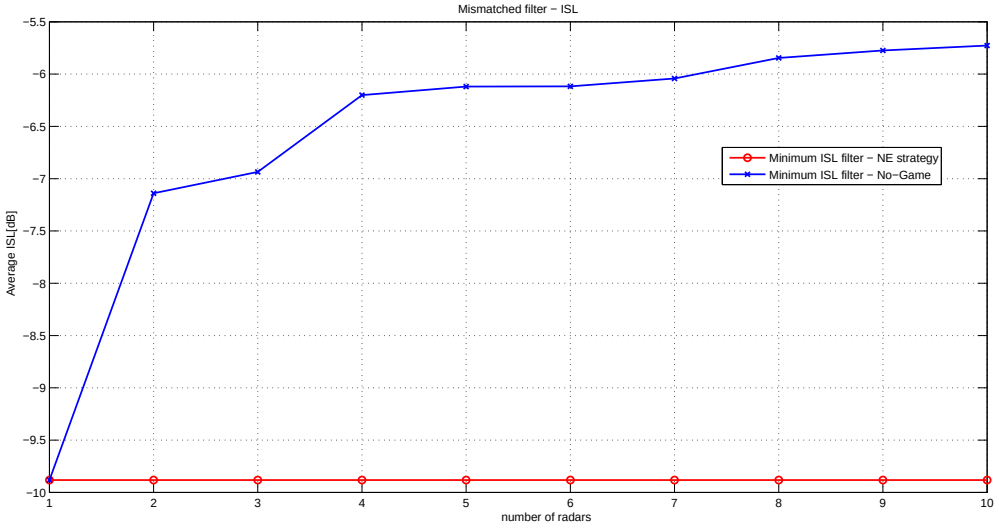

Figure 4.4: Average ISL versus the number of active players, Algorithm 6. ISL at the NE points (solid-circle red line); ISL with a random choice (solid-cross blue line).

at hand, we assume a maximum of 10 radars), obtained with the **Algorithm 6** and the no-game strategy, respectively. In the setup of this simulation, random initial strategies have been selected for the radars and the results have been averaged over 25 independent trails. The plots highlight that the no-game approach is very sensitive to the number of sensors composing the network; in fact increasing values of ISL can observed when the number of active radars increases. On the contrary, the updating procedure of **Algorithm 6** is capable of ensuring a quite flat ISL behavior.

In **Figures 4.5a** and **4.5b**, we focus on the performance of **Algorithm 7**, and similar comments as for the previous two algorithms can be made. It is here observed an even greater average increase, in terms of SINR, than in the

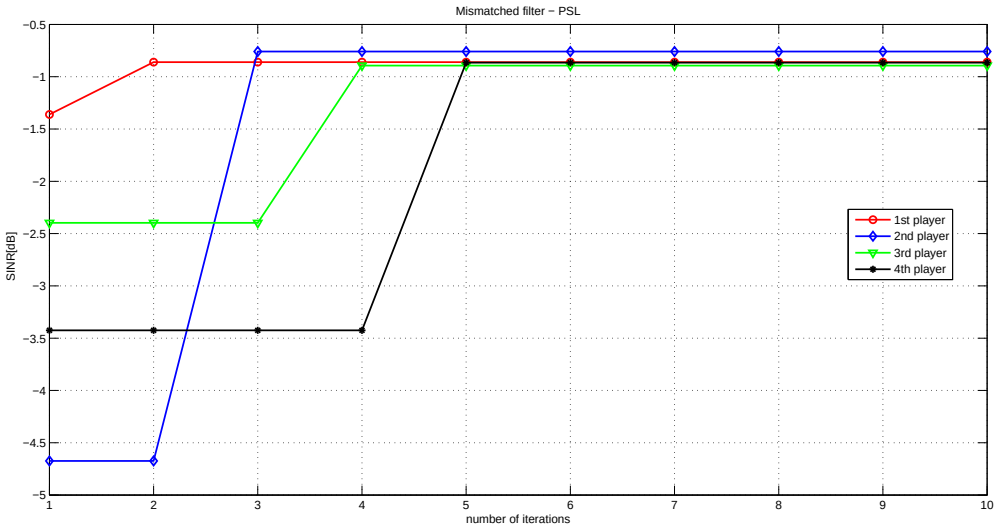

(a) SINR versus the number of iterations, for a set of $L = 4$ players, Algorithm 7.

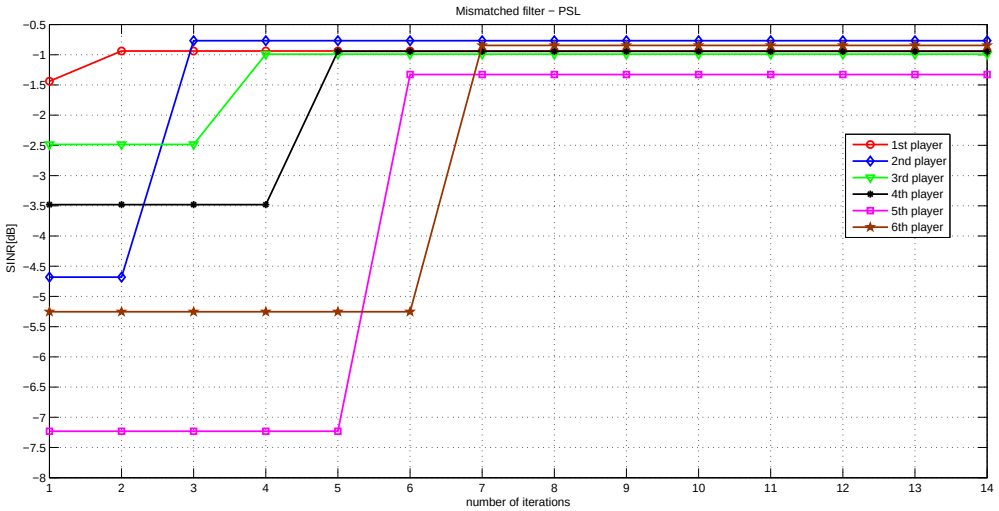

(b) SINR versus the number of iterations, for a set of $L = 4$ players, Algorithm 7.

Figure 4.5: SINR versus the number of iterations, Algorithm 7.

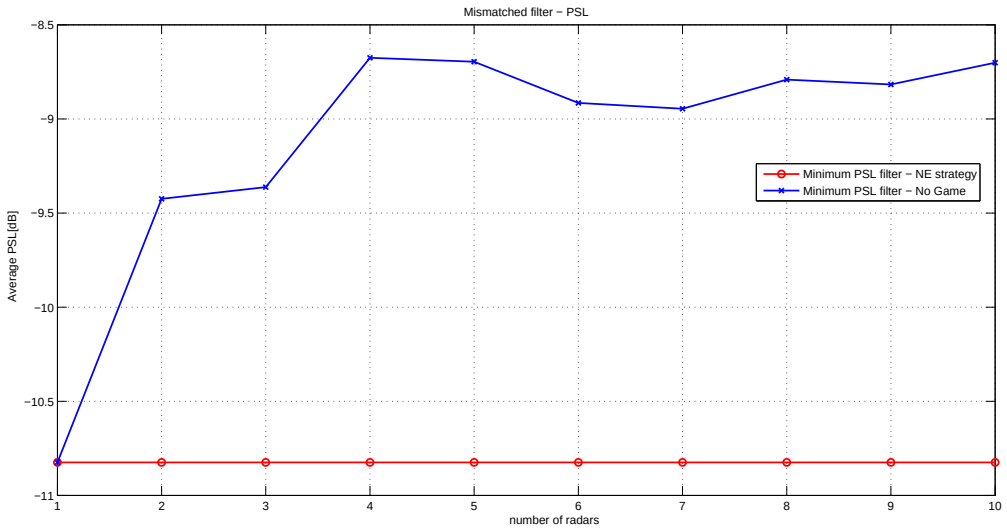

Figure 4.6: Average PSL versus the number of active players, Algorithm 7. PSL at the NE points (solid-circle red line); PSL with a random choice (solid-cross blue line).

aforementioned two techniques, which can be quantified in 2.12 dB for the first game, and 3.12 dB for the second one.

In **Figure 4.6**, we consider the average PSL versus the number of active radars, for both the no-game approach and the non-cooperative game technique of **Algorithm 7**. The same simulation conditions as in Fig. 3c have been considered concerning the initial choice. Notice that the average PSL for the no-game approach appears quite unpleasant, as worse and worse PSL values are obtained increasing the number of active sensors. On the contrary, **Algorithm 7** seems quite robust in terms of PSL with respect to the number of active radars.

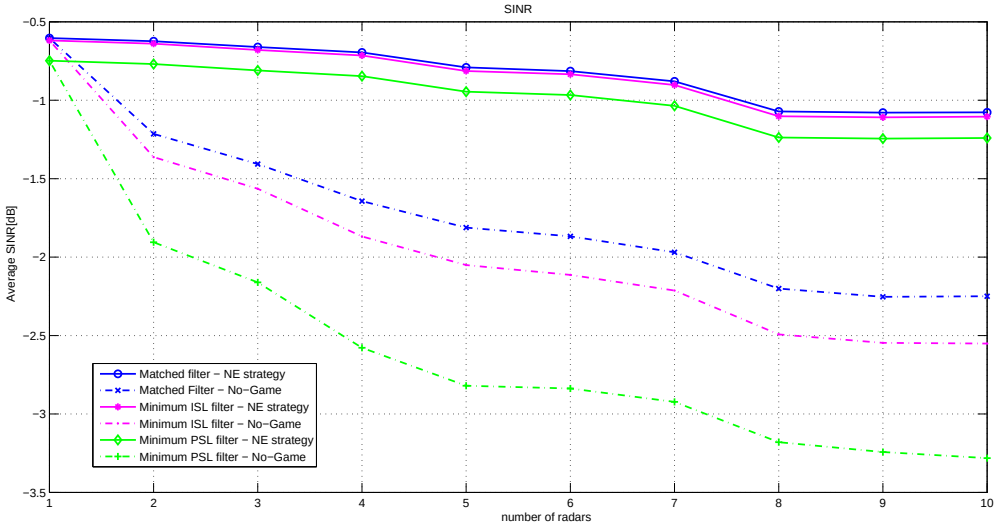

Figure 4.7: Average SINR versus the number of active radars. Algorithm 5: SINR at the NE points (solid-circle blue line); SINR with a random choice (dotted-cross blue line). Algorithm 6: SINR at the NE points (solid-star magenta line); SINR with a random choice (dotted-point magenta line). Algorithm 7: SINR at the NE points (solid-diamond green line); SINR with a random choice (dotted-plus green line).

Finally, in **Figure 4.7**, we analyze the average SINR among all the radars, at the NE, versus the number of active radars in the network, with respect to **Algorithms 5**, **6**, and **7**; in particular, for the latter two algorithms, the curves refer to the SINR values for the NE points of **Figures 4.4** and **4.5** (as such random initial strategies have been considered for the radars operate according to a no-game approach and the results are averaged over 25 independent trials); for comparison purposes, we also report the average SINR obtained when the radars operate in a no-game scenario. The plots confirm that, at the Nash equilibria, the radar network actually may enjoy an increase in terms of SINR, with respect to the case in which no-game is allowed. Moreover, as expected,

the performance gracefully decades as the number of active radars increases. This is a pretty natural behavior, since the larger the number of radars the larger the power of the interfering signals.

Overall, the results of this section confirm the effectiveness of the proposed algorithms, as well as that all the considered games converge to an equilibrium.

4.5 Conclusion

In this chapter, we have considered a network of radars sharing the same frequency band, and tuning their transmitted waveforms in order to improve their SINR.

We have assumed that each radar can select the waveform to be transmitted from a finite set. Hence, we have proposed code updating strategies according to some non-cooperative games, based on the potential games framework, to account for the cases of matched filter detection, minimum ISL and minimum PSL detection. Finally, we have discussed the situation where a non-negligible Doppler shift exists in the received data. In all the considered scenarios, the existence of Nash equilibria is analytically proven.

Numerical results have confirmed that the proposed games are effective in improving the system performance, in the sense that at the NE each radar may enjoy a SINR that is larger than that corresponding to the case of a random choice of the coded waveform to transmit. Moreover, it has also been verified that there is a graceful performance degradation as the number of active radars increases.

Possible future research tracks might account for the possibility of some form of cooperation between the radars of the network as well as the extension of the procedure to the case where more advanced decision strategies (in place of the linear filter followed by an envelope detector) are used. By doing so, we can also confer to the system additional desired robust features such as for instance the Constant False Alarm Rate (CFAR) property.

4.6 Appendix

4.6.1 Code design procedure

We choose our N dimensional radar codes so that $||\boldsymbol{c}|| = 1$, $\boldsymbol{c} \in \mathbb{C}^N$; otherwise stated, we fill the set Ω with sequences lying on the unit-norm sphere. To this

end, we consider both standard codes available in open literature and ad-hoc coding procedure.

As to the former class, we refer to some well known phase-coding techniques [18] to design the first 13 possible transmit sequences of the set Ω. Specifically, we assume that $\boldsymbol{c}_l = \frac{1}{\sqrt{N}} e^{\sqrt{-1}\boldsymbol{\phi}_l}$, where $\boldsymbol{\phi}_l = [\phi_l(1), \ldots, \phi_l(N)]^T$ is the phase sequence of the l-th code, and $l = 1, \ldots, 13$. In Table 4.1, we summarize the classes of phase codes herein used, as well as the values of the parameters applied in the respective design procedures[4].

Additionally, to properly test our non-cooperative procedures, we increase the number of possible strategies enriching with other suitable codes the set Ω. We resort to the following construction procedure. First of all, we force the coefficients $c_l(i)$, $i = 1, \ldots, N$, to belong to a well defined finite set Ω_* with cardinality M. Then, we obtain the transmit sequences picking up randomly the codes from the set Ω_*^N with cardinality M^N. Finally, we normalize the selected sequences so as to get unit-norm codes. For the specific case at hand, we set $c_l(i) \triangleq \{a_i + \sqrt{-1}b_i\}/\sqrt{2N}$ for $l = 14, \ldots, 113$, with $\{a_i, b_i\} \in \{-1, +1\}^2$. With such a choice we can produce up to 2^{2N} possible codes. Thus, we randomly

[4]The reader might refer to [18], which is an exhaustive compendium of the classic radar coding techniques.

choose 100 codes from such a set, and use them in our simulations.

The aforementioned construction procedure does not provide sequences very attractive from the radar point of view; indeed, it can lead to signals with significant modulus variations, poor range resolution, high peak sidelobe levels, and more in general, to signals with an undesired ambiguity function behavior. This drawback can be circumvented imposing a control on the aforementioned performance metrics at the code design stage. Precisely, we can start from a good (in the sense of the ambiguity function properties) code $\boldsymbol{c}_0$ and devise some additional sequences which inherit some attractive properties of $\boldsymbol{c}_0$. This goal can be achieved forcing the new sequences to lie in a suitable norm-ball centered around $\boldsymbol{c}_0$. In other words, we consider sequences which are solutions to the feasibility problem

$$\begin{cases} ||\boldsymbol{c} - \boldsymbol{c_0}||^2 \leq \epsilon \\ \\ ||\boldsymbol{c}||^2 = 1 \end{cases} . \tag{4.35}$$

where the parameter $\epsilon \in [0, 2]$ quantifies the desired similarity level; the smaller ϵ, the higher the degree of similarity among the ambiguity functions of the designed radar code and the reference sequence.

Solutions to problem (4.35) can be found according to the following algorithm.

1. Denote by $\boldsymbol{a}$ an N-dimensional complex vector whose elements are continuous random variables.

2. Construct the unit-norm vector $\boldsymbol{c}_{\mathbf{0}}^{\perp} = (\boldsymbol{I} - \boldsymbol{c}_{\mathbf{0}}\boldsymbol{c}_{\mathbf{0}}^{\dagger})\boldsymbol{a}/\|(\boldsymbol{I} - \boldsymbol{c}_{\mathbf{0}}\boldsymbol{c}_{\mathbf{0}}^{\dagger})\boldsymbol{a}\|$.

3. Define the sequence $\boldsymbol{c}^t = \sqrt{t}\boldsymbol{c}_{\mathbf{0}} + \sqrt{1-t}\boldsymbol{c}_{\mathbf{0}}^{\perp}$, where the parameter t complies with $t \geq (1-\epsilon/2)^2 = \delta_\epsilon$ and $t \leq 1$.

Exploiting the above procedure, we have updated the set Ω, so as to include additional 540 transmit sequences. In Table II, we show the set of reference codes; for each sequence, we solve problem (4.35) $K = 15$ times (with 15 different feasible values of t), thus devising $9K$ possible codes. Finally, the procedure is implemented for $\delta_\epsilon \in \{0.41, 0.63, 0.75, 0.9\}$.

Table 4.1: Classes of phase-codes ϕ; length $N = 16$; $\{r, q\}$ design parameters [18].

parameters	ϕ_l	parameters	ϕ_l
$r = 15$	Golomb-Zhang	//	Palindronic P4
//	MPS	$r = 3$	Chu
//	Zadoff-Chu	$r = 13$	Golomb-Zhang
$r = 5, q = 10$	Zadoff	$r = 17$	Chu
$r = 27, q = 8$	Zadoff	$r = 3, q = 16$	Zadoff
//	P3	$r = 21, q = 0$	Zadoff
$r = 3$	Golomb-Zhang	//	//

Table 4.2: Set of similarity codes. $\boldsymbol{c}_0 = \frac{1}{\sqrt{N}} e^{j\boldsymbol{\phi}_0}$: reference code; length $N = 16$; $\{r, q\}$ design parameters [18].

parameters	ϕ_0	parameters	ϕ_0
$r = 3$	Chu	//	Px
//	Frank	$r = 17$	Golomb-Zhang
//	MPS	$r = 6, q = 6$	Zadoff
//	P4	//	Polyphase Barker
//	P1	//	//

Chapter 5

Design of Pareto-Optimal Radar Receive Filters

5.1 Introduction

The design of optimized low sidelobe receive filters for pulse compression radar systems is a hot research topic among the radar signal processing community since 1960's [41, 90]. It is of fundamental interest for many radar applications including ground-based surveillance, Air Traffic Control (ATC), anti-wind shear, and radar metereology.

Some early studies can be dated back to 1967-1968 [91, 92], with reference to the IEEE journals, while to 1970 [83, 88], in the context of Russian literature. In [93], a literary survey and a selected reference list on this interesting problem is provided together with some new contributions concerning issues related to the filter length and the choice of the design criterion. According

to [93], the receiving filters proposed over the years can be classified into two main categories. The former, data independent class, does not require any prior knowledge about the surrounding environment, whereas the latter, data dependent class, depends on the assumed (possibly estimated) parameters of the environment. With reference to the former class, we quote [88, 84], and [85] where the minimum Integrated Sidelobe Level (ISL) filter [88] and the minimum Peak Sidelobe Level (PSL) filter [84, 85] are respectively designed. While the minimum ISL system shares a closed form solution, the computation of the minimum PSL filter requires the solution of a Linear Programming (LP) problem [84, 85], with reference to real optimization variables and transmitted code sequence, or the solution of a convex optimization Second Order Cone Programming (SOCP) problem [93] in the case of complex variables. Indeed, SOCP [94] problems represent a family of convex optimization programs of great interest for many signal processing applications such as beamforming [95] and target localization [96].

In this chapter, we still focus on the problem of radar receive filter optimization, assuming the same signal model as in [93]. We propose a new design algorithm, based on the following criterion: joint optimization of the sidelobe

energy and the peak sidelobe level. This task is tantamount to jointly minimizing quadratic forms, so that the resulting design problem can be formulated in terms of a multi-objective optimization problem. In order to solve it, we resort to the scalarization technique, where the original vectorial problem is reduced to a scalar one through the use of the Pareto-optimal theory. Thus, the proposed filters are chosen as *Pareto-optimal points*[1] of the previously mentioned multi-objective optimization problem. The performance of the algorithm is evaluated in terms of filter response, ISL, and PSL highlighting the role played by the Pareto weight in the design procedure. Particular emphasis is given to the trade-off existing between the aforementioned metrics. Indeed, it is possible to show that a low peak sidelobe level can be swaped for a reduction of the total sidelobe energy. The trade-off is ruled by the Pareto weight, which indeed represents the parameter defining the relative importance of the two objectives in the optimization problem, namely the cost required for improving a given objective (namely, the ISL) making worse the other (namely, the PSL).

The chapter is organized as follows. In Section 5.2, we present both the signal and the receiver models; then we formulate the design problem provid-

[1] A Pareto-optimal solution of a multi-objective optimization problem is defined as any solution that can't be improved with respect to a component without worsening the others [22].

ing the algorithm for the Pareto-optimal filter construction. In Section 5.3, we assess the performance of the filter design scheme, also in comparison with the minimum ISL and the minimum PSL filters. Finally, conclusions are given in Section 5.4.

5.1.1 Notation

We adopt the notation of using boldface for vectors $\boldsymbol{a}$ and matrices $\boldsymbol{A}$. The i-th element of $\boldsymbol{a}$ and the (l,m)-th entry of $\boldsymbol{A}$ are respectively denoted by $a(i)$ and $\boldsymbol{A}(l,m)$. The transpose operator and the conjugate transpose operator are denoted by the symbols $(\cdot)^T$ and $(\cdot)^H$ respectively. The letter j represents the imaginary unit (i.e. $j = \sqrt{-1}$). $\mathbb{C}$ is the set of real and complex numbers. For any complex number x, we use $\Re(x)$ and $\Im(x)$ to denote respectively the real and the imaginary part of x, $|x|$ and $\arg(x)$ represent the modulus and the argument of x. $v^\star(\cdot)$ stands for the optimal value of the problem $(\cdot)$. The Euclidean norm of the vector $\boldsymbol{x}$ is denoted by $\|\boldsymbol{x}\|$. Finally, $\mathbf{0}$ denotes a zero vector or matrix as long as the size of it is clear from the context.

5.2 Problem Formulation and Mismatched Filter Design

Assume that the transmitted signal is a coded pulse; denote by M the number of subpulses and by $[s(1), \ldots, s(M)]^T$ the radar code. The waveform at the receiver end is down-converted to baseband, undergoes a subpulse matched filtering operation, and then is sampled. The vector $\boldsymbol{r} = [r(1), \ldots, r(P)]^T$ ($P = 2L + M$, with L being a design parameter) of the samples from the range cell under test can be written as [93, 81][2]

$$\boldsymbol{r} = \alpha_0 \boldsymbol{s} + \sum_{n=-N+1, n\neq 0}^{N-1} \alpha_n \boldsymbol{J}_n \boldsymbol{s} + \boldsymbol{n}\,, \tag{5.1}$$

where $N = P - L(= L + M)$, $\boldsymbol{s} = [\boldsymbol{0}, s(1), \ldots, s(M), \boldsymbol{0}]^T \in \mathbb{C}^P$ ($\boldsymbol{0}$ is the zero row vector of dimension L), α_n's are complex scalars accounting for the Radar Cross Sections (RCS's) of the range cells illuminated by the radar and for the channel propagation effects (in particular α_0 refers to the RCS of the cell under test), $\boldsymbol{n}$ is the vector (assumed white) containing the filtered noise samples, and

[2] See these references for more details on the system model.

$\forall n \in \{1, \ldots, N-1\}$

$$\boldsymbol{J}_n(l,m) = \begin{cases} 1 \quad \text{if} \quad m-l=n \\ \\ 0 \quad \text{if} \quad m-l \neq n \end{cases} \qquad (l,m) \in \{1,\ldots,P\}^2$$

denotes the shift matrix. Finally $\boldsymbol{J}_{-n} = \boldsymbol{J}_n^T$.

In order to estimate α_0, as in [93], we focus on estimators whose analytic form is

$$\hat{\alpha}_0 = \frac{\boldsymbol{x}^H \boldsymbol{r}}{\boldsymbol{x}^H \boldsymbol{s}}\,, \tag{5.2}$$

where $\boldsymbol{x}$ is a suitable P-dimensional complex vector (receive filter) which can be designed according to several criteria. In particular, if $\boldsymbol{x} = \boldsymbol{s}$, it is the classic matched filter to the signal $\boldsymbol{s}$. Otherwise, it is usually referred to, in open literature, as mismatched filter or instrumental variable filter [93, 89].

Relevant performance metrics to optimize in the design of a receive filter are related to the energies in the sidelobes of the filter, i.e. $\frac{|\boldsymbol{x}^H \boldsymbol{J}_n \boldsymbol{s}|^2}{|\boldsymbol{x}^H \boldsymbol{s}|^2}$, $n = \pm 1, \ldots, \pm(N-1)$. Specifically, if one wants to optimize the total energy underlying the range sidelobes, it is possible to minimize the ISL $\triangleq \sum_{n=-N+1, n\neq 0}^{N-1} \frac{|\boldsymbol{x}^H \boldsymbol{J}_n \boldsymbol{s}|^2}{|\boldsymbol{x}^H \boldsymbol{s}|^2}$ [81, 88], so as to obtain the minimum ISL filter as an

optimal solution to the optimization problem

$$\min_{\boldsymbol{x}\in\mathbb{C}^P} \sum_{n=-N+1,n\neq 0}^{N-1} \frac{\left|\boldsymbol{x}^H \boldsymbol{J}_n \boldsymbol{s}\right|^2}{\left|\boldsymbol{x}^H \boldsymbol{s}\right|^2}. \tag{5.3}$$

Conversely, if the main concern is to optimize the level of sidelobe peaks, the metric to be considered is the PSL $\triangleq \max_{n=\pm 1,\ldots,\pm(N-1)} \frac{|\boldsymbol{x}^H \boldsymbol{J}_n \boldsymbol{s}|^2}{|\boldsymbol{x}^H \boldsymbol{s}|^2}$. Hence, the minimum PSL filter coincides with an optimal solution to the optimization problem

$$\min_{\boldsymbol{x}\in\mathbb{C}^P} \max_{n=\pm 1,\ldots,\pm(N-1)} \frac{\left|\boldsymbol{x}^H \boldsymbol{J}_n \boldsymbol{s}\right|^2}{\left|\boldsymbol{x}^H \boldsymbol{s}\right|^2}. \tag{5.4}$$

Both ISL and PSL approaches are included in the more general problem of minimizing the L_p-norm of the vector containing the energies of the sidelobes. This mismatched filter design criterion is proposed in [97], where an iterative algorithm attempting to obtain an optimal solution to the problem is introduced. However, the iterative technique of [97] has no known convergence properties even if simulation results show its effectiveness in some analyzed scenarios.

Indeed, providing a filter jointly optimized with respect to the two aforementioned metrics represents an attractive task. Such a need is in part jus-

tified by the growing demand for more and more involving signal processing procedures, with particular emphasis to those capable of adapting their characteristics to different clutter features.

The idea pursued in this chapter is to formulate the problem in terms of the following multi-objective optimization problem [22, pp. 174-187]:

$$\min_{\boldsymbol{x}\in\mathbb{C}^P} \left(\sum_{n=-N+1,\, n\neq 0}^{N-1} \frac{|\boldsymbol{x}^H \boldsymbol{J}_n \boldsymbol{s}|^2}{|\boldsymbol{x}^H \boldsymbol{s}|^2}, \max_{n=\pm 1,\pm 2\ldots,\pm(N-1)} \frac{|\boldsymbol{x}^H \boldsymbol{J}_n \boldsymbol{s}|^2}{|\boldsymbol{x}^H \boldsymbol{s}|^2} \right) \tag{5.5}$$

where the objective is now a vector-valued function which accounts for both ISL and PSL. The main goal is to design an algorithm capable of combining a low energy profile with acceptable range sidelobe peaks. We resort to the scalarization technique in order to find filters which are Pareto-optimal solutions for (5.5) (more details about this topic can be found in [22, 98]).The resulting scalarized problem is proved equivalent to a convex SOCP problem which can be easily solved through interior point methods with a polynomial-time computational complexity.

5.2.1 Pareto-Optimal Receive Filter Design

This section is devoted to the design of Pareto-optimal mismatched filters; namely, we focus on filters which are Pareto-optimal solutions of problem (5.5). To this end, let us denote by $\boldsymbol{a}_n = \boldsymbol{J}_n \boldsymbol{s}$, $n = \pm 1, \ldots, \pm(N-1)$, $\boldsymbol{a}_0 = \boldsymbol{s}$, and

$$\boldsymbol{A} = [\boldsymbol{a}_{-N+1}, \ldots, \boldsymbol{a}_{-1}, \boldsymbol{a}_1, \ldots, \boldsymbol{a}_{N-1}]^H \in \mathbb{C}^{(2N-2)\times P} .$$

As a consequence, $|\boldsymbol{x}^H \boldsymbol{J}_n \boldsymbol{s}|^2 = |\boldsymbol{a}_n^H \boldsymbol{x}|^2$, $\sum_{n=-N+1, n\neq 0}^{N-1} |\boldsymbol{x}^H \boldsymbol{J}_n \boldsymbol{s}|^2 = \boldsymbol{x}^H (\boldsymbol{A}^H \boldsymbol{A}) \boldsymbol{x}$ and $|\boldsymbol{x}^H \boldsymbol{s}|^2 = |\boldsymbol{a}_0^H \boldsymbol{x}|^2$.

In the following, we exploit the scalarization technique [22, pp. 174-187] to determine the Pareto-optimal points of the vector optimization problem (5.5). Precisely, let us choose any $\boldsymbol{\lambda} \succ_{\mathbb{R}^2} \boldsymbol{0}$[3], consider the scalar optimization problem

$$\min_{\boldsymbol{x}\in\mathbb{C}^P} \left[\lambda_1 \left(\sum_{n=-N+1,\, n\neq 0}^{N-1} \frac{|\boldsymbol{a}_n^H \boldsymbol{x}|^2}{|\boldsymbol{a}_0^H \boldsymbol{x}|^2} \right) + \lambda_2 \left(\max_{n=\pm 1, \pm 2 \ldots, \pm(N-1)} \frac{|\boldsymbol{a}_n^H \boldsymbol{x}|^2}{|\boldsymbol{a}_0^H \boldsymbol{x}|^2} \right) \right] , \tag{5.6}$$

and let $\boldsymbol{x}$ be an optimal point. Then, according to the scalarization technique, $\boldsymbol{x}$ is a Pareto-optimal point for problem (5.5). The parameter $\boldsymbol{\lambda}$ represents the Pareto weight vector; namely, the vector containing the coefficients ruling the

[3]We say that $\boldsymbol{\lambda} \triangleq (\lambda_1, \lambda_2) \succ_{\mathbb{R}^2} \boldsymbol{0}$ if $\lambda_1 > 0$ and $\lambda_2 > 0$.

relative importance of the scalar components. The choice of the parameter $\boldsymbol{\lambda}$ plays a primary role in the determination of the Pareto points; indeed, it quantifies our desire to advantage a metric with respect to the other. We explicitly notice that, setting in (5.6) $\lambda_1 \neq 0$ and $\lambda_2 = 0$, we obtain the minimum ISL filter, while, if $\lambda_1 = 0$ and $\lambda_2 \neq 0$, we come up with the minimum PSL filter. Other values of $\boldsymbol{\lambda} \succ_{\mathbb{R}^2} \mathbf{0}$ lead to different compromises between the ISL and the PSL.

In order to find Pareto-optimal solutions to (5.6), we recast problem (5.6) into the following problem

$$\begin{aligned} \min_{\boldsymbol{x}\in\mathbb{C}^P} \quad & \lambda_1 \left[\boldsymbol{x}^H(\boldsymbol{A}^H\boldsymbol{A})\boldsymbol{x}\right] + \lambda_2 \left[\max_{n=\pm1,\ldots,\pm(N-1)} \boldsymbol{x}^H(\boldsymbol{a}_n\boldsymbol{a}_n^H)\boldsymbol{x}\right] \\ \text{s.t.} \quad & \boldsymbol{x}^H(\boldsymbol{a}_0\boldsymbol{a}_0^H)\boldsymbol{x} = 1 \end{aligned}, \tag{5.7}$$

Additionally, we observe that multiplying $\boldsymbol{x}$ for a scalar complex exponential does not affect both the constraint and the objective function; therefore, prob-

lem (5.7) is equivalent to

$$\begin{aligned} \min_{\boldsymbol{x}\in\mathbb{C}^P} \quad & \lambda_1 \left[\boldsymbol{x}^H(\boldsymbol{A}^H\boldsymbol{A})\boldsymbol{x}\right] + \lambda_2 \left[\max_{n=\pm1,\ldots,\pm(N-1)} \boldsymbol{x}^H(\boldsymbol{a}_n\boldsymbol{a}_n^H)\boldsymbol{x}\right] \\ \text{s.t.} \quad & \Re(\boldsymbol{a}_0^H\boldsymbol{x}) = 1. \end{aligned} \tag{5.8}$$

Problem (5.8) can be reformulated as a convex optimization problem which belongs to the class of the SOCP problems [94]. Specifically, for $\lambda_2 \neq 0$ (if $\lambda_2 = 0$, we obtain the minimum PSL filter [84], [85]), problem (5.8) can be written as

$$\begin{aligned} \min_{\boldsymbol{x}\in\mathbb{C}^P} \max_{n=\pm1,\ldots,\pm(N-1)} \quad & \boldsymbol{x}^H\left(\gamma\boldsymbol{A}^H\boldsymbol{A} + \boldsymbol{a}_n\boldsymbol{a}_n^H\right)\boldsymbol{x} \\ \text{s.t.} \quad & \Re(\boldsymbol{a}_0^H\boldsymbol{x}) = 1, \end{aligned} \tag{5.9}$$

where $\gamma \triangleq \frac{\lambda_1}{\lambda_2}$, or equivalently as

$$\begin{aligned} \min_{\boldsymbol{x},t} \quad & t \\ \text{s.t.} \quad & \|\boldsymbol{A}_n \boldsymbol{x}\|^2 \leq t,\ n = \pm 1, \ldots, \pm(N-1)\,, \\ & \Re(\boldsymbol{a}_0^H \boldsymbol{x}) = 1, \\ & \boldsymbol{x} \in \mathbb{C}^P\,, t \in \mathbb{R}\,, \end{aligned} \tag{5.10}$$

where $\boldsymbol{A}_n \triangleq \begin{bmatrix} \sqrt{\gamma}\boldsymbol{A} \\ \boldsymbol{a}_n^H \end{bmatrix}$.

The parameter γ can be interpreted as the *weight* given to the second objective (namely, the total energy under the sidelobes) with respect to the first one (namely, the peak level of the sidelobes); this clearly implies that an optimal solution to problem (5.8) is a function of the Pareto weight.

5.3 Performance Analysis

In this section, we assess the performance of the receive filter introduced in the previous section in terms of output modulus when the input is the transmitted sequence (zero-Doppler cut of the cross-ambiguity function), ISL, and PSL. Additionally, we provide the Pareto-optimal curve, i.e.

$$\begin{cases} \text{ISL}^{\star} \triangleq \boldsymbol{x}^{\star H}(\gamma)(\boldsymbol{A}^H\boldsymbol{A})\boldsymbol{x}^{\star}(\gamma), \\ \\ \text{PSL}^{\star} \triangleq \max\limits_{n=0,\pm 1,\ldots,\pm(N-1)} \boldsymbol{x}^{\star H}(\gamma)(\boldsymbol{a}_n\boldsymbol{a}_n^H)\boldsymbol{x}^{\star}(\gamma), \end{cases}$$

(where $\text{ISL}^{\star}$ and $\text{PSL}^{\star}$ represent, respectively, the objective values of (5.3) and (5.4) in correspondence of an optimal solution $\boldsymbol{x}^{\star}(\gamma)$ to (5.9)); namely, the set of Pareto-optimal values, obtained through scalarization and varying the relative weight γ, for the considered optimization problem. To this end, we resort to a four-phase, length $M = 34$, code with a quite low peak to sidelobe level equal to -19.49 dB, designed according to the method described in Appendix-A of [81]. Moreover, we use SeDuMi software [25] in our simulations to solve the SOCP problem.

In **Figure 5.1**, we show the output modulus of the receive filter in Section II-A for $P = 74$ and for some values of the Pareto weight γ. In the same figure,

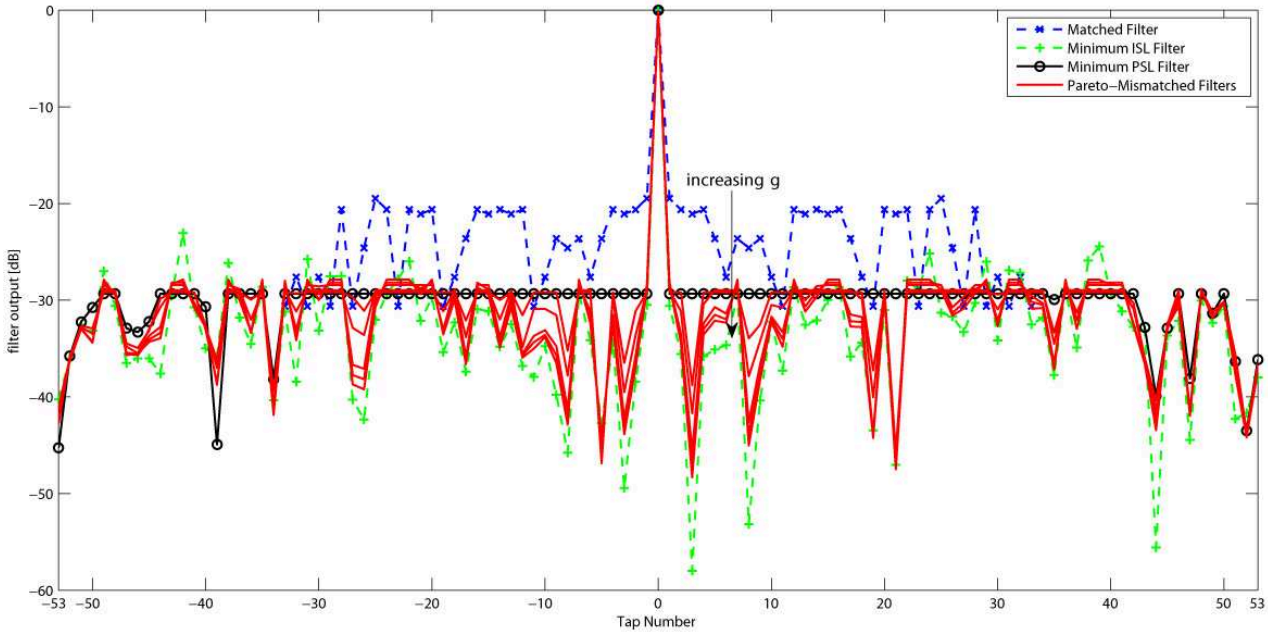

Figure 5.1: Filter Output modulus versus the tap number. Minimum ISL filter (plus-dashed green curve); minimum PSL filter (circle-solid black curve); matched filter (cross-dashed blue curve); Pareto-optimal mismatched filter (5.9) with $\gamma \in \{0.01, 0.02, 0.05, 0.07, 0.1\}$ (solid red curves).

we also plot the outputs of the minimum ISL filter, the minimum PSL filter, and the matched filter. From the plots, we can notice that the parameter γ rules the tradeoff between ISL and PSL of the filter output. Indeed, increasing γ we obtain filter responses which are closer and closer to the minimum ISL filter output. This is of course expected, as the greater γ, the higher the importance, in the optimization procedure, of the ISL feature with respect to the PSL one. This aspect is emphasized in **Figure 5.2**, where the related Pareto-optimal curve is plotted, as γ ranges in the interval $[0, 0.1]$. The curve is generally referred to as *optimal trade-off curve*, because it highlights the con-

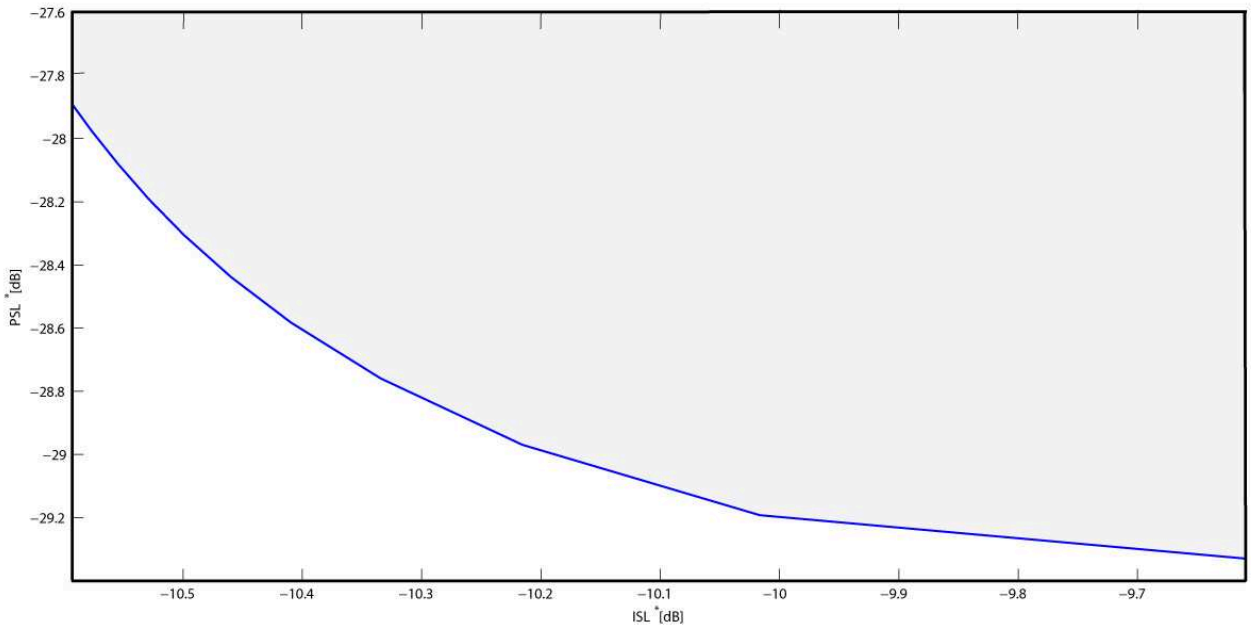

Figure 5.2: Pareto-optimal curve for $\gamma \in [0, 0.1]$, with a four-phase code of length $M = 34$. The set of achievable values above the curve is shaded in gray.

nection between the two objectives, ISL* and PSL*, highlighting the role of the weight in the determination of their Pareto-optimal values and the cost paid for increasing one component with respect to the other. The shaded region indicates the set of all the achievable values (ISL, PSL); for example, intercepting the curve with the vertical line ISL$= \eta$ (thus considering a certain fixed value for the ISL), we can observe how big PSL has to be in order to achieve ISL$= \eta$. The same interpretation arises intercepting the curve with an horizontal line PSL$= \beta$ (thus considering a certain fixed value for the PSL), which makes evident the minimum achievable value ISL in order to ensure PSL$= \beta$. The slope of the optimal trade-off curve at a Pareto-optimal value shows the

Table 5.1: ISL and PSL in dB for the Pareto-optimal mismatched filter (5.9), $P = 74$ and $\gamma \in \{0.01, 0.02, 0.05, 0.07, 0.1.\}$

γ	**ISL**	**PSL**
0.01	-10.017	-29.192
0.02	-10.215	-28.970
0.05	-10.460	-28.440
0.07	-10.582	-28.193
0.1	-10.593	-27.890
Matched Filter	-4.675	-19.49
Minimum ISL Filter	-10.885	-23.064
Minimum PSL Filter	-9.610	-29.330

local optimal trade-off between the two objectives; steep slopes lead to large variations of ISL* in correspondence of small changes in PSL* (this is actually what happens in the lower right region of the curves in **Figure 5.2**). In **Table 5.1**, we explicitly report the tradeoff between ISL and PSL; as already pointed out, increasing γ is tantamount of getting lower and lower PSL values, at the price of higher and higher ISL levels.

In **Figures 5.3a-5.3b**, we analyze the behavior of the ISL and PSL (still for the filter designed according to the criterion of Section II-A) versus the param-

eter L, which rules the length of the filter. For comparison, in the same figures, we also report the behavior of the minimum ISL filter, the minimum PSL filter, and the matched filter. The plots confirm that the longer the filter, the lower the corresponding ISL and PSL values. Indeed, this result is expected, since increasing L is tantamount to providing more degrees of freedom to the filter optimization process.

Finally, in **Figures 5.4a-5.4b**, we analyze the Doppler tolerance of the filters shown in **Figure 5.1**. Specifically, we assess the degradation of the actual ISL and PSL due to the presence of a Doppler shift in the useful signal. The curves in the figures, representing either ISL or PSL versus the normalized Doppler frequency ν_d, ranging in the interval $[-\Delta_\nu, \Delta_\nu]$, highlight that the higher the target Doppler (i.e. the discrepancy from the nominal condition), the worse the ISL and PSL associated with the filter (for all the considered values of the parameter γ). Nevertheless, for the simulated shift values, the new filters still guarantee a performance level which is superior than that ensured by the matched filter, both in terms of ISL and PSL.

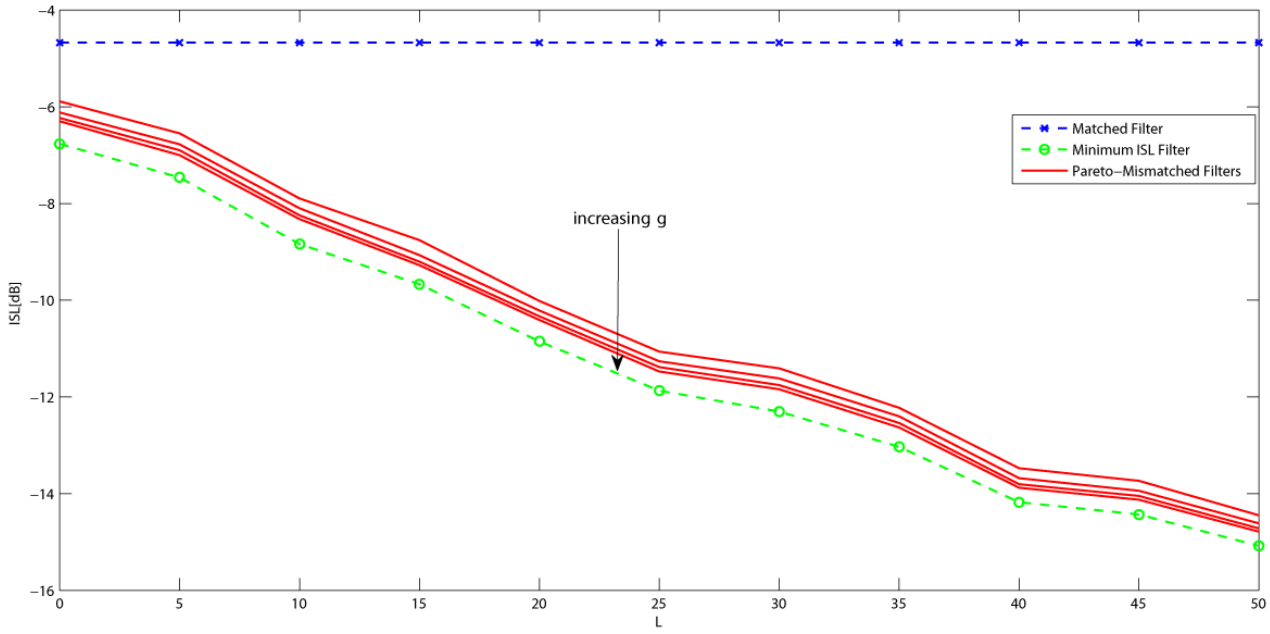

(a) ISL versus L for the Filters in **Figure 5.1**.

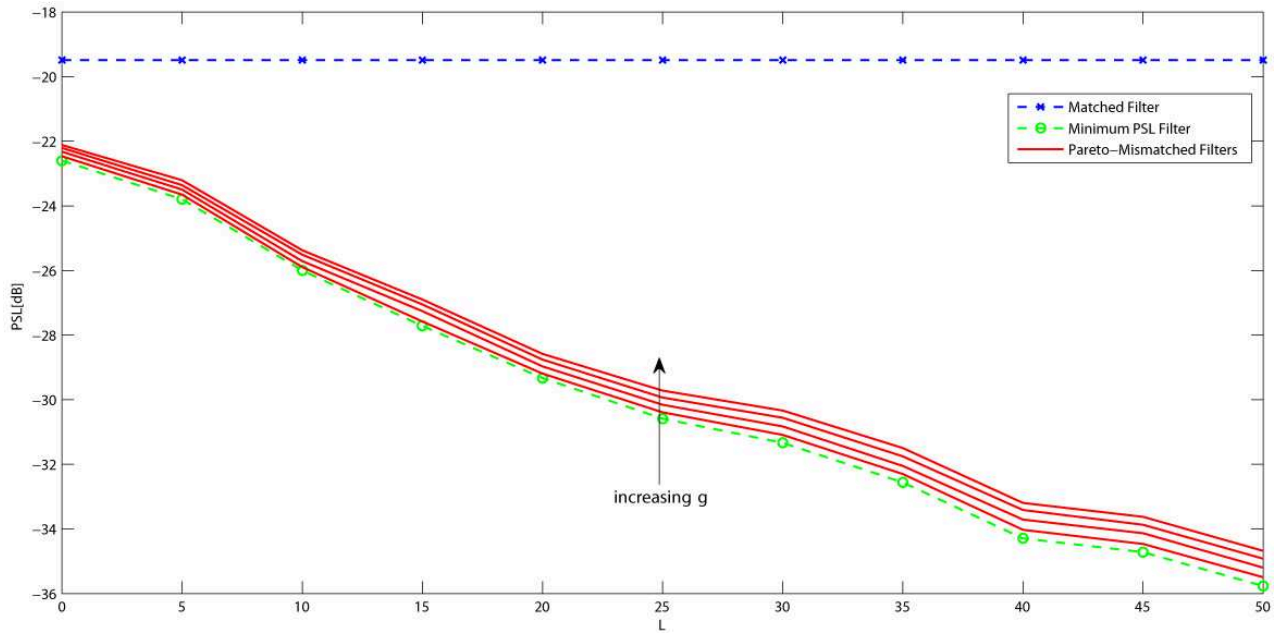

(b) PSL versus L for the Filters in **Figure 5.1**.

Figure 5.3: a) ISL versus L for the Filters in **Figure 5.1**; b) PSL versus L for the Filters in **Figure 5.1**. $L = [0, 5, 10, 15, 20, 25, 30, 35, 40, 45, 50]$. Matched-Filter (blu x-dashed curve). Minimum ISL filter (green circle-dashed curve). Pareto-optimal mismatched filters (red-solid curves).

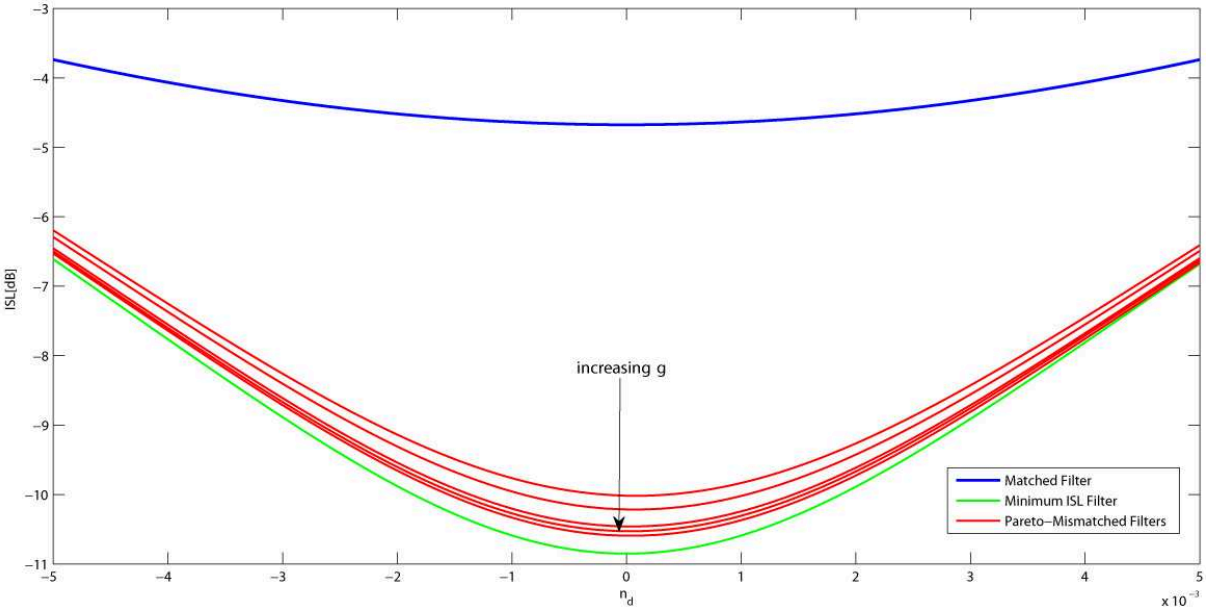

(a) ISL versus ν_d for the Filters in **Figure 5.1**.

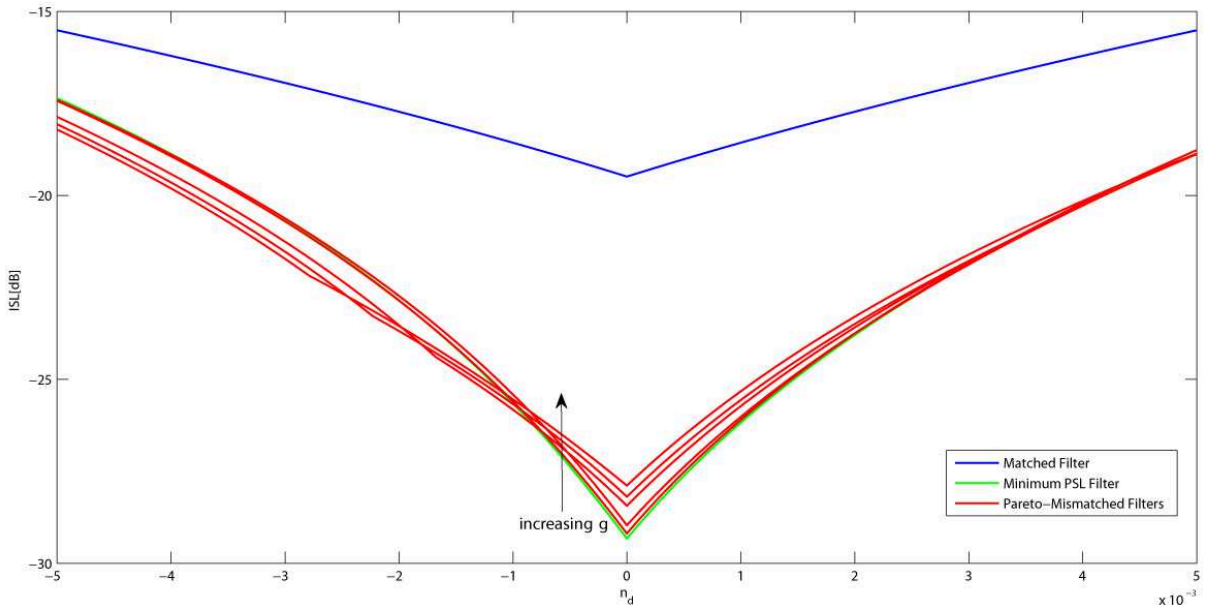

(b) PSL versus ν_d for the Filters in **Figure 5.1**.

Figure 5.4: a) ISL versus ν_d for the Filters in **Figure 5.1**; b) PSL versus ν_d for the Filters in **Figure 5.1**. $\Delta_\nu = 0.005$. Matched Filter (blue-solid curve). Minimum ISL Filter (green-solid curve). Pareto-optimal Mismatched Filters (red-solid curves).

5.4 Conclusions

In this chapter, we have considered the design of radar receive filters according to the following criterion: joint optimization of the ISL and PSL performance metrics. The problem has been formulated in terms of a multi-objective optimization problem. In order to solve it, we have resorted to the scalarization technique, thus focusing on the solutions which are Pareto-optimal for the aforementioned problem. At the analysis stage, we have assessed the performance of the considered receive systems providing filter responses and highlighting the tradeoff between ISL and PSL. Moreover, we have studied the Pareto-optimal curve, showing the effects of the Pareto weight on the performance trade-off. Finally, we have analyzed the Doppler tolerance associated with the considered receive systems.

Possible future developments might be focused on the comparison between the proposed design criterion and that based on the L_p norm minimization of the filter sidelobe energies. Additionally, it might be of interest the study of quantization effects on the filter coefficients as well as of the possible imbalance between the I and Q channels of the processing chain.

Chapter 6

Cognitive Design of the Receive Filter and Transmitted Phase Code in Reverberating Environment

6.1 Introduction

The problem of radar waveform diversity and receiver optimization has been addressed over and over during the last few decades, due to the increasing performance requirements in terms of target tracking accuracy, range-Doppler resolution, mainlobe clutter rejection and low sidelobe signal and/or filter design. The growth in terms of technology, such as new computing architectures, high speed and Off The Shelf (OTS) processors, and digital arbitrary waveform generators, had made possible to perform very complex and effective signal processing [41, Ch. 6, 11, 25], leading the path to the recent cognitive paradigm (see [42], [43], [44], and [70]), which states indeed a new success

frontier for radar signal processing. Its main innovation concerns the smart use of some a-priori information and previous radar experiences about the operating environment (as for instance location of electromagnetic interferences, reflectivity characteristic of the environment, weather conditions and discretes clutter).

Two principal research modalities, exploiting the waveform diversity to improve the radar performances, have emerged. The first is focused on the signal-independent interference and well models, but is not limited to, radar environments where the main contribution to the disturbance is represented by thermal noise, and/or intentional interference (Jammers), and/or unintentional emissions by information sources, and/or terrain scattering due to signals from other radar platforms (hot clutter), [30, 24, 46, 47]. The latter assumes a reverberant environment, namely a signal-dependent clutter scenario, with disturbances produced by radar reflections from terrain or non-threating targets in the surveillance volume. For a point-like target embedded in signal-dependent clutter, optimization of the transmit signal and receive filter to maximize the Signal to Interference plus Noise Ratio (SINR) has been accomplished, assuming both an energy constraint [48] and a dynamic range

constraints [49], on the transmitted waveform. Implementation errors [49], amplitude and phase modulation limitations [51], and quantization error effects [52], have also been considered, modifying the procedure of [48]. In [99], a cognitive approach for the design of the transmit signal (amplitude-phase modulated pulse train) and receive filter, accounting for a similarity between the transmitted sequence and a prescribed radar code, has been devised. In [82], innovative algorithms for optimizing the mean-square error of a target backscattering estimate in the presence of signal-dependent clutter, have been derived. Either a constant-modulus or a low Peak to Average power Ratio (PAR) constraint has been enforced on the transmitted waveform. For a zero-Doppler Gaussian point target in the presence of signal-dependent Gaussian clutter, modeled as the output of a stochastic Linear-Time-Invariant (LTI) filter with a stationary Gaussian shaped impulse response, analytic approaches to optimizing the energy-constrained transmit signal spectrum while maximizing detection performance have been introduced [55].

In this chapter, we address the joint optimization of the transmit signal and receive filter for a radar system which operates in a highly reverberant environment, focusing on both continuous and finite alphabet phase codes. Specifi-

cally, we suppose that the radar system can predict the actual scattering environment, using a dynamic environmental database, including a geographical information system, meteorological data, and some electromagnetic reflectivity and spectral clutter models. Thus, exploiting the aforementioned information and considering as figure of merit the SINR, we devise a suitable radar phase code and receive filter, under a similarity constraint between the sought waveform and a reference code [30], [24].

The devised constrained optimization procedure sequentially improves the SINR. Each iteration requires the solution of both a convex problem and an NP-hard optimization problem. As to the NP-hard quadratic fractional optimization problem, we resort to the relaxation and randomization approach [24] in order to find a good quality solution. The resulting computational complexity is linear with the number of iterations and trials in the randomized procedure, and polynomial with the receive filter length. The performance of the new algorithm is analyzed in a homogeneous clutter environment, showing that interesting SINR improvements can be obtained jointly optimizing the transmitter and the receiver.

The chapter is organized as follows. In Section 6.2, we describe the system

model. In Section 6.3, we formulate the constrained optimization problems for the design of (continuous or finite alphabet) radar phase codes and the receive filters. Additionally, we introduce two sequential optimization procedures to obtain high quality solutions to these problems. In Section 6.4, we assess the performance of the proposed algorithms. Finally, in Section 6.5, we draw conclusions and discuss possible future research tracks.

6.1.1 Notation

We adopt the notation of using boldface for vectors $\boldsymbol{a}$, and matrices $\boldsymbol{A}$; the i-th element of $\boldsymbol{a}$ and the (l,m)-th entry of $\boldsymbol{A}$ are respectively denoted by $a(i)$ and $\boldsymbol{A}(l,m)$. The conjugate transpose operator is denoted by the symbol $(\cdot)^\dagger$, while $(\cdot)^*$ and $(\cdot)^T$ denote, respectively, the conjugate and the transpose operator. $\boldsymbol{I}$ indicates the identity matrix (its size is determined from the context). $\mathbb{C}^N$ and $\mathbb{H}^N$ are respectively the sets of the sets of N-dimensional vectors of complex numbers and $N \times N$ Hermitian matrices. The curled inequality symbol $\succeq$ is used to denote generalized matrix inequality: for any $\boldsymbol{A} \in \mathbb{H}^N$, $\boldsymbol{A} \succeq \boldsymbol{0}$ means that $\boldsymbol{A}$ is a positive semidefinite matrix. $\mathrm{tr}(\cdot)$ is the trace of the square matrix argument, while $\mathrm{diag}\{\boldsymbol{a}\}$ indicates the N-dimensional diagonal matrix

whose i-th diagonal element is $a(i)$, for $i = 1, \ldots, N$. The Euclidean norm of the vector $\boldsymbol{x}$ is denoted by $\|\boldsymbol{x}\|$. The l_∞ norm of the vector $\boldsymbol{x}$ is defined as $||\boldsymbol{x}||_\infty = \max_{k\in(1,\ldots,N)} |\boldsymbol{x}(k)|$, while $\lfloor\cdot\rfloor$ denotes the integer floor operation. For any complex number x, we use $\Re(x)$, $|x|$, and $\arg(x)$ to indicate respectively the real part, the modulus, and the argument of x. $\mathbb{E}[\cdot]$ denotes the statistical expectation. The letter j represents the imaginary unit. Finally, $\odot$ indicates the Hadamard product.

6.2 System Model

We consider a monostatic radar system which transmits a coherent burst of N pulses. The waveform at the receiver end is down-converted to baseband, undergoes a pulse matched filtering operation, and then is sampled. The N-dimensional column vector $\boldsymbol{v} = [v(1), v(2), \ldots, v(N)] \in \mathbb{C}^N$ of the observations, from the range-azimuth cell under test, can be expressed as

$$\boldsymbol{v} = \alpha_T \boldsymbol{s} \odot \boldsymbol{p}(\nu_{d_T}) + \boldsymbol{c} + \boldsymbol{n}, \tag{6.1}$$

with $\boldsymbol{s} = [s(1), s(2), \ldots, s(N)]^T \in \mathbb{C}^N$ the radar code, α_T a complex parameter accounting for the target response, $\boldsymbol{p}(\nu_{d_T}) = [1, e^{j2\pi\nu_{d_T}}, \ldots, e^{j2\pi(N-1)\nu_{d_T}}]^T$, ν_{d_T} the normalized target Doppler frequency, $\boldsymbol{c} \in \mathbb{C}^N$ the vector of clutter samples, and $\boldsymbol{n} \in \mathbb{C}^N$ the vector of noise samples.

The clutter vector $\boldsymbol{c}$ is modeled as the superposition of returns from different uncorrelated scatterers, each from the $(r, i)-$th range-azimuth bin, namely:

$$\boldsymbol{c} = \sum_{r=0}^{N_c-1} \sum_{i=0}^{L-1} \alpha_{(r,i)} \boldsymbol{J}_r \left(\boldsymbol{s} \odot \boldsymbol{p}(\nu_{d_{(r,i)}}) \right),$$

where $N_c \leq N$ is the number of range rings that interfere with the range-azimuth bin of interest $(0, 0)$, L is the number of discrete azimuth sectors, $\alpha_{(r,i)}$ and $\nu_{d_{(r,i)}}$ are, respectively, the echo and the normalized Doppler frequency of the scatterer in the range-azimuth bin (r, i); furthermore, $\forall r \in \{0, \ldots, N-1\}$

$$\boldsymbol{J}_r(l, m) = \begin{cases} 1 \quad \text{if} \quad l - m = r \\ \qquad\qquad\qquad\qquad (l, m) \in \{1, \ldots, N\}^2, \\ 0 \quad \text{if} \quad l - m \neq r \end{cases}$$

where $\boldsymbol{J}_r = \boldsymbol{J}_{-r}^T$ denotes the shift matrix. As to the statistical characterization of the noise vector $\boldsymbol{n}$, we assume that it is zero-mean and white, i.e.:

$$\mathbb{E}[\boldsymbol{n}] = 0, \qquad \mathbb{E}\left[\boldsymbol{n}\boldsymbol{n}^\dagger\right] = \sigma_n^2 \boldsymbol{I}.$$

Now, let us focus on the statistical characterization of the clutter vector $\boldsymbol{c}$. As previously stated, we suppose that the scatterers are uncorrelated; moreover, for each scatterer, we denote by $\sigma_{(r,i)}^2 = \mathbb{E}\left[|\alpha_{(r,i)}|^2\right]$, assume that the expected value of its complex amplitude is zero, i.e. $\mathbb{E}\left[\alpha_{(r,i)}\right] = 0$, and that its normalized Doppler frequency, statistically independent of $\alpha_{(r,i)}$, is uniformly distributed around a mean Doppler frequency $\bar{\nu}_{d_{(r,i)}}$, i.e. $\nu_{d_{(r,i)}} \sim \mathcal{U}\left(\bar{\nu}_{d_{(r,i)}} - \frac{\epsilon_{(r,i)}}{2}, \bar{\nu}_{d_{(r,i)}} + \frac{\epsilon_{(r,i)}}{2}\right)$. As a consequence, we have: $\mathbb{E}[\boldsymbol{c}] = 0$ and

$$\boldsymbol{\Sigma}_{\boldsymbol{C}}(\boldsymbol{s}) = \mathbb{E}\left[\boldsymbol{c}\boldsymbol{c}^\dagger\right] = \sum_{r=0}^{N_c-1}\sum_{i=0}^{L-1} \sigma_{(r,i)}^2 \boldsymbol{J}_r \boldsymbol{\Gamma}(\boldsymbol{s},(r,i))\boldsymbol{J}_r^T, \tag{6.2}$$

where

$$\boldsymbol{\Gamma}(\boldsymbol{s},(r,i)) = \mathrm{diag}\{\boldsymbol{s}\}\boldsymbol{\Phi}_{\epsilon_{(r,i)}}^{\bar{\nu}_{d_{(r,i)}}}\mathrm{diag}\{\boldsymbol{s}\}^\dagger,$$

and, $\forall\,(l,m)\in\{1,\ldots,N\}^2$,

$$\mathbf{\Phi}_{\epsilon}^{\bar{\nu}_d}(l,m)=e^{(j2\pi\bar{\nu}_d(l-m))}\frac{\sin[\pi\epsilon(l-m)]}{[\pi\epsilon(l-m)]}.$$

A relevant scenario, which can be described and modeled according to (6.2), is now described (see also [99]). Let us assume that, for any (r,i) range-azimuth bin, the Radar Cross Section (RCS) $\sigma_0^{(r,i)}$ of the scatterer is predicted through the interaction between a digital terrain map, such as the National Land Cover Data (NLCD) and RCS clutter models. Whenever $\sigma_0^{(r,i)}$ has been estimated, according to the previous information, we can evaluate $\sigma^2_{(r,i)}$ as

$$\sigma^2_{(r,i)}=\sigma_0^{(r,i)}K_r|G\left(\theta_i\right)|^2,$$

where K_r is a constant accounting for the channel propagation effects, such as the free space two-way path loss and additional system losses (radar equation), θ_i is the azimuth angle of the bin (r,i), and $G\left(\theta\right)$ is the one-way antenna gain for the angle θ.

6.3 Problem formulation and Design Issues

We deal with the design of a suitable radar code and receive filter maximizing the SINR, under some constraints on the shape of the code. Specifically, assuming that the vector of observations $\boldsymbol{v}$ is filtered through $\boldsymbol{w}$, the SINR at the output of the filter[1] can be written as:

$$\text{SINR} = \frac{|\alpha_T|^2 \left| \boldsymbol{w}^\dagger \left(\boldsymbol{s} \odot \boldsymbol{p}(\nu_{d_T}) \right) \right|^2}{\boldsymbol{w}^\dagger \boldsymbol{\Sigma_C}(\boldsymbol{s}) \boldsymbol{w} + \sigma_n^2 \|\boldsymbol{w}\|^2}, \tag{6.3}$$

where $|\alpha_T|^2 \left| \boldsymbol{w}^\dagger (\boldsymbol{s} \odot \boldsymbol{p}(\nu_{d_T})) \right|^2$ is the useful energy at the output of the filter, while $\sigma_n^2 \|\boldsymbol{w}\|^2$ and $\boldsymbol{w}^\dagger \boldsymbol{\Sigma_C}(\boldsymbol{s}) \boldsymbol{w}$ represent, respectively, the noise and the clutter energy at the filter output. Notice that the clutter energy $\boldsymbol{w}^\dagger \boldsymbol{\Sigma_C}(\boldsymbol{s}) \boldsymbol{w}$ functionally depends both on the receive processing $\boldsymbol{w}$ and the transmitted waveform through $\boldsymbol{\Sigma_C}(\boldsymbol{s})$ (namely it is a quartic polynomial in variables $\boldsymbol{w}$ and $\boldsymbol{s}$). This observation represents the main difference between a signal-dependent and a signal-independent environment where the output clutter energy is only a function of $\boldsymbol{w}$, being a homogeneous quadratic form in that variable.

To develop our SINR optimization algorithm, we make use of the following technical Lemma (whose proof is given in [99]) providing an alternative

[1] Obviously, we assume that $\boldsymbol{w} \neq \boldsymbol{0}$.

expression to the SINR:

Lemma 6.3.1. *An equivalent expression of the SINR is given by:*

$$SINR = \frac{|\alpha_T|^2 \left| \boldsymbol{s}^T \left(\boldsymbol{w}^* \odot \boldsymbol{p}(\nu_{d_T}) \right) \right|^2}{\boldsymbol{s}^T \boldsymbol{\Theta}_{\boldsymbol{C}} \left(\boldsymbol{w} \right) \boldsymbol{s}^* + \sigma_n^2 \|\boldsymbol{w}\|^2} \tag{6.4}$$

where:

$$\boldsymbol{\Theta}_{\boldsymbol{C}} \left(\boldsymbol{w} \right) = \sum_{r=1}^{N_c-1} \sum_{i=0}^{L-1} \sigma_{(r,i)}^2 \mathrm{diag}\{\boldsymbol{J}_{-r} \boldsymbol{w}^*\} \boldsymbol{\Phi}_{\epsilon_{(r,i)}}^{\bar{\nu}_{d_{(r,i)}}} \mathrm{diag}\{\boldsymbol{J}_{-r} \boldsymbol{w}\} + \sum_{i=0}^{L-1} \sigma_{(0,i)}^2 \mathrm{diag}\{\boldsymbol{w}^*\} \boldsymbol{\Phi}_{\epsilon_{(0,i)}}^{\bar{\nu}_{d_{(0,i)}}} \mathrm{diag}\{\boldsymbol{w}\} \, .$$

As to the shape of the code, the focus is on both continuous alphabet phase codes, i.e. $|s(k)| = 1$, $k = 1, \ldots, N$, and finite alphabet phase code, namely $s(k) \in \{1, e^{j2\pi/M}, \ldots, e^{j2\pi(M-1)/M}\}$, $k = 1, \ldots, N$. Furthermore, a similarity constraint [30, 24] is enforced, namely

$$\|\boldsymbol{s} - \boldsymbol{s}_0\|_\infty \leq \delta \, , \tag{6.5}$$

where the parameter $\delta \geq 0$ rules the size of the similarity region and $\boldsymbol{s}_0$ is a prefixed phase code. By doing so, it is required the solution to be similar to a known code $\boldsymbol{s}_0$, which shares some nice properties such as reasonable range-

Doppler resolution and peak sidelobe level. In other words, imposing (6.5) is tantamount to indirectly controlling the ambiguity function of the considered coded pulse train: the smaller δ the higher the degree of similarity between the ambiguity functions of the devised radar code and $\boldsymbol{s}_0$.

Summarizing, the joint design of the radar code and receive filter can be formulated in terms of the following constrained optimization problems:

- $$\mathcal{P}^c \begin{cases} \max\limits_{\boldsymbol{s},\boldsymbol{w}} & \dfrac{|\alpha_T|^2 \left|\boldsymbol{w}^\dagger \left(\boldsymbol{s} \odot \boldsymbol{p}(\nu_{d_T})\right)\right|^2}{\boldsymbol{w}^\dagger \boldsymbol{\Sigma}_{\boldsymbol{C}}\left(\boldsymbol{s}\right) \boldsymbol{w} + \sigma_n^2 \|\boldsymbol{w}\|^2} \\ \text{s.t.} & |s(k)| = 1,\ k = 1, \ldots, N \\ & \|\boldsymbol{s} - \boldsymbol{s}_0\|_\infty \leq \delta \end{cases} \tag{6.6}$$

  for a continuous alphabet phase code;

- $$\mathcal{P}^d \begin{cases} \max\limits_{\boldsymbol{s},\boldsymbol{w}} & \dfrac{|\alpha_T|^2 \left|\boldsymbol{w}^\dagger \left(\boldsymbol{s} \odot \boldsymbol{p}(\nu_{d_T})\right)\right|^2}{\boldsymbol{w}^\dagger \boldsymbol{\Sigma}_{\boldsymbol{C}}\left(\boldsymbol{s}\right) \boldsymbol{w} + \sigma_n^2 \|\boldsymbol{w}\|^2} \\ \text{s.t.} & s(k) \in \{1, e^{j2\pi/M}, \ldots, e^{j2\pi(M-1)/M}\},\ k = 1, \ldots, N, \\ & \|\boldsymbol{s} - \boldsymbol{s}_0\|_\infty \leq \delta \end{cases} \tag{6.7}$$

for a discrete alphabet phase code.

Problems $\mathcal{P}^c$ and $\mathcal{P}^d$ are non-convex optimization problems, since the objective function is a non-convex function and the constraints $|s(k)|^2 = 1$, $k = 1, \ldots, N$, and $s(k) \in \left\{1, e^{j2\pi/M}, \ldots, \ e^{j2\pi(M-1)/M}\right\}$, $k = 1, \ldots, N$, define non-convex sets. The technique that we adopt to find a good quality solution for $\mathcal{P}^c$ and $\mathcal{P}^d$ is based on a sequential optimization procedure. The idea is to iteratively improve the SINR. Specifically, given $\boldsymbol{w}^{(n-1)}$, we search for an admissible radar code $\boldsymbol{s}^{(n)}$ at step n improving the SINR corresponding to the receive filter $\boldsymbol{w}^{(n-1)}$ and the transmitted signal $\boldsymbol{s}^{(n-1)}$. Whenever $\boldsymbol{s}^{(n)}$ is found, we fix it and search for the adaptive filter $\boldsymbol{w}^{(n)}$ which improves the SINR corresponding to the radar code $\boldsymbol{s}^{(n)}$ and the receive filter $\boldsymbol{w}^{(n-1)}$, and so on. Otherwise stated, $\boldsymbol{w}^{(n)}$ and $\boldsymbol{s}^{(n)}$ are used as starting point at step $n+1$. To trigger the procedure, the optimal receive filter $\boldsymbol{w}^{(0)}$ to an admissible code $\boldsymbol{s}^{(0)}$ is considered.

From an analytical point of view, $\boldsymbol{w}^{(n)}$ is an optimal solution to the optimization problem:

$$\mathcal{P}_{\boldsymbol{w}}{}^{(n)} \left\{ \max_{\boldsymbol{w}} \ \frac{|\alpha_T|^2 \left| \boldsymbol{w}^\dagger \left(\boldsymbol{s}^{(n)} \odot \boldsymbol{p}(\nu_{d_T}) \right) \right|^2}{\boldsymbol{w}^\dagger \boldsymbol{\Sigma_c} \left(\boldsymbol{s}^{(n)} \right) \boldsymbol{w} + \sigma_n^2 \|\boldsymbol{w}\|^2} \right. . \tag{6.8}$$

As shown in [99], $\mathcal{P}_{\boldsymbol{w}}{}^{(n)}$ is solvable and a closed form optimal solution $\boldsymbol{w}^{(n)}$ can be found for any feasible $\boldsymbol{s}^{(n)}$. Specifically, an optimal solution to $\mathcal{P}_{\boldsymbol{w}}{}^{(n)}$ is

given by:

$$\boldsymbol{w}^{(n)} = \frac{\left(\boldsymbol{\Sigma_C}\left(\boldsymbol{s}^{(n)}\right) + \sigma_n^2\boldsymbol{I}\right)^{-1}\left(\boldsymbol{s}^{(n)} \odot \boldsymbol{p}(\nu_{d_T})\right)}{\left\|\left(\boldsymbol{\Sigma_C}\left(\boldsymbol{s}^{(n)}\right) + \sigma_n^2\boldsymbol{I}\right)^{-1/2}\left(\boldsymbol{s}^{(n)} \odot \boldsymbol{p}(\nu_{d_T})\right)\right\|^2}, \tag{6.9}$$

from which it is evident the dependence of $\boldsymbol{w}^{(n)}$ on $\boldsymbol{s}^{(n)}$ and the steering vector $\boldsymbol{p}(\nu_{d_T})$. Furhermore, $\boldsymbol{s}^{(n)}$ is given by:

$$\boldsymbol{s}^{(n)} = \arg\max\left\{\frac{|\alpha_T|^2\left|\boldsymbol{w}^{(n-1)^\dagger}\left(\boldsymbol{s}^{(n-1)} \odot \boldsymbol{p}(\nu_{d_T})\right)\right|^2}{\boldsymbol{w}^{(n-1)^\dagger}\boldsymbol{\Sigma_C}\left(\boldsymbol{s}^{(n-1)}\right)\boldsymbol{w}^{(n-1)} + \sigma_n^2\|\boldsymbol{w}^{(n-1)}\|^2}, \frac{|\alpha_T|^2\left|\boldsymbol{w}^{(n-1)^\dagger}\left(\boldsymbol{s}^{(\star)} \odot \boldsymbol{p}(\nu_{d_T})\right)\right|^2}{\boldsymbol{w}^{(n-1)^\dagger}\boldsymbol{\Sigma_C}\left(\boldsymbol{s}^{(\star)}\right)\boldsymbol{w}^{(n-1)} + \sigma_n^2\|\boldsymbol{w}^{(n-1)}\|^2}\right\}$$

where $\boldsymbol{s}^{(\star)}$ is a good solution of problem $\mathcal{P}^{c\,(n)}_{\boldsymbol{s}}$ if the focus is on $\mathcal{P}^c$, and a good solution of problem $\mathcal{P}^{d\,(n)}_{\boldsymbol{s}}$ if the focus is on $\mathcal{P}^d$, respectively given by:

- $$\mathcal{P}^{c\,(n)}_{\boldsymbol{s}}\begin{cases}\max\limits_{\boldsymbol{s}} & \dfrac{|\alpha_T|^2\left|\boldsymbol{w}^{(n-1)^\dagger}\left(\boldsymbol{s} \odot \boldsymbol{p}(\nu_{d_T})\right)\right|^2}{\boldsymbol{w}^{(n-1)^\dagger}\boldsymbol{\Sigma_C}\left(\boldsymbol{s}\right)\boldsymbol{w}^{(n-1)} + \sigma_n^2\|\boldsymbol{w}^{(n-1)}\|^2} \\ \text{s.t.} & |s(k)| = 1,\, k = 1, \ldots, N, \\ & \|\boldsymbol{s} - \boldsymbol{s}_0\|_\infty \leq \delta\end{cases}; \tag{6.10}$$

- $$\mathcal{P}_{\boldsymbol{s}}^{d\,(n)} \begin{cases} \max\limits_{\boldsymbol{s}} & \dfrac{|\alpha_T|^2 \left| \boldsymbol{w}^{(n-1)^\dagger} \left(\boldsymbol{s} \odot \boldsymbol{p}(\nu_{d_T}) \right) \right|^2}{\boldsymbol{w}^{(n-1)^\dagger} \boldsymbol{\Sigma}_{\boldsymbol{C}} \left(\boldsymbol{s} \right) \boldsymbol{w}^{(n-1)} + \sigma_n^2 \|\boldsymbol{w}^{(n-1)}\|^2} \\ \text{s.t.} & s(k) \in \{1, e^{j2\pi/M}, \ldots, e^{j2\pi(M-1)/M}\},\ k = 1, \ldots, N, \\ & \|\boldsymbol{s} - \boldsymbol{s}_0\|_\infty \leq \delta \end{cases} . \tag{6.11}$$

Making use of [99, Proposition 2.1], the following Proposition 6.3.2 holds true:

Proposition 6.3.2. *Let $\left\{ \left(\boldsymbol{s}^{(n)}, \boldsymbol{w}^{(n)} \right) \right\}$ be a sequence of points obtained through the proposed sequential optimization procedure, either for the continuous or the discrete alphabet case; let SINR$^{(n)}$ be the SINR value corresponding to the point $\left(\boldsymbol{s}^{(n)}, \boldsymbol{w}^{(n)} \right)$ at the $n-$th iteration. Then:*

- *the sequence SINR$^{(n)}$ is a monotonic increasing sequence;*
- *the sequence SINR$^{(n)}$ converges to a finite value SINR*;*
- *starting from the sequence $\left\{ \left(\boldsymbol{s}^{(n)}, \boldsymbol{w}^{(n)} \right) \right\}$, it is possible to construct another sequence $\left\{ \left(\tilde{\boldsymbol{s}}^{(n')}, \tilde{\boldsymbol{w}}^{(n')} \right) \right\}$, that converges to a feasible point $(\tilde{\boldsymbol{s}}^\star, \tilde{\boldsymbol{w}}^\star)$ of problems $\mathcal{P}^c$ or $\mathcal{P}^d$, such that the SINR evaluated in $(\tilde{\boldsymbol{s}}^\star, \tilde{\boldsymbol{w}}^\star)$ is equal to SINR*.*

Let us observe that, from a practical point of view, the proposed optimization procedure requires a condition to stop the iterations; to this end, an

iteration gain constraint can be forced, namely $|\text{SINR}^{(n)} - \text{SINR}^{(n-1)}| \leq \zeta$, where ζ is the desired gain. The next subsections will be devoted to the study of the optimization problems $\mathcal{P}_{\boldsymbol{s}}^{c\,(n)}$ and $\mathcal{P}_{\boldsymbol{s}}^{d\,(n)}$ required for implementing the proposed sequential optimization procedures.

6.3.1 Radar Code Optimization: Solution of the Problem $\mathcal{P}_{\boldsymbol{s}}^{c\,(n)}$

An algorithm to find in polynomial time a good quality solution to the NP-hard problem $\mathcal{P}_{\boldsymbol{s}}^{c\,(n)}$ is now described. Using Lemma 6.3.1, $\mathcal{P}_{\boldsymbol{s}}^{c\,(n)}$ can be equivalently recast as the following problem $\mathcal{P}_1$:

$$\mathcal{P}_1 \begin{cases} \max\limits_{\boldsymbol{s}} & \dfrac{\left|\boldsymbol{s}^T\left(\boldsymbol{w}^{(n-1)^*} \odot \boldsymbol{p}(\nu_{d_T})\right)\right|^2}{\boldsymbol{s}^T \boldsymbol{\Theta}_{\boldsymbol{C}}\left(\boldsymbol{w}^{(n-1)}\right)\boldsymbol{s}^* + \sigma_n^2 \|\boldsymbol{w}^{(n-1)}\|^2} \\ \text{s.t.} & |s(k)| = 1,\, k = 1, \ldots, N \\ & \|\boldsymbol{s} - \boldsymbol{s}_0\|_\infty \leq \delta \end{cases}, \tag{6.12}$$

This is a non-convex fractional quadratic problem. Notice that, since $|s(k)| = |s_0(k)| = 1,\ k = 1, \ldots, N$, the similarity constraint $\max\limits_{k \in [1,\ldots,N]} |\boldsymbol{s}(k) - \boldsymbol{s}_0(k)| \leq \delta$ can

be equivalently written as $\Re\left[\boldsymbol{s}^*(k)\boldsymbol{s}_0(k)\right] \geq 1-\delta^2/2$ for $k=1,\ldots,N$, which is tantamount to imposing $\arg(\boldsymbol{s}(k)) \in [\gamma_k, \gamma_k+\delta_c]$, where $\gamma_k = \arg(\boldsymbol{s}_0(k)) - \arccos(1-\delta^2/2)$ and $\delta_c = 2\arccos\left(1-\delta^2/2\right)$ for $k=1,\ldots,N$, [24]. Thus, problem (6.12) is equivalent to:

$$\mathcal{P}_1' \begin{cases} \max\limits_{\boldsymbol{s}} & \dfrac{\left|\boldsymbol{s}^T\left(\boldsymbol{w}^{(n-1)^*} \odot \boldsymbol{p}(\nu_{d_T})\right)\right|^2}{\boldsymbol{s}^T\boldsymbol{\Theta}_{\boldsymbol{C}}\left(\boldsymbol{w}^{(n-1)}\right)\boldsymbol{s}^* + \sigma_n^2\|\boldsymbol{w}^{(n-1)}\|^2} \\ \text{s.t.} & |s(k)|=1,\ k=1,\ldots,N \\ & \arg(s(k)) \in [\gamma_k, \gamma_k+\delta_c],\ k=1,\ldots,N \end{cases} . \tag{6.13}$$

Let us observe that problem $\mathcal{P}_1'$, even in the simpler formulation corresponding to $\epsilon = 2$, is generally NP-hard, consequently one cannot find polynomial time algorithms for computing its optimal solutions. Hence, we focus on approximation techniques and propose a relaxation and randomization algorithm which provides a randomized feasible solution to (6.13). To this end, let us indicate with

$$\boldsymbol{S} = \left(\boldsymbol{w}^{(n-1)} \odot \boldsymbol{p}(\nu_{d_T})^*\right)\left(\boldsymbol{w}^{(n-1)} \odot \boldsymbol{p}(\nu_{d_T})^*\right)^\dagger, \tag{6.14}$$

and

$$\boldsymbol{M} = \boldsymbol{\Theta}_{\boldsymbol{C}} \left(\boldsymbol{w}^{(n-1)}\right)^* + \frac{\sigma_n^2}{N} \|\boldsymbol{w}^{(n-1)}\|^2 \boldsymbol{I}. \tag{6.15}$$

The relaxed version of problem $\mathcal{P}_1'$, obtained neglecting the similarity constraint, namely the conditions $\arg(s(k)) \in [\gamma_k, \gamma_k + \delta_c]$, $k = 1, \ldots, N$, is given by the following fractional quadratic problem $\mathcal{P}_1''$;

$$\mathcal{P}_1'' \begin{cases} \max\limits_{\boldsymbol{s}} & \dfrac{\left|\boldsymbol{s}^T \left(\boldsymbol{w}^{(n-1)^*} \odot \boldsymbol{p}(\nu_{d_T})\right)\right|^2}{\boldsymbol{s}^T \boldsymbol{\Theta}_{\boldsymbol{C}} \left(\boldsymbol{w}^{(n-1)}\right) \boldsymbol{s}^* + \sigma_n^2 \|\boldsymbol{w}^{(n-1)}\|^2} \\ \text{s.t.} & |s(k)| = 1,\ k = 1, \ldots, N \end{cases}, \tag{6.16}$$

which is equivalent to

$$\mathcal{P}_1''' \begin{cases} \max\limits_{\boldsymbol{X},\, \boldsymbol{s}} & \dfrac{\mathrm{tr}\,(\boldsymbol{S}\boldsymbol{X})}{\mathrm{tr}\,(\boldsymbol{M}\boldsymbol{X})} \\ \text{s.t.} & \boldsymbol{X}(k,k) = 1,\ k = 1, \ldots, N \\ & \boldsymbol{X} = \boldsymbol{s}\boldsymbol{s}^\dagger, \quad \boldsymbol{s} \in \mathbb{C}^N \end{cases}. \tag{6.17}$$

The Semidefinite Relaxation (SDP) [29] of problem $\mathcal{P}_1'''$, obtained dropping

the rank-one constraint, is:

$$\begin{cases} \max\limits_{\boldsymbol{X}} & \dfrac{\mathrm{tr}\,(\boldsymbol{S}\boldsymbol{X})}{\mathrm{tr}\,(\boldsymbol{M}\boldsymbol{X})} \\ \text{s.t.} & \boldsymbol{X}(k,k)=1,\, k=1,\ldots,N \\ & \boldsymbol{X}\succeq \boldsymbol{0} \end{cases}. \tag{6.18}$$

In order to solve the fractional problem (6.18), following the guidelines of [67], it suffices to solve the equivalent SDP problem:

$$(\text{SDP}) \begin{cases} \max\limits_{\boldsymbol{X},\, u} & \mathrm{tr}\,(\boldsymbol{S}\boldsymbol{X}) \\ \text{s.t.} & \mathrm{tr}\,(\boldsymbol{M}\boldsymbol{X})=1 \\ & \boldsymbol{X}(k,k)=u \\ & \boldsymbol{X}\succeq \boldsymbol{0},\, u>0 \end{cases}. \tag{6.19}$$

Indeed, both problems (6.18) and (6.19) are solvable and have equal optimal value; in fact, if $\left(\hat{\boldsymbol{X}},\hat{u}\right)$ is an optimal solution of (6.19), than it can be shown straightforward that $\hat{\boldsymbol{X}}/\hat{u}$ is an optimal solution of (6.18); also, if $\hat{\boldsymbol{X}}$ solves

(6.18), than $\left(\hat{\boldsymbol{X}}/\mathrm{tr}(\boldsymbol{M}\hat{\boldsymbol{X}}), 1/\mathrm{tr}(\boldsymbol{M}\hat{\boldsymbol{X}})\right)$ solves (6.19). Thus, following the same approach as in [24, pp. 8-9], a randomized feasible solution $\boldsymbol{s}^{(\star)}$ to problem $\mathcal{P}^{c\,(n)}_{\boldsymbol{S}}$ can be computed using **Algorithm 8**, where H indicates the number of randomizations involved in the procedure.

Algorithm 8 : Radar Phase Code Optimization

Input: $\boldsymbol{M}, \boldsymbol{S}, H, \{\gamma_i\}, \delta_c$.

Output: A randomized approximate solution $\boldsymbol{s}^{(\star)}$ to $\mathcal{P}^{c\,(n)}_{\boldsymbol{S}}$;

1: Let $(\boldsymbol{X}^\star, u^\star)$ be an optimal solution to problem (6.19).

2: Denote by $\hat{\boldsymbol{X}} = \boldsymbol{X}^\star/u^\star$.

3: Generate random vectors $(\boldsymbol{\xi})_h \in \mathbb{C}^N$, $h = 1, \ldots, H$, from the complex normal distribution $\mathcal{N}_{\mathbb{C}}(0, \boldsymbol{Y})$ where $\boldsymbol{Y} = \hat{\boldsymbol{X}} \odot \boldsymbol{y}_c\boldsymbol{y}_c^\dagger$, where $\boldsymbol{y}_c = [e^{-j\gamma_1}, \ldots, e^{-j\gamma_N}]^T$.

4: Let $(s(k))_h = y_c^*(k)\sigma((\xi_k)_h)$, $k = 1, \ldots, N$, $h = 1, \ldots, H$, where $\sigma(x) = e^{j\frac{\arg(x)}{2\pi}\delta_c}$, $x \in \mathbb{C}$.

5: Compute

$$t_h = \frac{\mathrm{tr}\left(\boldsymbol{s}_h^\dagger \boldsymbol{S}\boldsymbol{s}_h\right)}{\mathrm{tr}\left(\boldsymbol{s}_h^\dagger \boldsymbol{M}\boldsymbol{s}_h\right)}, \quad h = 1 \ldots, H.$$

6: Pick the maximal value over $\{t_1, \ldots, t_H\}$, say t_1, and output $\boldsymbol{s}^{(\star)} = \boldsymbol{s}_1$.

We point out that the H randomizations involved into steps 3-6 are meant to improve the approximation quality; in fact the randomized feasible solution yielding the largest objective value will be chosen as the approximate solution. As to the computational complexity connected with the implementation of the algorithm, the solution of the SDP relaxation requires $O(N^{3.5})$ floating point

operations (flops)[2] whereas each randomization involves $O(N^2)$ flops [23]. It follows that, for a modest number of randomizations, the most relevant contribution to the computational complexity is connected with the SDP solution.

6.3.2 Radar Code optimization: Solution of the Problem $\mathcal{P}_{\boldsymbol{s}}^{d\,(n)}$

At the current state of the art, most radar systems use phase coded waveforms, where the phases are taken from a finite and regularly spaced alphabet. As a consequence, in this subsection, we describe an algorithm to find in polynomial time good solutions to the NP-hard problem $\mathcal{P}_{\boldsymbol{s}}^{d\,(n)}$.

Firstly, we assume that $s_0(k) \in \{1, e^{j2\pi\frac{1}{M}}, \ldots, e^{j2\pi\frac{M-1}{M}}\}, k = 1, \ldots, N$, and[3] $M \geq 2$. Then, using Lemma 6.3.1, we equivalently recast $\mathcal{P}_{\boldsymbol{s}}^{d\,(n)}$ in terms of the following

[2]Herein, we use the Landau notation $O(n)$; hence, an algorithm is $O(n)$ if its implementation requires a number of flops proportional to n [69].

[3]Notice that, for $M = 2$ and $\delta < 2$, the optimal solution to problem (6.20) is the trivial one, i.e. $\boldsymbol{s}^{(\star)} \triangleq \boldsymbol{s}_0$.

problem $\mathcal{P}_2$:

$$\mathcal{P}_2 \begin{cases} \max\limits_{\boldsymbol{s}} & \dfrac{\left|\boldsymbol{s}^T\left(\boldsymbol{w}^{(n-1)^*} \odot \boldsymbol{p}(\nu_{d_T})\right)\right|^2}{\boldsymbol{s}^T \boldsymbol{\Theta}_{\boldsymbol{C}}\left(\boldsymbol{w}^{(n-1)}\right)\boldsymbol{s}^* + \sigma_n^2 \|\boldsymbol{w}^{(n-1)}\|^2} \\ \text{s.t.} & s(k) \in \{1, e^{j2\pi\frac{1}{M}}, \ldots, e^{j2\pi\frac{M-1}{M}}\},\ k = 1, \ldots, N \\ & \|\boldsymbol{s} - \boldsymbol{s}_0\|_\infty \leq \delta \end{cases} . \tag{6.20}$$

This is a non-convex fractional quadratic problem. Notice that, accounting for $\{s(k), s_0(k)\} \in \left\{1, e^{j2\pi\frac{1}{M}}, \ldots, \ e^{j2\pi\frac{M-1}{M}}\right\}^2$, $k = 1, \ldots, N$, the constraint $\max\limits_{k\in[1,\ldots,N]} |\boldsymbol{s}(k) - \boldsymbol{s}_0(k)| \leq \delta,\ k = 1, \ldots, N$, can be equivalently written as $\Re[\boldsymbol{s}^*(k)\boldsymbol{s}_0(k)] \geq 1 - \delta^2/2$ for $k = 1, \ldots, N$, which in turn amounts to enforcing

$$s(k) \in \{e^{j2\pi\frac{\beta_k}{M}}, e^{j2\pi\frac{\beta_k+1}{M}}, \ldots, e^{j2\pi\frac{\beta_k+\delta_d-1}{M}}\},$$

where

$$\beta_k = [M \arg(s_0(k))/(2\pi)] - \lfloor [M \arccos(1 - \delta^2/2)]/(2\pi) \rfloor$$

depends on $s_0(k)$ and δ,

$$\delta_d = \begin{cases} 1 + 2\lfloor \frac{M \arccos(1-\delta^2/2)}{2\pi} \rfloor & \delta \in [0, 2) \\ M & \delta = 2 \end{cases}$$

depends only on δ [24].

Thus, problem (6.20) is equivalent to:

$$\mathcal{P}_2' \begin{cases} \max\limits_{\boldsymbol{s}} & \frac{\left| \boldsymbol{s}^T \left(\boldsymbol{w}^{(n-1)^*} \odot \boldsymbol{p}(\nu_{d_T}) \right) \right|^2}{\boldsymbol{s}^T \boldsymbol{\Theta}_{\boldsymbol{C}} \left(\boldsymbol{w}^{(n-1)} \right) \boldsymbol{s}^* + \sigma_n^2 \|\boldsymbol{w}^{(n-1)}\|^2} \\ \text{s.t.} & \arg(s(k)) \in \frac{2\pi}{M} \left[\beta_k, \beta_k + 1, \ldots, \beta_k + \delta_d - 1 \right], \\ & |s(k)| = 1,\ k = 1, \ldots, N. \end{cases} . \tag{6.21}$$

Let us observe that problem $\mathcal{P}_2'$, even in the simpler formulation corresponding to $\epsilon = 2$, is generally NP-hard, consequently one cannot find polynomial time algorithms for computing its optimal solutions. As a consequence, in the following, we focus on approximation techniques and propose a relaxation and randomization algorithm which provides a randomized feasible solution of (6.21). Thus, using $\boldsymbol{S}$ and $\boldsymbol{M}$ defined respectively in (6.14) and (6.15), re-

sorting to the same relaxation procedure as in (6.16)-(6.19), and following the same steps as in [24, pp. 13-14], a randomized feasible solution $\boldsymbol{s}^{(\star)}$ to problem $\mathcal{P}_{\boldsymbol{S}}^{d\,(n)}$ can be computed using algorithm **Algorithm 9**.

Algorithm 9 : Radar Quantized Phase Code Optimization

Input: $\boldsymbol{M}$, $\boldsymbol{S}$, H, $\{\beta_i\}$, M, δ_d.

Output: A randomized approximate solution $\boldsymbol{s}^{(\star)}$ of $\mathcal{P}_{\boldsymbol{S}}^{d\,(n)}$;

1: Let $(\boldsymbol{X}^\star, u^\star)$ be an optimal solution to problem (6.19).

2: Denote by $\hat{\boldsymbol{X}} = \boldsymbol{X}^\star / u^\star$.

3: Generate a random vector $(\boldsymbol{\xi})_h \in \mathbb{C}^N$, $h = 1, \ldots, H$, from the complex normal distribution $\mathcal{N}_{\mathbb{C}}(0, \boldsymbol{W})$ where $\boldsymbol{W} = \hat{\boldsymbol{X}} \odot \boldsymbol{y}_d \boldsymbol{y}_d^\dagger$, with $\boldsymbol{y}_d = [e^{-j\frac{2\pi}{M}\beta_1}, \ldots, e^{-j\frac{2\pi}{M}\beta_N}]^T$.

4: Let $(s(k))_h = y_d^*(k)\mu((\xi_k)_h)$, $k = 1, \ldots, N$, $h = 1, \ldots, H$, where

$$\mu(x) = \begin{cases} 1, & \text{if } \arg(x) \in [0, 2\pi\frac{1}{\delta_d}); \\ e^{j2\pi\frac{1}{M}}, & \text{if } \arg(x) \in [2\pi\frac{1}{\delta_d}, 2\pi\frac{2}{\delta_d}); \\ \vdots & \\ e^{j2\pi\frac{\delta_d - 1}{M}}, & \text{if } \arg(x) \in [2\pi\frac{\delta_d - 1}{\delta_d}, 2\pi). \end{cases}$$

5: Compute

$$t_h = \frac{\mathrm{tr}\left(\boldsymbol{s}_h^\dagger \boldsymbol{S} \boldsymbol{s}_h\right)}{\mathrm{tr}\left(\boldsymbol{s}_h^\dagger \boldsymbol{M} \boldsymbol{s}_h\right)}, \quad h = 1 \ldots, H.$$

6: Pick the maximal value over $\{t_1, \ldots, t_H\}$, say t_1, and output $\boldsymbol{s}^{(\star)} = \boldsymbol{s}_1$.

As for **Algorithm 8**, the H randomizations involved into steps 3-6 are meant to improve the approximation quality; moreover, the computational complexity is mostly related to the solution of the SDP problem ($O(N^{3.5})$ flops). Finally,

also with reference to the finite alphabet case, a modest number of randomizations is sufficient to ensure satisfactory performances.

6.3.3 Transmit-Receive System Design: Optimization Procedure

In this subsection, the proposed sequential optimization procedures for the receive filter and the radar code are summarized and schematized respectively as **Algorithm 10** for the continuous alphabet case and **Algorithm 11** for the finite alphabet case. To trigger the recursion, an initial radar code $\boldsymbol{s}^{(0)}$, from which we obtain the optimal receive filter $\boldsymbol{w}^{(0)}$, is required; a natural choice is obviously $\boldsymbol{s}^{(0)} = \boldsymbol{s}_0$.

The computational complexity, connected with the implementation of both **Algorithm 10** and **Algorithm 11**, depends on the number of iterations $\overline{N}$ as well as on and the complexity involved in each iteration. Precisely, the overall complexity is linear with respect to $\overline{N}$, while each iteration includes the computation of the inverse of $\boldsymbol{\Sigma_c}\left(\boldsymbol{s}^{(n)}\right)$ and the complexity effort of **Algorithm 8** and **Algorithm 9**, respectively. The former is in the order of $O(N^3)$ [69]. The latter, for a modest number of randomizations, is connected with the SDP

Algorithm 10 : Transmit-Receive System Design

Input: $\left\{\sigma_{(r,i)}\right\}, \left\{\bar{\nu}_{d_{(r,i)}}, \epsilon_{(r,i)}\right\}, \sigma_n^2, \boldsymbol{s}_0, \nu_{d_T}, H, \delta, \zeta$.

Output: A solution $(\boldsymbol{s}^\star, \boldsymbol{w}^\star)$ of $\mathcal{P}^c$.

1: Set $n = 0$, $\boldsymbol{s}^{(n)} = \boldsymbol{s}_0$,

$$\boldsymbol{w}^{(n)} := \frac{\left(\boldsymbol{\Sigma_C}\left(\boldsymbol{s}_0\right) + \sigma_n^2 \boldsymbol{I}\right)^{-1}\left(\boldsymbol{s}_0 \odot \boldsymbol{p}(\nu_{d_T})\right)}{\left\|\left(\boldsymbol{\Sigma_C}\left(\boldsymbol{s}_0\right) + \sigma_n^2 \boldsymbol{I}\right)^{-1/2}\left(\boldsymbol{s}_0 \odot \boldsymbol{p}(\nu_{d_T})\right)\right\|^2},$$

and $\text{SINR}^{(n)} = \text{SINR}$.

2: **do**

3: $n := n + 1$;

4: Construct the matrices

$\boldsymbol{S} = \left(\boldsymbol{w}^{(n-1)} \odot \boldsymbol{p}(\nu_{d_T})^*\right)\left(\boldsymbol{w}^{(n-1)} \odot \boldsymbol{p}(\nu_{d_T})^*\right)^\dagger$ and $\boldsymbol{M} = \boldsymbol{\Theta_C}\left(\boldsymbol{w}^{(n-1)}\right)^* + \sigma_n^2 \|\boldsymbol{w}^{(n-1)}\|^2 \boldsymbol{I}$, and the parameters $\{\gamma_i\}$, δ_c.

5: Find a good quality solution $\boldsymbol{s}^{(\star)}$ to problem $\mathcal{P}_{\boldsymbol{s}}^{c\,(n)}$, through the use of **Algorithm 8**.

6: Set

$$\boldsymbol{s}^{(n)} = \arg\max \left\{ \frac{|\alpha_T|^2 \left|\boldsymbol{w}^{(n-1)^\dagger}\left(\boldsymbol{s}^{(n-1)} \odot \boldsymbol{p}(\nu_{d_T})\right)\right|^2}{\boldsymbol{w}^{(n-1)^\dagger}\boldsymbol{\Sigma_C}\left(\boldsymbol{s}^{(n-1)}\right)\boldsymbol{w}^{(n-1)} + \sigma_n^2 \|\boldsymbol{w}^{(n-1)}\|^2}, \frac{|\alpha_T|^2 \left|\boldsymbol{w}^{(n-1)^\dagger}\left(\boldsymbol{s}^{(\star)} \odot \boldsymbol{p}(\nu_{d_T})\right)\right|^2}{\boldsymbol{w}^{(n-1)^\dagger}\boldsymbol{\Sigma_C}\left(\boldsymbol{s}^{(\star)}\right)\boldsymbol{w}^{(n-1)} + \sigma_n^2 \|\boldsymbol{w}^{(n-1)}\|^2} \right\}.$$

7: Construct the matrix $\boldsymbol{\Sigma_C}\left(\boldsymbol{s}^{(n)}\right)$.

8: Solve problem $\mathcal{P}_{\boldsymbol{w}}{}^{(n)}$ finding an optimal receive filter

$$\boldsymbol{w}^{(n)} := \frac{\left(\boldsymbol{\Sigma_C}\left(\boldsymbol{s}^{(n)}\right) + \sigma_n^2 \boldsymbol{I}\right)^{-1}\left(\boldsymbol{s}^{(n)} \odot \boldsymbol{p}(\nu_{d_T})\right)}{\left\|\left(\boldsymbol{\Sigma_C}\left(\boldsymbol{s}^{(n)}\right) + \sigma_n^2 \boldsymbol{I}\right)^{-1/2}\left(\boldsymbol{s}^{(n)} \odot \boldsymbol{p}(\nu_{d_T})\right)\right\|^2},$$

and the value of the SINR for the pair $\left(\boldsymbol{s}^{(n)}, \boldsymbol{w}^{(n)}\right)$.

9: Let $\text{SINR}^{(n)} = \text{SINR}$.

10: **until** $|\text{SINR}^{(n)} - \text{SINR}^{(n-1)}| \leq \zeta$.

11: Output $\boldsymbol{s}^\star = \boldsymbol{s}^{(n)}$ and $\boldsymbol{w}^\star = \boldsymbol{w}^{(n)}$.

Algorithm 11 : Transmit-Receive System Design

Input: $\left\{\sigma_{(r,i)}\right\}$,$\left\{\bar{\nu}_{d_{(r,i)}}, \epsilon_{(r,i)}\right\}$,$\sigma_n^2$,$\boldsymbol{s}_0$,$\nu_{d_T}$,$H$,$\delta$,$\zeta$,$M$.

Output: A solution $(\boldsymbol{s}^\star, \boldsymbol{w}^\star)$ of $\mathcal{P}^d$.

1: Set $n = 0$, $\boldsymbol{s}^{(n)} = \boldsymbol{s}_0$,

$$\boldsymbol{w}^{(n)} := \frac{\left(\boldsymbol{\Sigma_C}\left(\boldsymbol{s}_0\right) + \sigma_n^2\boldsymbol{I}\right)^{-1}\left(\boldsymbol{s}_0 \odot \boldsymbol{p}(\nu_{d_T})\right)}{\left\|\left(\boldsymbol{\Sigma_C}\left(\boldsymbol{s}_0\right) + \sigma_n^2\boldsymbol{I}\right)^{-1/2}\left(\boldsymbol{s}_0 \odot \boldsymbol{p}(\nu_{d_T})\right)\right\|^2},$$

and $\text{SINR}^{(n)} = \text{SINR}$.

2: **do**

3: $n := n + 1$;

4: Construct the matrices

$\boldsymbol{S} = \left(\boldsymbol{w}^{(n-1)} \odot \boldsymbol{p}(\nu_{d_T})^*\right)\left(\boldsymbol{w}^{(n-1)} \odot \boldsymbol{p}(\nu_{d_T})^*\right)^\dagger$ and $\boldsymbol{M} = \boldsymbol{\Theta_C}\left(\boldsymbol{w}^{(n-1)}\right)^* + \sigma_n^2\|\boldsymbol{w}^{(n-1)}\|^2\boldsymbol{I}$,

and the parameters $\{\beta_i\}$, δ_d.

5: Find a good quality solution $\boldsymbol{s}^{(\star)}$ of problem $\mathcal{P}_{\boldsymbol{s}}^{d\,(n)}$, through the use of **Algorithm 9**.

6: Set

$$\boldsymbol{s}^{(n)} = \arg\max\left\{\frac{|\alpha_T|^2\left|\boldsymbol{w}^{(n-1)^\dagger}\left(\boldsymbol{s}^{(n-1)} \odot \boldsymbol{p}(\nu_{d_T})\right)\right|^2}{\boldsymbol{w}^{(n-1)^\dagger}\boldsymbol{\Sigma_C}\left(\boldsymbol{s}^{(n-1)}\right)\boldsymbol{w}^{(n-1)} + \sigma_n^2\|\boldsymbol{w}^{(n-1)}\|^2}, \frac{|\alpha_T|^2\left|\boldsymbol{w}^{(n-1)^\dagger}\left(\boldsymbol{s}^{(\star)} \odot \boldsymbol{p}(\nu_{d_T})\right)\right|^2}{\boldsymbol{w}^{(n-1)^\dagger}\boldsymbol{\Sigma_C}\left(\boldsymbol{s}^{(\star)}\right)\boldsymbol{w}^{(n-1)} + \sigma_n^2\|\boldsymbol{w}^{(n-1)}\|^2}\right\}.$$

7: Construct the matrix $\boldsymbol{\Sigma_C}\left(\boldsymbol{s}^{(n)}\right)$.

8: Solve problem $\mathcal{P}_{\boldsymbol{w}}{}^{(n)}$ finding an optimal receive filter

$$\boldsymbol{w}^{(n)} := \frac{\left(\boldsymbol{\Sigma_C}\left(\boldsymbol{s}^{(n)}\right) + \sigma_n^2\boldsymbol{I}\right)^{-1}\left(\boldsymbol{s}^{(n)} \odot \boldsymbol{p}(\nu_{d_T})\right)}{\left\|\left(\boldsymbol{\Sigma_C}\left(\boldsymbol{s}^{(n)}\right) + \sigma_n^2\boldsymbol{I}\right)^{-1/2}\left(\boldsymbol{s}^{(n)} \odot \boldsymbol{p}(\nu_{d_T})\right)\right\|^2},$$

and the value of the SINR for the pair $\left(\boldsymbol{s}^{(n)}, \boldsymbol{w}^{(n)}\right)$.

9: Let $\text{SINR}^{(n)} = \text{SINR}$.

10: **until** $|\text{SINR}^{(n)} - \text{SINR}^{(n-1)}| \leq \zeta$.

11: Output $\boldsymbol{s}^\star = \boldsymbol{s}^{(n)}$ and $\boldsymbol{w}^\star = \boldsymbol{w}^{(n)}$.

solution, i.e. $O(N^{3.5})$ [99].

6.4 Performance Analysis

In this section, we present the performance analysis of the proposed algorithm for the joint optimization of the radar code and the receive filter. We consider an L-band radar whose operating frequency is $f_0 = 1.4$ GHz, and that exploits a broadside array with $N_a = 21$ elements pointing in the range-azimuth bin of interest $(0, 0)$. Specifically, we consider a uniformly weighted linear array with uniform spacing equal to $d = \lambda/2$. Consequently, the radiation pattern is given by:

$$G(\theta) = \begin{cases} \dfrac{1}{N_a} \dfrac{\sin\left(N_a \dfrac{\pi}{2}\cos(\theta)\right)}{\sin\left(\dfrac{\pi}{2}\cos(\theta)\right)} & \text{if} \quad 0 \leq \theta \leq \pi \\ 10^{-3} & \text{if} \quad \pi \leq \theta \leq 2\pi \end{cases} .$$

We focus on a scenario with a homogeneous range-azimuth clutter where the number of range rings that interfere with the range-azimuth bin of interest $(0, 0)$ is $N_c = 2$ and the number of azimuth cells in each ring is $L = 100$. Moreover, we set the pulse train length to $N = 20$ and select, as similarity code $\boldsymbol{s}_0$,

the N-dimensional generalized Barker code and its M-quantized version[4] for **Algorithm 10** and **Algorithm 11**, respectively. With reference to the continuous phase case, we remark that the choice for this similarity code is mainly due to its autocorrelation properties, namely its minimal peak-to-sidelobe ratio excluding the the outermost sidelobe. The description of generalized Barker codes can be found in [72] and [73], also for other values of N. The exit condition that we implement to stop the procedure assumes $\zeta = 10^{-5}$, namely:

$$|\mathrm{SINR}^{(n)} - \mathrm{SINR}^{(n-1)}| \leq 10^{-5}.$$

The randomizations for both **Algorithms 8** and **9** have been set to $H = 100$.

As to the parameters of the uniform clutter, we fix $\frac{\sigma_0}{\sigma_n^2} K_r = \mathrm{CNR}\, K_r = 30$ dB, a mean Doppler frequency $\bar{\nu}_d = 0$, and Doppler uncertainty $\frac{\epsilon}{2} = 0.35$ for each range-azimuth bin. Additionally, we suppose the presence of a target with Signal to Noise Ratio (SNR) $\frac{|\alpha_T|^2}{\sigma_n^2} = \mathrm{SNR} = 10$ dB and normalized Doppler

[4]Specifically, given the code $\boldsymbol{s}$, we construct its M-quantized version $\boldsymbol{s}^q$ as $s^q(k) = \bar{\mu}(s(k))$, $k = 1, \ldots, N$, where the non-linearity $\bar{\mu}(x)$ is defined by

$$\bar{\mu}(x) = \begin{cases} 1, & \text{if } \arg(x) \in [0, 2\pi\frac{1}{M}) \\ e^{j2\pi\frac{1}{M}}, & \text{if } \arg(x) \in [2\pi\frac{1}{M}, 2\pi\frac{2}{M}) \\ \vdots & \\ e^{j2\pi\frac{M-1}{M}}, & \text{if } \arg(x) \in [2\pi\frac{M-1}{M}, 2\pi) \end{cases}.$$

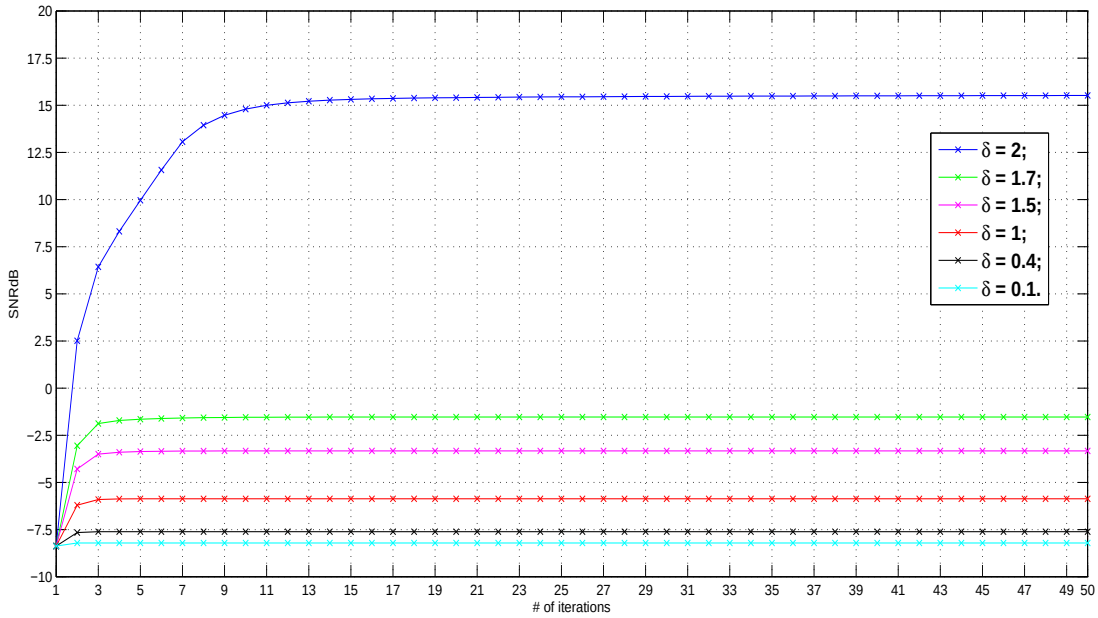

Figure 6.1: Algorithm 10 - SINR behavior for $\delta = [0.1, 0.4, 1, 1.5, 1.7, 2]$.

frequency $\nu_{d_T} = -0.4$.

The analysis is conducted in terms of the attainable SINR, in correspondence of the devised transmit code and receive filter, as well as the shape of the related auto- and cross-ambiguity function[5].

In **Figure 6.1**, the SINR behavior, averaged over 100 independent trials of **Algorithm 10**, is plotted versus the number of iterations, for different values of the similarity parameter δ. As expected, increasing δ, the optimal value of the SINR improves since the feasible set of the optimization problem becomes larger and larger. Actually, performance gains up to 22 dB, with respect to

[5]We exploit the MATLAB© toolbox SeDuMi [25] for solving the SDP relaxation, and the MATLAB© toolbox of [74] for plotting the ambiguity functions of the coded pulse trains.

step zero of our procedure, corresponding to the traditional adaptation on receive side only, can be observed for $\delta = 2$. Of course, this is just a potential value and in real conditions smaller gains could be experienced due to some inaccuracies in the a-priori information. Let us also observe that the number of iterations, required to achieve convergence, increases as well.

In **Figures 6.2**, the ambiguity function[6] of a synthesized code $\boldsymbol{s}^{\star}$, together with that of the reference code $\boldsymbol{s}_0$, is plotted for two different sizes of the similarity region. Indeed, we have an opposite behavior with respect to **Figure 6.1**. Precisely, increasing δ, the set of feasible points becomes larger and larger, and better and better SINR performances are swapped for worse and worse ambiguity behaviors.

In **Figures 6.3**, we analyze the frequency behavior of the radar code and the receive filter, corresponding to $\delta = 2$, for different values of the iteration number ($n = [0, 5, 20, 50]$). Precisely, we plot the contour map of the cross-ambiguity function,

$$\mathrm{g}^{(n)}(m, \nu_d) = \left| \boldsymbol{w}^{(n)^{\dagger}} \left(\boldsymbol{J}_m \left(\boldsymbol{s}^{(n)} \odot \boldsymbol{p}(\nu_d) \right) \right) \right|^2 \tag{6.22}$$

[6]We consider a coherent pulse train with ideal rectangular pulses of width T_p and pulse repetition time T_r.

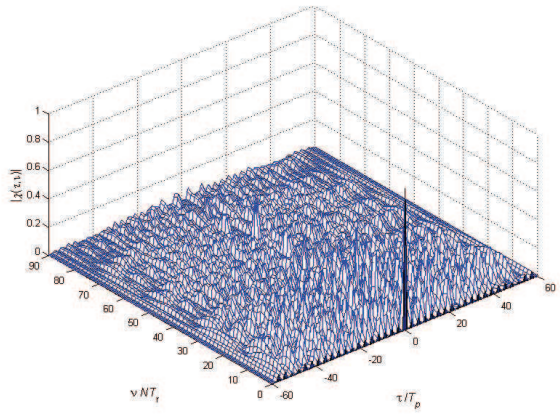

(a) Ambiguity Function modulus of the radar code s_0.

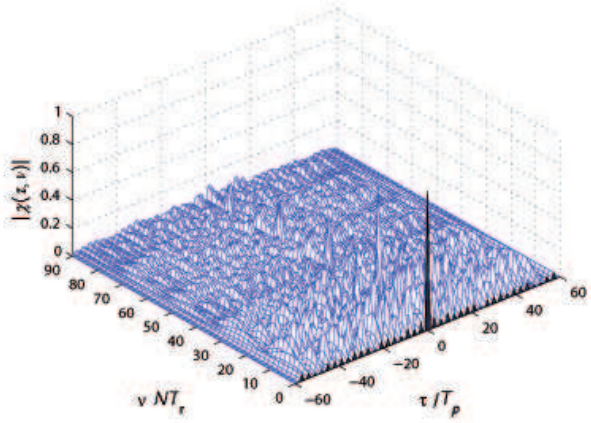

(b) Algorithm 10- Ambiguity Function modulus of the radar code $s^\star$ for δ=0.1

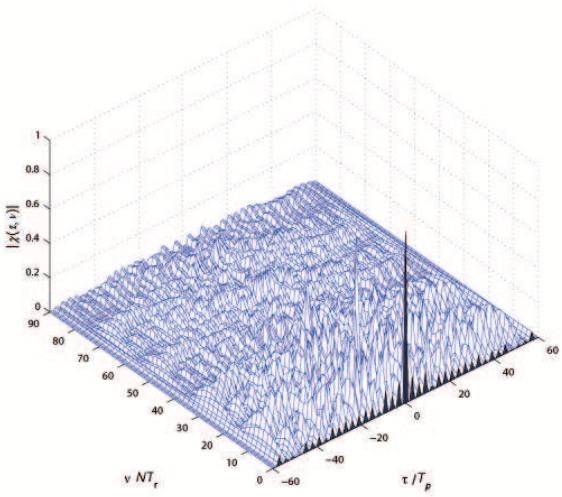

(c) Algorithm 10- Ambiguity Function modulus of the radar code $s^\star$ for δ=1

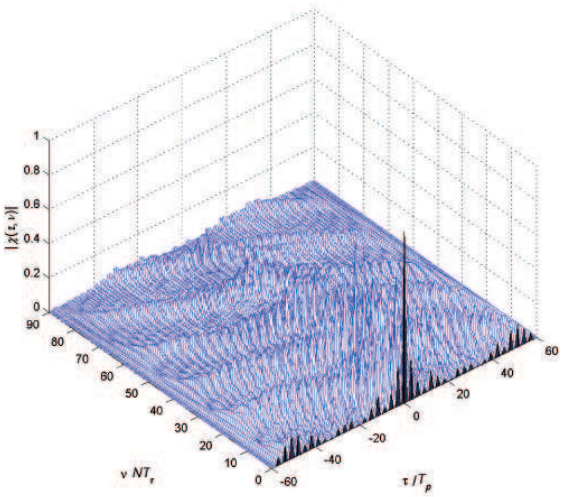

(d) Algorithm 10- Ambiguity Function modulus of the radar code $s^\star$ for δ=2

Figure 6.2: Ambiguity Function modulus, assuming $T_r = 3T_p$.

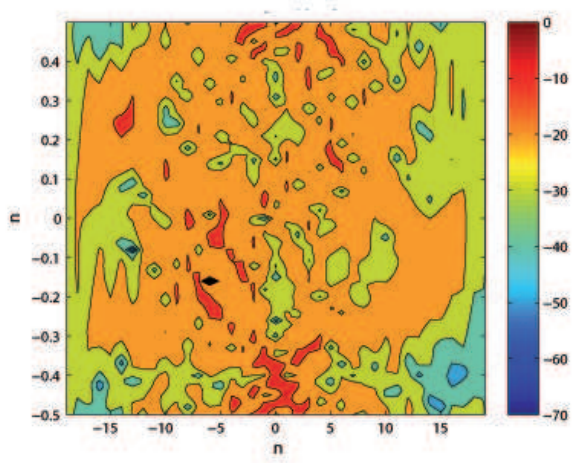

(a) Algorithm 10 - Cross-Ambiguity Function, in dB, of the radar code and receive filter $\left(\boldsymbol{s}^{(0)}, \boldsymbol{w}^{(0)}\right)$.

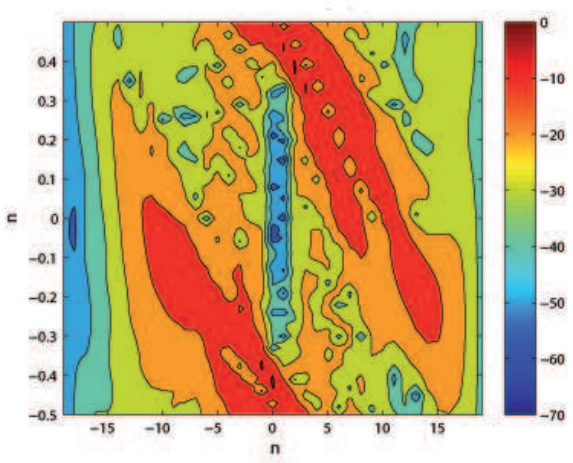

(b) Algorithm 10 - Cross-Ambiguity Function, in dB, of the radar code and receive filter $\left(\boldsymbol{s}^{(5)}, \boldsymbol{w}^{(5)}\right)$.

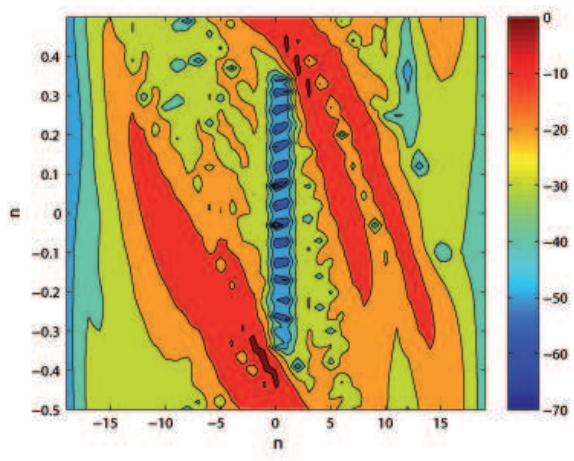

(c) Algorithm 10 - Cross-Ambiguity Function, in dB, of the radar code and receive filter $\left(\boldsymbol{s}^{(19)}, \boldsymbol{w}^{(19)}\right)$.

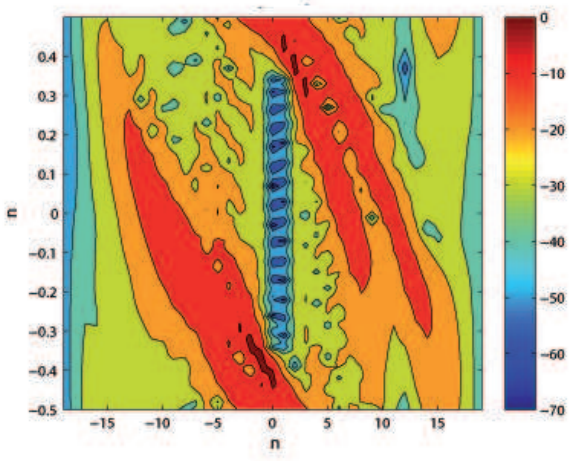

(d) Algorithm 10 - Cross-Ambiguity Function, in dB, of the radar code and receive filter $\left(\boldsymbol{s}^{(50)}, \boldsymbol{w}^{(50)}\right)$.

Figure 6.3: Algorithm 10 - Cross-Ambiguity Function, in dB.

where m is the delay-lag and ν_d is the Doppler frequency of the incoming signal. As forced by the design procedure, the cross-ambiguity function is equal to one at $(m, \nu_d) = (0, -0.4)$, which is the range-Doppler position of the nominal target. Moreover, lower and lower values of $\mathrm{g}^{(n)}(m, \nu_d)$ can be observed in the strip $0 \leq m \leq 2$ $-0,35 \leq m \leq 0.35$ as the iteration step n grows up. Interestingly, this performance trend reflects the capability of the proposed joint transmit-receive optimization procedure to sequentially refine the shape of the cross-ambiguity function in order to get better and better clutter suppression levels.

In **Figure 6.4**, the SINR behavior, averaged over 100 independent trials of **Algorithm 11**, is plotted versus the number of iterations, for different values of the similarity parameter δ, and for $M = 16$. The same considerations as for the analysis conducted in **Figure 6.1** hold true; indeed, increasing δ, we experience better and better SINR values, due to the enlargement of the feasible set. Performance gains up to approximatively 12 dB, with respect to step zero of our procedure can be observed for $\delta = 2$.

In **Figures 6.5**, the ambiguity function of a synthesized code $\boldsymbol{s}^{\star}$, together with that of the reference quantized code $\boldsymbol{s}_0^q$, is plotted for three different sizes of the similarity region, assuming $M = 16$. Again, we experience an opposite

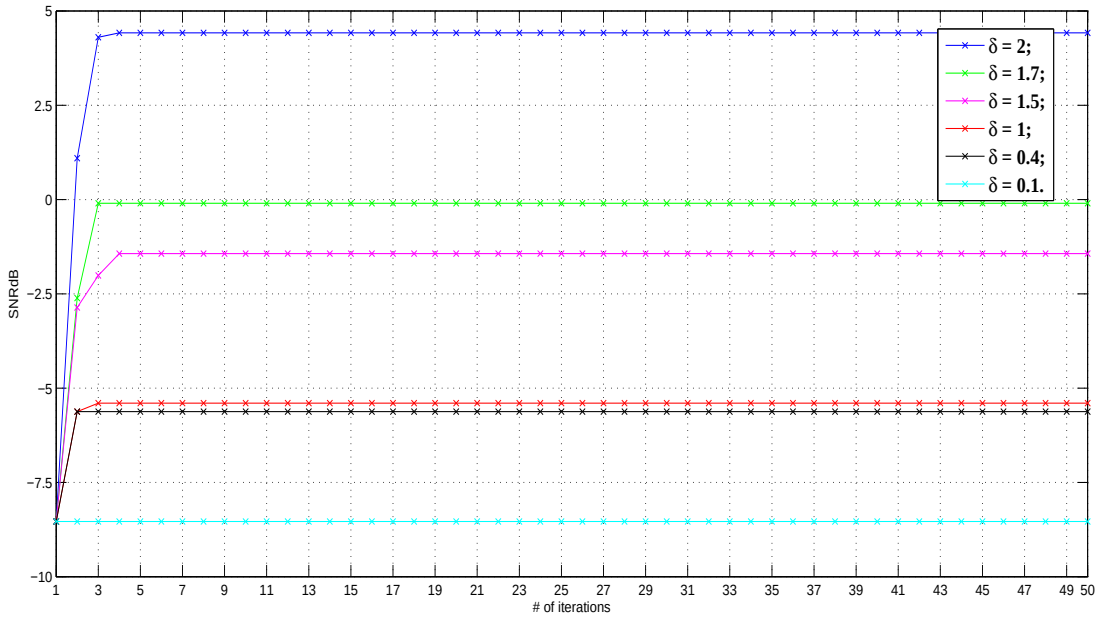

Figure 6.4: Algorithm 11 - SINR behavior for δ=$[0.1, 0.4, 1, 1.5, 1.7, 2]$, M =16.

trend with respect to **Figure 6.4**, which reflects how δ rules the trade-off between SINR performance and ambiguity behavior. Precisely, increasing δ, the set of feasible points becomes larger and larger, and better and better SINR performances are swapped for worse and worse ambiguity shapes.

In **Figure 6.6**, we analyze the impact of the number of quantization level on the devised code for a fixed similarity parameter $\delta = 2$. As expected, the achieved average SINR increases as the number of levels involved into the quantization procedure increases. Indeed, the greater the cardinality of the alphabet, the higher the degrees of freedom available in the choice of the radar code.

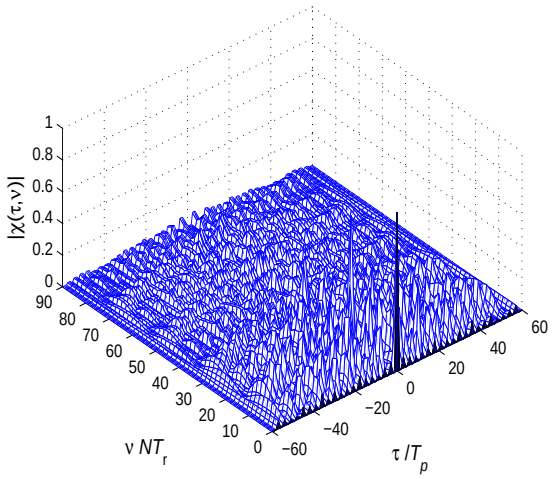

(a) Ambiguity Function modulus of the radar code s_0^q.

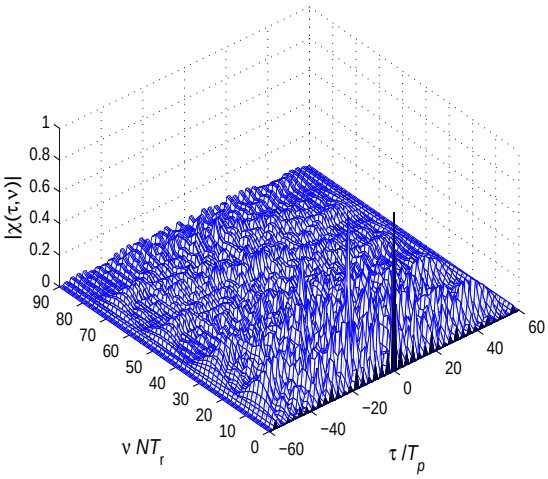

(b) Algorithm 11 - Ambiguity Function modulus of the radar code $s^\star$ for δ=0.4.

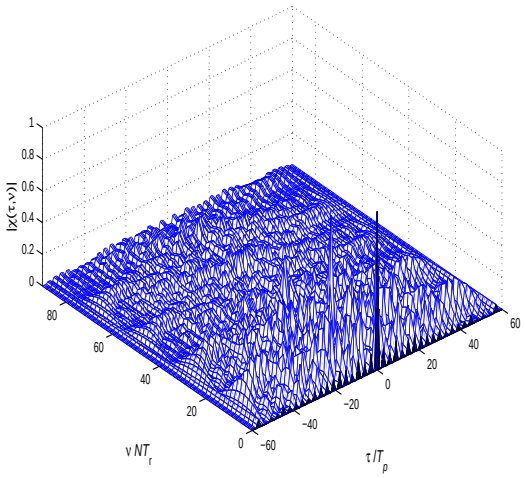

(c) Algorithm 11 - Ambiguity Function modulus of the radar code $s^\star$ for δ=1.

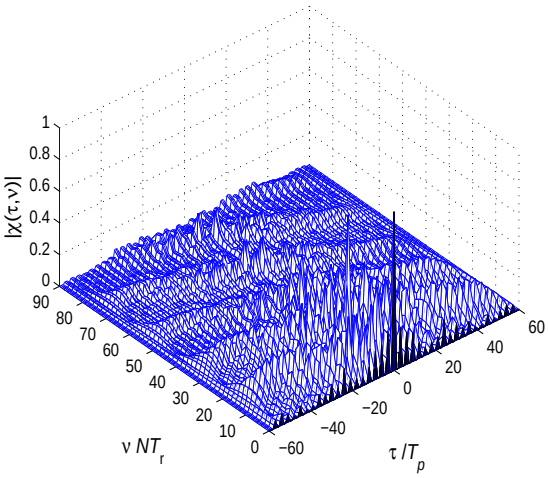

(d) Algorithm 11 - Ambiguity Function modulus of the radar code $s^\star$ for δ=2.

Figure 6.5: Ambiguity Function modulus of the radar code, assuming $T_r = 3T_p$ and $M = 16$.

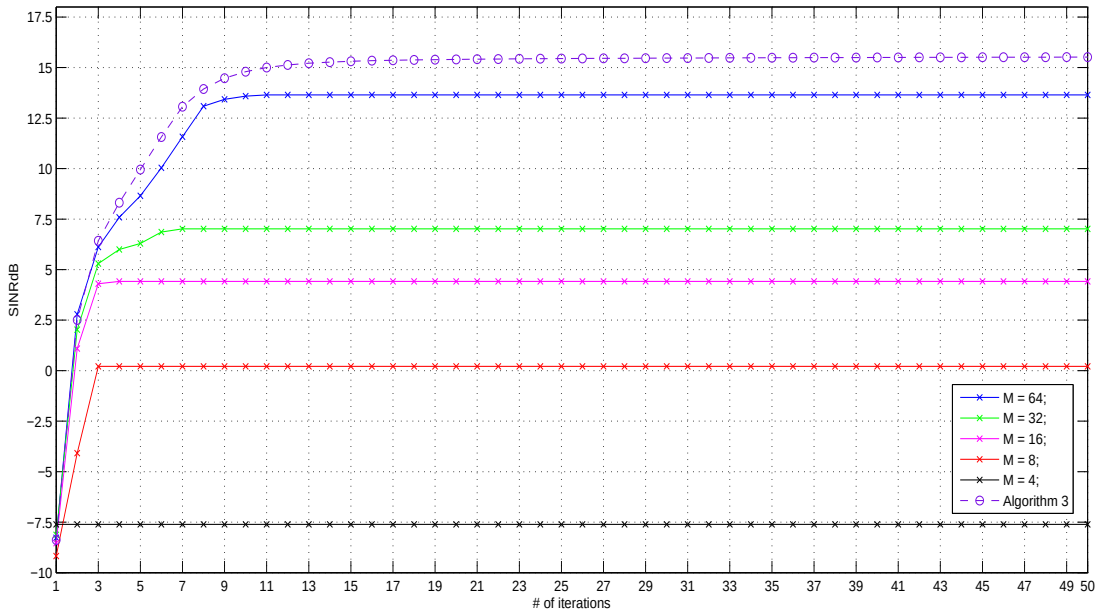

Figure 6.6: Algorithm 11 - SINR$^{(n)}$ behavior for $\delta = 2$, $M = [4, 8, 16, 32, 64]$; Algorithm 10 (o-marked violet dashed line).

6.5 Conclusions

In this chapter, we have considered the problem of cognitive constant envelope transmit signal and receive filter joint optimization in a signal-dependent clutter environment. We have devised iterative algorithms trying to optimize the SINR while accounting for a similarity constraint on the transmitted sequence. At each step, the proposed procedures require the solution of both convex and NP-hard problems. In order to find a good quality solution to the latter, we have resorted to relaxation and randomization techniques. At the analysis stage, we have assessed the performance of the proposed algorithms

in terms of average SINR (versus the number of iterations) and ambiguity function of the resulting phase code and cross-ambiguity function of the transmit signal and receive filter pair. Furthermore, with reference to the finite alphabet case, we analyzed the impact of the quantization level on the system performance. The results have highlighted that, in the presence of a perfect a-priori knowledge, with a modest number of trials, significant SINR gains (up to 22 dB or 12 dB, respectively) can be obtained jointly optimizing the transmitter and receiver. Possible future research tracks might concern the study of further constraints on the receive filter, so as to keep under control other key parameters such as the Integrated-to-Sidelobe Level or the Peak-to-Sidelobe Level.

Bibliography

[1] C. J. Baker and A. L. Hume, "Netted radar sensing", *IEEE Aerospace and Electronic System Magazine*, Vol. 18, no. 2, pp. 3 - 6, Febr. 2003.

[2] E. Fishler, A. Haimovich, R. Blum, L. Cimini, D. Chizhik, and R. Valenzuela, "Spatial diversity in radars: models and detection performance", *IEEE Transactions on Signal Processing*, Vol. 54, no. 3, pp. 823 - 838, Mar. 2006.

[3] J. Li and P. Stoica, *MIMO radar signal processing*, John Wiley & Sons, 2008.

[4] A. De Maio, G. A. Fabrizio, A. Farina, W. L. Melvin, and L. Timmoneri, "Challenging issues in multichannel radar array processing", *Proceedings of the IEEE International Radar Conference 2007*, Edinburgh (UK), pp. 856 - 862, Apr. 2007.

[5] L. Landi and R. Adve, "Time-orthogonal-waveform-space-time adaptive processing for distributed aperture radars", Principles of Waveform Diversity and Design, *SciTech Publishing*, Sect. B - part III, ch. 19, 2011.

[6] R. S. Adve, R. A. Schneible, G. Genello, and P. Antonik, "Waveform-space-time adaptive processing for distributed aperture radars", *Proceedings of the IEEE International Radar Conference 2005*, Arlington (US), pp. 93 - 97, May 2005.

[7] K. H. Berthke, B. Röde, M. Schneider, and A. Schroth, "A novel non-cooperative near-range radar network for traffic guidance and control on

airport surfaces", *IEEE Transactions on Control Systems Technology*, Vol. 1, no. 3, pp. 168 - 178, Sept. 1993.

[8] H. Huang and D. Lang, "The comparison of attitude and antenna pointing design strategies of non-cooperative spaceborne bistatic radar", *Proceedings of the IEEE International Radar Conference 2005*, Arlington (US), pp. 568 - 571, May 2005.

[9] H. D. Ly and Q. Liang, "Spatial-temporal-frequency diversity in radar sensor networks", *Proceedings of the IEEE Military Communications Conference 2006*, Washington (US), pp. 1 - 7, Oct. 2006.

[10] N. Levanon, "Multifrequency complementary phase-coded radar signal", *Proceeding of IEE Radar, Sonar and Navigation*, Vol. 147, no. 6, pp. 276 - 284, Dec. 2000.

[11] J. Li, L. Xu, P. Stoica, K.W. Forsythe, and D.W. Bliss, "Range compression and waveform optimization for MIMO radar: a Cramér–Rao bound based study", *IEEE Transactions on Signal Processing*, Vol. 56, no. 1, pp. 218 - 232, Jan. 2008.

[12] A. De Maio and M. Lops, "Design principles of MIMO radar detectors", *IEEE Transactions on Aerospace and Electronic System*, Vol. 43, no. 3, pp. 886 - 898, July 2007.

[13] N. Subotic, K. Cooper, and P. Zulch, "Conditional and constrained joint optimization of radar waveforms", *Proceedings of the International Waveform Diversity and Design Conference 2007*, Pisa (IT), pp. 387, June 2007.

[14] M. Greco, F. Gini, A. Farina, and J. B. Billingsley, "Analysis of clutter cancellation in the presence of measured L-band radar ground clutter data," *2000 IEEE Radar Conference*, pp. 422 - 427, Washington, D.C., 7 - 12 May 2000.

[15] A. d'Aspermont and S. Boyd, "Relaxations and Randomized Methods for Nonconvex QCQPs", *EE392o Class Notes, Stanford University*, Autumn 2003.

[16] Z.-Q. Luo, N. D. Sidiropoulos, P. Tseng, and S. Zhang, "Approximation Bounds for Quadratic Optimization with Homogeneous Quadratic Constraints", *SIAM Journal of Optimization*, Vol. 18, no. 1, pp.1 - 28, February 2007.

[17] R. A. Horn and C. R. Johnson, *Matrix Analysis*, Cambridge University Press, 1985.

[18] N. Levanon and E. Mozeson, *Radar signals*, John Wiley & Sons, 2004.

[19] J. S. Goldstein, I. S. Reed, and P. A. Zulch, "Multistage Partially Adaptive STAP CFAR Detection Algorithm", *IEEE Transactions on Aerospace and Electronic Systems*, Vol. 35, no. 2, pp. 645 - 661, April 1999.

[20] C. Ballantine, "On the Hadamard Product", *Mathematische Zeitschrift*, Vol. 105, no. 5, pp. 365 - 366, October 1968.

[21] S. Zhang, "Conic Optimization and SDP", *SEG5120 Class Notes, Chinese University of Hong Kong*, 2007.

[22] S. Boyd and L. Vandenberghe, *Convex Optimization*, Cambridge University Press, 2003.

[23] W.-K. Ma, T. N. Davidson, K. M. Wong, Z.-Q. Luo, and P.-C. Ching, "Quasi-Maximum-Likelihood Multiuser Detection Using Semi-Definite Relaxation With Application to Synchronous CDMA", *IEEE Transactions on Signal Processing*, Vol. 50, no. 4, pp. 912 - 922, April 2002.

[24] A. De Maio, S. De Nicola, Y. Huang, Z. Q. Luo, and S. Zhang, "Design of phase Codes for radar performance optimization with a similarity constraint," *IEEE Transactions on Signal Processing*, Vol. 57, no. 2, pp. 610 - 621, February 2009.

[25] J. F. Sturm, "Using SeDuMi 1.02, a MATLAB toolbox for optimization over symmetric cones," *Optimization Methods and Software*, Vol. 11 - 12, pp. 625 - 653, August 1999.

[26] D. Huffman, "The Generation of Impulse-Equivalent Pulse Trains", *IRE Transactions on Information Theory*, Vol. 8, no. 5, pp. 10 - 16, September 1962.

[27] R. Gold, "Optimal Binary Sequences for Spread Spectrum Multiplexing", *IEEE Transactions on Information Theory*, Vol. 13, no. 4, pp. 154-156, October 1967.

[28] D. V. Sarwate and M. B. Pursley, "Cross-correlation Properties of Pseudorandom and Related Sequences", *IEEE Proceedings*, Vol. 68, no. 5, pp. 593 - 619, May 1980.

[29] A. Nemirovski, *Lectures on modern convex optimization*, http://www.isye.gatech.edu/faculty-staff/profile.php?entry=an63.

[30] J. Li, J. R. Guerci, and L. Xu, "Signal waveform's optimal-under-restriction design for active sensing," *IEEE Signal Processing Letters*, Vol. 13, no. 9, pp. 565 - 568, September 2006.

[31] A. De Maio, S. De Nicola, Y. Huang, S. Zhang, and A. Farina, "Code design to optimize radar detection performance under accuracy and similarity constraints," *IEEE Transactions on signal processing*, Vol. 56, no. 11, pp. 5618 - 5629, November 2008.

[32] A. Farina, "Waveform Diversity: Past, Present, and Future", *Third International Waveform Diversity & Design Conference*, Plenary Talk, Pisa, June 2007.

[33] A. Nehorai, F. Gini, M. S. Greco, A. Papandreou-Suppappola, and M. Rangaswamy, "Adaptive waveform design for agile sensing and communications," *IEEE Journal of Selected Topics in Signal Processing (Special Issue on Adaptive Waveform Design for Agile Sensing and Communications)*, Vol. 1, no. 1, pp. 2 - 213, June 2007.

[34] J. S. Bergin, P. M. Techau, J. E. Don Carlos, and J. R. Guerci, "Radar waveform optimization for colored noise mitigation," *2005 IEEE International Radar Conference*, pp. 149 - 154, Washington, DC, 9 - 12 May 2005.

[35] L. K. Patton and B. D. Rigling, "Modulus constraints in adaptive radar waveform design," *2008 IEEE International Radar Conference*, pp. 1 - 6, Rome, Italy, 26 - 30 May 2008.

[36] A. De Maio, S. De Nicola, Y. Huang, D. P. Palomar, S. Zhang and A. Farina, "Code Design for Radar STAP via Optimization Theory", *IEEE Transactions on Signal Processing*, Vol. 58, n. 2, pp. 679 - 694, February 2010.

[37] I. S. Reed, J. D. Mallet, and L. E. Brennan, "Rapid convergence rate in adaptive arrays", *IEEE Trans. Aerosp. and Electron Syst.*, vol. 10, no.6, pp. 853-863, November 1974

[38] A. Farina and S. Pardini, "A Track-While-Scan Algorithm Using Radial Velocity in a Clutter Environment", *IEEE Transactions on Aerospace and Electronic Systems,* Vol. 14, n. 5, pp. 769 - 779, September 1978.

[39] H. L. Van Trees, *Optimum Array Processing. Part IV of Detection, Estimation and Modulation Theory*, John Wiley & Sons, 2002.

[40] A. Farina, H. Griffiths, G. Capraro, and M. Wicks, "Knowledge- based radar signal & data processing," *NATO RTO Lecture Series 233*, November 2003.

[41] M. Skolnik, *Radar handbook, 3rd Ed.*, Mc Graw Hill, 2008.

[42] P. Antonik, H. Shuman, P. Li, W. Melvin, and M. Wicks, "Knowledge-based space-time adaptive processing," *1997 IEEE National Radar Conference*, Syracuse, NY, May 1997.

[43] P. A. Antonik, H. Griffiths, D. D. Wiener, and M. C. Wicks, "Novel diverse waveform," *Air Force Research Lab.*, New York, In-House Rep., June 2001.

[44] F. Gini and M. Rangaswamy, *Knowledge based radar detection, tracking and classification*, John Wiley & Sons, Inc., 2008.

[45] H. L. Van Trees, "Optimum signal design and processing for reverberation-limited environments," *IEEE Transactions on Military Electronics*, Vol. 9, no. 3, pp. 212 - 229, July 1965.

[46] L. K. Patton, "On the satisfaction of modulus and ambiguity function constraints in radar waveform optimization for detection," *Doctor of Philosophy (PhD) Dissertation*, Wright State University, Engineering PhD, 2009.

[47] A. De Maio, Y. Huang, M. Piezzo, S. Zhang, and A. Farina, "Design of optimized radar codes with a peak to average power ratio constraint," *Accepted for pubblication on IEEE Transactions on Signal Processing*.

[48] W. D. Rummler, "A technique for improving the clutter performance of coherent pulse trains signals," *IEEE Transactions on Aerospace and Electronic Systems*, Vol. AES-3, no. 6, pp. 689 - 699, November 1967.

[49] D. F. Delong JR. and E. M. Hofstetter, " The design of clutter-resistant radar waveforms with limited dynamic range," *IEEE Transactions on Information Theory*, Vol. IT-15, no. 3, pp. 376 - 385, May 1969.

[50] H. W. Kuhn and A. W Tucker, "Nonlinear programming," *Proceedings on the 2nd Berkeley Symposyum on Mathematical Statistics and Probability.* Berkeley, Calif.: University of California Press, pp. 481 - 492, 1951.

[51] J. S. Thompson and E. L. Titlebaum, "The design of optimal radar waveforms for clutter rejection using the maximum principle," *Supplement to IEEE Transactions on Aerospace and Electronic Systems*, Vol. AES-3, pp. 581 - 589, November 1967.

[52] A. I. Cohen, "An algorithm for designing burst waveforms with quantized transmitter weights," *IEEE Transactions on Aerospace and Electronic Systems*, Vol. AES-11, no. 1, pp. 56 - 64, Jannuary 1975.

[53] R. A. Romero and N. A. Goodman, " Waveform design in signal-dependent interference and application to target recognition with multiple transmissions," *IEE Proceedings on Radar, Sonar and Navigation*, Vol. 3, no. 4, pp. 328 - 340, April 2009.

[54] S. M. Kay and J. H. Thanos, "Optimal transmit signal design for active sonar/radar," *2002 IEEE Conference on Acoustics, Speech, and Signal Processing, ICASSP 02*, Vol. 2, pp. 1513 - 1516, Orlando, FL, USA, 2002.

[55] S. Kay, "Optimal signal design for detection of gaussian point targets in stationary gaussian clutter/reverberation," *IEEE Journal of Selected Topics in Signal Processing*, Vol. 1, no. 1, pp. 31 - 41, June 2007.

[56] S. Kay, "Optimal detector and signal design for STAP based on the frequency-wavenumber spectrum," *Submitted on IEEE Transactions on Aerospace and Electronic Systems*, October 25, 2010.

[57] J. Ward, *Space-time Space-time adaptive processing for airborne radar*, Technical Report 1015, 13 December 1994.

[58] National Land Cover Data (NLCD). Available at http://landcover.usgs.gov/prodescription.asp

[59] C. T. Capraro, G. T. Capraro, A. De Maio, A. Farina, and M. Wicks, "Demonstration of knowledge-aided space-time adaptive processing using measured airborne data," *IEE Proceedings on Radar, Sonar and Navigation*, Vol. 153, no. 6, pp. 487 - 494, December 2006.

[60] D. K. Barton, *Modern radar systems analysis*, Artech House, 1988.

[61] F. E. Nathanson, with J. P. Reilly and M. N. Cohen, *Radar design principles: signal processing and the environment, 2nd Ed.*, Scitech Publishing, Inc., New Jersey 1999.

[62] A. De Maio, A. Farina, and G. Foglia, " Knowledge-aided bayesian radar detectors & their application to live data," *IEEE Transactins on Aerospace and Electronic Systems*, Vol. AES-46, no. 1, pp. 170 - 183, January 2010.

[63] J. B. Billingsley, *Low-angle radar land clutter.* Raleigh, NC: Scitech Publishing, 2002.

[64] A. Farina, F. Gini, M. V. Greco, and P. H. Y. Lee, "Improvement factor for real sea-clutter doppler frequency spectra," *IEE Proceedings on Radar, Sonar and Navigation,* Vol 141, no.5, pp.341 - 344, October 1996.

[65] T. M. Cover and J. A. Thomas, *Elements of information theory*, John Wiley & Sons, Inc., New York 1991.

[66] H. L. Van Trees, *Optimum array processing, part IV of detection, estimation, and modulation theory*, John Wiley & Sons, Inc., New York 2002.

[67] A. De Maio, Y. Huang, D. P. Palomar, S. Zhang, and A. Farina, "Fractional QCQP with applications in ML steering direction estimation for radar detection," *IEEE Transactions on Signal Processing*, Vol. 59, no. 1, pp. 172 - 185, January 2011

[68] W. Ai, Y. Huang, and S. Zhang, "Further results on rank-one matrix decomposition and its application," *Math. Program*, January 2008.

[69] G. H. Golub and C. F. Van Loan, *Matrix computations, 3rd Ed.*, The Johns Hopkins University Press, Baltimore and London, 1996.

[70] J. R. Guerci, *Cognitive radar, the knowledge-aided fully adaptive approach*, Artech House, 2010.

[71] S. Haykin, "Cognitive radar: a way of the future," *IEEE Magazine on Signal Processing*, Vol. 23, no. 1, pp. 30 - 40, January 2006.

[72] L. Bomer and M. Antweiler, "Polyphase barker sequences," *Electronics Letters*, Vol. 25, n. 23, pp. 1577 - 1579, November 1989.

[73] M. Friese, "Polyphase barker sequences up to length 36," *IEEE Transactions on Information Theory*, Vol. IT-42, no. 4, pp. 1248 - 1250, July 1996.

[74] E. Mozeson and N. Levanon, "MATLAB code for plotting ambiguity functions," *IEEE Transactions on Aerospace and Electronic Systems*, Vol. AES-38, no. 3, pp. 1064 - 1068, July 2002.

[75] M. R. Bell, "Information theory and radar waveform design," *IEEE Transactions on Information Theory*, Vol. IT-39, no. 5, pp. 1578 - 1597, September 1993.

[76] A. Aubry, "MIMO multiple access channel with partial channel state information," *Doctor of Philosophy (PhD) Dissertation*, Naples University, Engineering PhD, 2011.

[77] H. Huang and D. Lang, "The Comparison of Attitude and Antenna Pointing Design Strategies of Noncooperative Spaceborne Bistatic Radar", *Proceedings of the IEEE International Radar Conference 2005*, Arlington (US), pp. 568 - 571, May 2005.

[78] M. Greco, F. Gini, P. Stinco, A. Farina, and L. Verrazzani, "Adaptive waveform diversity for cross-channel interference mitigation", *Proceedings of the IEEE Radar Conference 2008*, Roma (IT), pp. 1 - 6, May 2008.

[79] D. Fudenberg and J. Tirole, *Game theory*, Cambridge, MA: MIT Press, 1991.

[80] D. Monderer and L. Shapley, "Potential games," *Games and economic behavior*, Vol. 14, no. 44, pp. 124 - 143, 1996.

[81] K. R. Griep, J. A. Ritcey, and J. J. Burlingame, Poly-phase codes and optimal filters for multiple user ranging, *IEEE Transaction on Aereospace and Electronics Systems*, Vol. 31, no. 2, pp. 752 - 767, Apr. 1995.

[82] P. Stoica, J. Li, and M. Xue, "Transmit codes and receive filters for radar: a look at the design process," *IEEE Signal Processing Magazine*, Vol. 25, no. 6, pp. 94 - 109, Nov. 2008.

[83] Y. I. Abramovich and M. B. Sverdlik, "Synthesis of a filter which maximizes the signal-to-noise radio under additional quadratic constraints," *Radio Eng. Electron. Phys.*, Vol. 15, no.11, pp. 1977 - 1984, Nov. 1970.

[84] Y. I. Abramovich and M. B. Sverdlik, "Synthesis of filters maximizing the signal-to- noise ratio in the case of a minimax constraint on the sidelobes of the crossambiguity function," *Radio Engineering and Electronic Physics*, Vol. 16, pp. 253 - 258, Feb. 1971.

[85] S. Zoraster, "Minimum peak range sidelobe filters for binary phase-coded waveforms," *Transaction on Aereospace and Electronics Systems*, Vol. 16, no. 1, pp. 112 - 115, Jan. 1980.

[86] J.C. Liberti Jr. and T.S. Rappaport, "Analytical results for capacity improvements in CDMA," *IEEE Transaction on Vehicular Technology*, Vol. 43, no. 3, pp. 680 - 690, Aug. 1994.

[87] S. Anderson, M. Millnert, M. Viberg, and B. Wahlberg, "An adaptive array for mobile communication systems," *IEEE Transaction on Vehicular Technology*, Vol. 40, no. 1, pp. 230, Feb. 1991.

[88] V. T. Dolgochub and M. B. Sverdlik, "Generalized γ-filters," *Radio Engineering and Electronic Physics*, Vol. 15, pp. 147 - 150, Jan. 1970.

[89] P. Stoica, J. Li, and M. Xue, "On binary probing signals and instrumental variables receivers for radar," *IEEE Transactions on Information Theory*, Vol. 54, no. 8, pp. 3820 - 3825, Aug. 2008.

[90] C. E. Cook and M. Bernfield, *Radar signals: nn introduction to theory and application*, New York. Academic Press, 1967.

[91] D. F. DeLong and E. M. Hofstetter, "On the design of optimum radar waveforms for clutter rejection," *IEEE Trans. Inform. Theory*, vol. 13, no. 3, pp. 454 - 463, Jul. 1967.

[92] C. Stutt and L. Spafford, "A best mismatched filter response for radar clutter discrimination," *IEEE Trans. Inform. Theory*, vol. 14, no. 2, pp. 280 - 287, Mar. 1968.

[93] P. Stoica, J. Li, and M. Xue, "Transmit codes and receive filters for radar," *IEEE Signal Processing Magazine*, vol. 25, no. 6, pp. 94 - 109, Nov. 2008.

[94] A. Nemirovski, "*Lectures on modern convex optimization*," Class Notes, Georgia Institute of Technology, Fall 2005.

[95] S. A. Vorobyov, A. B. Gershman, and Z.-Q. Luo, "Robust adaptive beamforming using worst-case performance optimization: a solution to the signal mismatch problem," *IEEE Trans. Signal Processing*, vol. 51, no. 2, pp. 313 - 324, Feb. 2003.

[96] K. Yang, G. Wang, and Z.-Q. Luo, "Efficient convex relaxation methods for robust target localization by a sensor network using time differences of arrivals," *IEEE Trans. Signal Processing*, vol. 57, no. 7, pp. 2775 - 2784, July 2009.

[97] J. E. Cilliers and J. C. Smit, "Pulse compression sidelobe reduction by minimization of L_p-norms," *IEEE Trans. Aerosp. Electron. Syst.*, vol. 43, no. 3, pp. 1238 - 1247, July 2007.

[98] K. Deb, Multi-objective optimization using evolutionary algorithms, *John Wiley Sons*, 1st ed. , June 2001.

[99] A. Aubry, A. De Maio, A. Farina, and M. Wicks, "Knowledge-Aided (Potentially Cognitive) Transmit Signal and Receive Filter Design in Signal-Dependent Clutter", *accepted for pubblication on IEEE Trans. on Aerosp. Electron. Syst.*, September 2011.